UNIVERZITA KARLOVA
Přírodovědecká fakulta

Studijní program: Molekulární a buněčná biologie, genetika a virologie

Mgr. Iva Filová

Molekulární mechanismy v transkripční regulaci neurosenzorického vývoje

Molecular mechanisms in transcriptional regulation of neurosensory development

Disertační práce

Vedoucí disertační práce: RNDr. Gabriela Pavlínková, Ph.D.
Biotechnologický ústav AV ČR, v. v. i.

Praha, 2019

Prohlášení

Prohlašuji, že jsem závěrečnou práci zpracovala samostatně a že jsem uvedla všechny použité informační zdroje a literaturu. Tato práce ani její podstatná část nebyla předložena k získání jiného nebo stejného akademického titulu.

V Praze dne 14. listopadu 2019 Mgr. Iva Filová

Poděkování

Touto cestou bych ráda poděkovala mé trpělivé a laskavé školitelce RNDr. Gabriele Pavlínkové, Ph.D. za odborné vedení a cenné rady během mého doktorského studia. Dále bych chtěla poděkovat Ing. Romaně Bohuslavové, Ph.D. a celému kolektivu Laboratoře molekulární patogenetiky z Biotechnologického ústavu AV ČR, v. v. i. za vytvoření výborného pracovního prostředí a za pomoc během experimentálních prací. Také bych chtěla poděkovat spolupracovníkům z jiných insitucí, kteří se podíleli na uvedených publikacích.

V neposlední řadě patří velké díky mé rodině a přátelům za podporu během celého mého dlouhého studia.

Abstrakt

Vývoj, maturace a životaschopnost neurosenzorických buněk vnitřního ucha je závislá na přesné časové a prostorové expresi transkripčních faktorů. Předmětem studia předkládané práce je objasnění funkce transkripčních faktorů ISL1, SOX2 a NEUROD1 v neurosenzorickém vývoji vnitřního ucha za použití tří myších modelů [Tg(*Pax2-Isl1*)], *Sox2CKO* a *Neurod1CKO*.

Myší mutant [Tg(*Pax2-Isl1*)] má ve svém genomu transgenní sekvenci kódující gen *Isl1*, jehož exprese je řízena regulační sekvencí pro gen *Pax2*. Ektopická exprese ISL1 řízená regulační sekvencí *Pax2* vedla ke zvětšení kochleovestibulárního ganglia a urychlený růst neuritů vnitřního ucha u embryí [Tg(*Pax2-Isl1*)]. V dospělosti u těchto mutantů docházelo k urychlené ztrátě sluchu v důsledku zhoršující se funkce vnějších vláskových buněk. Tyto změny korelovaly se ztrátou eferentních vláken z mediální olivy superior inervující vnější vláskové buňky. Poprvé jsme ukázali, že podstatou stařecké nedoslýchavosti (presbyakuze) kromě ztráty vláskových buněk a neuronů spirálního ganglia může být i poškození eferentní inervace. Kromě presbyakuze byly myši [Tg(*Pax2-Isl1*)] hyperaktivní. Po podání pikrotoxinu, blokátoru chloridových kanálů spjatých s GABA receptory, došlo u těchto mutantů k významnému potlačení hyperaktivity. Tyto analýzy ukázaly, že nadměrná a ektopická exprese ISL1 ovlivnila funkci GABAergních neuronů. Kromě změn v GABA signalizaci měli tito mutanti zmenšený *colliculus inferior* a nesprávně morfologicky formovaný mozeček, což souvisí s abnormálním vestibulárním fenotypem myší [Tg(*Pax2-Isl1*)].

Pro analýzy funkce SOX2 ve vývoji vnitřního ucha byl pomocí systému Cre-loxP vytvořen nový myší model s podmíněnou delecí *Sox2* v buňkách exprimujících ISL1 (*Sox2CKO*). U *Sox2CKO* docházelo k diferenciaci pouze omezeného počtu vláskových buněk v utrikulu, sakulu a bázi kochley, zatímco kristy a kochleární apex zůstaly zcela bez vláskových buněk. Jeden z hlavních rozdílů mezi vláskovými buňkami v těchto dvou skupinách orgánů vnitřního ucha je jejich původ. Vláskové buňky krist a kochleárního apexu se vyvíjí výhradně ze senzorických prekurzorů, zatímco část vláskových buněk v utrikulu, sakulu a bázi kochley vzniká z neurosenzorických prekurzorů, což by mohlo ovlivnit jejich diferenciaci u *Sox2CKO*. Analýzy neurálního vývoje vnitřního ucha ukázaly, že raně se vyvíjející neurony, které inervují vestibulární orgány a kochleární bázi, se diferencovaly u *Sox2CKO*, avšak časem podléhaly apoptóze v důsledku nedostatku neurotrofických faktorů, které jsou produkované vláskovými buňkami. Naopak později vznikající neurony v apexu se u *Sox2CKO* vůbec nediferencovaly.

SOX2 je tedy nutný pro diferenciaci později se vyvíjejících apikálních sluchových neuronů, pro přežití vestibulárních a bazálních sluchových neuronů a pro diferenciaci vláskových buněk senzorického původu.

Pomocí systému Cre-loxP byl také vytvořen unikátní model s tkáňově specifickou delecí *Neurod1* pouze ve vnitřním uchu a se zachováním exprese NEUROD1 v komponentech centrální sluchové dráhy v mozku (*Neurod1CKO*). Využitím tohoto modelu bylo možné ukázat, jak vývojové změny na periferii ovlivňují funkce centrální sluchové dráhy. Primárním důsledkem delece *Neurod1* byla zkrácená kochlea se sníženým počtem neuronů spirálního ganglia, dezorganizovanou inervací a chybějícím tonotopickým uspořádáním. Důsledkem změn ve vnitřním uchu docházelo sekundárně k vývoji zmenšeného kochleárního jádra postrádajícího tonotopické uspořádání. Tyto změny vedly ke změnám vlastností neuronů v *colliculus inferior* projevující se zhoršenými funkcemi při zpracování akustického signálu – omezené vnímání slyšitelných frekvencí, zhoršená selektivita frekvencí a abnormální odpovědi při behaviorálních testech.

Klíčová slova: ISL1, SOX2, NEUROD1, transkripční faktor, vývoj vnitřního ucha, sluchový a vestibulární systém

Abstract

The development, maturation, and viability of inner ear neurosensory cells depend on the spatiotemporal expression of multiple transcriptional factors. Based on three mouse models [Tg(*Pax2-Isl1*)], *Sox2CKO*, and *Neurod1CKO,* this thesis investigates the function of three transcriptional factors ISL1, SOX2 and NEUROD1 in the neurosensory development of the inner ear.

The mouse mutant [Tg(*Pax2-Isl1*)] carries transgenic sequence containing *Isl1* gene under *Pax2* regulatory sequence in its genome. ISL1 ectopic expression driven by *Pax2* regulatory sequence resulted in the enlarged cochleovestibular ganglion and accelerated neurite extension in [Tg(*Pax2-Isl1*)] embryos. In adult mutants, we detected an early onset of age-related hearing loss correlating with the worsening function of outer hair cells. These changes were associated with the loss of medial olivocochlear efferent neuron fibers innervating outer hair cells. For the first time, we showed that the age-related hearing loss (presbyacusis) might be caused by efferent innervation defects besides hair cell loss and spiral ganglion degeneration. In addition to presbyacusis, [Tg(*Pax2-Isl1*)] mice suffered from hyperactivity that was diminished by the administration of picrotoxin – channel blocker for GABA receptor chloride channels. This indicates that ISL1 overexpression impacts GABAergic neuron function. Besides changes in GABAergic signalization, [Tg(*Pax2-Isl1*)] mice had the reduced size of inferior colliculus and the aberrant morphology of the cerebellum, corresponding to the abnormal vestibular phenotype of these mutant mice.

For analysis of SOX2 function during inner ear development, we generated a new mouse model with conditional deletion of *Sox2* in ISL1 positive cells using the Cre-loxP system (*Sox2CKO*). In *Sox2CKO*, a limited number of hair cells of neurosensory origin differentiated in the utricle, saccule, and cochlear base, while all cristae and the cochlear apex were devoid of any hair cells derived from sensory precursors. Early developed neurons innervating the vestibular end organs and cochlear base differentiated in *Sox2CKO.* However, all these early differentiated neurons died later by apoptosis due to a lack of neurotrophins that are produced by hair cells. Late forming apical neurons in the cochlea did not differentiate at all in *Sox2CKO*. Our results demonstrate that transcriptional factor SOX2 is necessary for the differentiation of late forming neurons in the cochlear apex, for the maintenance of vestibular and basal spiral ganglion neurons, and for the differentiation of hair cells derived from sensory progenitors.

We used the Cre-loxP system to conditionally delete *Neurod1* gene in the inner ear but to retain NEUROD1 expression in the auditory nuclei and auditory midbrain (*Neurod1CKO*). Using *Neurod1CKO,* we demonstrated how developmental changes in the periphery affect the function of the central auditory system. The primary consequence of *Neurod1* deletion was shortened cochlea containing reduced number of spiral ganglion neurons with disorganized innervation and missing tonotopy. Abnormalities in the inner ear resulted in the size reduction of the cochlear nucleus and a loss of tonotopic organization of the central auditory pathway. These changes altered tuning properties of inferior colliculus neurons – truncated frequency range, worsened frequency selectivity, and abnormal responses in behavioral tests.

Key words: ISL1, SOX2, NEUROD1, transcriptional factor, inner ear development, auditory and vestibular system

Obsah

Seznam zkratek

ABR	Vyšetření sluchových kmenových potenciálů (z angl. Auditory brainstem response test)
ADHD	Porucha pozornosti s hyperaktivitou (z angl. Attention deficit hyperactivity disorder)
ATOH1	Transkripční faktor ATOH1 (z angl. Protein atonal homolog 1)
BARHL1	Transkripční faktor BARHL1 (z angl. BarH-like 1 homeobox protein)
BDNF	Mozkový neurotrofní faktor (z angl. Brain-derived neurotrophic factor)
bHLH	Strukturní motiv zásadité šroubovice–smyčka–šroubovice (z angl. basic helix-loop-helix)
BMP4	Kostní morfogenetický protein 4 (z angl. Bone morphogenetic protein 4)
c-Fos	Protoonkogen c-Fos (z angl. Proto-oncogene c-Fos)
CACNG1	Podjednotka gama-1 napěťově řízeného vápníkového kanálu (z ang. Voltage-dependent calcium channel gamma-1 subunit)
CALB2	Protein kalretinin (z ang. Calretinin), produkt genu *Calb2*
CDKN1B	Inhibitor cyklin-dependentní kinázy 1B (z angl. Cyclin-dependent kinase inhibitor 1B)
CKO	Podmíněná (tkáňově specifická) delece (z angl. Conditional knock out)
CN	Kochleární jádro (z ang. Cochlear nucleus)
DCN	Dorsální kochleární jádro (z ang. Dorsal cochlear nucleus)
DLG4	Protein DLG4 (z ang. Disks large homolog 4)
DLL1	Ligandový protein DLL1 (z ang. Delta-like protein 1)
DLX5	Transkripční faktor DLX5 (z angl. Homeobox protein DLX-5)
DPOAE	Měření otoakustických emisí (z angl. Distortion Product Otoacoustic Emission)
E	Embryonální den
EN1	Transkripční faktor EN1 (z angl. Homeobox protein engrailed-1)
EYA1	Transkripční faktor EYA1 (z angl. Eyes absent homolog 1)
FGF	Fibroblastový růstový faktor (z angl. Fibroblast growth factor)
FOXG1	Transkripční faktor FOXG1 (z angl. Forkhead box protein G1)

GABA	Kyselina gama-aminomáselná (z angl. gamma-Aminobutyric acid)
GATA3	Transkripční faktor GATA3 (z angl. Trans-acting T-cell-specific transcription factor GATA-3)
GBX2	Transkripční faktor GBX2 (Homeobox protein GBX-2)
HMG	Proteinová rodina vysoké mobility v elektroforetickém poli (z ang. High mobility group)
HOX2	Transkripční faktory HOX2 (z angl. Homeobox proteins Hox2)
ISL1	Transkripční faktor ISL1 (z angl. Insulin gene enhancer protein ISL-1)
JAG	Ligandy JAG signalizační dráhy Notch (z angl. Protein jagged)
LIM	Strukturní motiv LIM (z angl. **L**IN11 - **I**SL1 - **M**EC3)
NEUROD1	Neurogenní diferenciační faktor 1 (z angl. Neurogenic differentiation factor 1)
NEUROD4	Neurogenní diferenciační faktor 4 (z ang. Neurogenic differentiation factor 4)
NEUROG1	Transkripční faktor Neurogenin-1 (z angl. Neurogenin-1)
NHLH1	Transkripční faktor NHLH1 (z ang. Helix-loop-helix protein 1)
NHLH2	Transkripční faktor NHLH2 (z ang. Helix-loop-helix protein 2)
NOTCH1	Receptor NOTCH1 (z angl. Neurogenic locus notch homolog protein 1)
NTF-3	Neurotrofin-3 (z angl. Neurotrophin-3)
OCT4	Transkripční faktor OCT4 (z angl. Octamer-binding protein 4)
OTX2	Transkripční faktor OTX2 (z ang. Homeobox protein OTX2)
P	Postnatální den
PAX2	Transkripční faktor PAX2 (z angl. Paired box protein Pax-2)
PAX8	Transkripční faktor PAX8 (z angl. Paired box protein Pax-8)
PCR	Polymerázová řetězová reakce (z angl. Polymerase chain reaction)
POU4F3	Transkripční faktor POU4F3 (z angl. POU domain, class 4, transcription factor 3)
PROX1	Transkripční faktor PROX1 (z angl. Prospero homeobox protein 1)
RIF	Velikost odpovědi neuronu v závislosti na intenzitě zvuku (z angl. rate-intensity function)
SHH	Morfogen SHH (z angl. Sonic hedgehog protein)

SIX1	Transkripční faktor SIX1 (z angl. Homeobox protein SIX1)
Snca	Gen pro α-synuklein
SOX10	Transkripční faktor SOX10 (z ang. Transcription factor SOX-10)
SOX2	Transkripční faktor SOX2 (z angl. Transcription factor SOX-2)
TBX1	Transkripční faktor TBX1 (z angl. T-box transcription factor TBX1)
TNFα	Nádor nekrotizující faktor α (z ang. Tumor necrosis factor α)
VCN	Ventrální kochleární jádro (z ang. Ventral cochlear nucleus)
WNT	Signalizační kaskáda WNT (z angl. Wingless/Integrated)

1 Úvod

Ztrátou či poškozením sluchu trpí přes 5 % lidské populace - 432 milionů dospělých a 34 milionů dětí a předpokládá se, že v roce 2050 bude každý desátý člověk postižen nedoslýchavostí (World Health Organization, 20. března 2019). Příčiny ztráty sluchu mohou být vrozené nebo získané. Mezi vrozené příčiny se řadí genetické poruchy či komplikace během těhotenství a porodu (nízká porodní hmotnost novorozence, závažná novorozenecká žloutenka, užívání aminoglykosidových antibiotik matkou v těhotenství atd.). V průběhu života může být sluch poškozen v důsledku infekčních onemocnění, při úrazech hlavy a krku, ale nejčastější příčinou poškození sluchu je nadměrný hluk. Všechny zmíněné vlivy negativně působí na neurony a senzorické buňky vnitřního ucha, které nejsou schopny regenerace. Pokud se tyto buňky poškodí nadměrným hlukem, biologickým či chemickým působením, podléhají apoptóze a jejich ztráta je nevratná.

V současné době jsou jedinou možností léčby naslouchadla či kochleární implantáty, které zesilují a modulují zvuk. Avšak i tyto pomůcky mají své limity a nejsou vhodné pro každého pacienta trpícího poškozením sluchu. Současný výzkum je zaměřen na biologickou léčbu, při které by bylo možné naprogramovat buňky vnitřního ucha k transdiferenciaci na neurosenzorické buňky, čímž by bylo možné nahradit chybějící poškozené neurony a senzorické buňky. Za tímto účelem je nezbytné důkladně zmapovat transkripční regulaci a signální dráhy účastnící se embryonální i postnatální fáze vývoje vnitřního ucha a centrální sluchové dráhy. Tato disertační práce je zaměřena na objasnění funkce klíčových transkripčních faktorů (ISL1, SOX2 a NEUROD1) během proliferace, maturace a diferenciace neurosenzorických buněk vnitřního ucha i dalších úrovní sluchové dráhy, což přispívá k poznatkům základního výzkumu pro biologickou léčbu nedoslýchavosti.

2 Teoretický úvod

2.1 Sluchově rovnovážné ústrojí

Lidské ucho je sluchově rovnovážným orgánem, které má tři části – vnější (zevní), střední a vnitřní ucho (Obrázek 1)(Králíček 2004, Čihák 2016). Zevní ucho začíná boltcem (*auricola*), pokračuje zvukovodem (*meatus acusticus externus*) a je ukončeno membránou zvanou bubínek (*membrana tympani*). Hlavní funkcí vnějšího ucha je zachycení a vedení zvuku do dalších částí sluchového ústrojí. Za bubínkem se nachází dutina bubínková (*cavitas tympani*), kde jsou uloženy středoušní kůstky kladívko (*malleus*), kovadlinka (*incus*) a třmínek (*stapes*). Střední ucho zajišťuje amplifikaci signálu, neboť se energie z relativně velké plochy bubínku přenáší pákovým systémem na malé oválné okénko, které přiléhá k třmínku. Výsledkem tohoto mechanismu je 22násobné zesílení akustického tlaku na oválné okénko, kterým začíná vnitřní ucho. Vnitřní ucho je komplexní blanitý orgán tvořený kochleou a rovnovážným systémem a je uloženo v kostěném labyrintu. Buňky vnitřního ucha detekují vibrace vznikající zvukem či pohybem a transformují je na elektrický signál pro neurony VIII. hlavového nervu.

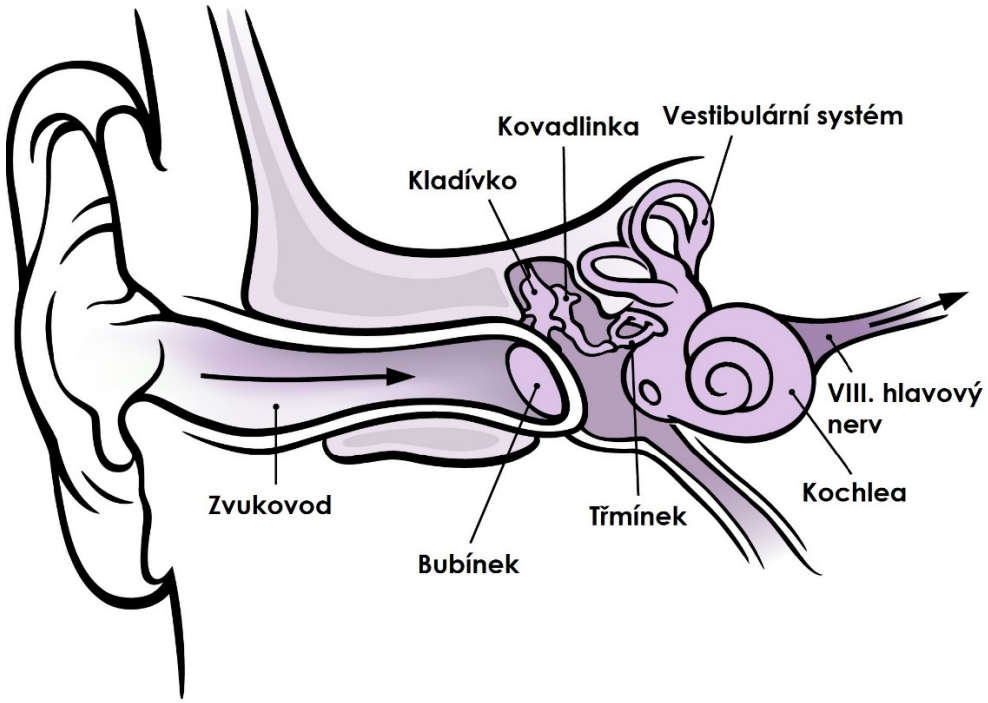

Obrázek 1: Schématické znázornění lidského ucha. Zvuky jsou do ucha přiváděny zvukovodem, jenž je ukončen bubínkem. V bubínkové dutině se nalézají tři středoušní kůstky (kladívko, kovadlinka a třmínek) zesilující přicházející signál vedoucí do vnitřního ucha, jenž se skládá ze sluchového (kochlea) a rovnovážného (vestibulárního) orgánu. Převzato a upraveno z (Chittka a Brockmann 2005).

2.2 Morfologie vnitřního ucha

Kostěný labyrint vnitřního ucha je uložen v kosti spánkové, je vyplněn tekutinou zvanou perilymfa a obsahuje membránový labyrint s endolymfou (Králíček 2004, Čihák 2016). Sluchově rovnovážný orgán vnitřního ucha je tvořen šesti blanitými orgány. Cortiho orgán detekující zvuk se nachází v kochlee (*cochlea*). Rovnovážný (vestibulární) systém obsahuje tři polokruhovité kanálky (*ductus semicircularis*) pro detekci úhlového zrychlení a dva na sebe kolmé váčky sakulus (*sacculus*) a utrikulus (*utriculus*), které zaznamenávají zrychlení lineární.

2.2.1 Kochlea (*Cochlea*)

Kochlea je membránami podélně rozdělena na tři části – *scala vestibuli*, *scala media* a *scala tympani* (Obrázek 2)(Králíček 2004, Čihák 2016). Mezi *scala vestibuli* a *scala media* se nachází Reisnerova membrána, zatímco basilární membrána rozděluje *scala media* a *scala tympani*. *Scala vestibuli* a *scala tympani* jsou propojeny ve vrcholu kochley (apexu) tzn. *helicotremou* a obsahují perilymfu, která je svým složením podobná krevní plazmě či mozkomíšnímu moku (vysoká koncentrace sodných iontů a nízká koncentrace draselných iontů). Naopak *scala media* je zcela uzavřena a vyplněna endolymfou, jenž má obdobné složení jako nitrobuněčná tekutina (vysoká koncentrace draselných kationtů a nízká koncentrace sodných kationtů). Koncentrace iontů endolymfy je udržována aktivním transportem buňkami uloženými ve *stria vascularis* (Forge a Wright 2002). Ve *scala media* je uložen Cortiho orgán, který obsahuje senzorický epitel.

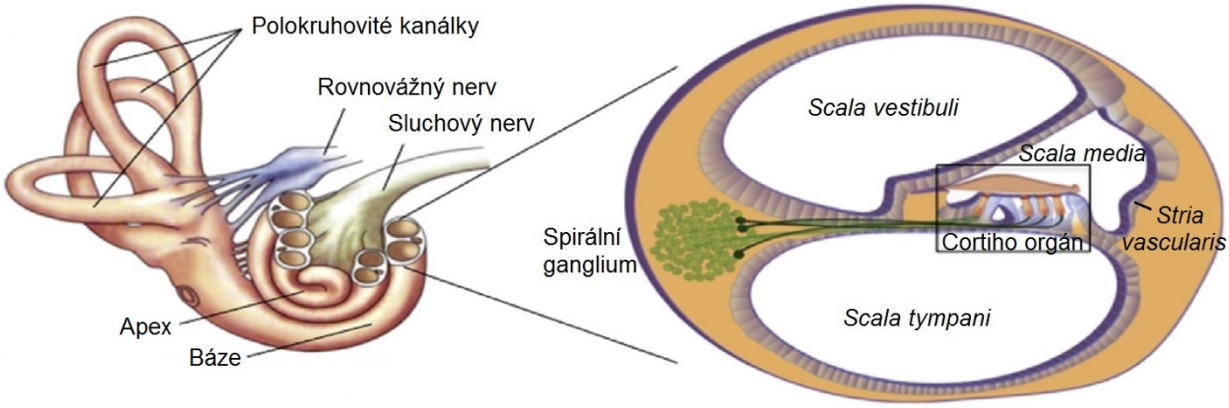

Obrázek 2: Struktura kochley. Sluchový Cortiho orgán je uložen ve *scala media* nacházející se mezi *scala vestibuli* a *scala tympani*. Převzato a upraveno z (Delacroix a Malgrange 2015).

Epitelové buňky Cortiho orgánu leží na basilární membráně (Obrázek 3)(Forge a Wright 2002). Za percepci zvuku a přeměnu mechanických akustických vibrací na elektrický signál

zodpovídají specializované senzorické vláskové buňky. Ty jsou v kochlee uspořádané do jedné řady vnitřních a tří řad vnějších vláskových buněk. Mezi vnitřními a vnějšími buňkami se nachází Cortiho tunel. Vláskové buňky mají na apikální straně tenké výběžky zvané stereocilie, které se v případě vnějších vláskových buněk dotýkají extracelulární tektoriální membrány. Na bazální straně vláskových buněk se nacházejí nervová zakončení aferentních vláken neuronů sluchového (spirálního) ganglia a eferentních vláken neuronů komplexu olivy superior (*nucleus olivaris superior*) z mozkového kmene. Žádná vlásková buňka přímo nesousedí s další vláskovou buňkou, ale je obklopena buňkami podpůrnými.

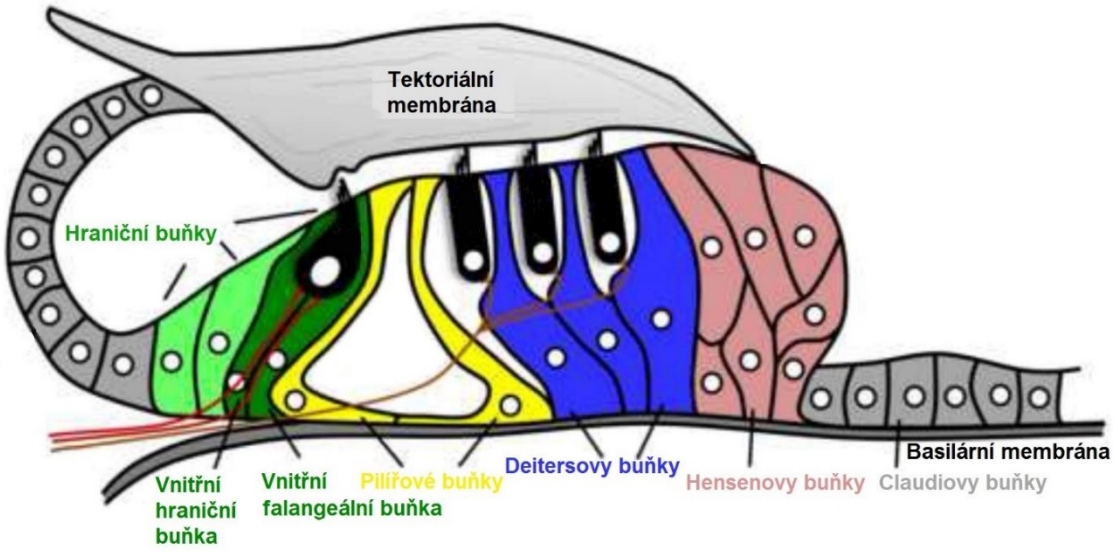

Obrázek 3: Řez Cortiho orgánem znázorňující epitelové buňky. Senzorické buňky jsou znázorněny černou barvou a jsou uspořádány do jedné řady vnitřních a tří řad vnějších vláskových buněk. Vláskové buňky jsou inervovány nervovými vlákny spirálního ganglia. Různé typy podpůrných buněk obklopující vláskové buňky jsou barevně odlišeny. Zmíněné epitelové buňky leží na basilární membráně a tektoriální membrána se klene nad stereociliemi vláskových buněk. Převzato a upraveno z (Wan, Corfas *et al.* 2013).

Charakteristickým znakem epitelových vláskových buněk jsou mechanosenzorické stereocilie tvořené aktinovými vlákny spojené myosiny. Rigidní stereocilie jsou na apikální straně buněk organizovány do řad se zvětšující se výškou, přičemž nejvyšší řada stereocilií je na všech sluchových vláskových buňkách orientována stejným směrem (Lim 1986). Řady stereocilií jsou ve svém vrcholu spojeny. Na vnitřních vláskových buňkách tvoří stereocilie jednu vyšší téměř rovnou řadu a několik nižších řad, zatímco na vnějších vláskových buňkách jsou uspořádány ve třech až čtyřech pravidelně odstupňovaných řadách do písmene W.

U vnějších vláskových buněk lze pozorovat rozdíly v počtu stereocílií mezi apexem a bází (u člověka obsahuje jedna vnější vlásková buňka v apexu 50 a v bázi 120 stereocilií). Výška vnějších vláskových buněk roste od báze k apexu. Senzorické buňky jsou nejmenší v bázi a nejvyšší v apexu. Obdobně je to i s výškou stereocilií, které jsou nejvyšší v apexu kochley. Žádné podobné gradienty nebyly zaznamenány u vnitřních vláskových buněk, ty však obsahují stereocilie o 30-50% širší než vnější vláskové buňky. Vnitřní a vnější vláskové buňky se liší nejen vzhledem, ale mají také odlišné funkce. Vnitřní vláskové buňky detekují zvuk ve formě chvění basilární membrány a pomocí mechanotransdukce převádějí mechanické vibrace na elektrický signál předávaný aferentním neuronů spirálního ganglia. Vnější vláskové buňky zastávají funkci mechanického zesilovače vibrací díky proteinu zvaného prestin (Zheng, Shen *et al.* 2000, Liberman, Gao *et al.* 2002).

Vláskové buňky jsou inervovány aferentními vlákny vedoucími z neuronů spirálního ganglia. Toto ganglium obsahuje dva druhy bipolárních neuronů (Fuchs a Glowatzki 2015). Většinu spirálního ganglia (90-95 %) tvoří senzorické neurony I. typu, které svými širšími, myelinovými a nerozvětvenými dendrity inervují výhradě vnitřní vláskové buňky. Na jedné vnitřní vláskové buňce se nalézají nervová zakončení z více neuronů, ale jeden neuron spirálního ganglia inervuje vždy jen jednu vnitřní vláskovou buňku. Synapse mezi vnitřní vláskovou buňkou a neuronem I. typu se nazývá „ribbon“ synapse (Nouvian, Beutner *et al.* 2006). Hlavní funkcí neuronů spirálního ganglia I. typu je přenos informací z vláskových buněk do vyšších vrstev centrální sluchové dráhy. Neurony vnitřního ucha I. typu se dále dělí na tři poddruhy na základě odlišného transkriptomu – Ia, Ib a Ic (Shrestha, Chia *et al.* 2018, Sun, Babola *et al.* 2018). Na druhou stranu několik vnějších vláskových buněk je inervováno jediným vláknem neuronu typu II, které zaujímají pouze 5-10 % spirálního ganglia. Vlákna neuronů II. typu jsou užší a nemyelinová (Fuchs a Glowatzki 2015). Na rozdíl od neuronů I. typu nejsou neurony II. typu aktivovány zvukovými podněty, ale nejspíše hrají důležitou roli při detekci poškození vnějších vláskových buněk. Kromě aferentních vláken spirálního ganglia lze také na všech vláskových buňkách nalézt eferentní zakončení vycházející z mozkového kmene modulující funkci senzorických buněk. Vlákna z laterální olivy superior zpětně kontrolují „ribbon“ synapse, zatímco vlákna neuronů mediální olivy superior končí na vnějších vláskových buňkách (Rabbitt a Brownell 2011, Fuchs a Lauer 2018).

Neméně důležité pro funkce kochley jsou podpůrné buňky, vyskytující se mezi buňkami vláskovými. Podpůrná buňka je spojena s vláskovou či jinou podpůrnou buňkou těsnými či adhezními spoji a podpůrné buňky mezi sebou komunikují pomocí vodivých spojů (Wan, Corfas *et al.* 2013). Podle odlišností v morfologii můžeme v kochlee rozlišit šest druhů podpůrných buněk: Claudiovy buňky, Hensenovy buňky, Deitersovy buňky, pilířové buňky, vnitřní falangeální buňky a hraniční buňky (Obrázek 3). Podpůrné buňky mají ve vnitřním uchu několik důležitých funkcí – udržují rigidní a velmi organizovanou strukturu Cortiho orgánu (zejména pilířové a Deitersovy buňky), regulují rovnováhu iontů důležitou pro vláskové buňky, produkují složky tektoriální membrány a jsou schopny odstranit poškozené vláskové buňky pomocí fagocytózy.

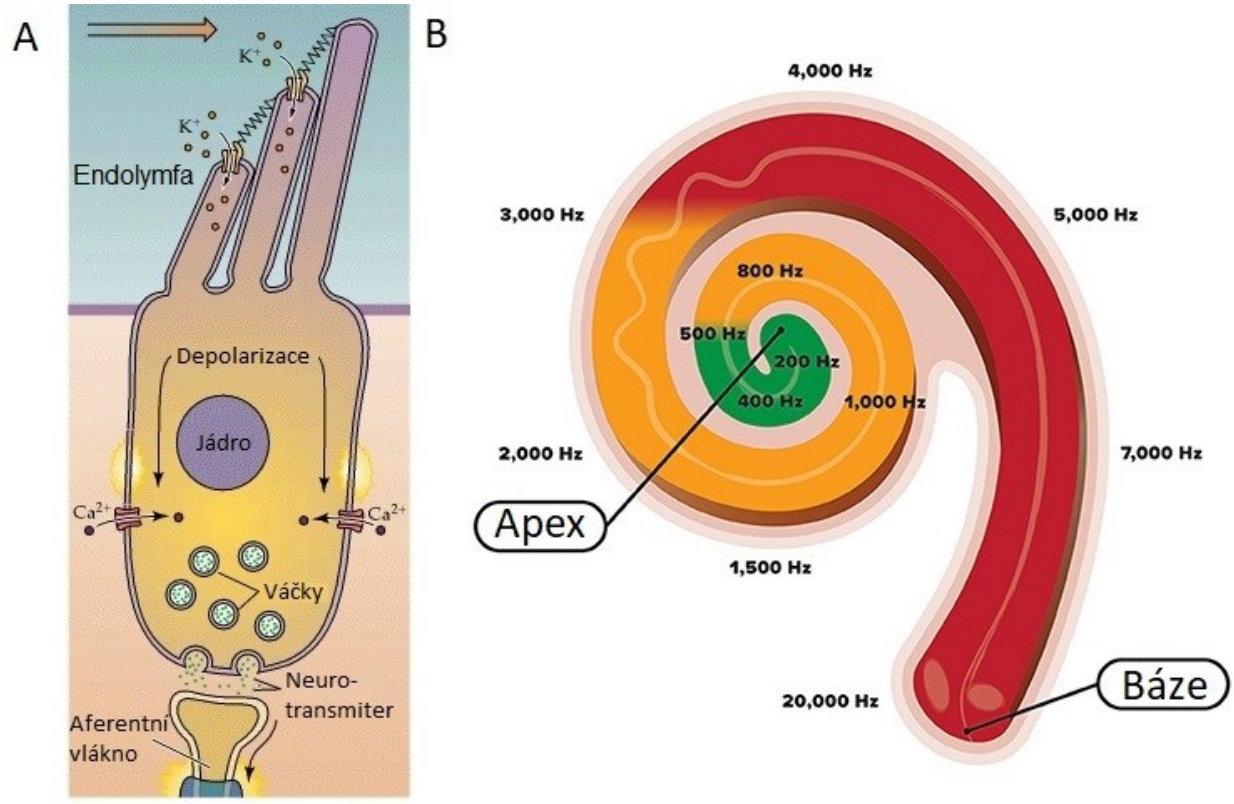

Obrázek 4: Schématické znázornění procesu mechanotransdukce vláskové buňky a tonotopického uspořádání lidské kochley. A – Při vychýlení stereocilií na vnitřní vláskové buňcedochází k otevření mechanicky řízených iontových kanálů a k následné depolarizaci buňky vedoucí ke změně v propustnosti napěťově řízených kanálů. Vstupující vápenaté ionty způsobí vylití neurotransmiteru do synaptické štěrbiny. **B –** Proměnlivá tuhost basilární membrány umožňuje detekovat nízké frekvence v apexu a vysoké frekvence v bázi. Uvedené frekvence odpovídají sluchovému rozsahu zdravého člověka. Převzato a upraveno z (Purves, Augustine *et al.* 2001, Lahav a Skoe 2014).

Hlavní úlohou Cortiho orgánu je převod mechanických vln na elektrický impuls procesem zvaný mechanotransdukce (Obrázek 4A)(Fettiplace 2017). Zvukové vlny po vstupu do zvukovodu rozechvějí bubínek a dále se vibrace šíří středoušními kůstkami a oválným okénkem až ke kochlee. Vzniklé vibrace na oválném okénku způsobí pohyb perilymfy uzavřené ve *scala vestibuli*, čímž se rozpohybuje basilární membrána a tím i Cortiho orgán, jenž na basilární membráně leží. V důsledku vlnění dochází k vychýlení stereocilií zanořených do tektoriální membrány a k otevření mechanicky ovládaných iontových kanálů na apikální straně vnitřních vláskových buněk. Z endolymfy bohaté na draselné ionty vstupují do buňky kationty způsobující depolarizaci senzorických buněk. Změna membránového potenciálu spouští otevření kanálů řízených napěťově, které jsou umístěny na bazolaterální straně vláskových buněk. Těmito kanály do buňky začnou proudit vápenaté ionty způsobující vylití neurotransmiteru glutamátu ze synaptického váčku vnitřní vláskové buňky do synaptické štěrbiny „ribbon“ synapse, čímž dojde k přenosu vzruchu na aferentní neurony spirálního ganglia.

Vláskové buňky umístěné v bazální části kochley se depolarizují při zvucích o vysoké frekvenci (u člověka 20 kHz a u myši 70 kHz), zatímco apikální část je zodpovědná za detekci nízkých frekvencí (u člověka 20 Hz a u myši 1 kHz)(Obrázek 4B). To je způsobeno unikátní vlastností basilární membrány, která je širší a flexibilnější v apikální části, zatímco v bázi je úzká a tuhá (Teudt a Richter 2014). Prostorová aktivace určitých vláskových buněk a neuronů v daném místě a danou frekvencí se označuje termínem tonotopie. Místo dosažení maximální amplitudy je pro jednotlivé frekvence charakteristické. Z konkrétního místa v Cortiho orgánu vedou aferentní nervová vlákna zvukovou informaci o jediné frekvenci do mozku. Tonotopické uspořádání je udržováno po celou dobu přenosu akustického signálu nervovým systémem až do mozkové kůry.

2.2.2 Rovnovážné ústrojí (Vestibulární systém)

Ve vestibulárním systému se nalézá celkem pět blanitých orgánů pro detekci úhlového a lineárního zrychlení, které zajišťují vnímání polohy hlavy vůči tělu (Obrázek 5). Orgány rovnovážného ústrojí obsahují podobně jako Cortiho orgán endolymfu, vláskové a podpůrné buňky a také nervová zakončení. Na apikální straně vláskových buněk se nachází 70–100 aktinových stereocilií odstupňovaných opět podle velikosti a jedno tubulinové kinocilium, které stereocilie převyšuje (Khan a Chang 2013)(kinocilium se v Cortiho orgánu nachází pouze

v embryonálním vývoji a po narození mizí). Vestibulární vláskové buňky se dají rozdělit na dva typy lišící se buněčným tvarem a typem nervového zakončení. Vlásková buňka I. typu je kulatá a je obklopena kalichem (*calyx*) aferentního vlákna, zatímco II. typ vestibulární senzorické buňky je cylindrického tvaru a nervové vlákno je zakončeno synaptickým knoflíkem (*bouton*) na bazální straně vláskové buňky. Vláskové buňky II. typu v rovnovážném ústrojí tvoří většinu.

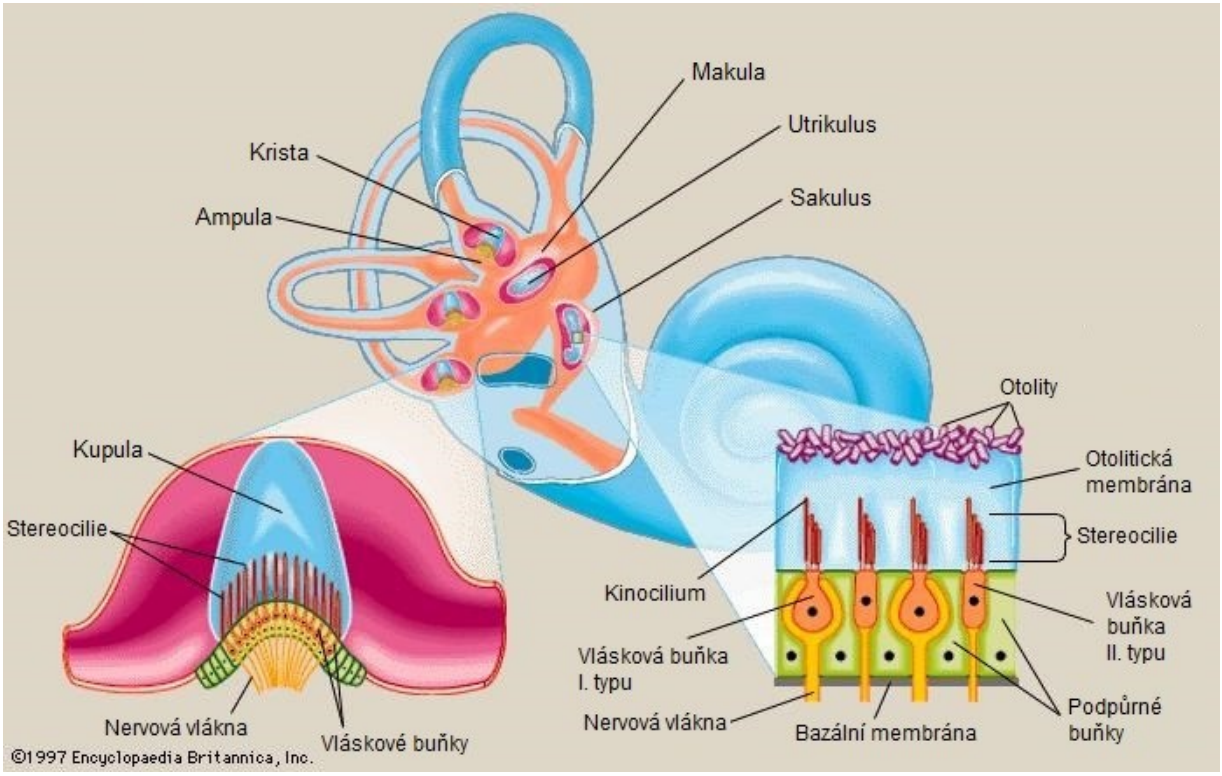

Obrázek 5: Rovnovážné ústrojí. Vestibulární systém obsahuje pět orgánů – dvě makuly a tři kristy uložené v ampulách. Makuly utrikulu a sakulu detekují lineární zrychlení díky otolitům, zatímco kristy umožňují vnímat rotační zrychlení způsobující proudění endolymfy v polokruhovitých kanálcích. Převzato a upraveno z (Hawkins 2017).

V utrikulu a sakulu se nacházejí senzorické orgány zvané makuly (*maculae staticae*). Stereocilie a kinocilie vláskových buněk makul jsou zanořeny do otolitické membrány, nad kterou leží krystalky uhličitanu vápenatého tzv. otolity (Obrázek 5)(Králíček 2004, Čihák 2016). Tyto dvě makuly spolu svírají téměř pravý úhel - vláskové buňky v sakulu leží v ose lidského těla a detekují změny v horizontální poloze, zatímco na něj kolmý utrikulus zpracovává informace o vertikální poloze. Při pohybu dochází vlivem gravitace k přesunu otolitů, což způsobuje ohyb stereocilií na vláskových buňkách. Mechanotransdukce rovnovážných vláskových buněk poté probíhá podobně jako v Cortiho orgánu. Obě makuly jsou uprostřed rozděleny striolou. V utrikulu jsou vláskové buňky orientovány kinociliem ke striole, ale

v sakulu jsou orientovány směrem opačným, tzn. kinocilium směřuje od strioly. Toto složité rozmístění vláskových buněk v makulách pomáhá přesně lokalizovat pozici hlavy k tělu.

Tři polokruhovité kanálky (anteriorní, posteriorní a laterální; *ductus semicircularis anterior, posterior et lateralis*) leží v na sobě kolmých rovinách a každý kanálek je ukončen rozšířením zvaném ampula (*ampulla membranacea*) obsahující kristu (*crista ampullaris*), což je senzorický orgán pro detekci úhlového zrychlení. Nad vláskovými buňkami krist leží gelovitá kupula (*cupula ampullaris*) bohatá zejména na glykoproteiny. Při otáčení hlavy nebo celého těla dochází k pohybu endolymfy v polokruhovitých kanálcích a k následnému vychýlení kupuly ze své osy, což spouští proces mechanotransdukce popsaný výše. V kristách jsou vláskové buňky na rozdíl od makul orientovány pouze jedním směrem.

Vestibulární vláskové buňky jsou inervovány aferentními vlákny vestibulárního neboli Scarpova ganglia, jenž se nachází mimo kostěný labyrint ve vnitřním zvukovodu (*meatus acusticus internus*)(Khan a Chang 2013). Vestibulární ganglium obsahuje bipolární neurony a je rozděleno na dvě části – superiorní vestibulární ganglium s nervovými zakončeními v utrikulu, anteriorní a laterální kristě a inferiorní vestibulární ganglium inervující posteriorní kristu a sakulus. Vestibulární vlákna odchází z vnitřního ucha vnitřním zvukovodem společně se sluchovými vlákny jako sluchově rovnovážný nerv neboli VIII. hlavový nerv. Většina vláken míří do vestibulárních jader umístěných v mozkovém kmeni a některá končí v mozečku (Králíček 2004).

2.3 Embryonální a postnatální vývoj vnitřního ucha

Lidské vnitřní ucho je strukturou i vývojem velmi podobné myšímu sluchově rovnovážnému orgánu. Z tohoto důvodu se pro studium vnitřního ucha často využívá myší model. Výhodami myšího modelu jsou krátký životní cyklus, početnost potomstva, nenáročnost chovu a v neposlední řadě velká genetická homologie s člověkem (DeBry a Seldin 1996). Avšak mezi lidskou a myší kochleou existují určité rozdíly (Robles a Ruggero 2001). Lidská kochlea je dlouhá 3,5 centimetru a je stočena do dvou a půl otáčky, zatímco myší sluchové ústrojí má jednu a tři čtvrtě otáčky o délce 7 milimetrů. Lidské ucho detekuje zvuky o frekvenci 20-20 000 Hz na rozdíl od myši, která je schopna rozpoznat zvuky o frekvenci 1 – 100 000 Hz. Pro studium funkce transkripčních faktorů exprimovaných ve vnitřním uchu byl v této disertační práci využit myší model, a proto budou následující kapitoly zaměřeny na vývoj vnitřního ucha u myši.

U myši domácí (*mus musculus*) začíná vývoj vnitřního ucha přibližně osmý den embryonálního vývoje (E8), kdy poblíž vyvíjejícího se zadního mozku vzniká z přilehlého ektodermu ušní ploténka neboli otická plakoda (Obrázek 6)(Torres a Giraldez 1998). Vchlipováním plakody vzniká otická jamka a po jejím uzavření poté otický váček ve věku E10,5. Otický váček neboli otocysta je dutina ve tvaru hrušky, ze které se až na výjimky (Sandell, Butler Tjaden *et al.* 2014) tvoří všechny buňky vnitřního ucha (Magarinos, Contreras *et al.* 2012, Xu, Ueno *et al.* 2017). Do otocysty také migrují buňky z neurální lišty, ze kterých se následně diferencují některé neurony a gliové buňky kochleovestibulárního nervu i vláskové a podpůrné buňky kochley a makul (Freyer, Aggarwal *et al.* 2011). Od E9,5 se z otické jamky a následně otocysty oddělují prekurzory sluchově rovnovážného (statoakustického) ganglia procesem delaminace. Neurony vnitřního ucha se tak diferencují mnohem dříve než senzorický epitel, jehož diferenciace z buněk otocysty začíná přibližně od E12 (Torres a Giraldez 1998).

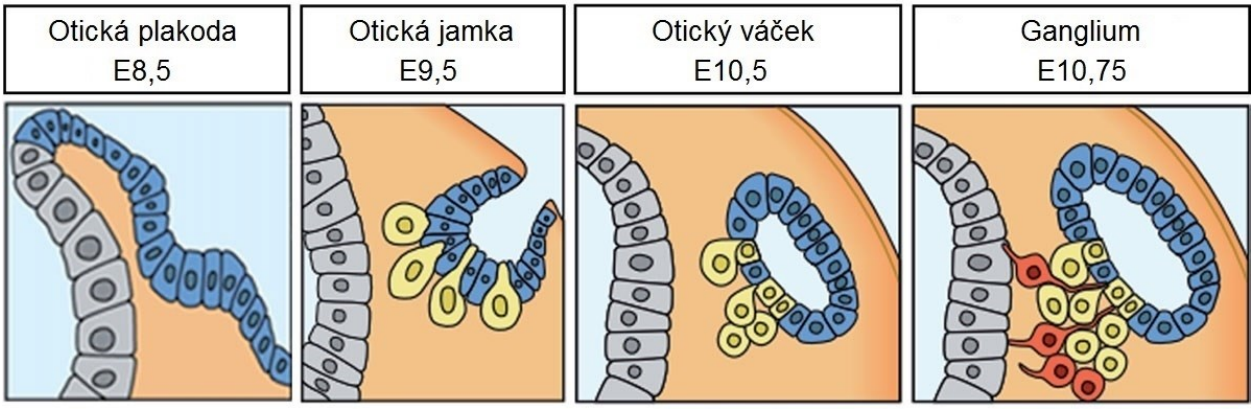

Obrázek 6: Raný vývoj vnitřního ucha na myším modelu. Z ektodermu vzniká vchlipováním otická jamka, jejímž uzavřením se vytvoří otický váček, který obsahuje prekurzorové buňky vnitřního ucha (modře). Z otického váčku delaminují neuroblasty (žlutě), které diferencují na sluchově rovnovážné neurony (červeně). Převzato a upraveno z (Magarinos, Contreras *et al.* 2012).

Myší otocysta prochází četnými morfologickými změnami, které vedou k vytvoření šesti senzorických orgánů sluchu a rovnováhy (Obrázek 7)(Morsli, Choo *et al.* 1998). V E11,5 se z ventrální strany otického váčku začíná tvarovat kochleární trubice a současně se dorsolaterálně rozšiřuje primordium anteriorního a posteriorního polokruhovitého kanálku vestibulárního systému. Ve věku E12 se začínají formovat polokruhovité kanálky, které vznikají resorpcí okolní tkáně. V tomto věku se vytváří první otáčka kochley a utrikulus je již také rozeznatelný. O den později (E13) jsou kanálky zcela oddělené, ventrálně od utrikulu se objevuje sakulus a kochlea má vyvinutou jednu polovinu první otáčky. V dalším vývoji orgány vnitřního ucha

rostou a dostávají svou konečnou podobu. Kristy polokruhovitých kanálků se formují a kochlea se dále prodlužuje – v E15 má jednu a půl otáčky a v E17 dosáhne své konečné jedné a tři čtvrtě otáčky.

Po narození dochází hlavně k maturaci buněk vnitřního ucha a dokončování růstu všech jeho orgánů (Mikaelian a Ruben 1965). V kochlee se prodlužují vláskové buňky a vytváří se Cortiho tunel mezi vnitřními a vnějšími senzorickými buňkami. V postnatálním dni 8 (P8) jsou vláskové a podpůrné buňky srovnatelné se senzorickým epitelem dospělé myši. Spirální ganglium se vyvíjí o něco déle a neurony maturují až do věku P10, kdy myši začínají slyšet.

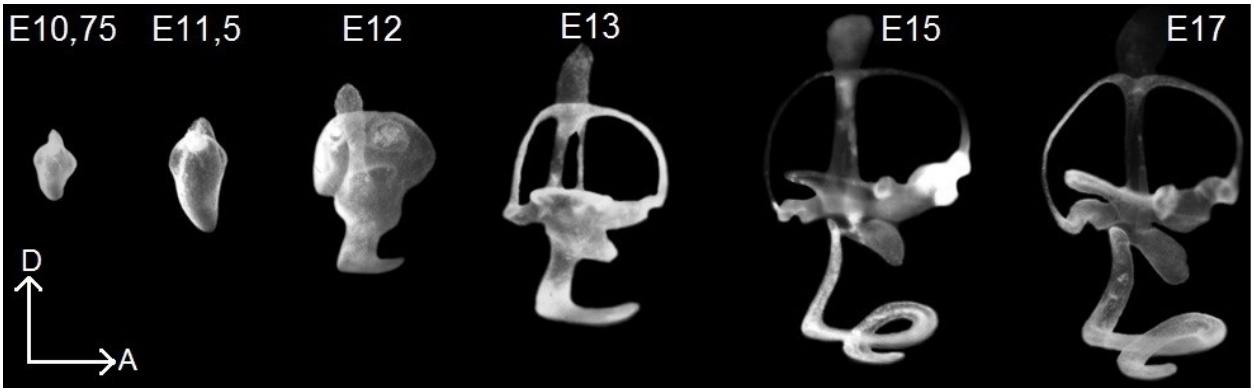

Obrázek 7: Morfologické změny během embryonálního vývoje myšího vnitřního ucha. Z jednoduchého útvaru myší otocysty se postupně vytváří šest orgánů vnitřního ucha (A – anteriorně; D – dorsálně). Převzato a upraveno z (Morsli, Choo *et al.* 1998).

2.4 Molekulární regulace vývoje vnitřního ucha

Vývoj lidského i myšího vnitřního ucha je řízen regulační sítí transkripčních faktorů a protenů signálních drah, jejichž přesná časová a prostorová exprese je klíčová pro specifikaci, proliferaci a diferenciaci všech buněk vnitřního ucha.

Pro indukci formování otocysty jsou klíčové difúzní signální proteiny exprimované v okolních buňkách i ve vznikající ušní plakodě. V blízkém mesodermu a neuroektodermu jsou exprimovány fibroblastové růstové faktory (FGF); ve struně hřbetní (notochordu) je exprimován morfogen „Sonic hedgehog protein" (SHH); proteiny signalizační dráhy „Wingless/Integrated" (WNT) difundují ze zadního mozku a kostní morfogenetický faktor 4 (BMP4) je uvolňován z neuroektodermu i z prekurzorů otické plakody (Fritzsch, Beisel *et al.* 2006). Kombinace výše zmíněných proteinů vede ke specifikaci buněk ektodermu na prekurzory vnitřního ucha v otické plakodě a k začátku formování otického váčku. Důležitost těchto proteinů byla prokázána na myších či kuřecích modelech s částečnou či úplnou delecí genů kódujících tyto proteiny.

Fibroblastové růstové faktory jsou exprimovány v neuroektodermu zadního mozku (FGF3 a 10) a blízké mesenchymální tkáni (FGF10)(Alvarez, Alonso *et al.* 2003). Role FGF3 a FGF10 během formování otocysty jsou do značné míry zastupitelné, neboť delece pouze jednoho z faktorů se na fenotypu neprojeví, avšak současná delece *Fgf3* a *Fgf10* u myšího modelu má za následek vznik velmi malé či dokonce žádné otocysty.

Nejranější exprese morfogenu SHH byla ukázána na myším embryu ve věku E10,5 v notochordu sousedícím s ventrální částí otocysty (Liu, Li *et al.* 2002). Tento protein hraje důležitou roli ve specifikaci neuronů vnitřního ucha, formování kochley a chrupavkového obalu vnitřního ucha, který se postnatálně mění na kostěný labyrint. Naopak ligandy signalizační dráhy WNT můžeme nalézt již v E8,5 v zadním mozku, který se nalézá v těsné blízkosti dorsální části ušní plakody (Riccomagno, Takada *et al.* 2005). Tato signalizační kaskáda reguluje expresi BMP4 a vývoj krist. Z ventrální části otocysty se vyvíjí kochlea, což je řízeno morfogenem SHH, zatímco dorsální část otického váčku dává vzniknout vestibulárnímu systému a na tomto procesu se podílí zejména proteiny WNT1/3 a BMP4 (Basch, Brown *et al.* 2016).

U myši je BMP4 exprimován od E9 a je přítomný v epitelu vnitřního ucha až do P1 (Blauwkamp, Beyer *et al.* 2007, Chang, Lin *et al.* 2008). Výsledky studií ukazují na významnou roli BMP4 ve specifikaci senzorických i nesenzorických buněk. Delece genu *Bmp4* má u myši za následek malformaci polokruhovitých kanálků, deformaci Cortiho orgánu a úbytek vláskových a podpůrných buněk. Tyto změny se poté negativně promítají do sluchových a rovnovážných funkcí vnitřního ucha. Studie *in vitro* potvrdila důležitost BMP4 pro přežívání postnatálních neuronů spirálního ganglia a růst neuritů (Waqas, Sun *et al.* 2017).

Známými ranými transkripčními faktory exprimovanými v myší otocystě jsou: „Trans-acting T-cell-specific transcription factor GATA-3“ (GATA3); „T-box transcription factor TBX1“ (TBX1); „Paired box protein Pax-2/8“ (PAX2 a PAX8); „Homeobox protein DLX-5“ (DLX5); „Forkhead box protein G1“ (FOXG1); „Eyes absent homolog 1“ (EYA1); „Homeobox protein SIX1“ (SIX1) a „Octamer-binding protein 4“ (OCT4)(Fritzsch, Beisel *et al.* 2006). Funkce zmíněných transkripčních faktorů jsou různorodé a jejich exprese se různě prolínají. To naznačuje složitou síť interagujících transkripčních faktorů podílejících se na proliferaci, specifikaci a diferenciaci buněk vnitřního ucha. GATA3 je exprimován již od E8 až do postnatálního období v různých částech vnitřního ucha (Lawoko-Kerali, Rivolta *et al.* 2002). Je důležitý pro vývoj spirálního ganglia, vznik polokruhovitých kanálků a struktury kochley a

diferenciaci vláskových buněk (Appler, Lu *et al.* 2013, Duncan a Fritzsch 2013, Luo, Deng *et al.* 2013). TBX1 je aktivní v posterolaterální části otocysty, kde reguluje vývoj epitelu, a naopak inhibuje neurální vývoj (Raft, Nowotschin *et al.* 2004). Dále se také podílí na morfogenezi vnitřního ucha. Transkripční faktor PAX2 hraje důležitou roli ve vývoji senzorického epitelu i inervace kochley a sakulu ve ventrální části otocysty (Burton, Cole *et al.* 2004), zatímco DLX5 je spojován s vývojem dorsálních vestibulárních struktur (Merlo, Paleari *et al.* 2002). Delece genu *Foxg1* v myším modelu je zodpovědná za zkrácení kochley a ztrátu kanálků i krist (Pauley, Lai *et al.* 2006, Hwang, Simeone *et al.* 2009). Také inervace sluchového a vestibulárního systému je u těchto mutantů poškozena. Transkripční faktory EYA1 a SIX1 tvoří heterodimer vázající se na zesilovač genu *Atoh1* („Protein atonal homolog 1“), což je první diferenciační marker vláskových buněk (Ahmed, Wong *et al.* 2012). OCT4 reguluje expresi *Neurogeninu-1* (*Neurog1*)(Fritzsch, Beisel *et al.* 2006), který je ve vnitřním uchu detekovatelný od E8,75. Protein NEUROG1 je nezbytný pro vývoj statoakustického ganglia a jeho delece vede k úplné ztrátě senzorických neuronů (Ma, Anderson *et al.* 2000, Matei, Pauley *et al.* 2005). Jeho hlavní funkcí je regulace delaminace neuroblastů z otocysty a aktivace Neurogenního diferenciačního faktoru 1 (NEUROD1). Ztráta NEUROG1 má negativní vliv i na regulaci diferenciace vláskových buněk, kterých je méně u myší s mutací v genu *Neurog1* ve srovnání s kontrolami.

Otocysta obsahuje buňky, které proliferují a následně diferencují v senzorické neurony, vláskové a podpůrné buňky. Na základě expresních studií se předpokládá, že z buněk otocysty vznikají tři prekurzorové linie (Fritzsch, Beisel *et al.* 2006). Neurální prekurzory dávají vzniknout pouze neuronům sluchově rovnovážného ganglia, ze senzorických prekurzorů se vyvíjí vláskové a podpůrné buňky a z neurosenzorických prekurzorů se diferencují senzorické buňky i neurony (Obrázek 8). Společným rysem všech prekurzorových linií je exprese transkripčního faktoru „Insulin gene enhancer protein ISL-1“ (ISL1)(Radde-Gallwitz, Pan *et al.* 2004).

Neurální prekurzory jsou charakteristické zejména expresí výše zmíněných transkripčních faktorů NEUROG1 a NEUROD1 (Liu, Pereira *et al.* 2000, Ma, Anderson *et al.* 2000). U myší se nejprve začíná vyvíjet vestibulární ganglium, jehož neurony se stávají postmitotickými mezi E9,5 a E12,5 (Ruben 1967). Od E10,5 ukončují buněčný cyklus i senzorické neurony spirálního ganglia v bázi kochley a neurony v apexu přestávají proliferovat ve věku E15,5.

Vývoj ganglií je zpočátku nezávislý na senzorickém epitelu, který se začíná formovat o několik dní později.

Na specifikaci senzorických prekurzorů se podílí především transkripční faktory ISL1 a „Transcription factor SOX-2“ (SOX2)(Radde-Gallwitz, Pan *et al.* 2004, Kiernan, Pelling *et al.* 2005). Terminální mitóza senzorických prekurzorů tří krist a obou makul začíná přibližně dvanáctý den embryonálního vývoje (Ruben 1967). Většina epitelových buněk vestibulárního systému ukončuje buněčné dělení ve věku E16, nicméně některé buňky rovnovážného ústrojí proliferují až do P6. Protein zodpovědný za terminaci mitózy ve vestibulárním systému nebyl doposud identifikován na rozdíl od ústrojí sluchového.

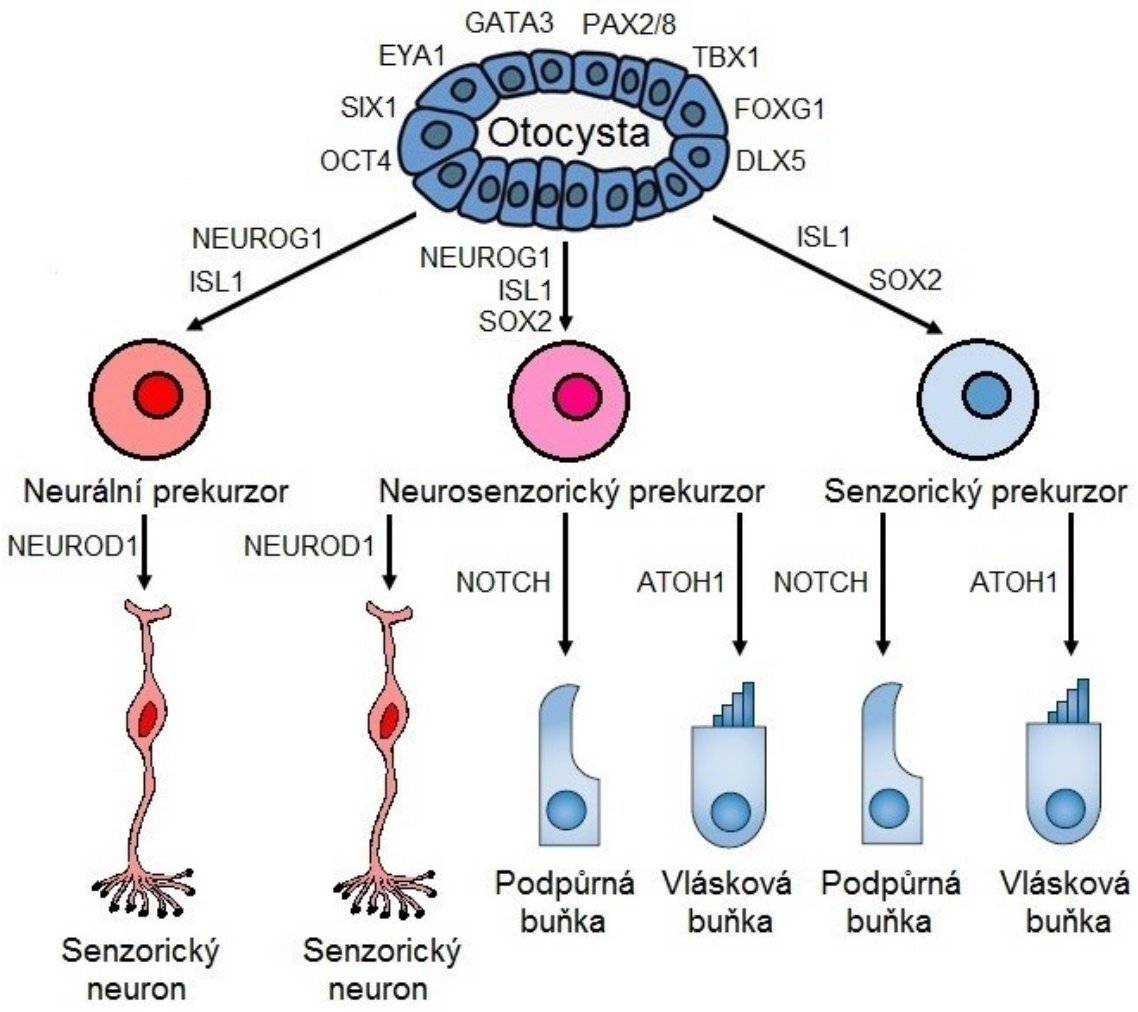

Obrázek 8: Zjednodušené schéma exprese transkripčních faktorů řídící specifikaci a diferenciaci buněk vnitřního ucha. Z otocysty vznikají tři prekurzorové linie, z nichž se vyvíjí senzorické neurony, podpůrné a vláskové buňky. Specifikace a diferenciace buněk je regulována rozmanitou sítí transkripčních faktorů. Převzato a upraveno z (Fritzsch, Beisel *et al.* 2006, Kelley 2006, Magarinos, Contreras *et al.* 2012).

Proliferace v kochlee je negativně regulována inhibitorem cyklin dependentní kinázy 1B (CDKN1B, dříve označovaný jako $p27^{kip1}$)(Chen a Segil 1999). Buněčné dělení v senzorickém epitelu kochley končí v apexu v E12,5 a v bázi o dva dny později (Ruben 1967). Naopak diferenciace epitelových prekurzorů na vláskové buňky začíná nedaleko báze přibližně v E13,5 a pokračuje směrem k apexu (Basch, Brown *et al.* 2016). Jinými slovy buňky v apexu, které jako první ukončily buněčný cyklus, se diferencují nejpozději, zatímco buňky v bázi diferencují krátce po ukončení proliferace. To znamená, že směr ukončení buněčného cyklu a diferenciace je ve sluchovém orgánu opačný. Existuje teorie, že pro aktivaci diferenciace vláskových a podpůrných buněk jsou nutné signální proteiny maturovaných sluchových neuronů (Ruben 1967).

Laterální inhibice iniciovaná signální dráhou Notch je zodpovědná za vysoce organizovanou strukturu senzorického epitelu, kde spolu vláskové buňky nesousedí, nýbrž každá vlásková buňka je obklopena buňkami podpůrnými. Po ukončení proliferace začínají prekurzory vláskových buněk exprimovat ligandy „Protein jagged-2“ (JAG2) a „Delta-like protein 1“ (DLL1), které se váží na receptor „Neurogenic locus notch homolog protein 1„ (NOTCH1) na membránách okolních buněk (Lanford, Lan *et al.* 1999). Tato vazba spouští v cílové buňce signalizační kaskádu, která zabraňuje diferenciaci na vláskovou buňku. Pokud signalizační proteiny JAG2 a DLL1 ve vnitřním uchu chybí, dochází k redukci podpůrných buněk a ke zmnožení buněk vláskových, které jsou organizovány neuspořádaně a jejichž stereocilie jsou orientované různými směry (Kiernan, Cordes *et al.* 2005).

Z daného výčtu vyplývá, že se na regulaci proliferace, specifikace a diferenciace buněk vnitřního ucha podílí velké množství signalizačních proteinů a transkripčních faktorů. Následující kapitoly budou zaměřeny na několik vybraných transkripčních faktorů, které byly předmětem výzkumu tohoto projektu.

2.4.1 PAX2

Transkripční faktor PAX2 („Paired box protein 2“) patří do početné rodiny PAX proteinů (UniProt 2019). Tento transkripční faktor je důležitý pro vývoj centrální nervové soustavy, ledvin, oka i optického nervu a vnitřního ucha (Torres, Gomez-Pardo *et al.* 1996, Ohyama a Groves 2004).

Exprese PAX2 ve vnitřním uchu je pravděpodobně aktivována morfogenem SHH (Liu, Li *et al.* 2002). PAX2 je považován za jeden z nejranějších faktorů důležitých pro indukci otické

plakody. Tento protein je detekovatelný ve ventrální části otocysty, ze které vzniká kochlea a sakulus (Torres, Gomez-Pardo *et al.* 1996). Důsledkem úplné delece genu *Pax2* je nevyvinutá kochlea, jenž zůstává ve tvaru koule a neobsahuje Cortiho orgán, protože ztráta tohoto genu vede k masivní apoptóze prekurzorových epitelových buněk v kochlee (Burton, Cole *et al.* 2004). U myší neexprimující PAX2 je sakulus často menší a deformovaný, ale utrikulus a polokruhovité kanálky s kristami se vyvíjí podobně jako u kontrolních jedinců. Spirální ganglium u mutantů také chybí, což je zapříčiněno nedostatkem neurotrofinů produkovaných vláskovými buňkami. Nicméně existují další studie, které ukazují expresi tohoto transkripčního faktoru ve všech senzorických oblastech vnitřního ucha a nejenom v kochlee a sakulu (Lawoko-Kerali, Rivolta *et al.* 2002, Liu, Wang *et al.* 2018). Z jakého důvodu má delece *Pax2* vliv pouze na vývoj kochley a sakulu, nebylo dokázáno, ale předpokládá se, že PAX2 je omezeně zastupitelný PAX8 ve vývoji vnitřního ucha (Bouchard, de Caprona *et al.* 2010).

2.4.2 ISL1

ISL1 („Insulin gene enhancer protein ISL-1“) je protein z rodiny LIM – homeodoménových transkripčních faktorů (UniProt 2019). Označení pro doménu LIM je zkratka utvořená z prvních písmen proteinů obsahující tuto sekvenci (**L**IN11 – **I**SL1 - **M**EC-3)(Hobert a Westphal 2000). Proteinová doména LIM je složená ze dvou motivů zinkových prstů a zodpovědná za protein – proteinové interakce. Homeodoména obsahující tři helixy zprostředkovává vazbu na regulační oblasti DNA. Expresní profil ISL1 ukazuje důležitost tohoto proteinu během vývoje srdce, slinivky, motorických neuronů centrální i periferní nervové soustavy, endodermu trávící soustavy a vnitřního ucha (Zhuang, Zhang *et al.* 2013). Delece obou alel genu *Isl1* v myším modelu vede k abnormálnímu vývoji srdce a k letalitě v brzkém embryonálním věku (E10,5), protože nedochází k srdeční segmentaci (Cai, Liang *et al.* 2003).

ISL1 je ve vnitřním uchu exprimován v otické plakodě v E8,5 (Huang, Sage *et al.* 2008). Exprese ISL1 byla detekována ve vznikajícím kochleovestibulárním gangliu a v otocystě, kde se jeho exprese částečně prolíná s PAX2 (Radde-Gallwitz, Pan *et al.* 2004). V senzorických neuronech můžeme ISL1 najít až do P6, avšak v epitelu po diferenciaci vláskových buněk ISL1 zůstává exprimován pouze v podpůrných buňkách. ISL1 tedy specifikuje neurální i senzorické prekurzory vnitřního ucha.

Jelikož úplná delece genu *Isl1* je letální v brzkém embryonálním věku, kdy otický váček teprve vzniká, je nutné přistoupit k dalším metodám a myším modelům pro objasnění funkce

ISL1 během vývoje vnitřního ucha. Jednou z možností je tkáňově specifická delece genu *Isl1* nebo naopak jeho ektopická exprese. Zvýšená exprese ISL1 v diferencovaných vláskových buňkách kochley vede k ochraně vláskových buněk před hlukem (Huang, Kantardzhieva *et al.* 2013). Tento protektivní efekt může být způsoben inhibicí nádor nekrotizujícího faktoru α (TNFα) a jím spouštěné zánětlivé dráhy. Vláskové buňky jsou také odolnější vůči stárnutí v důsledku nadprodukce ISL1. Toto je zatím jediný popsaný myší model pro studium funkce ISL1 ve vývoji vnitřního ucha a zaměřuje se pouze na vliv tohoto transkripčního faktoru na plně maturované vláskové buňky. Přesná role ISL1 na specifikaci a diferenciaci vláskových buněk nebyla zatím plně objasněna.

2.4.3 SOX2

SOX2 („Transcription factor SOX-2“) patří do proteinové rodiny vysoké mobility v elektroforetickém poli („High mobility group“, HMG), které jsou schopny se vázat na DNA (UniProt 2019). SOX2 je důležitý pro kmenové buňky a pluripotenci, ale jeho zvýšená aktivita vede k rakovinotvornému bujení (Liu, Lin *et al.* 2013).

Prvotní experimenty zaměřené na objasnění funkce SOX2 ve vývoji vnitřního ucha byly provedeny na myších modelech, jejichž gen *Sox2* byl pozměněn insercí vektoru (pAA2) či pomocí radioaktivního záření (Kiernan, Pelling *et al.* 2005). Tyto experimentální modely ukázaly, že transkripční faktor SOX2 je nezbytný pro vytvoření senzorické oblasti epitelu, neboť pokud není exprimován, nediferencují se vláskové ani podpůrné buňky. Dále je nepostradatelný pro tvorbu polokruhovitých kanálků a prodlužování kochley. Tyto závěry byly dále potvrzeny i v dalších studiích, kde byla prokázána exprese SOX2 v senzorických epitelových prekurzorech (Liu, Wang *et al.* 2018). Pro diferenciaci vláskových buněk je však důležitá následná inhibice exprese SOX2 a naopak pro podpůrné buňky je exprese SOX2 nezbytná (Dabdoub, Puligilla *et al.* 2008). SOX2 se přímo váže na zesilovač genu *Atoh1* a tím spouští diferenciaci vláskových buněk. Zároveň SOX2 působí i jako inhibitor *Atoh1* v podpůrných buňkách, kde reguluje expresi genu *Prox1* („Prospero homeobox protein 1“). Přesná úloha SOX2 bude nejspíše záležet na míře jeho exprese v dané tkáni a také na vazebných partnerech (Kempfle, Turban *et al.* 2016, Puligilla a Kelley 2017). Exprese genu *Sox2* v senzorických prekurzorech je spuštěna aktivací signalizační dráhy Notch navázáním ligandu JAG1 na receptor NOTCH1 (Kiernan, Xu *et al.* 2006).

Transkripční faktor SOX2 je exprimován také během vývoje bipolárních neuronů statoakustického ganglia. Nejprve je exprimován během procesu delaminace neuroblastů (E9,5 a 10,5), následně je jeho exprese utlumena v diferencujících se neuronech, což je charakterizováno expresí NEUROG1 a NEUROD1 (Nishimura, Noda *et al.* 2017). SOX2 je v senzorických neuronech vnitřního ucha opět detekovatelný krátce po narození, jeho exprese klesá v druhém postnatálním týdnu a v dospělosti jeho přítomnost ve vnitřním uchu nebyla prokázána. Na základě experimentů ukazující vznik neuronů z epitelových buněk po *Sox2*-transfekci bylo předpokládáno, že SOX2 je nezbytný pro formování neuronů vnitřního ucha (Puligilla, Dabdoub *et al.* 2010). Další experimenty ukázaly, že delece *Sox2* pomocí inducibilní rekombinázy Sox2-CreRT2 vede ke snížení exprese NEUROG1 a NEUROD1, zastavení migrace neuroblastů z otického váčku a ke vzniku zmenšeného kochleovestibulárního ganglia, jehož prekurzory podléhají apoptóze (Steevens, Sookiasian *et al.* 2017). Poslední experimenty pomocí tkáňově specifické delece *Sox2* (myší model *Foxg1-Cre; Sox2*$^{f/f}$) nicméně ukázaly, že specifikace a diferenciace vestibulárních neuronů probíhá v nepřítomnosti SOX2, ale vývoj neuronů spirálního ganglia kriticky závisí na přítomnosti SOX2 (Dvorakova, Macova *et al.* 2019).

2.4.4 NEUROD1

NEUROD1 („Neurogenic differentiation factor 1“) je transkripční faktor obsahující motiv α-šroubovice-smyčka-α-šroubovice a patří do tzv. „basic helix-loop-helix“ (bHLH) skupiny proteinů (UniProt 2019). Jeho funkce je nezbytná pro vývoj Langerhansových ostrůvků pankreatu a mutantní myši postrádající NEUROD1 umírají do 5 dnů po narození v důsledku hyperglykémie a ketonurie, což jsou jedny z hlavních příznaků *diabetes mellitus* (Naya, Huang *et al.* 1997). Neméně důležitou úlohu hraje NEUROD1 během vývoje neuronů nervové soustavy. Jeho exprese byla ukázána v mozkové kůře, hipokampu, limbickém systému a v granulárních buňkách mozečku (Miyata, Maeda *et al.* 1999, Cho a Tsai 2004).

Ve vnitřním uchu byl protein NEUROD1 detekován již ve věku E8,75 v proliferujících a migrujících neuroblastech (Liu, Pereira *et al.* 2000). V těchto neurálních prekurzorech je NEUROD1 exprimován dříve než ISL1, ale jeho exprese klesá s ukončením buněčného cyklu a v maturovaných neuronech již není detekovatelný (Deng, Yang *et al.* 2014). NEUROD1 je exprimován v senzorickém epitelu otocysty a poté ve věku, kdy se začínají diferencovat vláskové buňky (E13,5 v rovnovážném ústrojí a E15,5 v kochlee)(Kim, Fritzsch *et al.* 2001).

Výsledky fyziologických sluchových testů ukázaly, že mutanti s delecí *Neurod1* trpí nedoslýchavostí v důsledku ztráty 95 % neuronů spirálního ganglia (Liu, Pereira *et al.* 2000, Kim, Fritzsch *et al.* 2001). Tyto myši jsou také hyperaktivní a běhají v kruzích. NEUROD1 je totiž důležitý i pro vývoj vestibulárního ganglia a po jeho deleci byl počet rovnovážných neuronů redukován na 15 % oproti kontrolám. Ztráta sluchu a rovnovážných funkcí je nejen důsledkem ztráty neuronů ve spirálním a vestibulárním gangliu, ale je to také výsledek delece *Neurod1* v mozku (kochleární jádro a mozeček)(Miyata, Maeda *et al.* 1999, Pan, Jahan *et al.* 2009). Vzhledem ke sníženému množství sluchově rovnovážných neuronů byla redukována i nervová vlákna inervující senzorický epitel. U myší s delecí genu *Neurod1* byla prokázána výrazně nižší exprese neurotrofinových tyrosinkinázových receptorů v neurálních prekurzorech, zatímco hladina neurotrofinů produkovaných epitelem byla srovnatelná u kontrol a mutantů. To naznačuje, že NEUROD1 se přímo či nepřímo podílí na regulaci exprese neurotrofinových receptorů. Nedostatečná aktivace neurotrofinové signalizační kaskády má za následek buněčnou smrt neuronů.

Úplná delece *Neurod1* způsobuje také změny v morfologii vnitřního ucha (Liu, Pereira *et al.* 2000, Kim, Fritzsch *et al.* 2001). Kochlea je kratší a širší, zatímco vestibulární systém zůstává zachován. Zkrácení kochley má za následek zmnožení řad vnějších vláskových buněk a narušení orientace stereocilií v apexu.

Další experimenty byly provedeny na myších modelech s tkáňově specifickou delecí *Neurod1* pouze v buňkách exprimujících PAX2 (*Pax2-Cre; Neurod1*$^{f/f}$)(Jahan, Kersigo *et al.* 2010). Tito jedinci mají ve vnitřním uchu defekty popsané výše – redukovaná inervace a snížený počet neuronů v gangliích vnitřního ucha, které umírají apoptózou. Vestibulární i spirální ganglium je u mutanttů umístěno odlišně než u kontrol a obě ganglia inervují všechny orgány vnitřního ucha. NEUROD1 se totiž nejspíše podílí na segregaci sluchových a rovnovážných neuronů. NEUROD1 zůstává exprimován pouze ve vestibulárních nervových buňkách, zatímco jeho exprese mizí v neuronech spirálního ganglia, kde je exprimován GATA3 (Lawoko-Kerali, Rivolta *et al.* 2004). Navíc u mutantů *Pax2-Cre; Neurod1*$^{f/f}$ vedou vlákna spirálních neuronů I. typu k více než jedné vnitřní vláskové buňce, což ukazuje na porušení tonotopie. Expresní profil neuronů ganglií ukázal, že delece *Neurod1* negativně ovlivňuje *Nhlh1* a *Nhlh2* („Helix-loop-helix protein“), zatímco exprese genu *Neurog1* je zvýšená (Seo, Lim *et al.* 2007). To potvrzuje

negativní zpětnou vazbu transkripčního faktoru NEUROD1 na expresi NEUROG1 (Jahan, Kersigo *et al.* 2010).

U myšího modelu *Pax2-Cre; Neurod1$^{f/f}$* byl také zkoumán vliv NEUROD1 na vývoj vláskových buněk (Jahan, Pan *et al.* 2010). Výsledky ukázaly, že NEUROD1 působí inhibičně na expresi genů důležitých pro diferenciaci vláskových buněk *Atoh1, Fgf8* a *Pou4f3* („POU domain, class 4, transcription factor 3“) a že v důsledku absence této inhibice chybí v kochlee diferenciační gradient vláskových buněk od báze k apexu. V nepřítomnosti NEUROD1 dochází také k diferenciaci ektopických vláskových a podpůrných buněk ve spirálním i vestibulárním gangliu.

Pozdější experimenty však ukázaly, že delece pomocí Pax2-Cre je ve vnitřním uchu neúplná a k deleci nedochází ve všech neurosenzorických buňkách vnitřního ucha (Pan, Jahan *et al.* 2011). Navíc PAX2 je aktivní i v mozku (Torres, Gomez-Pardo *et al.* 1996, Cai, Kardon *et al.* 2016), tudíž některé vlivy delece *Neurod1* na vývoj vnitřního ucha mohou být také ovlivněny delecí *Neurod1* v mozku. Pro úplné odhalení funkce transkripčního faktoru NEUROD1 během vývoje vnitřního ucha je tedy nutné získat nový model s delecí *Neurod1* pouze ve vnitřním uchu bez delece tohoto genu v centrálních částech sluchové a rovnovážné dráhy. Takový model by také pomohl odhalit sekundární vliv delece *Neurod1* ve vnitřním uchu na vývoj a funkci centrální sluchově rovnovážné dráhy.

2.4.5 ATOH1

ATOH1 („Protein atonal homolog 1“) dříve označovaný jako MATH1 patří stejně jako NEUROD1 do proteinové rodiny bHLH (UniProt 2019). Tento transkripční faktor je důležitý během vývoje centrální nervové soustavy (Ben-Arie, Bellen *et al.* 1997, Huang, Tupal *et al.* 2012), některých druhů kožních buněk (Van Keymeulen, Mascre *et al.* 2009) a exokrinních buněk tenkého střeva (Yang, Bermingham *et al.* 2001). Myši s úplnou delecí *Atoh1* umírají krátce po narození kvůli dýchacím problémům, které souvisí s nedokonalou formací respiračního komplexu v zadním mozku (Rose, Ren *et al.* 2009).

Protein ATOH1 je přítomný ve vestibulární ústrojí od E12,5 a v kochlee od E13,5 nedaleko báze v senzorických prekurzorech, které ukončily buněčné dělení (Chen, Johnson *et al.* 2002). Nejprve je exprese detekovatelná v celém senzorickém primordiu, ale následně (E15,5) je specifická pouze pro vláskové buňky. Na začátku vývoje je však přechodně přítomný i v prekurzorech podpůrných buněk (Woods, Montcouquiol *et al.* 2004, Driver, Sillers *et al.*

2013). Krátce po narození (P2) je ATOH1 exprimován ve vláskových buňkách rovnovážného ústrojí a ve vnitřních i vnějších vláskových buňkách kochley. Poté jeho exprese klesá a v dospělosti exprimován není (Hume, Bratt *et al.* 2007, Yang, Xie *et al.* 2010). Matei *et al*. odhalil jeho expresi také v obou gangliích vnitřního ucha (Matei, Pauley *et al.* 2005), kde jeho funkce ovšem zůstává neobjasněná.

Transkripční faktor ATOH1 je klíčový pro zahájení diferenciace vláskových buněk, zatímco podpůrné buňky se vyvíjí i bez jeho účasti (Bermingham, Hassan *et al.* 1999). Nedostatek ATOH1 vede k apoptóze prekurzorů vláskových buněk v rovnovážném i sluchovém ústrojí. V kochlee průběh buněčné smrti kopíruje časovou expresi ATOH1, tedy od báze k apexu (Chen, Johnson *et al.* 2002). Bez přítomnosti vláskových buněk dochází k následné ztrátě podpůrných buněk (Woods, Montcouquiol *et al.* 2004). Dalším důsledkem úplné delece *Atoh1* je transdiferenciace původně epitelových buněk sakulu a utrikulu na buňky nervové (Raft, Koundakjian *et al.* 2007).

Kompletní delece *Atoh1* má negativní vliv i na neurony vnitřního ucha (Fritzsch, Matei *et al.* 2005). Ačkoli se raně formující kochleovestibulární ganglium u myší postrádající *Atoh1* vyvíjí zprvu stejně jako u kontrol, v pozdějším embryonálním stádiu dochází k úbytku inervace všech orgánů vnitřního ucha. Ztráta inervace je pravděpodobně zapříčiněna nedostatkem neurotrofinů, zejména mozkového neurotrofního faktoru (BDNF), který je produkován vláskovými buňkami. Jeho hladina je u mutantů snížena, což vede k nedostatečné neurotrofinové podpoře neuronů a jejich následné buněčné smrti.

Protože úplná delece *Atoh1* je pro myši letální v P0, byly pro zkoumání vlivu ATOH1 v postnatálních stádiích připraveny myší modely s podmíněnou či zpožděnou delecí tohoto genu a s bodovou mutací v *Atoh1*. Myši s podmíněnou delecí *Atoh1* řízenou expresí Pax2-Cre *(Pax2-Cre; Atoh1$^{f/f}$)* přežívají tři týdny po narození (Pan, Jahan *et al.* 2011). Kochlea u tohoto mutanta dosahuje podobné délky jako u kontroly, avšak neobsahuje žádné vláskové buňky a podpůrné buňky tvoří nepravidelné „ostrůvky“. V důsledku nedostatečného zásobení neurotrofiny (BDNF a NTF-3; neurotrofin-3) ze senzorického epitelu podléhají neurony spirálního ganglia apoptóze. Superiorní vestibulární ganglium je redukované, zatímco inferiorní rovnovážné ganglium je u tohoto myšího modelu zvětšené. Tento nárůst je pravděpodobně zapříčiněn chybějící negativní zpětnou vazbou ATOH1 na expresi NEUROG1 a NEUROD1. Ztráta Cortiho orgánu má také nepříznivý vliv na formování basilární a tektoriální membrány, které jsou o polovinu

menší u mutantů *Pax2-Cre; Atoh1*$^{f/f}$. Zpožděná delece *Atoh1* (*Atoh1-Cre; Atoh1*$^{f/f}$) ukázala, že je tento transkripční faktor důležitý i pro správné formování stereocilií a pro polaritu vláskových buněk (Pan, Jahan *et al.* 2012). Na myším modelu s inducibilní delecí *Atoh1* bylo ukázáno, že v pozdějším embryonálním věku (E16,5) je ATOH1 důležitý pro přežití vláskových buněk pouze v apexu, ale polaritu stereocilí ovlivňuje v tomto věku ve všech orgánech vnitřního ucha (Chonko, Jahan *et al.* 2013). ATOH1 je nutný pro přežití vláskových buněk po dobu 72 hodin od počátku své exprese (Cai, Seymour *et al.* 2013). Bodová mutace způsobující záměnu metioninu za izoleucin na 200. aminokyselině snižuje aktivitu ATOH1. Hypomorfismus ATOH1 má za následek snížení počtu vláskových buněk a deformaci stereocilií vedoucích ke zhoršení sluchových funkcí (Sheykholeslami, Thimmappa *et al.* 2013). Funkce ATOH1 může být částečně nahrazena jiným bHLH proteinem - NEUROG1, který dokáže aktivovat expresi POU4F3 ale nikoli BARHL1 („BarH-like 1 homeobox protein), což jsou transkripční faktory nezbytné pro vláskové buňky. Tyto mutanti mají vláskové buňky, avšak trpí ztrátou sluchu, protože vláskové buňky mají nefunkční a neuspořádané stereocilie (Jahan, Pan *et al.* 2015).

Transfekce buněk vnitřního ucha expresním vektorem obsahující *Atoh1* vede k produkci ektopických vláskových buněk v blízkosti senzorického epitelu (Zheng a Gao 2000, Kawamoto, Ishimoto *et al.* 2003, Shou, Zheng *et al.* 2003, Yang, Cong *et al.* 2013) či aktivaci regenerace vláskových buněk, jenž nemají endogenní ATOH1 (Izumikawa, Minoda *et al.* 2005). Vnitřní hraniční a vnitřní falangeální buňky se po ektopické expresi ATOH1 dokáží transdiferencovat na vnitřní vláskové buňky a jeví se jako ideální cíl pro biologickou léčbu (Yang, Cong *et al.* 2013). Experimenty *ex vivo* a *in vivo* ukázaly, že při současné nadměrné expresi ATOH1 a ISL1 dochází k transdiferenciaci podpůrných buněk na buňky vláskové, což poukazuje na možnou spolupráci těchto dvou transkripčních faktorů při diferenciaci vláskových buněk (Yamashita, Zheng *et al.* 2018). Při těchto pokusech o regeneraci či diferenciaci však nejsou nově vzniklé vláskové buňky zcela vyvinuté a postrádají některé důležité funkční znaky a netvoří přesnou strukturu Cortiho orgánu. Často jsou také tyto experimenty prováděné na myší neonatální tkáni, která má ještě omezenou schopnost regenerace.

Na indukci exprese *Atoh1* se podílejí transkripční faktory SOX2, SIX1 a EYA1 (Ahmed, Wong *et al.* 2012). ATOH1 také reguluje svoji vlastní expresi positivní autoregulací (Raft, Koundakjian *et al.* 2007). Při překročení kritické hladiny se ATOH1 váže na vlastní promotor a

podporuje svou expresi. Exprese ATOH1 je ovlivňována také epigeneticky (Stojanova, Kwan *et al.* 2015). Metylace histonů v regulační sekvenci *Atoh1* vede k umlčování genu ve vláskových buňkách, zatímco acetylace způsobuje zvýšenou expresi tohoto genu (Stojanova, Kwan *et al.* 2015).

Exprese ATOH1 koreluje s expresí některých dalších proteinů důležitých pro vývoj vnitřního ucha – proteiny stereocilií myosin VI a VIIa, složky tektoriální membrány tektiny a transkripční regulátory JAG2, POU4F3, FGF8 (Yoon, Lee *et al.* 2011, Cai, Jen *et al.* 2015). ATOH1 přímo indukuje tvorbu dvou transkripčních faktorů nezbytných pro přežívání vláskových buněk - POU4F3 (Masuda, Pak *et al.* 2012) a BARHL1 (Chellappa, Li *et al.* 2008). Bez produkce POU4F3 dochází ke ztrátě vláskových buněk ve všech orgánech vnitřního ucha (Xiang, Gan *et al.* 1997) a BARHL1 je důležitý pro přežití sluchových vláskových buněk v postnatálních stádiích (Li, Price *et al.* 2002). ATOH1 se též podílí na zahájení exprese myosinu VIIa, což je jeden z prvotních znaků maturovaných vláskových buněk (Masuda, Pak *et al.* 2012).

Mezi ATOH1 a NEUROG1/NEUROD1 funguje negativní zpětná vazba (Jahan, Pan *et al.* 2010, Mulvaney a Dabdoub 2012, Galvez, Tena *et al.* 2017), ale proteiny bHLH spolu dokaží také tvořit heterodimery a ovlivňovat společně transkripci dalších genů či jsou vzájemně částečně zastupitelné (Jahan, Pan *et al.* 2015). Přesné vztahy mezi transkripčními proteiny bHLH ve vývoji vnitřího ucha však stále nejsou plně objasněné.

2.5 Sluchová dráha

Sluchová dráha je čtyřneuronová dráha přenášející informace z Cortiho orgánu vnitřního ucha do primární sluchové kůry (Obrázek 9)(Králíček 2004). Dendrity aferentních bipolárních neuronů spirálního ganglia tvoří „ribbon“ synapse s vláskovými buňkami Cortiho orgánu, kde je mediátorem přenosu glutamát (Nordang, Cestreicher *et al.* 2000). Sluchový nerv vede z vnitřního ucha do stejnostranného kochleárního jádra (*nucleus cochlearis*) nacházející se v mozkovém kmeni (Králíček 2004). Axony obou kochleárních jader se setkávají v interneuronovém svazku *lemniscus lateralis* a odtud dále pokračují do *colliculus inferior*. Z ventrálního kochleárního jádra mohou jít axony přímo do *colliculus inferior* či přes interneurony komplexu olivy superior. *Colliculus inferior* je část středního mozku, ze které sluchová dráha pokračuje do *corpus geniculatum mediale* v hrbolu mezimozkovém (*thalamus*). Konečným cílem je primární sluchová kůra (*cortex auditivus primus*) ve spánkovém laloku.

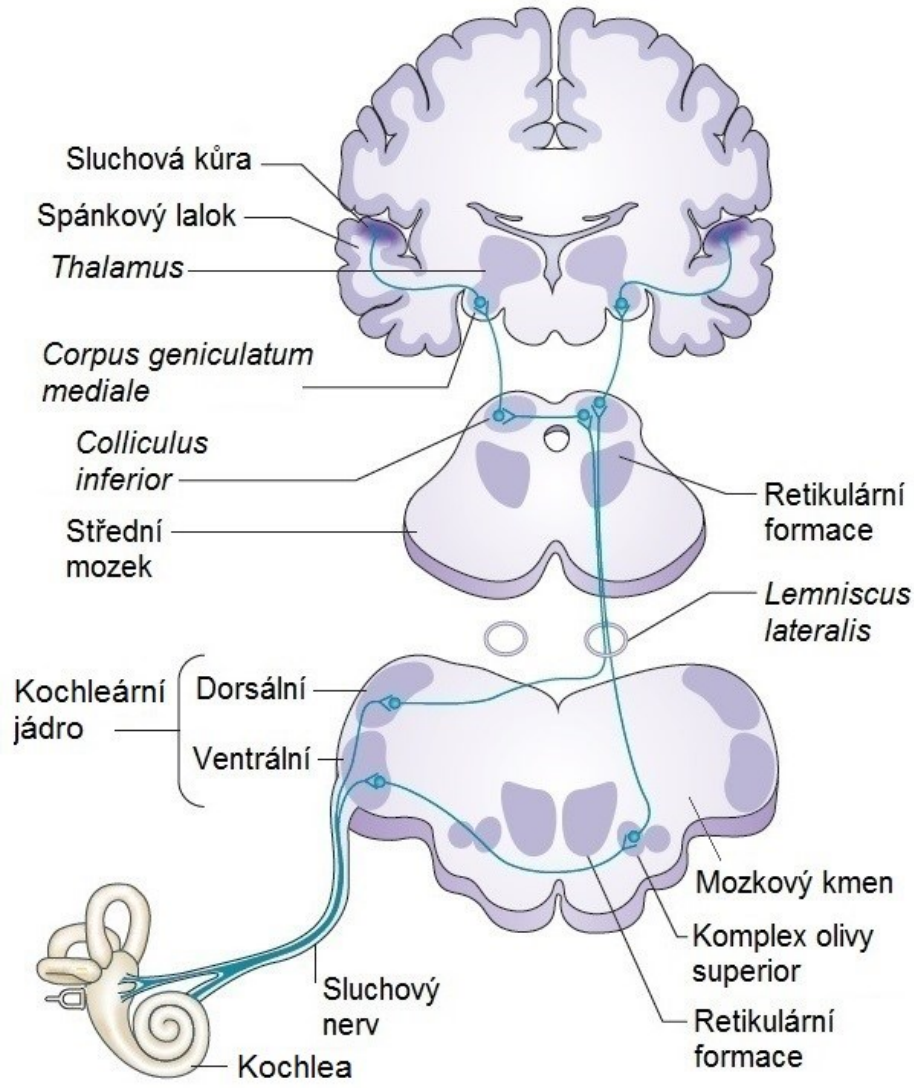

Obrázek 9: Vzestupná sluchová dráha. Aferentní sluchová dráha je čtyřneuronová – spirální ganglium, kochleární jádro, *colliculus inferior* a *corpus geniculatum mediale*. Součástí dráhy jsou i dvě interneuronová jádra – komplex olivy superior a *lemniscus lateralis*. Převzato a upraveno z (Javitt a Sweet 2015).

2.5.1 Kochleární jádro (*Nucleus cochlearis*)

Kochleární jádra obsahují druhé neurony sluchové dráhy a přijímají informace od axonů neuronů spirálního ganglia (první neurony sluchové dráhy)(Králíček 2004). Synapse mezi sluchovým nervem a kochleárním jádrem jsou glutamátové. Rozeznáváme dorsální (DCN) a ventrální kochleární jádro (VCN). Obě jádra zachovávají tonotopické uspořádání (Obrázek 10)(Muniak, Rivas *et al.* 2013). Vlákna přicházející z kochleární báze směřují do dorsálních části kochleárních jader (vysoké frekvence), zatímco apikální vlákna končí ve ventrálních oddílech DCN a VCN (nízké frekvence).

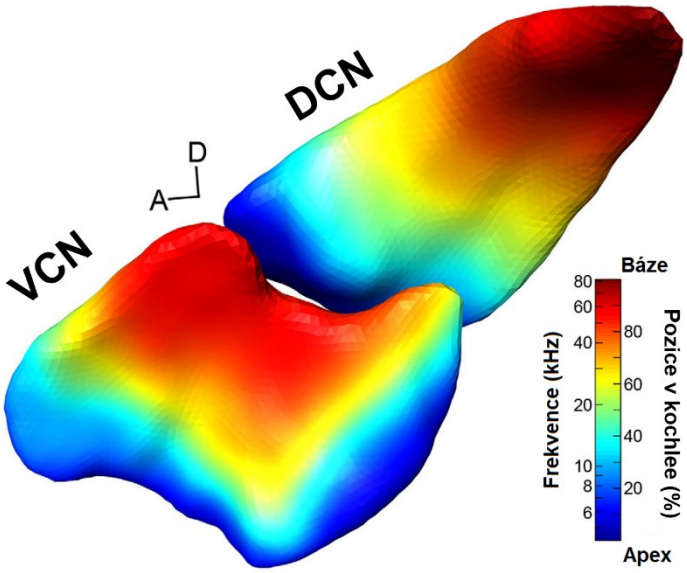

Obrázek 10: Tonotopické uspořádání myšího ventrálního a dorsálního kochleárního jádra. Barevná škála odpovídá jednotlivým frekvencím, které byly zpracovány v určité části kochley. (A – anteriorně; D – dorsálně; DCN – Dorsální kochleární jádro; VCN – Ventrální kochleární jádro) Převzato a upraveno z (Muniak, Rivas *et al.* 2013).

DCN je uspořádáno do čtyř vrstev (Webster a Trune 1982, Mao, Montgomery *et al.* 2015). Vnější vrstva gliových ependymálních buněk odděluje DCN a VCN. Pod ní se nachází molekulární vrstva, kde je nízká hustota neuronů, mezi nimž převažují malé hvězdicové („stellate“) a granulární nervové buňky. Dále v DCN můžeme nalézt vrstvu pyramidových neuronů, která dále zahrnuje i Golgiho interneurony, unipolární kartáčové buňky („unipolar brush cells”) a granulární buňky. Poslední částí je středová vrstva, kudy vstupuje sluchový nerv. Centrální vrstva obsahuje zejména obrovské („giant“) buňky. Jednou z hlavních funkcí DCN je odstínění zvuků produkovaných vlastním tělem (dýchání, žvýkání atd.) a naopak zaostření na neočekávané zvuky, které přichází z okolí (Shore a Zhou 2006).

VCN je heterogenní nevrstevnatý orgán složený z několika druhů neuronů. Nejpočetnější zastoupení mají chobotnicové („octopus”), chundelaté („bushy”) a hvězdicové multipolární buňky (Webster a Trune 1982). Jedna vnitřní vlásková buňka je inervovaná jedním myelinovým dendritem neuronu spirálního ganglia, jehož axon tvoří jednu velkou synapsi na chundelaté buňce („endbulb of Held“). Toto uspořádání umožňuje akustické zaostření v prostoru a přesné lokalizování zdroje zvuku (Sento a Ryugo 1989).

Většina neuronů kochleárních jader se diferencuje a migruje z rhombomer 2-5 ve věku E10,5-13,5 (Ivanova a Yuasa 1998, Wang, Rose *et al.* 2005), ale některé nervové buňky DCN proliferují až do E18,5 (Shepard, Scheffel *et al.* 2018). Ve VCN se nejprve diferencují neurony v dorsální části (vysoké frekvence) a poté diferenciace pokračuje směrem k ventrální oblasti (nízké frekvence), což koresponduje s vývojem spirálního ganglia vnitřního ucha, kde

diferenciace směřuje od báze (vysoké frekvence) k apexu (nízké frekvence). Oproti tomu vývoj neuronů v DCN nevykazuje žádný gradient (Shepard, Scheffel *et al.* 2018).

Z kochleárních jader odchází tři hlavní svazky neuronů (Králíček 2004). Z DCN vede *stria acustica dorsalis* do kontralaterálního *lemniscus lateralis* a *colliculus inferior*, z VCN směřuje část svazku *stria acustica intermedia* do komplexu olivy superior a další oddíl do *lemniscus lateralis*, poslední svazek kochleárního jádra *corpus trapezoideum* vede z VCN do komplexu olivy superior.

Na experimentálních modelech myši a pískomila bylo ukázáno, že po chirurgickém odstranění vnitřního ucha či ztrátě vláskových buněk dochází k negativním změnám i v kochleárních jádrech (Tierney, Russell *et al.* 1997, Tong, Strong *et al.* 2015). Při poškození vnitřního ucha se zmenšuje celkový objem kochleárních jader, snižuje se počet neuronů a také se zmenšují těla neuronů v této části mozku. Důležitá je však doba, během níž dochází k degeneraci vnitřního ucha. Negativní změny na kochleárních jádrech se projeví pouze při poškození vnitřního ucha během brzkého neonatálního vývoje, kdy ještě není sluch u hlodavců plně vyvinut. Při ztrátě plně maturovaných vláskových buněk po P14 mají kochleární jádra srovnatelné vlastnosti jako kontroly.

2.5.2 Komplex olivy superior (*Nucleus olivaris superior*)

Komplex olivy superior tvoří tři oblasti interneuronů v prodloužené míše (*medulla oblongata*) – mediální jádro trapézového tělesa (*nucleus medialis corporis trapezoidei*), laterální (*nucleus olivaris inferior lateralis*) a mediální oliva superior (*nucleus olivaris inferior medialis*). Tento komplex je první část sluchové dráhy, kde se setkávají aferentní vlákna z obou uší, což je nezbytné pro binaurální přenos informací.

2.5.3 Spodní párový hrbolek *(Colliculus inferior)*

Třetí neurony sluchové dráhy sídlí v *colliculus inferior*, kde se zpracovávají informace o frekvenci a intensitě zvuku z obou uší a kde se integrují senzorické signály sluchové dráhy a dalších smyslů, což je základem některých sluchových reflexů (např. lekavá/stresová reakce na neznámé či hlasité zvuky)(Henry, Wallick *et al.* 1972).

Na základě histochemických barvení byl tento oddíl středního mozku rozdělen na tři části: centrální jádro, dorsální kůra a (laterální) externí kůra (Faye-Lund a Osen 1985). Centrální jádro je vrstevnaté a má tonotopické uspořádání, jelikož zde končí většina vláken vedoucích z nižších oddílů sluchové dráhy (Stiebler a Ehret 1985, Ress a Chandrasekaran 2013). Externí kůra

přijímá vstupy z mimosluchových zdrojů (např. somatosenzorická dráha)(Aitkin, Dickhaus *et al.* 1978), zatímco dorsální kůra obsahuje zejména neurony sestupné sluchové dráhy (Winer, Larue *et al.* 1998).

2.6 Vestibulární dráha

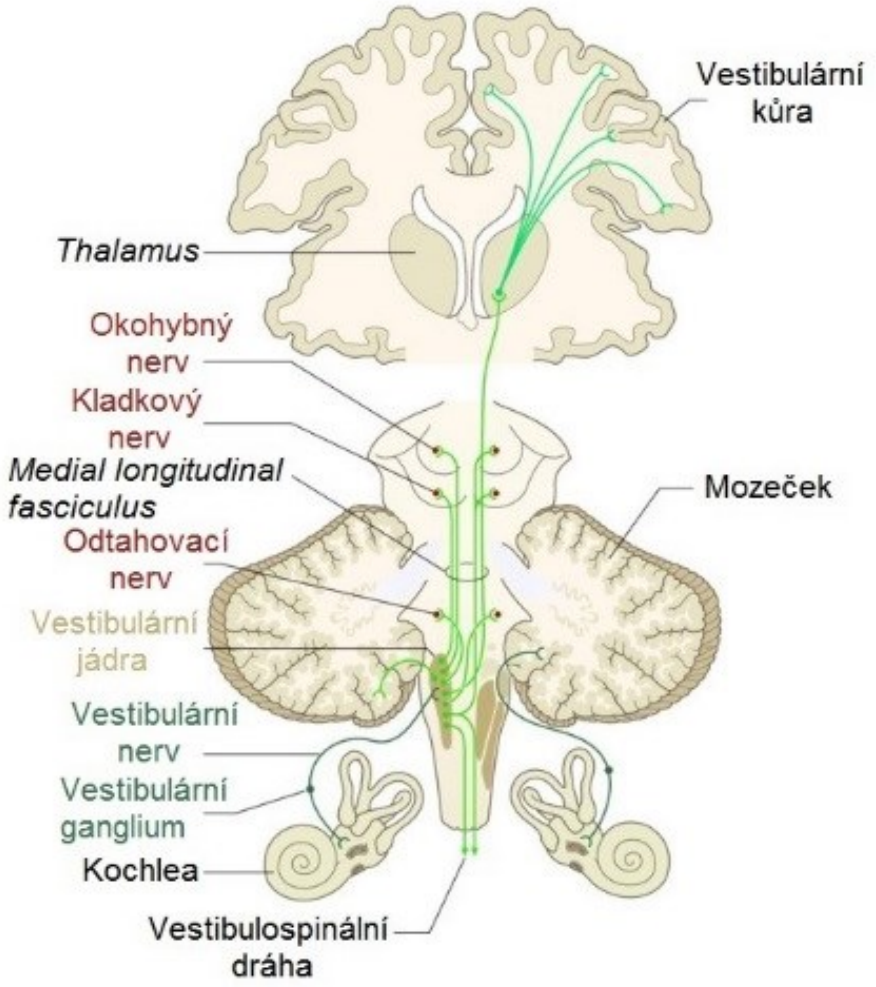

Obrázek 11: Vzestupná vestibulární dráha. Aferentní vestibulární dráha je tříneuronová – vestibulární ganglium, vestibulární jádra a *thalamus*. Vestibulární jádra jsou dále spojena s mozečkem, jádry hlavových nervů (okohybný, kladkový a odtahovací nerv) a s míchou. Převzato a upraveno z (Champney 2015).

Vestibulární dráha je tří neuronová (Obrázek 11)(Králíček 2004). První neurony se nachází ve vestibulárním neboli Scarpově gangliu vnitřního ucha. Následují nervové buňky vestibulárních jader a dráha končí ve vestibulární mozkové kůře.

Některé axony vestibulárního ganglia vedou přímo do mozečku (*cerebellum*), avšak většina vláken nejprve ústí do čtyř vestibulárních jader v mozkovém kmeni (Tascioglu 2005, Khan a

Chang 2013). Mediální neboli Schwalbeovo jádro je největší z vestibulárních jader a končí zde aferentní vlákna kristy laterálního polokruhovitého kanálku. Axony vedoucí od superiorního a posteriorního kanálku končí v superiorním neboli Bechtěrevově jádře. Největší nervové buňky jsou obsaženy v laterálním neboli Deitersově jádru, kde najdeme zakončení neuronů všech vestibulárních orgánů. Čtvrtým jádrem je jádro laterální neboli sestupné s nervovými zakončeními obou makul. Z těchto jader vedou také eferentní dráhy inervující oční svalstvo a míchu.

Z vestibulárních jader odchází nervová vlákna dále do mozečku nebo přes *thalamus* do vestibulární kůry. Vestibulární dráha je také spojena s páteřní míchou a s třemi jádry nervů inervující okohybné svaly (okohybný, kladkový a odtahovací hlavový nerv) a společně tak tvoří dráhy důležité pro vestibulospinální a vestibulookulární reflexy.

2.6.1 Mozeček (*Cerebellum*)

Mozeček je velmi členitý a rozložitý orgán skládající se ze dvou hemisfér a středové červovité části zvané *vermis* (Riley 1930). Na povrchu se nacházejí tři korové vrstvy šedé hmoty – molekulární vrstva, vrstva Purkyňových buněk a granulární vrstva. Ve středu mozečku se nacházejí čtyři jádra bílé hmoty. Z hlediska morfologie se mozeček rozděluje na tři laloky (lobi) – anteriorní, posteriorní a flokulonodulární (Obrázek 12). Tyto laloky se dají dále rozdělit na deset menší laloků označovaných římskými číslicemi (lobuli I-X) oddělených rýhami (fissury).

Podle fyziologie a fylogenetiky se mozeček rozděluje na tři odlišné oblasti – cerebrální, spinální a vestibulární mozeček (Obrázek 12)(Králíček 2004). Cerebrální oblast je fylogeneticky nejmladší (*neocerebellum*) a zahrnuje laterální části obou hemisfér. Předpokládá se, že *neocerebellum* je důležité pro plánování a úpravu volních pohybů těla. Spinální část je o něco starší (*paleocerebellum*) a skládá se z *vermis* a mediálních částí hemisfér. Spinální mozeček spolupracuje s mozkovou kůrou a kontroluje propriorecepci, postoj a chůzi. Fylogeneticky nejstarší oblastí je vestibulární mozeček (*archicerebellum*), který se skládá pouze z flokulonodulární laloku neboli laloku X. Podílí se na udržení vzpřímené polohy a řízení automatických očních pohybů.

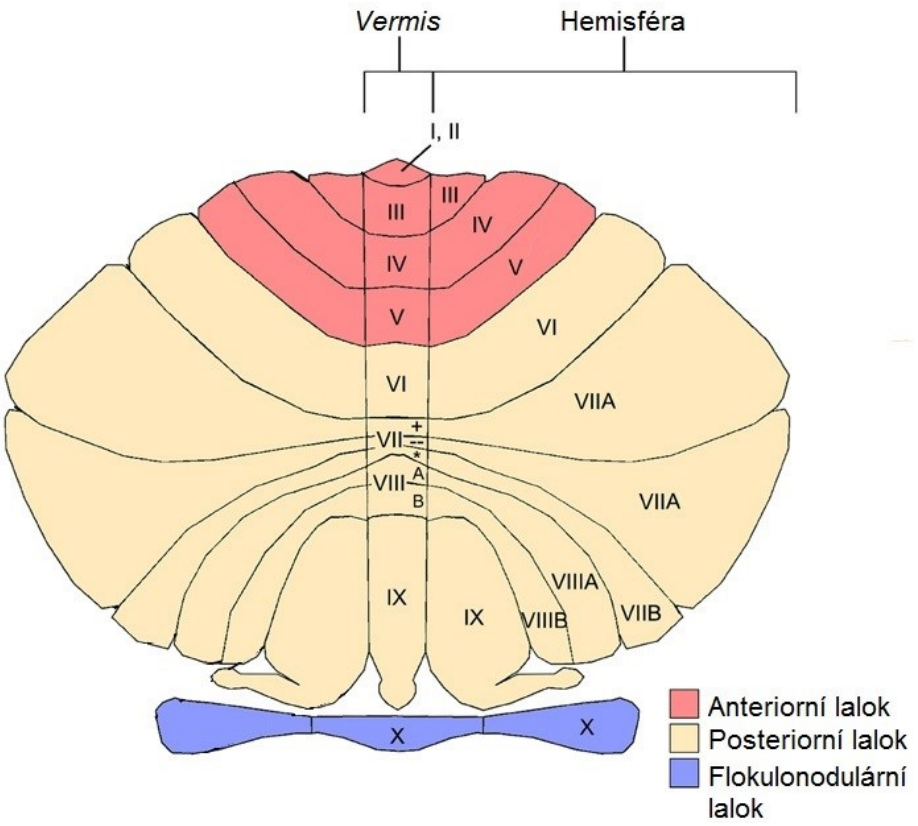

Obrázek 12: Anatomie mozečku. Převzato a upraveno z (D'Mello a Stoodley 2015).

Do mozečku vedou primární vlákna přímo z rovnovážných orgánů a sekudární vlákna vedoucí navíc přes vestibulární jádra. Oba tyto typy aferentních vláken se nazývají mechová vlákna („mossy fibers“) a tvoří aktivační glutamátové synapse s unipolárními kartáčovými buňkami. Dále je signál přenášen přes granulární buňky paralelními vlákny na Purkyňovy buňky, které zprostředkovávají motorickou odpověď. Tato odpověď je modulována inhibičními interneurony, které využívají kyselinu γ-aminomáselnou (GABA) jako neurotransmiter. Mezi tyto interneurony patří hvězdicové, košíčkové („basket“) a Golgiho buňky. (Ito 2006, Ango a Dos Reis 2019, Balmer a Trussell 2019).

3 Cíle práce

Náplní této práce bylo pomocí tří unikátních transgenních myších modelů odhalit dosud nepopsané funkce transkripčních faktorů ISL1, NEUROD1 a SOX2 a specifikovat jejich roli během vývoje vnitřního ucha. Cílem práce konkrétně bylo:

- Stanovit míru ektopické exprese transgenu pro transkripční faktor ISL1 s regulační sekvencí *Pax2* v nově vytvořeném myším modelu [Tg(*Pax2-Isl1*)]
- Určit vliv nadměrné exprese ISL1 na embryonální a postnatální vývoj sluchové dráhy a na sluchové funkce v [Tg(*Pax2-Isl1*)]
- Analyzovat změny v rovnovážném ústrojí a vestibulární centrální dráze u myší [Tg(*Pax2-Isl1*)]
- Zmapovat endogenní expresi ISL1 během vývoje vnitřního ucha pomocí myšího modelu *Isl1-Cre*
- Specifikovat roli SOX2 v neurosenzorickém vývoji pomocí experimentálního modelu s podmíněnou delecí *Sox2 (Isl1-Cre; Sox2$^{f/f}$)*
- Definovat vliv tkáňově specifické delece *Neurod1* ve vnitřním uchu na vývoj a funkci sluchové dráhy v modelu *Isl1-Cre; Neurod1$^{f/f}$*

4 Materiál a metody

Během experimentální části jsem využívala zejména tyto metody:

- Práce s myším modelem (perfúze, odběr orgánů a embryí, měření hladiny glukosy v krvi apod.)
- Genotypizace - izolace DNA a polymerázová řetězová reakce (PCR)
- Preparace embryí a mikrodisekce vnitřního ucha a jeho orgánů
- Příprava tkáňových řezů pomocí vibratomu
- Imunohistochemické barvení (řezů či celé tkáně)
- Histochemické barvení (detekce genu lacZ a tedy enzymu β-galaktosidázy pomocí chromogenního substrátu X-galaktózy)
- *In situ* hybridizace
- Mikroskopie (stereoskopický, fluorescenční, konfokální a elektronový mikroskop)
- Izolace RNA, příprava cDNA pomocí reverzní transkripce a kvantitativní PCR
- Analýza dat za využití programů ImageJ a GraphPad Prism

Ve spolupráci s dalšími laboratořemi bylo využito metod:

- Trasování nervových vláken pomocí značených lipofilních prób
- Měření otoakustických emisí (DPOAE)
- Vyšetření sluchových kmenových potenciálů (ABR)
- Behaviorální testy (měření reflexní úlekové reakce a prepulzní inhibice úlekové reakce)
- Testy rovnováhy (běh na rotarodu apod.)
- Měření elektrické aktivity neuronů v *colliculus inferior*

5 Výsledky

Výsledky získané během doktorského studia byly publikovány v těchto vědeckých článcích:

- Chumak T., Bohuslavova R., **Macova I.**, Dodd N., Buckiova D., Fritzsch B., Syka J., Pavlinkova G. (2016). "Deterioration of the Medial Olivocochlear Efferent System Accelerates Age-Related Hearing Loss in Pax2-Isl1 Transgenic Mice." Molecular Neurobioly **53**(4):2368-83.
- Bohuslavova R., Dodd N., **Macova I.,** Chumak T2., Horak M., Syka J., Fritzsch B., Pavlinkova G. (2017). "Pax2-Islet1 Transgenic Mice Are Hyperactive and Have Altered Cerebellar Foliation." Molecular Neurobiology **54**(2):1352-1368.
- Dvorakova M., Jahan I., **Macova I.**, Chumak T., Bohuslavova R., Syka J., Fritzsch B., Pavlinkova G. (2016). "Incomplete and delayed Sox2 deletion defines residual ear neurosensory development and maintenance. " Scientific Reports **6**:38253.
- **Macova I.,** Pysanenko K., Chumak T., Dvorakova M., Bohuslavova R., Syka J., Fritzsch B., Pavlinkova G. (2019) "Neurod1 Is Essential for the Primary Tonotopic Organization and Related Auditory Information Processing in the Midbrain." Journal of Neuroscience **39**(6):984-1004.

Pro studium transkripční regulace vývoje vnitřního ucha byly využity tři různé myší modely:
1) transgenní model [Tg(*Pax2-Isl1*)] s ektopickou expresí ISL1 řízenou regulační sekvencí pro gen *Pax2*
2) mutant *Sox2CKO* s podmíněnou delecí genu *Sox2* za využití *Isl1-Cre* nesoucí gen *Cre* vložený do endogenního lokusu *Isl1*
3) mutant *Neurod1CKO* s podmíněnou delecí genu *Neurod1* opět pomocí *Isl1-Cre*.

5.1 Negativní vliv transgenní exprese ISL1 na vývoj a funkci sluchově rovnovážného systému

Nový myší transgenní model [Tg(*Pax2-Isl1*)] byl připraven injekcí vektoru obsahující regulační oblast a promotor *Pax2*, kódující sekvenci genu *Isl1*, intron Wnt1 a poly(A) konec do oplodněného myšího vajíčka. Homozygotní mutace *Pax2-Isl1* je letální v E10,5 vzhledem k abnormálnímu vývoji mozku. Z tohoto důvodu byly experimenty prováděny pouze na jedincích s heterozygotní mutací *Pax2-Isl1*, u nichž byl pomocí kvantitativní PCR stanoven

počet kopií daného vektoru v myším transgenním genomu na dvě. Dospělosti se dožívalo pouze 60 % transgenních heterozygotů, zbývající mutanti umírali během dvou dnů po narození. V porovnání s kontrolními sourozenci byly myši [Tg(*Pax2-Isl1*)] hyperaktivní a pohybovaly se v kruzích.

Vliv ektopické exprese ISL1 na vývoj vnitřního ucha byl zkoumán metodami imunohistologického barvení, kvantitativního PCR, trasování neuronových vláken a fyziologickými testy. Ve věku E10,5 bylo v kochleovestibulárním gangliu detekováno více ISL1 pozitivních neuronů u [Tg(*Pax2-Isl1*)] než u kontrolních jedinců korespondující se zvýšenou produkcí ISL1 v našem novém myším modelu. U mutanta byla pozorována urychlená diferenciace aferentních nervových vláken v periferní i centrální části sluchově rovnovážné soustavy v E12,5. Ačkoli několik dní po narození (P3) nebyla nervová vlákna v kochlee transgenních myší organizována do svazků jako u kontrol, v dospělosti nebyly zaznamenány žádné změny v inervaci Cortiho orgánu. Měření otoakustických emisí (DPOAE) odhalilo, že s věkem se předčasně zhoršovala funkce vnějších vláskových buněk u mutantů [Tg(*Pax2-Isl1*)]. Podobný efekt byl zaznamenán také při vyšetření sluchových kmenových potenciálů (ABR), kdy se prahy ABR u mutanta zvyšovaly opět s věkem. Tyto výsledky naznačují urychlenou ztrátu sluchu při ektopické expresi ISL1. Navíc během stárnutí docházelo k předčasné ztrátě neuronů spirálního ganglia u myší [Tg(*Pax2-Isl1*)] v porovnání se stejně starými kontrolními jedinci. K výraznému zhoršení funkce vnějších vláskových buněk u mutanta [Tg(*Pax2-Isl1*)] nedocházelo v důsledku ztráty vnějších vláskových buněk, jak bylo ukázáno imunohistologicky i pomocí kvantitativní PCR. Naopak významná změna byla detekována v eferentní inervaci senzorického epitelu kochley myší [Tg(*Pax2-Isl1*)]. U dospělých mutantních myší byl počet eferentních zakončení na vnějších vláskových buňkách a podpůrných buňkách signifikantně snížen. Tato eferentní vlákna vycházejí z mediální olivy superior, kde byla u [Tg(*Pax2-Isl1*)] postnatálně detekována transgenní exprese ISL1, zatímco u kontrol ve stejném věku není tento transkripční faktor v mozkovém kmeni exprimován.

Kromě sluchové dráhy byl u myší [Tg(*Pax2-Isl1*)] také analyzován vestibulární systém kvůli jejich hyperaktivitě a pohybu v kruzích. Po podání pikrotoxinu, blokátoru chloridových kanálů spjatých s GABA receptory, se hyperaktivita u transgenních mutantů snížila. Na rotarodu však dosahovali lepších výsledků mutanti, což ukazuje spíše na defekt v centrální vestibulární dráze než ve vestibulárních orgánech vnitřního ucha. Tento závěr byl potvrzen imunohistologickými

analýzami, které neukázaly žádné rozdíly v rovnovážných orgánech vnitřního ucha u kontrolních myší a [Tg(*Pax2-Isl1*)]. Jediná změna v rovnovážném ústrojí byla zaznamenána v sakulu, který byl u transgenních myší menší s nižším počtem vláskových buněk a méně inervovaný. Pomocí protilátky proti kalretininu byl stanoven ve věku šesti a jedenácti měsíců počet vestibulárních neuronů, který byl stejný u mutantů a kontrol v obou věcích. Tyto výsledky ukazují, že periferní část vestibulárního systému nebyla mutací zásadně ovlivněna, a proto byly další analýzy zaměřeny na mozeček a *colliculus inferior*. Morfologická hodnocení ukázala, že oba uvedené orgány byly znatelně menší u mutantů [Tg(*Pax2-Isl1*)] a rýhování mozečku bylo abnormální, kdy laloky I-III byly často spojeny v jeden lalok a výjimečně také chyběly laloky VI a VII. Změny v mozečku byly také prokázány na molekulární úrovni. U [Tg(*Pax2-Isl1*)] byl detekován menší počet kalbindin pozitivních Purkyňových buněk v lobulech I-III a méně kalretinin pozitivních unipolárních kartáčových buněk v lobulech IX a X. Změny v expresi proteinů vázajících vápenaté ionty (kalbindin a kalretinin) značí možný zhoršený přenos informací u mutantů. Transkripční faktor ISL1 není u myší v mozečku exprimován, avšak u našeho transgenního modelu byl detekován v PAX2 pozitivních buňkách (GABAergní neurony - hvězdicové, košíčkové a Golgiho buňky). Expresní profil mozečku byl změněn v důsledku ektopické exprese ISL1, přičemž byly zaznamenány vyšší hladiny exprese genů pro transkripční faktory *Pax6* a *Neurod4* (neurogenní diferenciační faktor 4), pro proteiny důležité pro udržení vápníkové homeostáze *Calb2* (kalretinin) a *Cacng1* (podjednotka gama-1 napěťově řízeného vápníkového kanálu) či pro marker glutamátových neuronů *Dlg4* („Disks large homolog 4“).

Deterioration of the Medial Olivocochlear Efferent System Accelerates Age-Related Hearing Loss in *Pax2-Isl1* Transgenic Mice

Tetyana Chumak[1] · Romana Bohuslavova[2] · Iva Macova[2] · Nicole Dodd[2] · Daniela Buckiova[1] · Bernd Fritzsch[3] · Josef Syka[1] · Gabriela Pavlinkova[2]

Received: 18 December 2014 / Accepted: 7 May 2015 / Published online: 20 May 2015

Abstract The development, maturation, and maintenance of the inner ear are governed by temporal and spatial expression cascades of transcription factors that form a gene regulatory network. ISLET1 (ISL1) may be one of the major players in this cascade, and in order to study its role in the regulation of inner ear development, we produced a transgenic mouse overexpressing *Isl1* under the *Pax2* promoter. *Pax2*-regulated ISL1 overexpression increases the embryonic ISL1^{+} domain and induces accelerated nerve fiber extension and branching in E12.5 embryos. Despite these gains in early development, the overexpression of ISL1 impairs the maintenance and function of hair cells of the organ of Corti. Mutant mice exhibit hyperactivity, circling behavior, and progressive age-related decline in hearing functions, which is reflected in reduced otoacoustic emissions (DPOAEs) followed by elevated hearing thresholds. The reduction of the amplitude of DPOAEs in transgenic mice was first detected at 1 month of age. By 6–9 months of age, DPOAEs completely disappeared, suggesting a functional inefficiency of outer hair cells (OHCs). The timing of DPOAE reduction coincides with the onset of the deterioration of cochlear efferent terminals. In contrast to these effects on efferents, we only found a moderate loss of OHCs and spiral ganglion neurons. For the first time, our results show that the genetic alteration of the medial olivocochlear (MOC) efferent system induces an early onset of age-related hearing loss. Thus, the neurodegeneration of the MOC system could be a contributing factor to the pathology of age-related hearing loss.

Keywords Medial olivocochlear efferent system · Islet1 transcription factor · Age-related hearing loss · Outer hair cells · Transgenic mouse

Introduction

The morphogenesis of the inner ear is governed by temporal and spatial expression cascades of transcription factors that form a gene regulatory network [1]. Within the otic placode, the neurosensory phenotype is consolidated with upregulation of the proneural gene *Neurogenin1* (*Neurog1*). *Neurog1* null mice show not only a loss of all sensory neurons but also a significant reduction in hair cell and supporting cell formation, suggesting incompletely overlapping precursor populations common to neuron and sensory epithelia [2–4]. Other factors important for the general epithelia-neurosensory transition are also expressed, such as *Gata3*, *Pax2/8*, *Tbx1*, *Foxg1*, *Foxi1*, *Eya1/Six1*, and *Oct4* [5–7]. This combination of transcriptional factors provides a necessary context for the switch from epidermal to proneurosensory fate. The topological specification of prosensory patches represents the first step in the development of the sensory epithelia. Developing prosensory cells express a number of genes that have functional roles in prosensory specification, including *Tbx1*, *Bmp4*, *Jag1*, and SRY-box containing gene 2 (*Sox2*). Differentiation of sensory epithelia into hair cells and supporting cells is regulated by temporally expressed transcription factors [5, 8, 9]. However,

Electronic supplementary material The online version of this article (doi:10.1007/s12035-015-9215-1) contains supplementary material, which is available to authorized users.

✉ Gabriela Pavlinkova
gpavlinkova@ibt.cas.cz

[1] Institute of Experimental Medicine, CAS, Prague, Czechia

[2] Laboratory of Molecular Pathogenetics, Institute of Biotechnology, CAS, Prague 4, CZ-142 20 Prague, Czechia

[3] Department of Biology, University of Iowa, Iowa City, IA 52242, USA

the complete functional and molecular composition of the transcriptional network that controls neurosensory development remains unclear. Most importantly, the Lim-domain factor, *Lmx1a* [10], has been found to be essential for normal ear morphogenesis as well as normal neurosensory development whereas eliminating *Lmo4* results in formation of extra sensory epithelia [11].

Like *Lmx1a*, *Islet1* (*Isl1*) is a Lim homeodomain (LIM-HD) transcription factor that can bind to DNA in the form of monomeric or heteromultimeric transcription factor complexes [12]. LIM-HD transcription factors are characterized by two zinc finger motifs: the LIM domain for protein/protein interactions and a homeodomain for binding to the DNA control elements of target genes. ISL1 acts in a context-dependent fashion, requiring other factors to achieve specificity, and it has a unique potential for combinatorial interaction with other transcription regulators in a homomeric or heteromeric fashion [13]. Embryos lacking the *Isl1* gene die by embryonic day E10.5, indicating an essential requirement for ISL1 during normal embryonic development [14]. Loss-of-function studies in the mouse have revealed crucial roles for ISL1 in motor neuron, pancreatic, cardiac, and eye development [15–19]. Thus, ISL1 contributes to the development of neuronal and non-neuronal cell types, suggesting that its activity is context dependent. The dose-dependent requirement for *Isl1* is an interesting aspect of ISL1 regulation, which affects the specification of motor neurons [20] and modulates horizontal cell number in the mouse retina [19]. During normal ear development, ISL1 appears first in the otic placode and it is then upregulated in the cells that will form the cochleovestibular ganglion during placode invagination [21]. Subsequently, the expression of ISL1 in the neuronal lineage is maintained as the neuronal differentiation progresses in the terminally differentiated neurons. ISL1 is also one of the earliest markers of the developing sensory epithelia. ISL1 is expressed in all cells committed to form either hair cells or supporting cells, which suggests its role in the specification of the cell population committed to form these cell types [21–23]. Upon initiation of hair cell differentiation, the expression of ISL1 is downregulated in these differentiating cells [22]. The expression of ISL1 in the inner ear suggests a role in the inner ear development, such as specifying the neuronal/sensory competency. We hypothesize that ISL1-expressing cells are the common precursors for both sensory epithelia and neurons. By modulating the expression of *Isl1*, we expect to change the fate specification of cells in the inner ear [24].

To gain further insight into the role of ISL1 in ear development, we have expressed *Isl1* under the *Pax2* promoter in transgenic mice [Tg(*Pax2-Isl1*)]. The transgenic expression of *Pax2-Isl1* resulted in an enlargement of $ISL1^+$ expression domain with an increased number of $ISL1^+$ cells in the otic epithelium and delaminating neuroblasts of the ganglion in the E10.5 mouse otocyst. However, our data also show an increased postnatal lethality, motor hyperactivity and circling behavior, and an early onset of the age-related hearing loss in transgenic mice compared to littermate controls.

Material and Methods

Generation of Transgenic Mice

This study was conducted in accordance with the Guide for the Care and Use of Laboratory Animals (NIH Publication No. 85-23, revised 1996). The experimental protocol was approved by the Animal Care and Use Committee of the Institute of Molecular Genetics, Academy of Sciences of the Czech Republic. All efforts were made to minimize suffering. The experimental mice were housed in a controlled environment (23 °C; 12-h light/dark cycle) with free access to water and standard chow diet. All experiments were performed with male and female littermate mice that were either wild-type (WT) or heterozygous *Pax2-Isl1* transgenic mice ($Tg^{+/-}$) on an FVB background (strain code 207, Charles River). This strain background does not interfere with measurements of hearing loss attributable to the experimental transgenesis [25]. To generate *Pax2-Isl1* transgenic mice, we prepared the pGEM7f vector, containing *Pax2* regulatory sequences (8.5-kb regulatory element at the *Pax2* locus and promoter [26]), the Wnt1 intron and poly[A] sequences, and the *Isl1* gene insert [27]. A 14.3-kb *AatII* fragment (restriction map, Fig. 1a) was injected into the pronuclei of fertilized eggs from inbred FVB mouse strain. The transgenic mice were generated at the Mouse Genome Engineering Facility at the University of Nebraska Medical Center, Omaha, USA. Genotyping was carried out by PCR using 5′ primer (located in *Pax2* regulatory element), 5′-AAG TTG AGT TTG AGA GGC GAC ACG-3′, and 3′ primer (located in *Isl1* gene), 5′-TTG GCG CAT TTG ATC CCG TAC AAC-3′, yielding a 400-bp amplicon. PCR reactions were carried out using the following conditions: 35 cycles at 95 °C for 30 s, 60 °C for 30 s, and 72 °C for 30 s. The amplification products were run on agarose gels and visualized by ethidium bromide staining. We generated six different founder lines of [Tg(*Pax2-Isl1*)], which carried *Pax2-Isl1* transgene. The founder lines were outbred with FVB. We selected one line of heterozygous *Pax2-Isl1* transgenic mice ($Tg^{+/-}$) for detailed analyses.

Analysis of Hearing Functions

Animals from both experimental groups (WT, $n=58$ and $Tg^{+/-}$, $n=70$) were divided into three groups according to their age: 1 to 5, 6 to 9, and 10 to 15 months old. All tests were carried out on mice, anesthetized with ketamine (50 mg/kg) and xylazine (10 mg/kg), and maintained on a temperature-regulated blanket in a sound-attenuating and anechoic

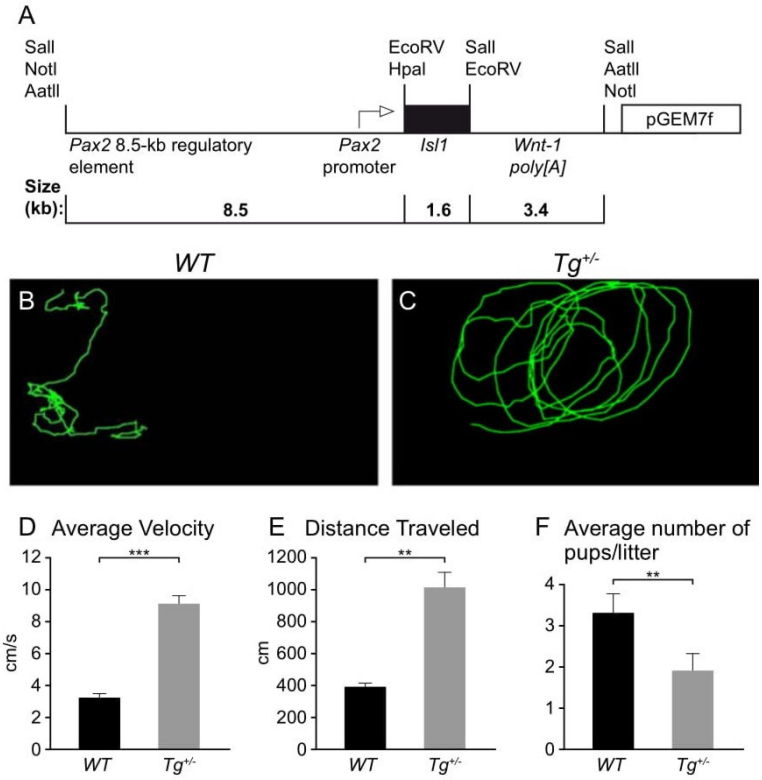

Fig. 1 *Pax2-Isl1* transgenic mice. **a** Diagram of the *Isl1* transgene, which comprises the 8.5-kb *Pax2* regulatory element and promoter, the *Wnt1* gene as a source of introns and poly [A] sequences, and *Isl1* gene cloned into the *EcoRV* site. **b**, **c** Traces and **d**, **e** quantification of mouse locomotion in an open field showing circling and hyperactivity of $Tg^{+/-}$ mice (n=3) in comparison to WT littermates (n=3). The total distance traveled was measured in a 2-min time period. **f** Average number of surviving $Tg^{+/-}$ offspring per litter is significantly decreased compared to their WT littermates (n=27 litters). The values represent means±SEM. $^{**}P<0.01$; $^{***}P<0.001$, t test

chamber. Acoustic stimuli were generated with a TDT (Tucker Davis Technologies, FL, USA) System III using Enhanced Real-Time Processor RP 2.1.

For auditory brainstem response (ABR) recording, needle electrodes were placed subcutaneously on the vertex (active electrode) and in the neck muscles (ground and reference electrodes). The responses to tone bursts (3-ms duration, 1-ms rise/fall times, frequencies of 2, 4, 8, 16, 32, and 40 kHz) were recorded. Acoustic stimuli were conveyed to the animal in free-field conditions via a two-way loudspeaker system (Jamo® woofer [Denmark] and SEAS® T25CF 002 tweeter [Norway]) placed 70 cm in front of the animal's head. The signal from an electrode was amplified 10,000 times and band-pass filtered over the range of 300 Hz to 3 kHz. The signal was processed with a TDT System III Pentusa Base Station and analyzed using BioSig™ (TX, USA) software. The response threshold to each frequency was determined as the minimal tone intensity that still evoked a noticeable potential peak in the expected time window of the recorded signal.

Cubic (2 F1–F2) distortion product otoacoustic emissions (DPOAEs) over a F2 frequency range from 4 to 38 kHz were recorded with a low-noise microphone system (Etymotic probe ER-10B+, Etymotic Research, IL, USA). Acoustic stimuli (ratio F2/F1=1.21, F1 and F2 primary tone levels of L1/L2=70/60 dB) were presented to the ear canal with two custom-made piezoelectric stimulators connected to the probe with 10-cm-long silastic tubes. The signal from the microphone was analyzed by the TDT System III (RP2 processor, sampling rate 100 kHz) using custom-made Matlab software. DPOAEs were successively recorded in both ears of the animals at individual frequencies over the frequency range 4–38 kHz with a resolution of four points per octave. The average values per group were calculated (mean±SD or SEM) and the results were plotted in audiograms (ABR thresholds) and DP-grams (distortion product otoacoustic emissions).

Behavior Testing

Twelve-week-old males, three WT and three $Tg^{+/-}$, were used for testing. All testing was carried out during the light cycle. Mice were individually placed in a chamber (37 cm length × 20 cm width × 14.5 cm height) and allowed to acclimatize for 30 min before testing. To analyze locomotor activity in an open-field environment, mice were recorded (Sony DCR-SX85Camcoder) in 2-min sequences during 30-min period. An average of five measurements was analyzed per mouse. The average of total distance over a 2-min time period and the average of velocity traveled were quantified using the NIH ImageJ program, (http://imagej.nih.gov/ij/download.html), with the Manual Tracking Plug-in.

Immunohistochemical Analyses of Embryos

Mouse embryos were isolated at E10.5 and E12.5 for additional analyses. The noon of the day on which the vaginal plug was found was designated as E0.5. The developmental stage was classified for each embryo by morphological criteria. The embryonic morphology was assessed using a Nikon SMZ dissection microscope. Frozen 8-μm-thick sections of E10.5 embryos were fixed in 4 % paraformaldehyde (PFA) for 15 min, incubated with 0.6 % H_2O_2 (to block endogenous peroxidase), blocked with serum, and followed by incubation with the primary mouse anti-ISL1 monoclonal antibody (#39.4D5, Developmental Hybridoma Bank, Iowa City, IA, USA). The sections were labeled with secondary anti-mouse IgG-peroxidase (#A9044, Sigma) and developed in diaminobenzidine substrate (DAB; #D3939, Sigma). Semi-quantitative analyses were performed to determine the relative number of cells expressing ISL1 per each field, using the threshold tool in the NIH ImageJ program (http://imagej.nih.gov/ij/download.html), as described [28]. The slides (n=3–4× 3 embryos/each group) were analyzed under a Nikon Eclipse 50i microscope with a ×20 magnification objective using the NIS-elements program.

For the dye-tracing experiment, the heads of E12.5 embryos were removed and fixed for a minimum of 24 h in 4 % PFA. NeuroVue® dye-coated filter microstrips were cut to appropriately sized pieces using microscissors and inserted into the brainstem and saccule nerve tracts and incubated at 60 °C for 4 days. A two-colour tracing system using NeuroVue® Maroon and Red, which have 647- and 568-nm excitation, respectively, was applied [29]. Progression of dye diffusion was monitored using epifluorescent microscopy. On completion of dye diffusion, wet mounts of inner ear and brain stem were prepared using glycerol and coverslips as spacers. Images were taken using a Leica SP5 confocal laser scanning system to generate stack of images. These stacks were subsequentially collapsed to generate single images.

Immunohistochemical Analyses of Adult Tissues

All animals older than P15 that were used for morphological analysis underwent hearing function tests. Mice were perfused with 4 % PFA. Auditory bullas were removed and fixed in 4 % PFA for 1–2 h for cochlear surface preparation or overnight for paraffin section preparation. For paraffin sections, fixed cochleae were decalcified in 0.12 M ethylendiaminotetraacetic acid for 1 week, dehydrated through a graded alcohol series, cleared in xylene, and embedded in paraffin. For cochlear surface preparation, the bone capsule was removed using tweezers sequentially from apex to base, and the basal membrane with the organ of Corti was dissected into 3–4 pieces per cochlea. Cochlear pieces aimed for nerve fiber visualization were decalcified 0.12 M ethylendiaminotetraacetic acid for 10 min prior to staining. Following overnight postfixation, the brain was cut into two hemispheres and sectioned serially into 50-μm-thick slices using a vibratome. The brain sections were stained with primary anti-ISL1 (#39.4D5, Developmental Hybridoma Bank, Iowa City, IA, USA) and anti-PAX2 (#PRB-276P, Covance) overnight. Dissected cochleae were stained using the following primary antibodies: anti-prestin (# sc-30163, Santa Cruz Biotechnology Inc., Dallas, TX, USA), anti-200-kDa neurofilament protein (NF200, # N4142, Sigma-Aldrich Co., St. Louis, MO, USA), anti-choline acetyltransferase (ChAT, # AB144P Millipore Corporation, MA, USA), and anti-myosin 7a (Myo7a, # 028918, Sigma-Aldrich Co., St. Louis, MO, USA). Phalloidin (# 59033, Dyomics) was used for F-actin and DAPI (# *D9542*, Sigma-Aldrich Co., MO, USA) for nuclei visualization. Preparations were examined under Zeiss 510 DUO laser confocal with ×40 Plan-Apochromat oil immersion objectives (numerical aperture 1.4). Z stacks through the thickness of the cochlea with step sizes from 0.5 to 1 μm depending on the aim were obtained. Unless stated otherwise, the cochlear region of 16–20 kHz is presented in the results, because this frequency region showed the most prominent functional decline in hearing tests. To determine the region of interest, the ImageJ plugin Line measure was used (http://www.masseyeandear.org/research/otolaryngology/investigators/laboratories/eaton-peabody-laboratories/epl-histology-resources/imagej-plugin-for-cochlear-frequency-mapping-in-whole-mounts/).

To plot cochleograms, photographs were taken consecutively from the whole length of the cochlea starting from the apical turn. The images were then manually superimposed using Corel Draw software to create a picture of the whole cochlea from apex to base. Cells were counted in each 7 % of the cochlear length using ImageJ software, and the loss of outer hair cells (OHCs) was calculated using Excel.

For quantitative analysis of ChAT positive ($ChAT^+$) staining, the 3D stacks from the 16–20 kHz cochlear region were analyzed. Three cochleae from each group were examined. To minimize the possibility of biased results, the analysis was carried out blindly. The volumes of $ChAT^+$ MOC terminals and volumes of $ChAT^+$ particles in the region of Deiters' cells (DCs) were calculated using the 3D object counter ImageJ plugin [30]. $ChAT^+$ particles in the DC area are shown as a volume per OHC.

The amount of spiral ganglion neurons (SGNs) was assessed in serial sections stained with diluted cresyl violet solution using the Zeiss confocal microscope 510 DUO [31]. Z stacks through the spiral ganglion were acquired for stereological analysis. SGNs were counted in the basal, middle, and apical regions of the cochlea in all three age groups, with a minimum of three ears per group, and five slices from each cochlea were analyzed. The numerical density was defined as the number of objects per cubic millimeter. For each animal, SGNs were quantified with the optical dissector method (×63 objective) in five cochlear sections at the base, middle, and

apex level. SGNs were quantified in counting boxes (counting frame 99×88 μm, dissector height 8.4 μm). SGNs were visualized by focusing through the dissector height, and the numerical density of cells per cubic millimeter was calculated. Quantification of SGNs was accomplished with Ellipse software.

Gene Expression Analysis by RT-qPCR

Total RNA was isolated from one or two cochleae per one mouse sample at P3, P28, or 7–11 months by TRIzol® Reagent (Thermo Fisher Scientific Inc., Waltham, MA, USA). After DNase I treatment (Thermo Fisher Scientific Inc., Waltham, MA, USA), RNA concentration and purity were determined by NanoDrop ND-1000 (Thermo Fisher Scientific Inc., Waltham, MA, USA). cDNA was obtained from RNA samples (0.25 or 0.5 μg) by reverse transcription using the RevertAid H Minus First Strand cDNA Synthesis Kit (Thermo Fisher Scientific Inc., Waltham, MA, USA). cDNA samples were diluted 10× or 20×, respectively. Each reaction for qPCR contained 4 μl diluted cDNA, 5 μl SYBR Green JumpStart Taq ReadyMix for qPCR (Sigma-Aldrich, St. Louis, MO, USA), 0.5 μl water, and 0.25 μl 10 mM forward primer and 0.25 μl 10 mM reverse primer. qPCR was performed with the initial activation at 94 °C for 120 s, followed by 39 cycles at 94 °C for 15 s, 59 °C for 30 s, and 72 °C for 30 s using CFX384™ Real-Time PCR Detection System (Bio-Rad Laboratories, Hercules, CA, USA). The *Hprt1* gene was selected as the best reference gene for our analyses from a panel of 12 control genes (TATAA Biocenter AB, Sweden). The relative expression of *prestin*, *Myo7a*, and *Isl1* with *Hprt1* as a reference gene was calculated using $-\Delta\Delta$Cq method, based on qPCR efficiencies (E) and the quantification cycle (Cq) difference (Δ) of Tg sample (Tg) versus WT (ratio= $(E_{\text{target}})^{\Delta\text{Cq(Mean WT}-\text{Mean Tg)}}/(E_{\text{Hprt1}})^{\Delta\text{Cq Hprt1(Mean WT}-\text{Mean Tg)}}$ [32]. Quantitative reverse transcription PCR (RT-qPCR) data were analyzed using the GenEX5 program (http://www.multid.se/genex/). Primer sets for *Myo7a* and *prestin* used are from Xia et al. [33], and *Hprt1* primers are from Bohuslavova et al. [34]. Primer sequences are listed in Table S1.

Transgene Copy Number Estimation by qPCR

The copy number of transgene was estimated as described previously [35]. Briefly, qPCR reactions were first performed on serial dilutions of genomic DNA from tail biopsies to identify an appropriate amount of DNA template for experimental reactions and primer efficiencies. Primers were designed to amplify sequences from *Isl1* exon 3 and a reference gene, *Hprt1* (Table S1). Primer sets were designed using Primer 3 software (http://frodo.wi.mit.edu/primer3/). Primers were selected according to the following parameters: length between 18 and 24 bases, melting temperature (Tm) 60 °C, and G+C content between 40 and 60 % (optimal 50 %). Genomic DNA from six mice of each genotype was diluted to use 20 ng/20-μl reactions. qPCR was performed as described above. Reactions were run on gels to confirm that primers amplified only a single product. Threshold cycles (Cp) were normalized to *Hprt1*, of which two copies are present in both WT and *Tg* DNA. ΔCq was calculated for each sample ($\text{Cq}_{Hprt1}-\text{Cq}_{Isl1}$). Fold change of a target transgene was calculated using $\Delta\Delta$Cq method as described [32, 35].

Statistical Analysis

A one-way or two-way analysis of variance (ANOVA) was used to investigate statistically significant differences (significance assigned at the $P<0.05$ level; GraphPad, 2005; San Diego, USA). The differences between WT and $Tg^{+/-}$ in behavior tests, in survival, qPCR and ChAT expression data were analyzed by Student's *t* test (significance assigned at the $P<0.05$ level; GraphPad, 2005; San Diego, USA).

Results

Decreased Survival of Pax2-Isl1 Transgenic Mice

The *Pax2-Isl1* transgenic mice [Tg*(Pax2-Isl1)*] were generated using a transgenic construct containing *Isl1* gene insert and the 8.5-kb *Pax2* regulatory sequences with regulatory activities in the midbrain-hindbrain region and otic vesicle, which closely mimic the activities of the endogenous *Pax2* gene at E9.5 (Fig. 1a). We produced six different founder lines of [Tg(*Pax2-Isl1*)], which carried the *Pax2-Isl1* transgene. We observed a decreased postnatal survival of transgenic heterozygous pups and abnormal circling behavior in all six transgenic lines. One transgenic line was selected for a detailed functional analysis. In order to estimate the number of transgene copies integrated into the genome, we used quantitative PCR to amplify *Isl1* from tail DNA from WT and heterozygous transgenic ($Tg^{+/-}$) littermates. The transgene copy number was 2 (data not shown). $Tg^{+/-}$ mice exhibited increased levels of motor hyperactivity, including augmented locomotion and circling behavior compared to WT littermates (Fig. 1b–e; supplemental files: movie S1, S2). The average velocity of $Tg^{+/-}$ mice was 2.8-fold higher compared to WT ($P<0.001$; Fig. 1d). The average distance traveled in 2 min was 10±0.9 and 3.9±0.2 m for $Tg^{+/-}$ and WT, respectively ($P<0.01$; Fig. 1e).

Mating produced a lower number of transgenic offspring at weaning than the expected Mendelian frequencies. The number of surviving offspring at weaning from WT and $Tg^{+/-}$ intercrosses was 89 WT and 52 $Tg^{+/-}$ pups in 27 litters. The average number of surviving transgenic heterozygous offspring per litter (1.926±0.2871, $n=27$) was significantly

lower compared to their WT littermates (3.296±0.3988; Fig. 1f). We noticed a decreased survival rate of the $Tg^{+/-}$ pups within 24 h after birth compared to their WT littermates. Death that occurs immediately at birth or within 24 h after birth is neonatal death. Neonatal death is not always the direct consequence of a primary defect but rather the extreme manifestation of a physiological problem secondary to a primary defect [28]. We did not notice any abnormal gross appearance in the pups, such as morphological defects or hemorrhages. However, these pups were found outside their nest, rejected by the mother and unable to feed, which could be associated with neuromuscular defects or/and absence or diminished vocalization of newborns. Neuromuscular defects may involve many structures of the brain, nerves, as well as the muscles and can result in respiratory failure or abnormal feeding. Suckling, like breathing, is regulated by the brain stem and involves motor neuronal pathways. Defects affecting breathing often also affect suckling activity. The survival of pups outside of a nest and exposed to hypothermia is even shorter than that of nested non-suckling newborns. The absence of vocalization or diminished vocalization of newborns could result in rejection by the mother due to her inability to recognize the babies.

Transgenic Expression of Pax2-Isl1 Causes Enlargement of the ISL1$^+$ Domain in the Otocyst at E10.5 and Faster Nerve Fiber Extension and Branching at E12.5

To establish the *Isl1* expression pattern in the otocyst of $Tg^{+/-}$ compared to WT mice, we analyzed the expression of ISL1 at E10.5 embryos. The ISL1$^+$ expression domain was enlarged in the $Tg^{+/-}$ otocysts. The size of the cochlear-vestibular ganglion delaminating from the otic epithelium and differentiating into ganglion neurons was increased in $Tg^{+/-}$ embryos compared to WT littermates (Fig. 2a, b). Likewise, the size of ISL1$^+$ domain was significantly enlarged in $Tg^{+/-}$ compared to WT littermates, likely reflecting the effects of transgenic *Isl1* expression (Fig. 2c). To date, we have been unable to produce homozygotes due to the hyperactivity of the transgenic males. However, using another founder line of [Tg(*Pax2-Isl1*)] with one transgene copy and a lower motor hyperactive phenotype, transgenic homozygous embryos showed severe abnormalities in the mid-hindbrain region and signs of developmental arrest at E10.5 (Fig. S1), similar to other *Pax2* mutants [36].

We injected lipophilic dyes into the cerebellum (Fig. 2d, e) or the ear (Fig. 2f, g) in order to analyze the nerve fiber extension and branching in E12.5 embryos. The saccule is the first to differentiate and extends to the brainstem and cerebellum. More branching is seen in the saccule, and more fibers going to the posterior canal can be observed in $Tg^{+/-}$ compared to WT mice (Fig. 2d, e). Ear injections revealed more fibers extending earlier already into the cerebellum in the transgenic embryos (Fig. 2f, g). Cochlea projections were not investigated as they just reach the brainstem at this stage [37]. Thus, increased expression levels of *Isl1* in mutant embryos were associated with more rapid differentiation of afferents.

Impaired Hearing Function of Pax2-Isl1 Transgenic Mice

We used DPOAE measurements to assess the function of OHCs in the cochlea. The age-related decline of DPOAE amplitudes started from the high-frequency region in both WT and $Tg^{+/-}$ groups. However, the loss of DPOAEs was much more rapid in $Tg^{+/-}$ animals. The DPOAE amplitudes at 32–40 kHz were reduced in 1-month-old $Tg^{+/-}$ compared to WT animals. This decline progressed with age. Five-month-old $Tg^{+/-}$ animals had significantly smaller DPOAE amplitudes at the majority of tested frequencies (8–25 kHz) and a complete loss of DPOAEs at 32–40 kHz compared to WT mice (Fig. 3a). $Tg^{+/-}$ mice completely lost DPOAEs by the age of 6–9 months (Fig. 3c), while DPOAEs of WT mice were only slightly decreased at high frequencies at this age and were still present at the middle frequencies in 15-month-old animals (Fig. 3e).

Differences in ABR hearing thresholds corresponded with changes in DPOAEs. Young mutant mice (1–5 months) had significantly higher ABR thresholds at 32 kHz than WT mice (Fig. 3b). However, the ABR thresholds of 6- to 9-month-old $Tg^{+/-}$ mice were significantly higher in overall frequency range with the smallest difference of 10 dB at 40 kHz and the highest of 35 dB at 16 kHz (Fig. 3d). The hearing thresholds of mutant mice at this age underwent the largest shift detected during the experiment (Fig. S2D). The hearing thresholds of $Tg^{+/-}$ animals at 8 and 16 kHz were the most affected by aging, and they shifted by 35 and 45 dB, respectively, when the youngest and the oldest tested groups were compared. In contrast, the shift in hearing thresholds during the aging of WT animals was more uniform over the whole frequency range. It did not differ by more than 22 dB between the youngest and oldest tested groups at any of the tested frequencies (Fig. S2C).

Cellular and Molecular Changes in Auditory Hair Cells

The nature and dynamics of functional changes (DPOAEs, hearing thresholds) in mutant mice suggest primary abnormalities in OHC function. To characterize the OHC state, we analyzed the OHC number, spatial organization, and expression of prestin, F-actin, and myosin 7a (Myo7a) using cochlear whole mount preparation. The spatial organization of hair cells was unaltered in transgenic mice. Hair cells were arranged in three OHC rows and one row of inner hair cells (IHCs) in both experimental groups of animals. We did not notice any visible differences between the young $Tg^{+/-}$ and WT animals in the hair cell stereocilia visualized by phalloidin

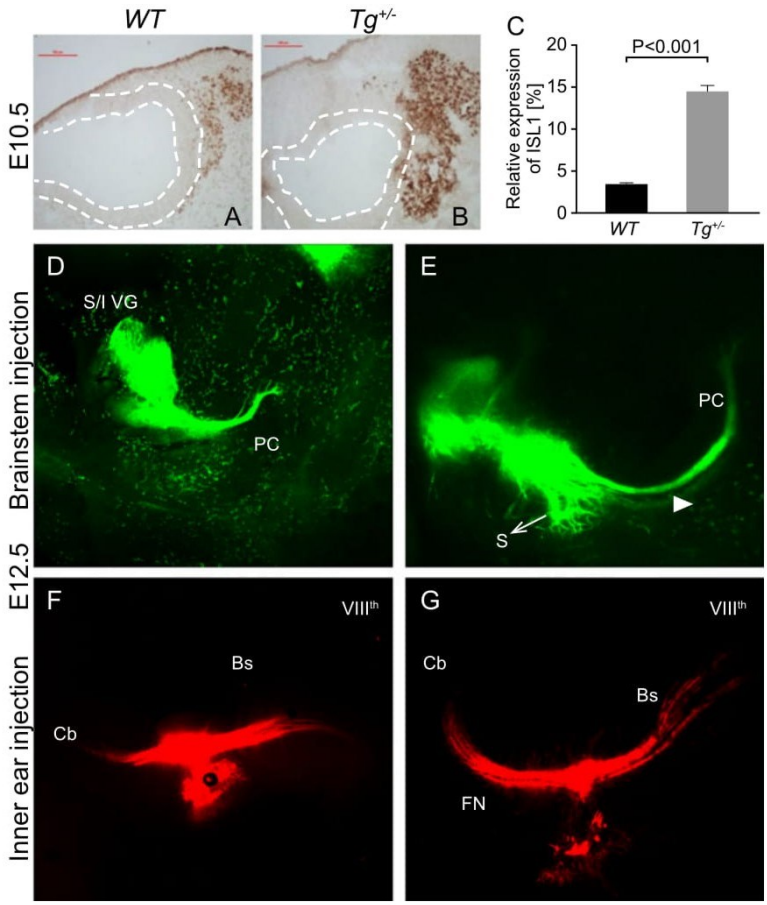

Fig. 2 ISL1 expression in the otocyst at E10.5 and nerve fiber extension in E12.5 embryos. **a**, **b** Transverse sections of embryos stained with anti-ISL1 antibody. Mutant embryos show increased ISL1 expression compared to WT at E10.5. The *dashed lines* indicate the borders of the otic epithelium. *Scale bar* 0.1 mm. **c** $ISL1^+$ area quantified as a percentage of total tissue area in the field using the ImageJ software. The values are means± SEM (n=5 for WT, n=3 for $Tg^{+/-}$; t test). **d**–**g** The lipophilic dye tracing of fiber extension and branching in E12.5 embryos (*false color green*, brainstem injection) shows more branching in the saccule and more fibers going through the posterior canal in $Tg^{+/-}$ (**e**) compared to WT embryos (**d**). The inner ear injection (*false color red*) shows more fibers going to the cerebellum in the $Tg^{+/-}$ (**g**) than in WT embryos (**f**). *S* saccule, *VG* vestibular ganglion, *Cb* cerebellum, *Pc* posterior canal, *Bs* brain stem

staining (Fig. 4a, b). In the oldest group of animals (11 months and older), $Tg^{+/-}$ mice demonstrated a greater degree of disorganization and loss of OHC stereocilia in the high-frequency cochlear region than WT animals (Fig. 4d, e). The hair cell marker, Myo7a, did not reveal any visible differences between the hair cells of WT and $Tg^{+/-}$ animals in all age groups (Fig. 4g, h). The number of present and missing cells in each 7 % of cochlear length was counted and the loss of OHCs was plotted as a cochleogram (Fig. 4c, f, i). Missing OHCs were rare in the cochleae of both experimental groups at P3 and P15. However, we detected OHC loss in 1- to 5-month-old animals averaging 24 % in WT and 37 % in $Tg^{+/-}$ animals (Fig. 4c, insert). The predominant OHC loss was detected in high-frequency regions and was lower in low-frequency regions. OHCs were the most preserved in the middle part of the cochlea in animals of all age groups. However, we detected a significantly higher loss of OHCs in the high-frequency region of the cochlea (above 30 kHz) in young transgenic mice compared to WT (Fig. 4c). While OHC loss extended from the high-frequency region to the direction of lower frequency regions in older $Tg^{+/-}$ and WT animals (6–9, 10–15 months; Fig. 4f, i, inserts), OHC loss was significantly higher in $Tg^{+/-}$ animals. However, the progression of OHC loss with age was the same for both groups with the difference of 13–14 % between WT and $Tg^{+/-}$ mice. The number of IHCs did not change along the whole cochlear length in most animals from both groups across age. However, we observed some IHC degeneration in the high-frequency region of the cochlea (30 kHz and above) in 11-month-old $Tg^{+/-}$ animals when the OHCs were completely lost.

Although mutant mice had a significantly higher loss of OHCs compared to WT animals, it does not fully explain the complete loss of DPOAEs by the age of 6–9 months. This suggests a loss of OHC function despite the continuing presence of the vast majority of OHCs in the cochleae of $Tg^{+/-}$ 6- to 9-month-old mice. In order to better understand this loss of function, we analyzed the expression and distribution of motor protein prestin in the OHCs of WT and transgenic mice (Fig. 5). The distribution of prestin did not differ between experimental groups. Prestin was localized in the cell wall from approximately the mid-nuclear level to the level of the cuticular plate on top of the cell (Fig. 5c, d) and corresponded to other published reports. The mRNA levels of *prestin* quantified by RT-qPCR were significantly lower in $Tg^{+/-}$ cochlea

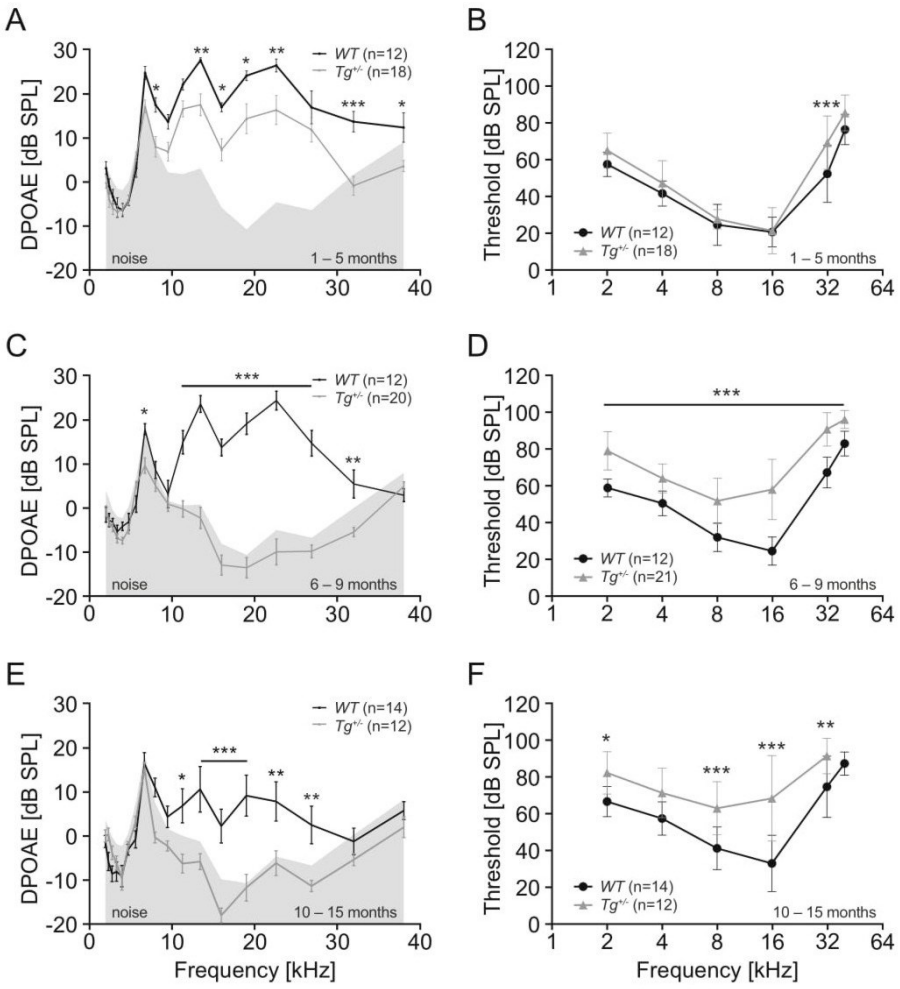

Fig. 3 Deteriorated distortion product otoacoustic emissions (*DPOAEs*) and hearing thresholds (*ABRs*) in transgenic mice. Results of hearing tests presented as DPOAE-grams (**a**, **c**, **e**) and audiograms (**b**, **d**, **f**) demonstrate significantly lower DPOAEs levels in 1- to 5-month-old $Tg^{+/-}$ animals (**a**) and complete loss of DPOAEs in 6- to 9-month-old $Tg^{+/-}$ mice (**c**). In contrast in WT mice, DPOAE levels only decrease in older animals and are still present in 10- to 15-month-old mice (**e**). Changes in ABR thresholds confirm changes in DPOAEs being significantly increased in 6- to 15-month-old $Tg^{+/-}$ compared to the WT mice of the same age (**d**, **f**). Results are means±SEM for DPOAEs and means±SD for hearing threshold. *P<0.05, **P<0.01, ***P<0.001, two-way ANOVA with the Bonferroni correction test

than in WT at 1 month of age (Fig. 5h), whereas the expression of *prestin* did not differ between WT and $Tg^{+/-}$ cochlea in P3 and in older mice (7- to 11-month-old mice; Fig. 5g, i).

Changes in Cochlear Innervation

Because we detected an increased branching of nerve fibers in E12.5 transgenic embryos, we examined the state of the cochlear innervation after birth. Compared to WT animals at P3, radial fibers of $Tg^{+/-}$ mice at 40–70 kHz were not organized in tight bundles (Fig. 6). We did not find noticeable changes in radial innervation in older animals (data not shown).

In the next step, we examined the peripheral part of the medial olivocochlear (MOC) system. The volume of MOC terminals was significantly reduced in $Tg^{+/-}$ compared to WT in all age groups (Fig. 7a, c, g, i, m). $Tg^{+/-}$ animals showed progressive age-related deterioration of the MOC terminals with a 30 % volume reduction in 10 to 15 months old compared to the younger $Tg^{+/-}$ group (Fig. 7c, i). In both $Tg^{+/-}$ and WT animals, the loss of OHCs was accompanied by the degeneration of the efferent terminals related to the missing cells (Fig. 7g, i, stars). The volume of $ChAT^{+}$ particles in the DC region was also decreased in $Tg^{+/-}$ (Fig. 7b, d, h, j, n). However, no progressive age-related decrease was detected in the $ChAT^{+}$ area in DCs of both WT and $Tg^{+/-}$ groups (Fig. 7n).

The MOC efferents originate in the medial portion of the superior olivary complex and project to OHCs. Since we detected degenerative changes in the MOC terminals at the base of OHCs, we additionally analyzed the postnatal expression of the *Pax2-Isl1* transgene in these olivary neurons prior to hearing. We found ISL1 expressed in $PAX2^{+}$ cells in the area of the superior olivary complex in the brain of P8 $Tg^{+/-}$ (Fig. 8b, f–h). There was no ISL1 expression in the WT littermates (Fig. 8a, c–e). Thus, the

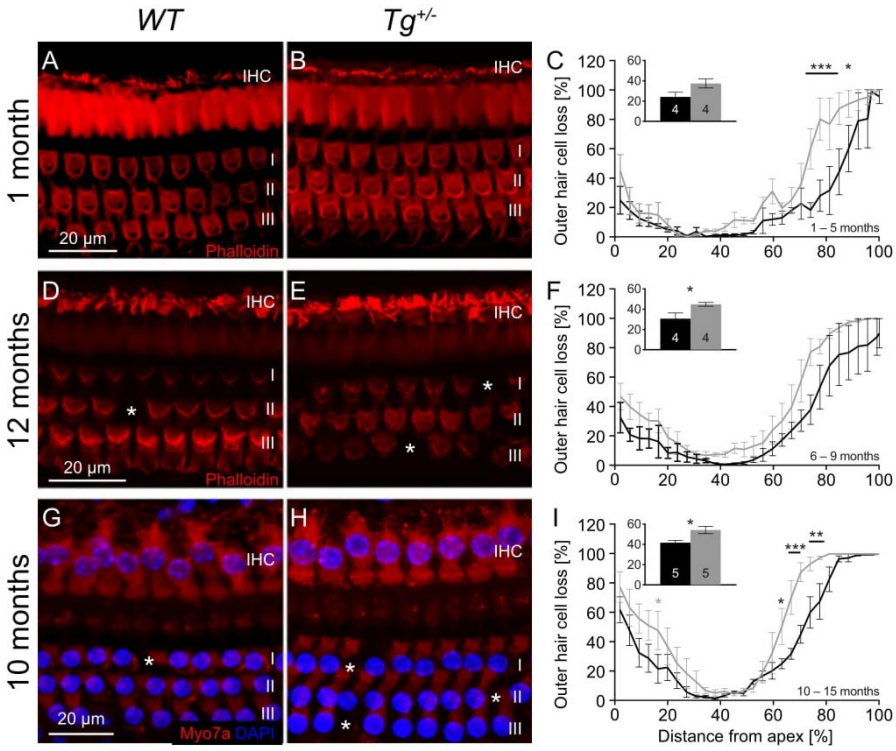

Fig. 4 Loss of high-frequency OHCs in $Tg^{+/-}$ mice with no evident alteration of HC morphology. HCs appear to be normal when visualized using phalloidin and anti-Myo7a antibodies (**a**, **b**, **d**, **e**, **g**, **h**). Moderate disorganization of OHC cilia is noticeable in 12-month-old $Tg^{+/-}$ mice (**e**). A decreased number of OHCs is already detected in 1- to 5-month-old animals, mainly in the high-frequency region of the cochlea (**c**), and the same trend continues in older animals (**f**, **i**). However, the progression of OHC loss with age is the same with the difference of 13–14 % between WT and $Tg^{+/-}$ mice for all ages (**c**, **f**, **i**, *inserts*), suggesting a similar level of OHC loss progression with age for both groups. Stars indicate missing OHCs.Values are presented as means±SEM; $*P<0.05$, $**P<0.01$, $***P<0.001$, one-way ANOVA with the Bonferroni correction test. *IHC* inner hair cells; *OHC* outer hair cells; *I, II, III* 3 rows of OHCs

misexpression of ISL1 might negatively affect the development and function of MOC neurons.

Changes in Cell Number in the Spiral Ganglion

Spiral ganglion neuron (SGN) degeneration is a function of age as shown in mice [38] and also in humans [39]. We observed no significant reduction in the number of SGNs in WT animals in any analyzed age group (Fig. 9c). In contrast, $Tg^{+/-}$ mice showed an age-related reduction in the number of SGNs (Fig. 9d) in the middle turn (from $6.932\times10^5/mm^3$ in young to $5.872\times10^5/mm^3$ in old mice, $P\leq0.001$) and the basal turn (from $5.945\times10^5/mm^3$ in young to $4.765\times10^5/mm^3$ in old mice, $P\leq0.001$). It is interesting that the premature loss of SGNs in the middle cochlear turn of $Tg^{+/-}$ corresponded with a significant shift in ABR thresholds at 8–16 kHz. No statistically significant loss of SGNs was detected in the basal turn of $Tg^{+/-}$ animals up to 10 months of age (Fig. 9d). However, the total number of SGNs in all cochlear turns was significantly smaller in $Tg^{+/-}$ animals compared to WT mice in all age groups (Fig. S3).

Discussion

In this study, we have examined the functional role of ISL1 in the development and maintenance of auditory sensory cells and neurons in the inner ear. We hypothesized that modulating ISL1 expression will change the fate specification of cells in the inner ear. *Pax2*-regulated *Isl1* overexpression increases the embryonic $ISL1^+$ domain and the size of the cochleovestibular ganglion in the inner ear at E10.5. It also induces premature nerve fiber extension and branching in E12.5 embryos. Despite these gains in early development, it has detrimental long-term effects on the maintenance and function of the organ of Corti hair cells.

Pax2 is one of the earliest genes to be expressed in the preotic region [40] but slightly after *Foxg1* [41]. PAX2 is a key regulator of otic cell identity, and shape in chick [42] and PAX2 combined with PAX8 is needed for mouse ear development [7]. PAX2 is required for the expression of otic transcription factors and for cell adhesion molecules, which in turn are necessary for epithelial integrity and subsequent placode invagination. In the mouse, PAX2 is expressed in all

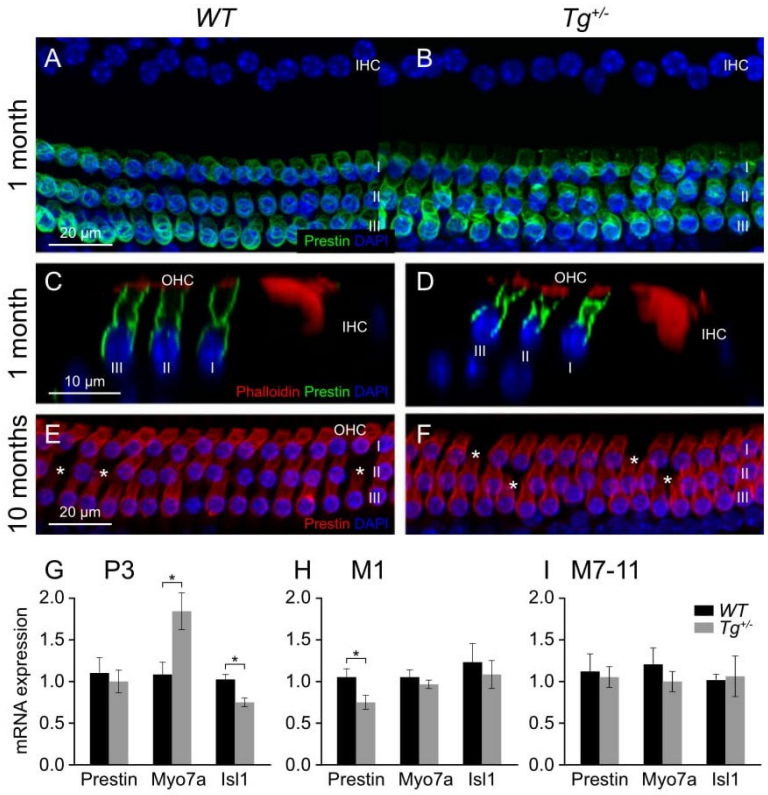

Fig. 5 Preserved prestin distribution and decreased levels of prestin mRNA in OHCs. Prestin location and distribution inside OHCs is not different between WT and $Tg^{+/-}$ mice and is not affected by aging (**a**–**f**). RT-qPCR analysis shows lower prestin levels of mRNA in 1-month-old $Tg^{+/-}$ mice compared to WT (**h**; n=6 mice/genotype). No significant differences in prestin expression are detected in P3 (**g**; n=5 $Tg^{+/-}$ and 7 WT) or M7-11-month-old cochlea (**i**; n=5 mice/genotype). Stars indicate missing OHCs.Values are presented as means±SEM; *P<0.05, t test. *IHC* inner hair cells; *OHC* outer hair cells; *I, II, III* 3 rows of OHCs

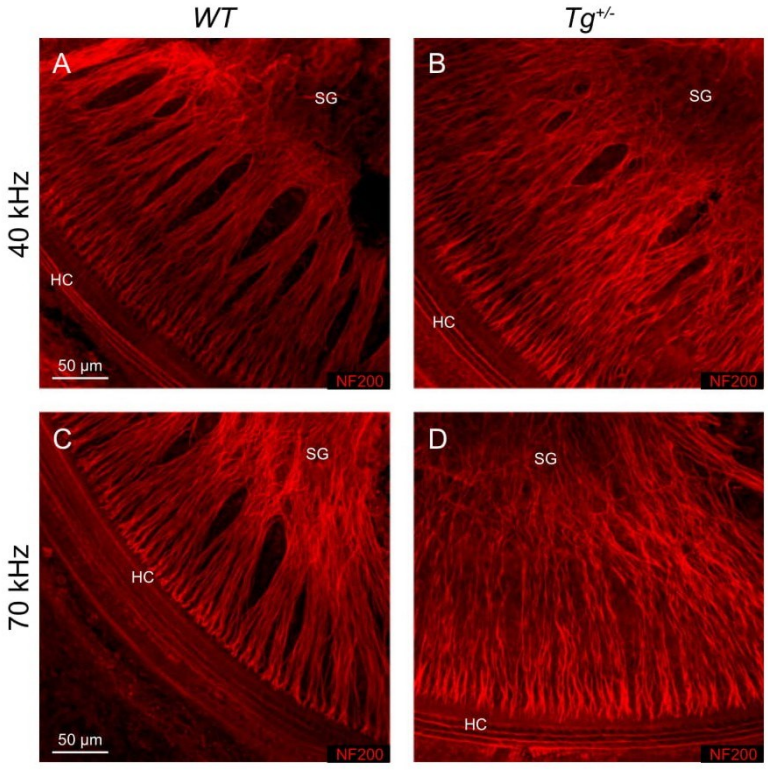

Fig. 6 Altered radial innervations. Spatial organization of radial fibers (NF200) in the basal part of the cochlea (40 kHz and above) is altered in $Tg^{+/-}$ mice at P3 (**b**, **d**) compared to *WT* littermates (**a**, **c**)

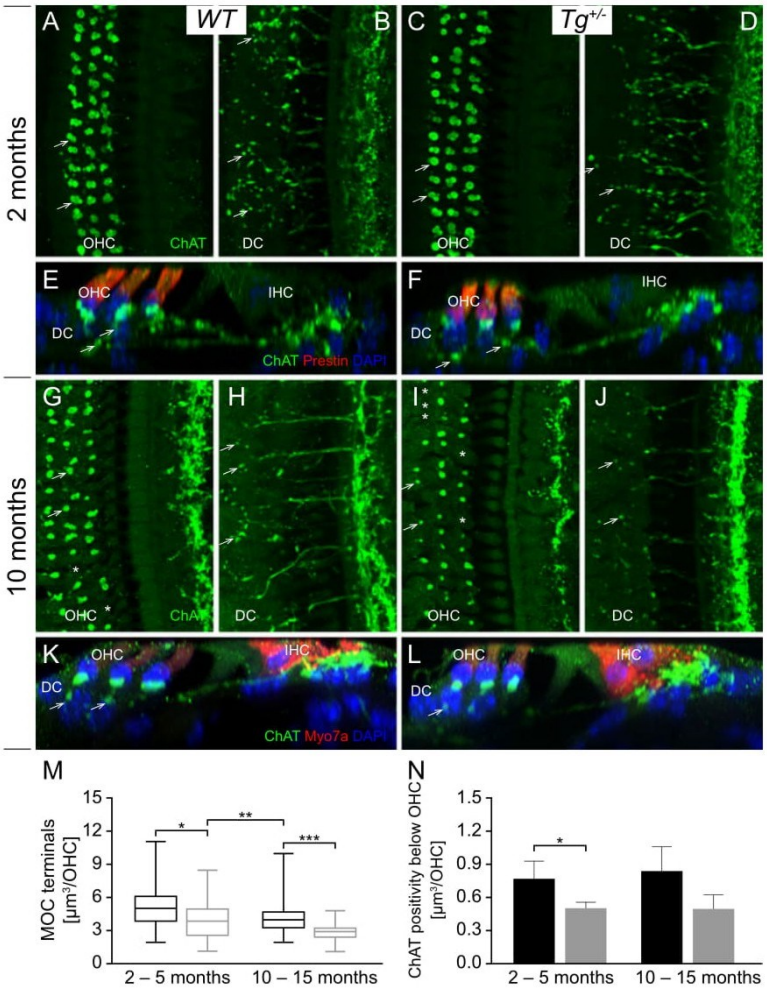

Fig. 7 Altered efferent innervations. Despite visible similarities, the quantitative analysis shows a decrease in the volume of MOC terminals of OHCs (**a**, **c**, arrows; quantified in **m**) and efferent vesiculated fibers in the region of Deiters' cells (**b**, **d**, arrows; quantified in **n**) in young $Tg^{+/-}$ mice (**i**, **m**) than in WT animals (**g**, **m**). The progressive loss of efferent fibers is visible in older $Tg^{+/-}$ (**j**) compared to WT (**h**). In both WT and $Tg^{+/-}$ groups, efferent endings are missing if the OHC is lost (**g**, **i**; stars). Side view (**e**, **f**, **k**, **l**) represents the maximum projection of a focal series through the thickness of one OHC, arrows here and in **b**, **d**, **h**, **j** point out ChAT positive particles in the region of Deiters' cells. Values are median with 25% and 75% percentiles (**m**) and means ± SEM; *$P<0.05$, **$P<0.01$, ****$P<0.0001$, *t* test. *IHC* inner hair cells, *OHC* outer hair cells, *DC* Deiters' cells

sensory and some non-sensory epithelia, but within sensory epithelia at E16.5, it is restricted to hair cells [43]. Although PAX2 is expressed in differentiating hair cells, mature murine hair cells do not express PAX2 protein. In *Pax2* null mouse, cochlear outgrowth is delayed and pattern of the cochlear sack and its innervation is heavily impaired [7]. A rudimentary cochlea sack of *Pax2* knockout inner ears lacks the spiral ganglion and contains a few scattered neuron-like cells. Thus, *Pax2* affects the regional patterning of the early otocyst and cellular patterning within the sensory epithelia of the inner ear.

Pax2-Isl1 transgenic mice were created on the basis of FVB strain, which is a mouse strain with a normal pattern of age-related hearing deterioration. Our results of hearing evaluation in the FVB strain are comparable to previous reports [44, 45] that show completely preserved DPOAEs up to at least 5 months of age and the minor ABR threshold shift of 20 dB in 14-month-old animals compared to 1-month-old mice. In contrast, $Tg^{+/-}$ mice displayed a significant functional hearing deficit already at the youngest analyzed group (1–5 months). The first signs of age-related sensory hearing loss are associated with the decrease of DPOAE amplitudes at the high-frequency cochlear region [46]. Although the initial changes in DPOAE amplitudes in this region were detected in 6- to 9-month-old WT mice, the premature decline in DPOAEs in the high-frequency region was already found in the youngest $Tg^{+/-}$ group. $Tg^{+/-}$ mice completely lost DPOAEs by the age of 6–9 months, whereas 10–15-month-old WT animals still had apparent otoacoustic emissions in the middle frequency region.

DPOAEs reflect the cochlear amplification facilitated by OHCs [47, 48]. Usually, a decrease of DPOAE amplitudes relates to the loss of OHCs [47, 48] or the decline in their function [49, 50]. Accordingly, we detected a higher OHC loss in the high-frequency region of the cochlea in 1- to 5-month-old $Tg^{+/-}$ mice compared to WT. Interestingly, we also found disorganized radial fibers that did not form regular bundles in the high-frequency basal cochlear region of P3 $Tg^{+/-}$ animals. At 40–70-kHz range, fibers were not or were only

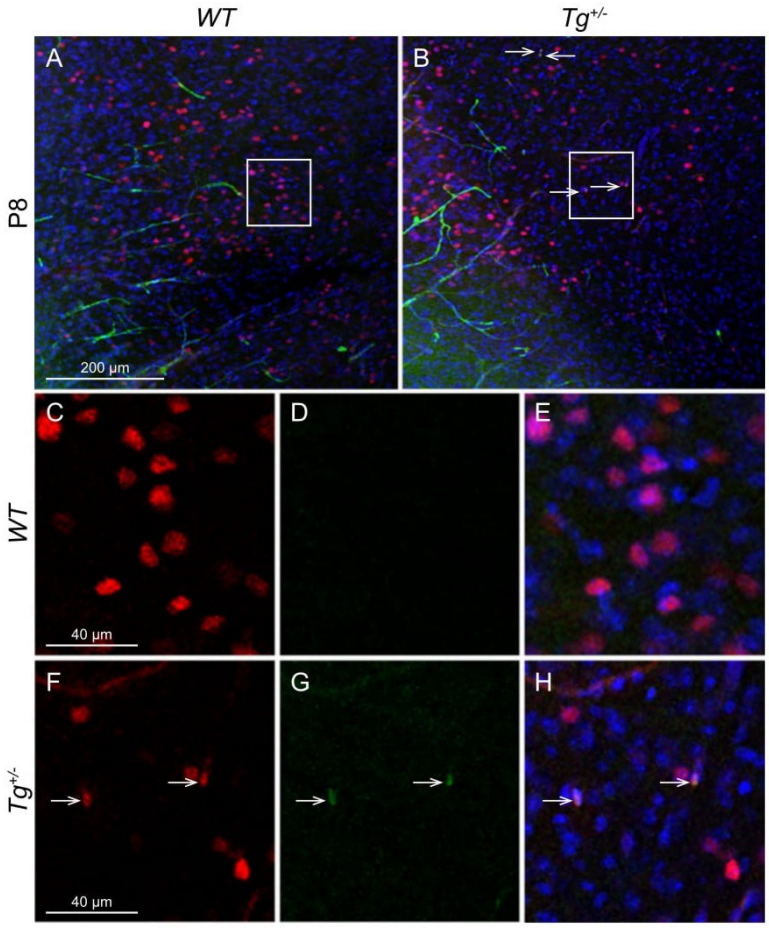

Fig. 8 ISL1 expression in the transgenic brainstem at P8. The immunostaining of neurons in the area of superior olivary complex in the brainstem with antibodies for PAX2 (*red*) and ISL1 (*green*) shows PAX2 and ISL1 co-expression in neurons in $Tg^{+/-}$ (**b**; *arrows*) but not in WT (**a**). *Boxed areas* are shown at a higher magnification, WT (**c**–**e**) and $Tg^{+/-}$ (**f**–**h**). Hoechst 33342 (*blue*) was used as a nuclear counterstain

rarely organized in radial fiber bundles (Fig. 6b, d). Within this broad sheet of fibers, several could be traced to cross obliquely to other bundles, something that is nearly impossible in radial bundles. The topological innervation of a given position of the organ of Corti is the neuronal basis for the tonotopic map reported for both afferents and efferents. How much such disorganization will affect the precision of the tonotopic map and whether it is restricted to afferents or efferents require single fiber recordings. The higher loss of OHCs in $Tg^{+/-}$ animals could be associated only with the loss of DPOAEs at high frequencies (32–40 kHz), whilst the number of OHCs in the middle frequency region of $Tg^{+/-}$ cochleae did not differ significantly from that in WT animals. Since the complete absence of DPOAEs could not be explained by the loss of OHCs, another possibility for the loss of cochlear amplification in $Tg^{+/-}$ might be an impaired function of OHCs.

Cochlear amplification is thought to be of two main sources: somatic, caused by prestin motility [51, 52], and streocilia based [53, 54]. Prestin is a motor protein located in the OHC lateral wall, and it is responsible for the OHC motility. Homozygous mice with targeted deletion of prestin gene showed a 40- to 60-dB loss of cochlear sensitivity across all frequencies [52], which represents a standard threshold shift in the case of the absent OHC motility. This corresponds to hearing loss found in our study. Although we found a moderate reduction in prestin mRNA expression in $Tg^{+/-}$ cochlea in 1-month-old mice compared to WT littermates, no significant changes in prestin mRNA levels were detected in older animals (7–11 months). We noticed no obvious difference in the prestin distribution in the OHCs between WT and $Tg^{+/-}$ animals. The analysis of stereocilia of the OHCs revealed that the stereocilia in 1- to 9-month-old $Tg^{+/-}$ and WT animals did not differ. We found more profound disorganized OHC stereocilia in 11-month-old and older $Tg^{+/-}$ animals than in WT, which points to the accelerated age-related degeneration of transgenic OHCs [55]. Thus, the premature and severe DPOAE loss in $Tg^{+/-}$ animals was unlikely due to prestin abnormalities or the deterioration of stereocilia.

Cochlear amplification facilitated by OHCs is highly dependent on the correct ionic environment in the scala media conditioned by the stria vascularis. The correct ionic balance is required for proper function of both, inner and outer HCs. In

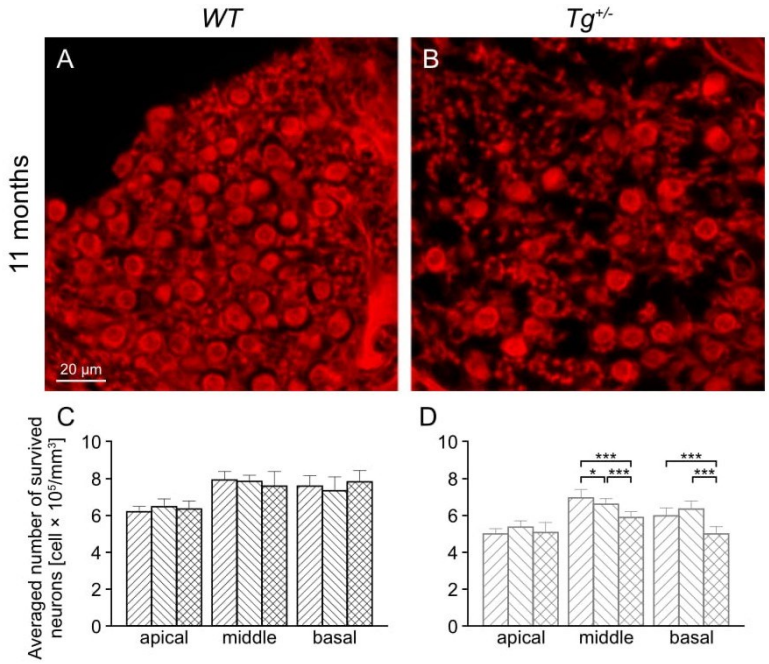

Fig. 9 Loss of spiral ganglion neurons in transgenic cochleae. The number of spiral ganglion neurons (SGNs) is preserved in all cochlear turns in WT mice in all ages (**a**, **c**). In contrast, a progressive age-related loss of SGNs is found in the middle cochlear turn of $Tg^{+/-}$ mice (**d**). A significant loss of SGNs is also noticeable in the oldest tested group of $Tg^{+/-}$ mice (**b**, **d**). Values are presented as means±SD; *$P<0.05$, ***$P<0.001$, one-way ANOVA with the Bonferroni correction test

our study, ABR threshold shift correlated with changes in DPOAEs in $Tg^{+/-}$ mice, suggesting that worsening of hearing thresholds was mainly due to the loss of cochlear amplification and that the function of IHCs remained preserved. Based on this, we can assume that the function of the stria vascularis in $Tg^{+/-}$ mice was not affected.

The MOC efferent innervation is important for the maintenance and function of OHCs. The activation of the MOC system enhances auditory processing of distracting noise [56–58], and it may thus protect the inner ear from acoustic trauma [59–61]. MOC terminals are the endings of the efferent fibers, which make OHCs hyperpolarized when activated. The MOC efferents originate in the superior olivary complex and enable modulation of the auditory periphery by higher auditory centers in the brain. We detected ISL1 misexpression in the neurons in the region of the superior olivary complex of $Tg^{+/-}$ mice, which may affect the formation of MOC efferent neurons. The reduced or altered MOC $Tg^{+/-}$ efferents may contribute to the reduction of MOC terminals and accelerate the deterioration of OHC function in mutant mice. Similarly, a surgical de-efferentation accelerates the age-related deterioration of DPOAEs without an extensive loss of OHCs [62]. The reduction in the MOC-negative-feedback-gain-control may also explain the particular deterioration in the hearing thresholds of $Tg^{+/-}$ animals at 16 kHz since this region has the maximal density of MOC terminals [63].

Although the main targets for the MOC pathway are OHCs, it has been shown that certain supporting cells (Deiter's cells; DCs), also receive efferent innervations [64] and are sensitive to acetylcholine in vitro [65]. The proper function of DCs is necessary for OHC electromotility. DCs are located between the basilar membrane and the reticular lamina, and their phalangeal processes create a scaffold for OHCs [66]. It is believed that DCs act as a transducer that transfers the force generated by OHC electromotility to the underlying basilar membrane [67]. In vitro analysis shows that electrical and mechanical stimulations of DCs or manipulation with the gap junctions between DCs can affect OHC electromotility [68]. Recent studies with mutant mice showed the crucial role of DCs in active cochlear amplification in vivo. For example, the deletion of connexin 26 in DCs and outer pillar cells reduces cochlear amplification and DPOAEs [69] or *Vangl2* conditional knockout mice changes the shape and distribution of outer pillar cell and DC phalangeal processes with the reduction in otoacoustic emissions [41]. The ablation of the pillar cells and DCs negatively affects OHCs [70]. Although we have not detected any loss of DCs (nuclear staining) in $Tg^{+/-}$ animals, the loss of $ChAT^{+}$ swellings of vesiculated efferent fibers in $Tg^{+/-}$ animals may affect DC function and, consequently, the function of OHCs.

Conclusions

In summary, our data show progressive hearing loss of $Tg^{+/-}$ mice starting at 1 month of age. This decline is particularly obvious in DPOAE reduction followed by a corresponding elevation of hearing thresholds. Functional and morphological

deterioration starts from the basal part of the cochlea. However, the largest functional changes occur at the 16-kHz area (see tonotopic map of Mueller). The timing of DPOAE reduction coincides with the appearance of visible signs of cochlear efferent innervation alterations. $Tg^{+/-}$ MOC terminals decrease in volume by 36 % compared to controls. In contrast to the effects of efferents, we only find a moderate loss of OHCs (Fig. 4) and SG neurons (Fig. 9) in $Tg^{+/-}$ cochlea. These results are in line with recent research suggesting that cochlear efferents sustain the long-term viability of hair cells and cochlear function [62]. ISL1 is highly expressed in developing motoneurons [14] and efferents are derived from facial branchial motoneurons [71]. It is possible that PAX2, known to be expressed in the hindbrain where efferents form, can affect the normal development of efferents and, as a side effect, the long-term viability of hair cells and overall hearing performance. Likewise *Pax2*-driven ISL1 overexpression alters the development of efferents and, consequently, the maintenance of OHCs and hearing functions. Because neuronal degeneration is the common predisposing factor for the pathology of age-related neurodegenerative diseases, this possibility is worth exploring. Our data provide the first evidence that the alternation of MOC efferent system accelerates the age-related functional decline of hearing without the loss of OHCs.

Acknowledgments We thank Z. Hampejsova for the experimental work on transgene copy estimation. This work was supported by the Czech Science Foundation (Grant Agreement No. 13-07996S), by BIOCEV CZ.1.05/1.1.00/02.0109 from the ERDF, "Biotechnological expert" CZ.1.07/2.3.00/30.0020 from the European Social Fund and the state budget of the Czech Republic, and by Grant No. AVOZ50520701 from the Czech Ministry of Education, Youth and Sports.

Conflict of Interest The authors declare that they have no competing interests.

References

1. Chen J, Streit A (2013) Induction of the inner ear: stepwise specification of otic fate from multipotent progenitors. Hear Res 297:3–12. doi:10.1016/j.heares.2012.11.018
2. Ma Q, Anderson DJ, Fritzsch B (2000) Neurogenin 1 null mutant ears develop fewer, morphologically normal hair cells in smaller sensory epithelia devoid of innervation. J Assoc Res Otolaryngol 1(2):129–143
3. Matei V, Pauley S, Kaing S, Rowitch D, Beisel KW, Morris K, Feng F, Jones K et al (2005) Smaller inner ear sensory epithelia in Neurog 1 null mice are related to earlier hair cell cycle exit. Dev Dyn 234(3):633–650
4. Raft S, Groves AK (2014) Segregating neural and mechanosensory fates in the developing ear: patterning, signaling, and transcriptional control. Cell Tissue Res. doi:10.1007/s00441-014-1917-6
5. Kelley MW (2006) Regulation of cell fate in the sensory epithelia of the inner ear. Nat Rev Neurosci 7(11):837–849
6. Fritzsch B, Beisel KW, Hansen LA (2006) The molecular basis of neurosensory cell formation in ear development: a blueprint for hair cell and sensory neuron regeneration? Bioessays 28(12):1181–1193
7. Bouchard M, de Caprona D, Busslinger M, Xu P, Fritzsch B (2010) Pax2 and Pax8 cooperate in mouse inner ear morphogenesis and innervation. BMC Dev Biol 10:89. doi:10.1186/1471-213X-10-89
8. Kiernan AE, Pelling AL, Leung KK, Tang AS, Bell DM, Tease C, Lovell-Badge R, Steel KP et al (2005) Sox2 is required for sensory organ development in the mammalian inner ear. Nature 434(7036):1031–1035
9. Jahan I, Pan N, Kersigo J, Fritzsch B (2013) Beyond generalized hair cells: molecular cues for hair cell types. Hear Res 297:30–41. doi:10.1016/j.heares.2012.11.008
10. Nichols DH, Pauley S, Jahan I, Beisel KW, Millen KJ, Fritzsch B (2008) Lmx1a is required for segregation of sensory epithelia and normal ear histogenesis and morphogenesis. Cell Tissue Res 334(3):339–358. doi:10.1007/s00441-008-0709-2
11. Deng M, Luo XJ, Pan L, Yang H, Xie X, Liang G, Huang L, Hu F et al (2014) LMO4 functions as a negative regulator of sensory organ formation in the mammalian cochlea. J Neurosci 34(30):10072–10077. doi:10.1523/JNEUROSCI.0352-14.2014
12. Bhati M, Lee C, Nancarrow AL, Lee M, Craig VJ, Bach I, Guss JM, Mackay JP et al (2008) Implementing the LIM code: the structural basis for cell type-specific assembly of LIM-homeodomain complexes. EMBO J 27(14):2018–2029. doi:10.1038/emboj.2008.123
13. Hobert O, Westphal H (2000) Functions of LIM-homeobox genes. Trends Genet 16(2):75–83
14. Pfaff SL, Mendelsohn M, Stewart CL, Edlund T, Jessell TM (1996) Requirement for LIM homeobox gene Isl1 in motor neuron generation reveals a motor neuron-dependent step in interneuron differentiation. Cell 84(2):309–320
15. Sun Y, Dykes IM, Liang X, Eng SR, Evans SM, Turner EE (2008) A central role for Islet1 in sensory neuron development linking sensory and spinal gene regulatory programs. Nat Neurosci 11(11):1283–1293. doi:10.1038/nn.2209
16. Lin L, Bu L, Cai CL, Zhang X, Evans S (2006) Isl1 is upstream of sonic hedgehog in a pathway required for cardiac morphogenesis. Dev Biol 295(2):756–763
17. Cai CL, Liang X, Shi Y, Chu PH, Pfaff SL, Chen J, Evans S (2003) Isl1 identifies a cardiac progenitor population that proliferates prior to differentiation and contributes a majority of cells to the heart. Dev Cell 5(6):877–889
18. Elshatory Y, Everhart D, Deng M, Xie X, Barlow RB, Gan L (2007) Islet-1 controls the differentiation of retinal bipolar and cholinergic amacrine cells. J Neurosci 27(46):12707–12720. doi:10.1523/jneurosci.3951-07.2007
19. Whitney IE, Raven MA, Ciobanu DC, Poche RA, Ding Q, Elshatory Y, Gan L, Williams RW et al (2011) Genetic modulation of horizontal cell number in the mouse retina. Proc Natl Acad Sci U S A 108(23):9697–9702. doi:10.1073/pnas.1103253108
20. Liang X, Song MR, Xu Z, Lanuza GM, Liu Y, Zhuang T, Chen Y, Pfaff SL et al (2011) Isl1 is required for multiple aspects of motor neuron development. Mol Cell Neurosci 47(3):215–222. doi:10.1016/j.mcn.2011.04.007
21. Li H, Liu H, Sage C, Huang M, Chen ZY, Heller S (2004) Islet-1 expression in the developing chicken inner ear. J Comp Neurol 477(1):1–10
22. Radde-Gallwitz K, Pan L, Gan L, Lin X, Segil N, Chen P (2004) Expression of Islet1 marks the sensory and neuronal lineages in the mammalian inner ear. J Comp Neurol 477(4):412–421
23. Huang M, Sage C, Li H, Xiang M, Heller S, Chen ZY (2008) Diverse expression patterns of LIM-homeodomain transcription factors (LIM-HDs) in mammalian inner ear development. Dev Dyn 237(11):3305–3312. doi:10.1002/dvdy.21735
24. Fritzsch B, Pan N, Jahan I, Elliott KL (2014) Inner ear development: building a spiral ganglion and an organ of Corti out of unspecified ectoderm. Cell Tissue Res. doi:10.1007/s00441-014-2031-5

25. Zheng QY, Johnson KR, Erway LC (1999) Assessment of hearing in 80 inbred strains of mice by ABR threshold analyses. Hear Res 130(1-2):94–107
26. Rowitch DH, Kispert A, McMahon AP (1999) Pax-2 regulatory sequences that direct transgene expression in the developing neural plate and external granule cell layer of the cerebellum. Brain Res Dev Brain Res 117(1):99–108
27. Muller YL, Yueh YG, Yaworsky PJ, Salbaum JM, Kappen C (2003) Caudal dysgenesis in Islet-1 transgenic mice. Faseb J 17(10):1349–1351
28. Turgeon B, Meloche S (2009) Interpreting neonatal lethal phenotypes in mouse mutants: insights into gene function and human diseases. Physiol Rev 89(1):1–26. doi:10.1152/physrev.00040.2007
29. Kersigo J, D'Angelo A, Gray BD, Soukup GA, Fritzsch B (2011) The role of sensory organs and the forebrain for the development of the craniofacial shape as revealed by Foxg1-cre-mediated microRNA loss. Genesis 49(4):326–341. doi:10.1002/dvg.20714
30. Bolte S, Cordelieres FP (2006) A guided tour into subcellular colocalization analysis in light microscopy. J Microsc 224(Pt 3): 213–232. doi:10.1111/j.1365-2818.2006.01706.x
31. Alvarez-Buylla A, Ling CY, Kirn JR (1990) Cresyl violet: a red fluorescent Nissl stain. J Neurosci Methods 33(2-3):129–133
32. Pfaffl MW (2001) A new mathematical model for relative quantification in real-time RT-PCR. Nucleic Acids Res 29(9), e45
33. Xia A, Song Y, Wang R, Gao SS, Clifton W, Raphael P, Chao SI, Pereira FA et al (2013) Prestin regulation and function in residual outer hair cells after noise-induced hearing loss. PLoS One 8(12), e82602. doi:10.1371/journal.pone.0082602
34. Bohuslavova R, Kolar F, Kuthanova L, Neckar J, Tichopad A, Pavlinkova G (2010) Gene expression profiling of sex differences in HIF1-dependent adaptive cardiac responses to chronic hypoxia. J Appl Physiol (1985) 109(4):1195–1202. doi:10.1152/japplphysiol.00366.2010
35. Schoen CJ, Burmeister M, Lesperance MM (2013) Diaphanous homolog 3 (Diap3) overexpression causes progressive hearing loss and inner hair cell defects in a transgenic mouse model of human deafness. PLoS One 8(2), e56520. doi:10.1371/journal.pone.0056520
36. Favor J, Sandulache R, Neuhauser-Klaus A, Pretsch W, Chatterjee B, Senft E, Wurst W, Blanquet V et al (1996) The mouse Pax2(1Neu) mutation is identical to a human PAX2 mutation in a family with renal-coloboma syndrome and results in developmental defects of the brain, ear, eye, and kidney. Proc Natl Acad Sci U S A 93(24):13870–13875
37. Fritzsch B (2003) Development of inner ear afferent connections: forming primary neurons and connecting them to the developing sensory epithelia. Brain Res Bull 60(5-6):423–433
38. Dazert S, Feldman ML, Keithley EM (1996) Cochlear spiral ganglion cell degeneration in wild-caught mice as a function of age. Hear Res 100(1-2):101–106
39. Makary CA, Shin J, Kujawa SG, Liberman MC, Merchant SN (2011) Age-related primary cochlear neuronal degeneration in human temporal bones. J Assoc Res Otolaryngol 12(6):711–717. doi:10.1007/s10162-011-0283-2
40. Hans S, Liu D, Westerfield M (2004) Pax8 and Pax2a function synergistically in otic specification, downstream of the Foxi1 and Dlx3b transcription factors. Development 131(20):5091–5102. doi:10.1242/dev.01346
41. Copley CO, Duncan JS, Liu C, Cheng H, Deans MR (2013) Postnatal refinement of auditory hair cell planar polarity deficits occurs in the absence of Vangl2. J Neurosci 33(35):14001–14016. doi:10.1523/JNEUROSCI.1307-13.2013
42. Christophorou NA, Mende M, Lleras-Forero L, Grocott T, Streit A (2010) Pax2 coordinates epithelial morphogenesis and cell fate in the inner ear. Dev Biol 345(2):180–190. doi:10.1016/j.ydbio.2010.07.007
43. Lawoko-Kerali G, Milo M, Davies D, Halsall A, Helyer R, Johnson CM, Rivolta MN, Tones MA et al (2004) Ventral otic cell lines as developmental models of auditory epithelial and neural precursors. Dev Dyn 231(4):801–814
44. Martin GK, Vazquez AE, Jimenez AM, Stagner BB, Howard MA, Lonsbury-Martin BL (2007) Comparison of distortion product otoacoustic emissions in 28 inbred strains of mice. Hear Res 234(1-2): 59–72. doi:10.1016/j.heares.2007.09.002
45. Jones JM, Montcouquiol M, Dabdoub A, Woods C, Kelley MW (2006) Inhibitors of differentiation and DNA binding (Ids) regulate Math1 and hair cell formation during the development of the organ of Corti. J Neurosci 26(2):550–558
46. Schuknecht HF (1964) Further observations on the pathology of presbycusis. Arch Otolaryngol 80:369–382
47. Hofstetter P, Ding D, Powers N, Salvi RJ (1997) Quantitative relationship of carboplatin dose to magnitude of inner and outer hair cell loss and the reduction in distortion product otoacoustic emission amplitude in chinchillas. Hear Res 112(1-2):199–215
48. Trautwein P, Hofstetter P, Wang J, Salvi R, Nostrant A (1996) Selective inner hair cell loss does not alter distortion product otoacoustic emissions. Hear Res 96(1-2):71–82
49. Li D, Henley CM, O'Malley BW Jr (1999) Distortion product otoacoustic emissions and outer hair cell defects in the hyt/hyt mutant mouse. Hear Res 138(1-2):65–72
50. Popelar J, Groh D, Pelanova J, Canlon B, Syka J (2006) Age-related changes in cochlear and brainstem auditory functions in Fischer 344 rats. Neurobiol Aging 27(3):490–500. doi:10.1016/j.neurobiolaging.2005.03.001
51. Dallos P, Wu X, Cheatham MA, Gao J, Zheng J, Anderson CT, Jia S, Wang X et al (2008) Prestin-based outer hair cell motility is necessary for mammalian cochlear amplification. Neuron 58(3): 333–339. doi:10.1016/j.neuron.2008.02.028
52. Liberman MC, Gao J, He DZ, Wu X, Jia S, Zuo J (2002) Prestin is required for electromotility of the outer hair cell and for the cochlear amplifier. Nature 419(6904):300–304. doi:10.1038/nature01059
53. Chan DK, Hudspeth AJ (2005) Ca2+ current-driven nonlinear amplification by the mammalian cochlea in vitro. Nat Neurosci 8(2): 149–155. doi:10.1038/nn1385
54. Kennedy HJ, Crawford AC, Fettiplace R (2005) Force generation by mammalian hair bundles supports a role in cochlear amplification. Nature 433(7028):880–883. doi:10.1038/nature03367
55. Adams JC, Schulte BA (1997) Histopathologic observations of the aging gerbil cochlea. Hear Res 104(1-2):101–111
56. Kawase T, Liberman MC (1993) Antimasking effects of the olivocochlear reflex. I Enhancement of compound action potentials to masked tones. J Neurophysiol 70(6):2519–2532
57. May BJ, McQuone SJ (1995) Effects of bilateral olivocochlear lesions on pure-tone intensity discrimination in cats. Audit Neurosci 1(4):385–400
58. Winslow RL, Sachs MB (1987) Effect of electrical stimulation of the crossed olivocochlear bundle on auditory nerve response to tones in noise. J Neurophysiol 57(4):1002–1021
59. Lauer AM, May BJ (2011) The medial olivocochlear system attenuates the developmental impact of early noise exposure. J Assoc Res Otolaryngol 12(3):329–343. doi:10.1007/s10162-011-0262-7
60. Liberman MC (1991) The olivocochlear efferent bundle and susceptibility of the inner ear to acoustic injury. J Neurophysiol 65(1):123–132
61. Maison SF, Luebke AE, Liberman MC, Zuo J (2002) Efferent protection from acoustic injury is mediated via alpha9 nicotinic acetylcholine receptors on outer hair cells. J Neurosci 22(24):10838–10846
62. Liberman MC, Liberman LD, Maison SF (2014) Efferent feedback slows cochlear aging. J Neurosci 34(13):4599–4607. doi:10.1523/JNEUROSCI.4923-13.2014
63. Maison SF, Adams JC, Liberman MC (2003) Olivocochlear innervation in the mouse: immunocytochemical maps, crossed versus

uncrossed contributions, and transmitter colocalization. J Comp Neurol 455(3):406–416. doi:10.1002/cne.10490
64. Burgess BJ, Adams JC, Nadol JB Jr (1997) Morphologic evidence for innervation of Deiters' and Hensen's cells in the guinea pig. Hear Res 108(1-2):74–82
65. Matsunobu T, Chung JW, Schacht J (2001) Acetylcholine-evoked calcium increases in Deiters' cells of the guinea pig cochlea suggest alpha9-like receptors. J Neurosci Res 63(3):252–256
66. Parsa A, Webster P, Kalinec F (2012) Deiters cells tread a narrow path—the Deiters cells-basilar membrane junction. Hear Res 290(1-2):13–20. doi:10.1016/j.heares.2012.05.006
67. Nam JH, Fettiplace R (2010) Force transmission in the organ of Corti micromachine. Biophys J 98(12):2813–2821. doi:10.1016/j.bpj.2010.03.052
68. Yu N, Zhao HB (2009) Modulation of outer hair cell electromotility by cochlear supporting cells and gap junctions. PLoS One 4(11), e7923. doi:10.1371/journal.pone.0007923
69. Zhu Y, Liang C, Chen J, Zong L, Chen GD, Zhao HB (2013) Active cochlear amplification is dependent on supporting cell gap junctions. Nat Commun 4:1786. doi:10.1038/ncomms2806
70. Mellado Lagarde MM, Cox BC, Fang J, Taylor R, Forge A, Zuo J (2013) Selective ablation of pillar and Deiters' cells severely affects cochlear postnatal development and hearing in mice. J Neurosci 33(4):1564–1576. doi:10.1523/JNEUROSCI.3088-12.2013
71. Simmons DJD, de Caprona DC, Fritzsch B (2011) Development of the inner ear efferent system. In: Auditory and vestibular efferents, vol 38. Springer, New York. doi:10.1007/978-1-4419-7070-1_7

Pax2-Islet1 Transgenic Mice Are Hyperactive and Have Altered Cerebellar Foliation

Romana Bohuslavova[1] · Nicole Dodd[1] · Iva Macova[1] · Tetyana Chumak[2] · Martin Horak[3] · Josef Syka[2] · Bernd Fritzsch[4] · Gabriela Pavlinkova[1]

Received: 7 September 2015 / Accepted: 12 January 2016 / Published online: 3 February 2016

Abstract The programming of cell fate by transcription factors requires precise regulation of their time and level of expression. The LIM-homeodomain transcription factor Islet1 (Isl1) is involved in cell-fate specification of motor neurons, and it may play a similar role in the inner ear. In order to study its role in the regulation of vestibulo-motor development, we investigated a transgenic mouse expressing *Isl1* under the *Pax2* promoter control ($Tg^{+/-}$). The transgenic mice show altered level, time, and place of expression of Isl1 but are viable. However, $Tg^{+/-}$ mice exhibit hyperactivity, including circling behavior, and progressive age-related decline in hearing, which has been reported previously. Here, we describe the molecular and morphological changes in the cerebellum and vestibular system that may cause the hyperactivity of $Tg^{+/-}$ mice. The transgene altered the formation of folia in the cerebellum, the distribution of calretinin labeled unipolar brush cells, and reduced the size of the cerebellum, inferior colliculus, and saccule. Age-related progressive reduction of calbindin expression was detected in Purkinje cells in the transgenic cerebella. The hyperactivity of $Tg^{+/-}$ mice is reduced upon the administration of picrotoxin, a non-competitive channel blocker for the γ-aminobutyric acid (GABA) receptor chloride channels. This suggests that the overexpression of Isl1 significantly affects the functions of GABAergic neurons. We demonstrate that the overexpression of Isl1 affects the development and function of the cerebello-vestibular system, resulting in hyperactivity.

Keywords Islet1 transcription factor · Vestibular system · Cerebellum · Foliation defects · Hyperactivity · GABA signaling · Transgenic mouse · Purkinje cells · Calcium homeostasis · Age-related deterioration of Purkinje cells · Attention deficit hyperactivity disorder

Introduction

The vestibular system of the ear provides a major input for balance [1]. Hair cells located within the five vestibular epithelia (the utricle, the saccule, and the lateral, superior, and posterior semicircular canal cristae) receive and convert stimuli in the three cardinal planes into electric signals [2]. The extracted information reaches the ipsilateral vestibular nucleus complex (VCN) in the brainstem and cerebellum [3, 4] via bipolar neurons, which form the vestibular part of the eighth cranial nerve. The region of the cerebellum that communicates most intimately with the vestibular system is the vestibulocerebellum, receiving afferents primarily from the vestibular ganglion and vestibular nuclei [4]. The cerebellum also receives proprioceptive input [5] and is part of a motor control loop to modify cortical signals for smooth, integrated movements [6] of the extraocular and skeletal muscles [7, 8]. The vestibular and proprioceptive signals are further processed and integrated together with other sensory, motor, and associative signals in the striatum, a central brain area for motor control (reviewed in [9]). The motor output pathways are regulated by

Electronic supplementary material The online version of this article (doi:10.1007/s12035-016-9716-6) contains supplementary material, which is available to authorized users.

✉ Gabriela Pavlinkova
gpavlinkova@ibt.cas.cz

[1] Institute of Biotechnology CAS, Prumyslova 595, Vestec, Prague-West District 25242, Czech Republic

[2] Institute of Experimental Medicine CAS, Prague, Czech Republic

[3] Institute of Physiology CAS, Prague, Czech Republic

[4] Department of Biology, University of Iowa, Iowa City, IA, USA

the cerebellum and the striatum [9]. A connection between inner ear dysfunction, behavioral disorders such as hyperactivity and circling phenotype, and the striatum has recently been shown [10].

The insulin gene enhancer protein Islet1 (Isl1), a LIM-homeodomain transcription factor, contains two LIM domains which act as protein–protein interaction motifs and a homeodomain for recognizing and binding to specific DNA sequences, the primary structure of which is highly conserved among species. The combinations of LIM-homeodomain proteins form a transcriptional "LIM code" required for the specification and maintenance of different cell types during development [11, 12]. A LIM code is particularly well characterized for the developmental program of motor neurons [11, 13]. A LIM code defines the subtypes of motor neurons with the ability to select distinct axonal pathways, to recognize specific targets in the periphery, and to regulate viability. Isl1 is required for the differentiation and survival of motor neurons [14–16]. Isl1 is also essential for the development of striatonigral neurons [17, 18], and Isl1 expression in the ear suggests a role in cell lineage specification and differentiation of prosensory progenitors [16, 19, 20] possibly in interaction with other LIM-homeodomain factors [12]. The precise function of Isl1 in the development of the inner ear and the vestibular system-mediated motor coordination is unknown due to the early lethality of *Isl1* null mutants.

To further understand the function of Isl1, we used an overexpression model of *Isl1* under the *Pax2* regulatory sequence to explore the gain-of-function role of *Isl1* in the developing cerebellar and vestibular system. *Pax2* is one of the earliest genes to be expressed in the pre-otic region [21] and the midbrain/hindbrain region, giving rise to the cerebellum [22, 23]. Pax2 is a key regulator of otic cell identity and placode morphogenesis [24], and Pax2 combined with Pax8 is essential for mouse ear development with Pax2 playing a major role in cochlea development [25]. Pax2 is also involved in the specification of the midbrain/hindbrain region [26] including the formation of the cerebellum [23, 27]. *Pax2* expression at E7.5 initiates the partitioning of the midbrain/hindbrain region. Starting at E13.5, *Pax2* is expressed in prospective γ-aminobutyric acid (GABA) interneuron precursors in the cerebellar cortex, which sequentially generate different types of inhibitory interneurons according to an inside out progression: first are GABAergic neurons in the cerebellar nuclei, then Golgi and Lugaro cells in the granular layer, and finally basket and stellate cells in the molecular layer [28]. *Pax2* expression is downregulated when these interneurons mature and establish functional synaptic contacts with their targets [23].

Previously, we showed Isl1 to play a role in auditory system maintenance [29]. The transgenic expression of *Isl1* under *Pax2* regulatory sequences impaired the maintenance and function of hair cells of the organ of Corti with an early onset of age-related hearing loss, reflected in reduced otoacoustic emissions and the deterioration of the medial olivocochlear efferent system derived from facial motoneurons [30]. Additionally, the mutant mice exhibited increased levels of motor hyperactivity, including augmented locomotion and circling behavior, compared to *WT* littermates. In the current study, we present data showing that *Isl1* overexpression also causes some aberrant development of the vestibular system and the central nervous system, in particular the cerebellum, which may relate to hyperactivity.

Materials and Methods

Generation of Transgenic Mice

The use of animals in this study was conducted in accordance with the Guide for the Care and Use of Laboratory Animals (NIH Publication No. 85-23, revised 1996). All animal procedures were approved by the Animal Care and Use Committee of the Institute of Molecular Genetics, Academy of Sciences of the Czech Republic, and all efforts were made to minimize suffering. The experimental mice were housed in a controlled environment (23 °C, 12 h light/dark cycle) with free access to water and standard chow diet. All experiments were performed with both male and female littermate mice that were either wild-type or heterozygous *Pax2-Isl1* transgenic mice [Tg(*Pax2-Isl1*)Gp300] ($Tg^{+/-}$) on an FVB (*WT*) background (strain code 207, Charles River). $Tg^{+/-}$ mice were generated as described previously [29]. Genotyping was carried out from tail DNA by PCR using 5′ primer (located in *Pax2* regulatory element), 5′-AAG TTG AGT TTG AGA GGC GAC ACG-3′, and 3′ primer (located in *Isl1* gene), 5′-TTG GCG CAT TTG ATC CCG TAC AAC-3′ yielding a 400-bp amplicon. PCR was preformed over 35 cycles at 95 °C for 30 s, 63 °C for 30 s, and 72 °C for 30 s. The amplification products were run on agarose gels and visualized by ethidium bromide staining.

Immunohistochemistry

Mice were perfused with 4 % paraformaldehyde (PFA), and temporal bones were dissected and fixed in 4 % PFA for 30 min. Sensory organs were dissected in phosphate-buffered saline (PBS) and decalcified in 0.12 M ethylendiaminotetraacetic acid. For brain dissections, the mice were first perfused with 4 % PFA and brains were stored overnight at 4 °C in 4 % PFA. The brains were sectioned in the sagittal plane at 80 μm/section using a vibratome and transferred free-floating into microplates containing 0.4 % PFA. The sections were defatted in 70 % ethanol for a minimum of 1 h and blocked with 2.5 % normal goat serum in PBS with 0.5 % Tween20 for 1 h. For histological analyses, dissected tissues were fixed with 4 % PFA in PBS (pH 7.4) at 4 °C overnight, dehydrated, and embedded in paraffin.

Paraffin-embedded brains were cut in 7-μm sections, and tissue sections were stained with hematoxylin and eosin. The following dilutions of antiserum were used for immunohistochemistry: anti-Islet1 (no. 39.4D5, Developmental Hybridoma Bank, Iowa City, IA, USA) 1:200, anti-myosin 7a (Myo7a, no. 028918, Sigma-Aldrich) 1:500, anti-Pax2 (no. PRB-276P, Covance) 1:100, anti-acetylated tubulin (no. T6793, Sigma-Aldrich) 1:400, anti-calretinin (no. sc-50453, Santa Cruz Biotechnology) 1:100, anti-neurofilament 200 (NF200, no. N4142, Sigma-Aldrich) 1:200, and anti-calbindin (no. C9848, Sigma-Aldrich) 1:250. The vibratome sections and whole mount samples were incubated with primary Ab for 72 h at 4 °C. Following several washing steps with PBS, the corresponding secondary antibodies (Alexa dyes 1:400, Jackson ImmunoResearch Laboratories) were added and incubated overnight at 4 °C. The sections and whole mounts were counter-stained with Hoechst stain, mounted with antifade mounting medium, and viewed using Zeiss 510 DUO laser confocal (sections), confocal Leica SPE (whole mount, sections), or fluorescent stereomicroscope Leica MZFLIII (sections). Measurements of the whole cerebellar area and the percentage of calretinin staining quantification were performed using ImageJ software version 1.46r (National Institutes of Health, Bethesda, MD, USA). Three different sagittal sections were taken per sample, and percentage area and staining were taken between them. The quantification of saccular and utricular macula areas stained with anti-Myo7a antibody and number of $Myo7a^+$ cells per 100 μm^2 was done with ImageJ.

Lipophilic Dye-Tracing

Heads of the pups were removed and fixed for a minimum of 24 h in 4 % PFA. NeuroVue® dye-coated filter microstrips were cut to appropriate size pieces using microscissors and inserted into the brainstem and saccule nerve tracts and incubated at 60 °C for 4 days [31]. A two-color tracing system using NeuroVue® Maroon and Orange, which have 647 and 538 nm excitation, respectively, was applied. Progression of dye diffusion was monitored using fluorescent dissection scopes. On completion of dye diffusion, whole mounts of the inner ear and brain stem were prepared using glycerol and coverslips as spacers [32]. Images were taken using Leica confocal laser scanning system, and the stack of images was collapsed into a single plane. Images were organized into plates using Corel Draw.

Gene Expression Analysis by RT-qPCR

Total RNA was isolated from the cerebellum halves of 1-month-old mice using TRIzol® Reagent (Thermo Fisher Scientific Inc., Waltham, MA, USA). After removing genomic DNA by DNase I treatment (Thermo Fisher Scientific Inc., Waltham, MA, USA), RNA concentration and purity were determined using NanoDrop ND-1000 (Thermo Fisher Scientific Inc., Waltham, MA, USA). Isolated RNA (1 μg) was reverse transcribed into cDNA (RevertAid H Minus First Strand cDNA Synthesis Kit, Thermo Fisher Scientific Inc., Waltham, MA, USA). The obtained cDNA samples were diluted 20×. Each reaction for qPCR analysis contained 4 μl diluted cDNA, 5 μl SYBR Green JumpStart Taq ReadyMix for qPCR (Sigma-Aldrich, St. Louis, MO, USA), 0.5 μl ultrapure water, 0.25 μl 10 mM forward primer, and 0.25 μl 10 mM reverse primer. The primer sequences are listed in Table S1. qPCR was performed with the initial activation at 94 °C for 120 s, followed by 39 cycles at 94 °C for 15 s, 60 °C for 30 s, and 72 °C for 30 s using the CFX384™ Real-Time PCR Detection System (Bio-Rad Laboratories, Hercules, CA, USA). The $-\Delta\Delta Cq$ method was used to quantify the relative mRNA expression [33] with *Hprt1* as a reference gene [34]. The *Isl1* reaction products were analyzed using agarose gel electrophoresis. Equivalent aliquots of each amplification reaction were separated on a 2 % agarose gel containing 0.5 μg/ml ethidium bromide.

Behavior and Systemic Drug Testing

All testing was carried out during the light cycle. We only used 7–13-week-old males for all behavior tests. The mice were individually placed in a chamber (37 cm length × 20 cm width × 14.5 cm height) and allowed to acclimatize for 30 min before testing. To analyze locomotor activity in an open-field environment, the mice were recorded (Sony DCR-SX85Camcoder) in 9-s sequences during a 20-min period. Six movement sequences were analyzed per mouse. The average of the total distance traveled over a 2-min time period and the average velocity were quantified using the NIH ImageJ program with the Manual Tracking Plug-in (http://imagej.nih.gov/ij/download.html). The vestibular function was evaluated by the ability of the mice to right themselves in the air (air-righting reflex) when held supine and dropped onto a soft surface from a height of 50 cm [35]. The average percentage of trials of each mouse landing on all four feet from five attempts/mouse was determined.

Rotarod assays were performed using the rotarod apparatus (Rota Rod 47600, Ugo Basile) to assess fine motor coordination and balance [36, 37]. Briefly, during the acclimatization period, mice with their heads in the direction of rotation were loaded on the rotarod at an initial speed of 4 rpm. This speed was maintained for 2 min and, if mice fell during this period, they were placed back on the rotarod. For the experimental measurements, the drum was slowly accelerated to a speed of 4–40 rpm for a maximum of 300 s for each trial. The latency to fall off the rotarod within 300 s was recorded. If the mouse clung to the grip of the rotating drum and failed to resume normal performance for three consecutive revolutions, the

sensor was manually triggered. Mice were tested in three consecutive trials in one session per day with a 15-min rest period between each trial.

The baseline levels of open-field measurements for each mouse were compared the day before and after drug administration at indicated times. The drugs were injected intraperitoneally, and open-field activity was recorded after injection at indicated times. We used the dopaminergic antagonist haloperidol and a long-acting haloperidol decanoate (0.25 mg/kg, [10, 38]), the glutamatergic *N*-methyl-D-aspartate receptor antagonist ketamine (3 mg/kg, [39]), picrotoxin, a non-competitive channel blocker for the GABA receptor chloride channels (1 mg/kg, [40]), and α-lobeline, nicotine acetylcholine receptor antagonist (1 mg/kg [41]) at a volume of 10 μl/1 g of mouse weight in sterile buffered saline or sesame oil for haloperidol decanoate.

Auditory Brainstem Response Testing

For auditory brainstem response (ABR) recording, needle electrodes were placed subcutaneously on the vertex (active electrode) and in the neck muscles (ground and reference electrodes). The click-evoked responses were recorded (angular pulse with alternating polarity, duration 0.1 ms, repetition rate of 11 Hz). Acoustic stimuli were conveyed to the animal in free-field conditions via a two-way loudspeaker system (Jamo® woofer [Denmark] and SEAS® T25CF 002 tweeter [Norway]) placed 70 cm in front of the animal's head. The signal was processed with a TDT System III Pentusa Base Station and analyzed using BioSig™ (TX, USA) software. The ABR responses of five *WT* and five $Tg^{+/-}$ mice were recorded.

Statistical Analysis

The differences between *WT* and $Tg^{+/-}$ in behavior tests were tested using one-way ANOVA with Bonferroni's multiple comparison test and two-way repeated measures ANOVA; qPCR expression, Myo7, and calretinin data were analyzed by Student's *t* test (significance assigned at the $P<0.05$ level; GraphPad, 2005; San Diego, USA).

Results

Behavioral Changes in $Tg^{+/-}$ Mice

In all experiments, only heterozygous *Pax2-Isl1* transgenic mice ($Tg^{+/-}$) were analyzed. Homozygosity for the [Tg(Pax2-Isl1)] allele is associated with severe abnormalities in the mid-hindbrain region and signs of developmental arrest at E10.5 [29]. Although the heterozygous transgenic mice are viable, approximately 40 % of the $Tg^{+/-}$ pups do not survive the first 2 days of life, suggesting altered early postnatal development [29]. The surviving adult $Tg^{+/-}$ mice exhibited significant ($P<0.001$) increased levels of motor activity and circling behavior compared to *WT* littermates, suggesting defects in the vestibular system (Fig. 1a; supplemental files: movie M1 and M2). During open-field observations, the mutant mice did not display any rapid sideway wagging movements of the head, rapid vertical bobbing movements of the head, or any sustained tonic contractions or tremor of the limbs or trunk. Hyperactivity and the abnormal circling behavior of $Tg^{+/-}$ mice started with full maturity (approximately at 6 weeks of age) and intensified with increasing age. The mice consistently displayed a unidirectional circling preference of either left-circling or right-circling. The average movement velocity of $Tg^{+/-}$ mice was significantly higher (8.5 ± 0.3 cm/s; $n=6$) compared to *WT* (2.1 ± 0.1 cm/s; $n=6$, $P<0.0001$; Fig. 1a). The hyperactivity phenotype was associated with a lower body weight of $Tg^{+/-}$ mice (23.1 ± 0.49 g, $N=6$, 7 weeks) compared to *WT* (28.5 ± 0.70 g, $N=5$, $P<0.0001$, *t* test) despite free access to the same food. A basic test of vestibular function, the air-righting test, showed both $Tg^{+/-}$ and *WT* mice landed on their feet most of the time dropped supine out of 50 cm height onto a soft padding. An additional test to measure motor functions was performed on the rotarod (Fig. 1b). The performance of $Tg^{+/-}$ mice in the accelerating rotarod motor learning paradigm was superior to *WT* littermates. Repeated measures ANOVA showed a significant genotype effect ($P<0.0001$) and a significant session (time) effect ($P<0.0117$). Unexpectedly, the performance of $Tg^{+/-}$ mice improved with the training as in the second session of the motor learning $Tg^{+/-}$ mice reached the maximum testing time of 300 s in all trials with one exception of a shorter trial period of 220 s. Both tests assessing motor coordination and balance showed that $Tg^{+/-}$ mice were hyperactive without any demonstrable motor deficiencies. An increase in locomotor activity is therefore not necessarily related to a dysfunction of the inner ear but rather implies an alternation of brain functions [10]. Consistent with this concept that the abnormal locomotor phenotype may originate in the brain instead of the ear, picrotoxin, a non-competitive channel blocker for the GABA receptor chloride channels normalized the open-field hyperactive behavior of $Tg^{+/-}$ mice. After 30 and 180 min, the hyperactivity of $Tg^{+/-}$ mice was decreased by 61 and 55 %, respectively, compared to untreated $Tg^{+/-}$ ($P<0.001$; Fig. 1a, c; supplemental files: movie M1–4). The same dose of pictrotoxin did not significantly affect the locomotor activity in control littermates compared to untreated *control* mice. We tested the effects of glutamatergic *N*-methyl-D-aspartate receptor antagonist (ketamine), dopaminergic antagonist (haloperidol), and nicotine acetylcholine receptor antagonist (α-lobeline; Fig. 1c). In all behavioral tests, the difference in the average velocity between $Tg^{+/-}$ and *control* mice was significant in all treatment groups. However, treatment with

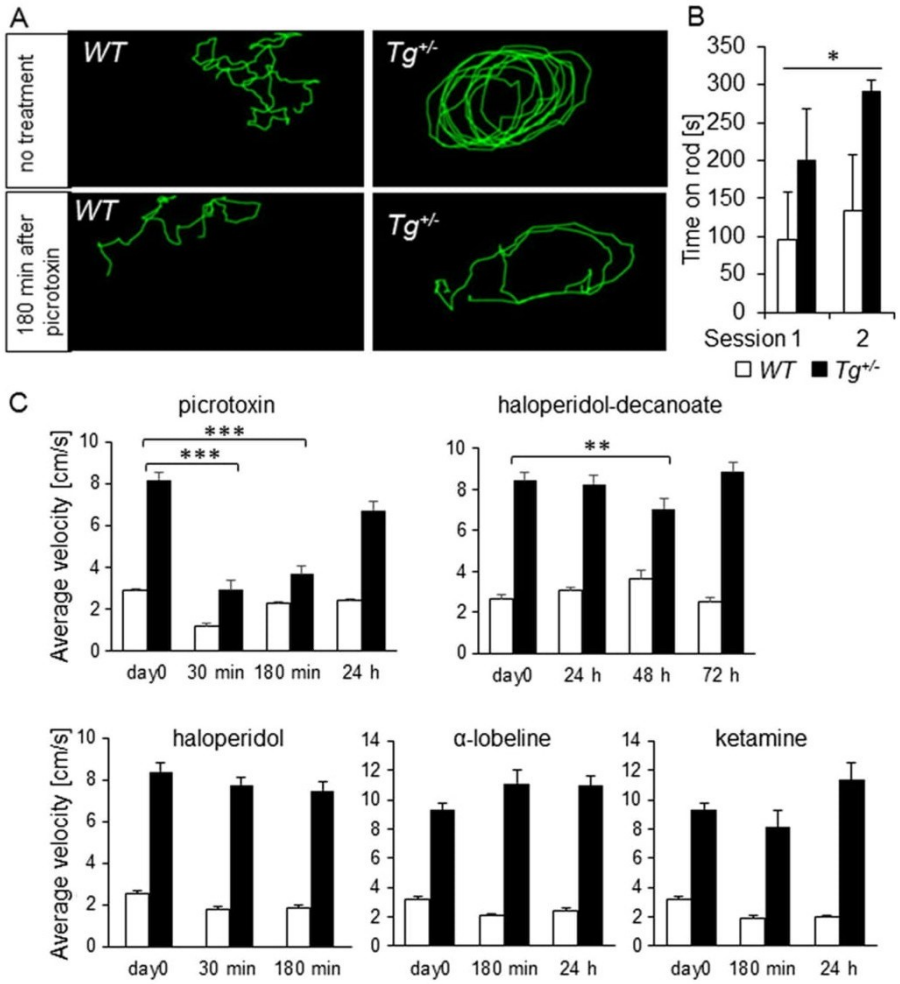

Fig. 1 Behavior tests in an open field. $Tg^{+/-}$ mice display GABA receptor-mediated increased locomotor activity. **a** Traces of locomotion in an open field show significant hyperactivity and circling of $Tg^{+/-}$ mice. **b** Motor coordination of *WT* ($n = 6$) and $Tg^{+/-}$ ($n = 3$) mice on the accelerating rotarod was analyzed in three trials/session (repeated measures ANOVA: genotype effect, $***P < 0.0001$; session effect, $*P < 0.0117$). The values represent means of three trials/session ± SEM. **c** Quantification of mouse locomotion in an open field showing that picrotoxin significantly reduced hyperactivity of mutants ($n = 6$ $Tg^{+/-}$, $n = 5$ *WT*) but did not correct circling. There was a significant alleviation of the locomotor activity of $Tg^{+/-}$ mice compared to *WT* after the application of haloperidol-decanoate at 48 h. Data represent mean ± SEM ($**P < 0.01$; $***P < 0.001$)

ketamine and α-lobeline had no effect on the hyperactivity of $Tg^{+/-}$ mice. Haloperidol, which acts in the brain to alleviate hyperactivity in humans, did not have a significant effect, although a moderate decrease of locomotor activity was noticeable (Fig. 1c). For a long-acting effect, we used haloperidol-decanoate that attenuated the hyperactivity in $Tg^{+/-}$ by 23 % compared to untreated $Tg^{+/-}$ at 48 h after the application ($P < 0.01$; Fig. 1c). The same dose of haloperidol did not significantly affect *WT* littermates at any time points. The systemic responsiveness to picrotoxin and to haloperidol indicates a disruption of brain functions that regulate movement in addition to the vestibular system dysfunction of $Tg^{+/-}$ mice. The apparent effects of picrotoxin, a non-competitive channel blocker of the GABA receptor chloride channels, suggest that the hyperactivity of transgenic mice is associated with altered GABA signaling. Although a trend of decreased activity after haloperidol treatment is evident, in comparison to picrotoxin, the effect of haloperidol on locomotor activity of $Tg^{+/-}$ mice is less prominent.

Changes in the Vestibular End Organs of $Tg^{+/-}$ Mice

To determine whether the behavioral disorders of $Tg^{+/-}$ could be associated with inner ear changes, we analyzed the vestibular end organs and patterns of innervation. The saccule is the first sensory epithelium to differentiate and connect to the brainstem and cerebellum [3, 42]. We observed more branching in the saccule, more fibers going to the posterior canal, and more fibers already extending into the cerebellum earlier in the transgenic embryos compared to *WT* at E12.5 [29]. The overall patterns of vestibular innervation were further investigated in $Tg^{+/-}$ mice after birth by immunohistochemistry using an anti-acetylated tubulin antibody (Fig. 2a, b). The innervation of the anterior vertical canal crista (AC), horizontal canal crista (HC), and utricle (U) in $Tg^{+/-}$ pups was comparable with that in the wild type with the exception of occasional nerve fibers with an aberrant trajectory in $Tg^{+/-}$ (Fig. 2b, arrow). In addition, we used lipophilic dye-tracing to examine the innervation patterns of *WT* and mutant inner

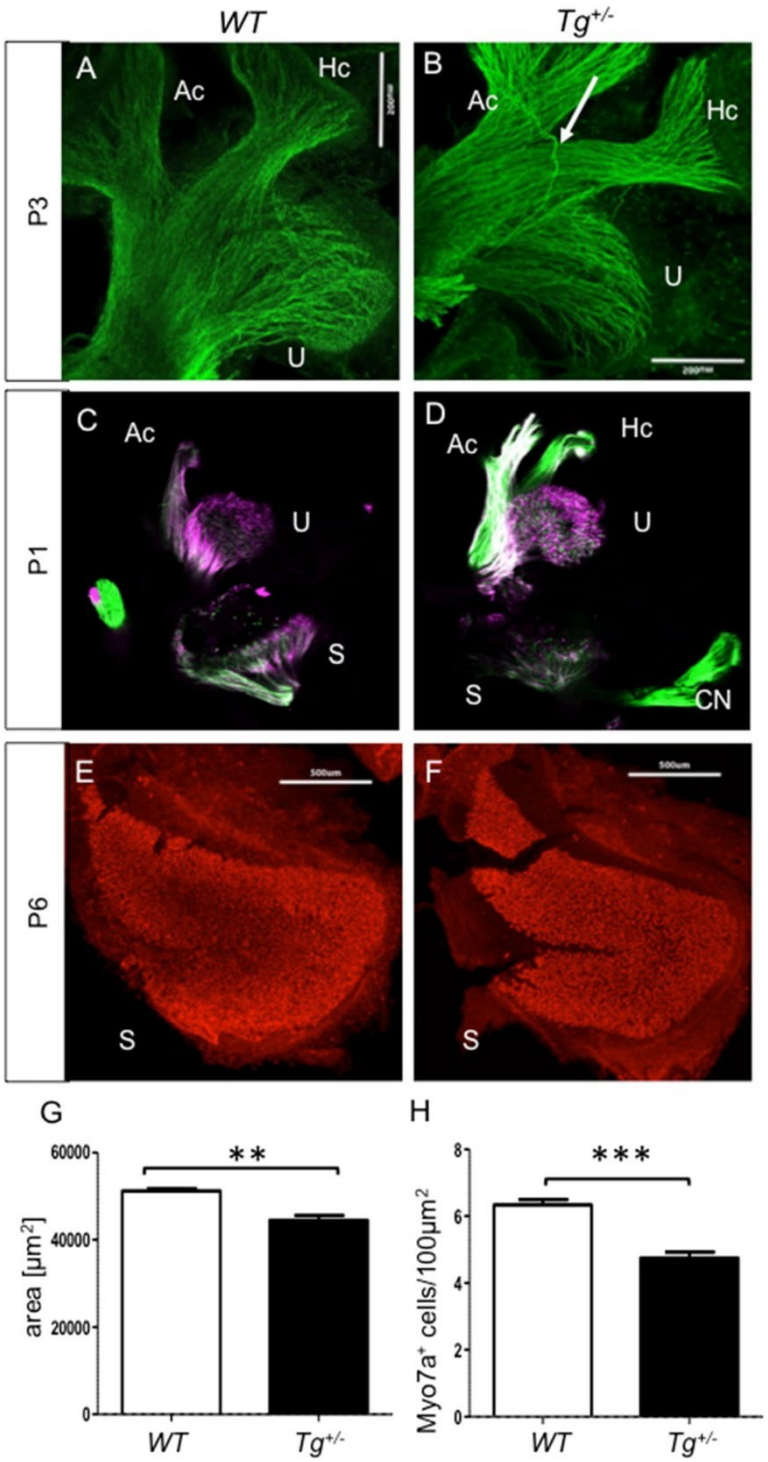

Fig. 2 The pattern of innervation in the vestibular system at P3 (**a**, **b**). Similar dense innervation of *WT* and $Tg^{+/-}$ sensory epithelia is shown by anti-tubulin staining of the fibers in whole mount. A misguided nerve fiber with the same aberrant trajectory was repeatedly observed in $Tg^{+/-}$ (*white arrow*). *Scale bar* 500 μm. **c**, **d** Less fibers in the transgenic saccule at P1. The utricle and anterior and horizontal canals are typically labeled at the same intensity. Lipophilic dyes were injected into the cerebellum. **e**, **f** A reduction of sensory epithelium of the saccular maculae in $Tg^{+/-}$ (**e**) compared to *WT* (**f**) at P6. Hair cells are visualized using anti-Myo7a (*red*) in whole-mount immunohistochemistry. Quantification of area saccule (**g**) and counting of $Myo7a^+$ cells per 100 μm^2 (**h**) is done by ImageJ. The values represent means ± SEM ($N = 3$ individuals/group and 6×100 μm^2/3 individuals/group). $^{**}P < 0.01$; $^{***}P < 0.001$. *Scale bar* 500 μm. *U*, Utricle; *Ac*, anterior canal crista; *Hc*, horizontal canal crista; *S*, saccule

ears. At P1, the utricle and anterior and horizontal canals were labeled at the same fiber density in the $Tg^{+/-}$ and *WT* littermates (Fig. 2c, d). However, the labeling intensity of the saccule in the $Tg^{+/-}$ was much lower (Fig. 2d). To check if this staining difference is related to aberration in the sensory epithelium, we analyzed the size of the saccule and utricle in a

whole mount preparation at P6. The size of the utricular maculae showed no measurable difference (data not shown), but the size of $Tg^{+/-}$ saccular maculae was significantly smaller ($P < 0.01$) compared to *WT* (Fig. 2e–g). Furthermore, the number of hair cells per 100 μm^2 of the sensory epithelium of the saccule was significantly reduced ($P < 0.001$) in $Tg^{+/-}$ (Fig. 2h), seemingly corresponding to the reduced innervation (Fig. 2d).

To further examine the properties of the vestibular afferents in the vestibular ganglion, we used calretinin, a marker of a selective population of large ganglion neurons that project centrally into the brainstem vestibular nuclei and the vestibular cerebellum [43–45]. The total number of calretinin$^+$ neurons in the vestibular ganglion was not significantly altered in $Tg^{+/-}$ compared to *WT* littermates (Fig. 3a–c). Both $Tg^{+/-}$ and *WT* ganglia were similarly affected by the aging process and showed the well-known age-related decline [46] when we compared 6- and 11-month-old mice (Fig. 3c).

Transgenic Isl1 Expression in the Cerebellum Causes Foliation and Cellular Changes

Since the relatively minor changes found in the inner ear could not be matched to the obvious motor deficits of transgenic mice, we next analyzed the cerebellum, a motor control system [6]. The area of the cerebellum was compared using three near midsagittal sections through the cerebellar vermis. The $Tg^{+/-}$ cerebella were smaller ($P < 0.0278$) compared to control littermates at P8 (9.227 ± 0.6 mm^2, $N = 6$ versus 11.16 ± 0.3 mm^2, $N = 5$). Changes differed by lobule. For example, lobule X and lobule IX trended to be smaller, but the difference was not significant ($P > 0.05$, *t* test). Transgenic mice had consistent foliation defects in the anterior lobe (I–V lobules) of the cerebellar vermis (Fig. 4). The predominant phenotype was the fusion of vermis lobules I–II and III. The fissure between anterior-folia I/II and III either failed to form, leading to the fusion of the lobules, or was shallower in the transgenic cerebella than in *WT* (Fig. 4d, f, h). Importantly, most of the transgenic mice had a hemilobule on top of or as part of the anterior medullary velum (Fig. 4b, f, h, arrow). A mild foliation defect in lobules IV and V was consistently detected in $Tg^{+/-}$ (Fig. 4g, h). In one of the 20 adult mutants analyzed, lobules VI–VIII failed to form. Additionally, sagittal sections of the $Tg^{+/-}$ brain revealed that the inferior colliculus was smaller (Fig. 4f). Although the brains of all adult $Tg^{+/-}$ mice analyzed ($n = 20$) appeared grossly normal, the inferior colliculus was noticeably reduced in the dorsal view of the adult brains (supplemental file: Fig. S1). The fiber bundle of the inferior colliculus reaching to the medial geniculate body (brachium of the inferior colliculus; BIC) was significantly reduced in the $Tg^{+/-}$ inferior colliculus, as shown by NF200 staining (Fig. 5c, d, arrow). Additionally, white matter fibers formed a distinctive tract in the $Tg^{+/-}$ cerebellum with an aberrant fiber bundle forming the outer layer of the anterior cerebellum (Fig. 5d, arrowhead). To analyze inferior colliculus activation, we performed ABR recordings. The amplitude of the IV wave was lower, and the latency of all ABR waves (I–IV) was prolonged in $Tg^{+/-}$ compared to *WT* mice (Fig. 5e, f). Since wave IV represents lateral lemniscus and inferior colliculus activation [47], the ABR data confirm functional abnormalities of the inferior colliculus of $Tg^{+/-}$ mice.

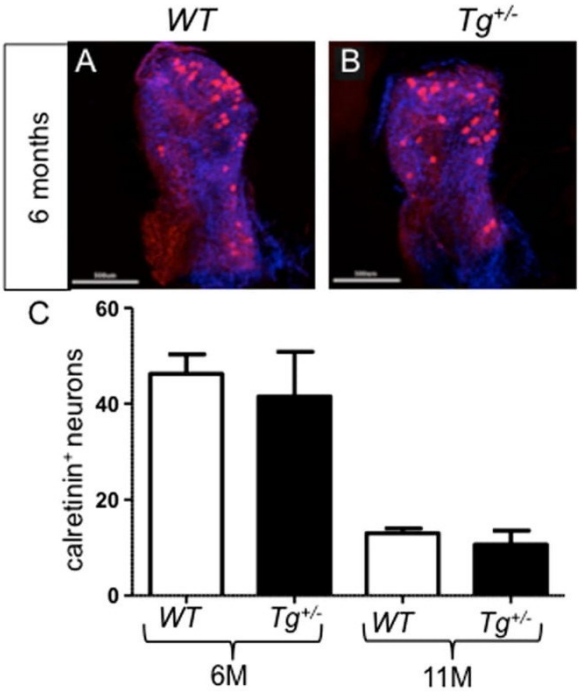

Fig. 3 Total number of calretinin-labeled neurons in the vestibular ganglion of *WT* (**a**) and $Tg^{+/-}$ (**b**). **c** The number of calretinin$^+$ neurons in *WT* and $Tg^{+/-}$ ganglia is similar at 6 months of age (*6M*) and it is declining with age at a similar rate in both *WT* and $Tg^{+/-}$ (11 months of age, *11M*). Single immunostaining with anti-calretinin (*red*) and visualization of nuclei with Hoechst (*blue*). *Scale bar* 500 μm

We observed a different penetrance of the cerebellar phenotype, from severe foliation defects with a significant reduction/fusion of lobules (Fig. 6a) to milder changes in the formation of lobules in the anterior lobe (Fig. 6b–f). One likely possibility for the variable phenotype is the mosaic expression of the transgene due to the heterozygosity of the mutation.

We compared the formation of the Purkinje cell (PC) layer in P16 mice. As in the controls, the PCs were oriented in a monolayer with dendrites projecting into the molecular layer throughout all lobules of the $Tg^{+/-}$ cerebellum. However, patches of PCs were missing in the anterior lobe, especially in lobules I–III, and the density of calbindin-labeled PC dendrites appeared to be reduced compared to *WT* littermates (detail of lobule I–II in Fig. 7a, b). With advancing age, PCs progressively

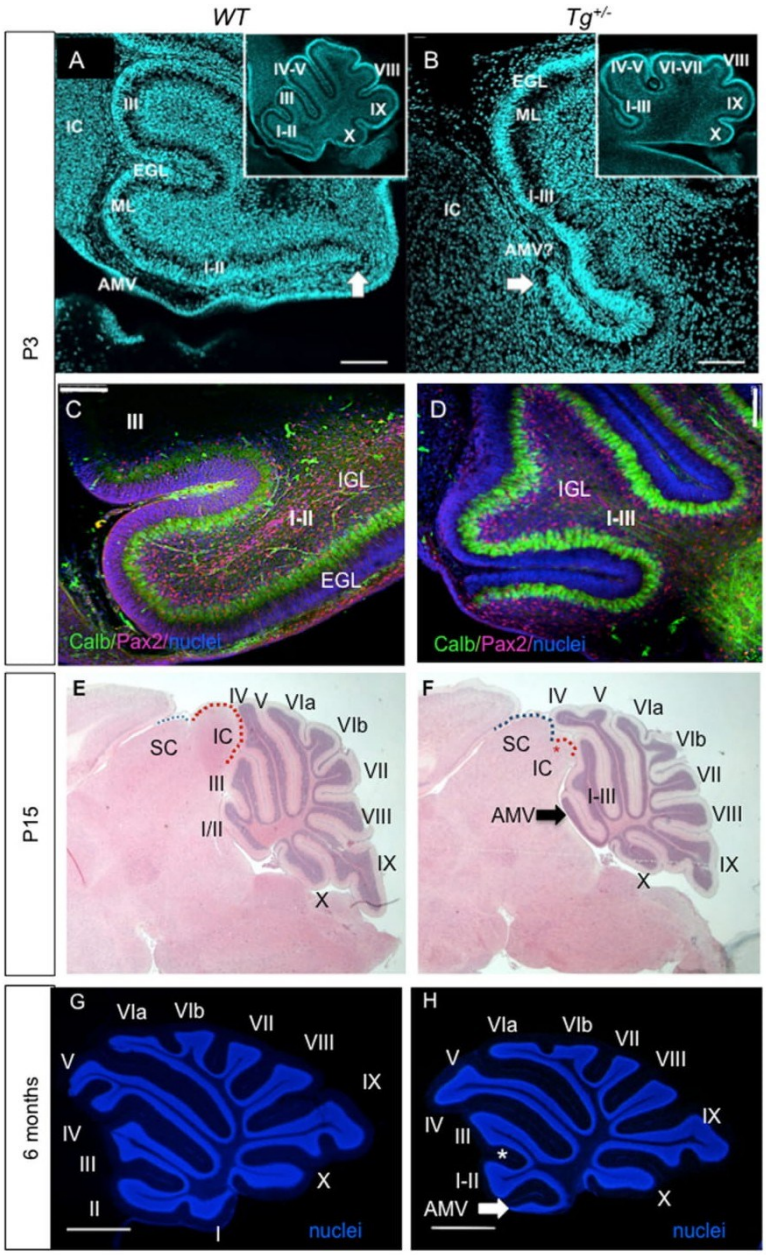

Fig. 4 Changes in the cerebellum. **a**, **b** P3 sagittal sections using Hoechst nuclear staining show the different organizations in the control (*WT*) and mutant ($Tg^{+/-}$) littermate cerebellar foliation (insert **a**, **b**) and disorganization of lobule I + II. Note absence of a recognizable anterior medullary velum (*AMV*) and the rostral expansion of a hemilobe only in the transgenic mouse (*arrowhead*). **c**, **d** Pax2 (*red*) and calbindin (*green*; Purkinje cells) staining of sagittal sections of the anterior lobe of the cerebellar vermis at P3 shows a comparable distribution of Purkinje cells and $Pax2^{+}$ cells in *WT* (C) and $Tg^{+/-}$ lobules (**d**). The altered foliation of lobules I–III is obvious in the $Tg^{+/-}$ cerebellum. **e**, **f** Hematoxylin-eosin staining of the brain sections at the level of vermis at P15. The predominant phenotype of altered formation of vermis lobules leading to the fusion of I–III and a hemilobule on top of or as part of the anterior medullary velum (*arrow*) is detected in the $Tg^{+/-}$ cerebellum. The remnant of the inferior colliculus (*IC*) is denoted by a *red asterisk* in the $Tg^{+/-}$ midbrain. The superior colliculus (*SC*) and IC are outlined by *blue-* and *red-dashed lines*, respectively. **g**, **h** The adult $Tg^{+/-}$ cerebellum shows the defect in the foliation of the anterior lobe compared to *WT* littermates as shown by Hoechst staining of the granule cell layer nuclei. The fissure (*) between anterior folia I/II and III failed to form properly, leading to the fusion of the lobules. A hemilobule is on top of or as part of the anterior medullary velum (*arrow*). The lobules IV–V in $Tg^{+/-}$ differ from controls. Roman numerals depict cerebellum lobules. *AMV*, anterior medullary velum; *Calb*, calbindin; *EGL*, external granule layer; *IGL*, internal granule layer; *IC*, inferior colliculus; *ML*, molecular layer; *SC*, superior colliculus. *Scale bar* 100 μm (**a**–**d**) and 1000 μm (**e**–**h**)

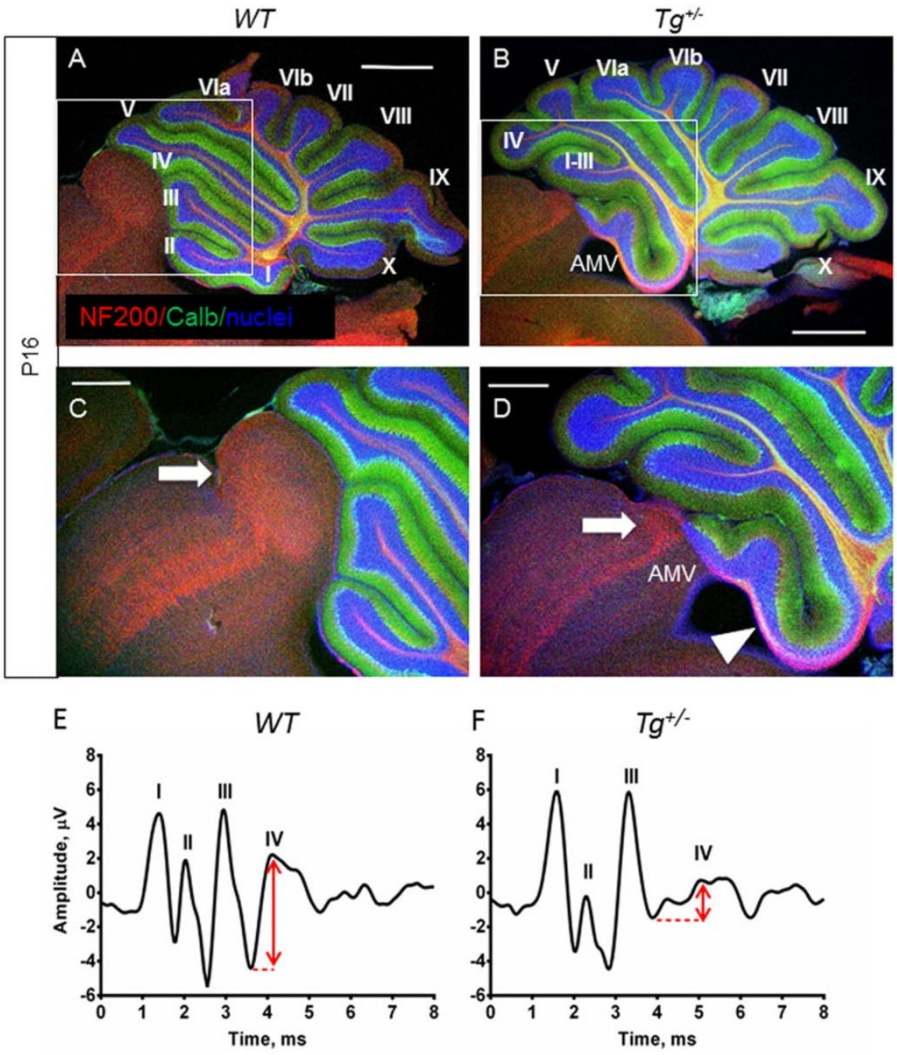

Fig. 5 Changes in the inferior colliculus of transgenic mice. Representative confocal images shows the expression of NF200 (*red*) and calbindin (*green*) in cerebellar sections from P16 *WT* (**a**, **c**) and transgenic (**b**, **d**) mice. **c**, **d** The brachium of the inferior colliculus (*arrow*) is profoundly reduced in $Tg^{+/-}$ compared to *WT* mice. An *arrowhead* indicates an aberrant tract of white matter fibers in the transgenic cerebellum expanding along the hemilobe that is fused with the anterior medullary velum (*AMV*). **e**, **f** The auditory brainstem response (*ABR*) waveforms of 3-week-old mice to a click stimulus. Individual responses at 80 dB SPL click are represented. Major waves I–IV are indicated above the peaks. The results show that the amplitude of ABR wave IV is lower, and the latency of ABR waves is prolonged in $Tg^{+/-}$ compared to *WT*. *Scale bar* 1000 μm (**a**, **b**) and 500 μm (**c**, **d**)

lost calbindin immunoreactivity, particularly, in the anterior lobe (Fig. 7c, d). The majority of PCs in lobules I–III lost the expression of calbindin at 4 months of age, although PCs were still present, since basket interneuron fibers (visualized by NF200 staining) were wrapped around PC bodies. At 6 months of age, the deterioration of PCs advanced in all lobules of the transgenic cerebella. The expression of calbindin was significantly diminished in the majority of PCs and their dendrites (Fig. 8a, b), in detail, lobules I–II and X (Fig. 8c–f). Given that there was no profound shrinkage of the molecular layer and Purkinje cell nuclei could still be detected, we presume that PC dendrites are still present but have been reduced or have lost immunopositivity for anti-calbindin. This conclusion is further supported by the presence of scattered patches of preserved PCs, with PC dendrites mostly in lobules V–VIII, and dorsal IX (supplemental file: Fig. S2). A significant attenuation of calbindin expression in PCs of the $Tg^{+/-}$ cerebellum may be caused by altered GABA signaling. Changes in calbindin expression may result in an alteration of Ca^{2+} homeostasis with the outcome of altered cerebellar control of motor function as PCs are well known to emit calcium spikes [6].

Another important calcium-binding protein expressed in the cerebellum is calretinin. Calretinin is expressed predominantly in unipolar brush cells (UBCs) in the posterior lobes (IX, X) of the cerebellum [48, 49]. UBCs receive direct input from the vestibular ganglion and vestibular nuclei [3, 50]. We specifically analyzed calretinin expression in lobules X and IX at P16 and in 8-month-old adult mice. A significant ($P < 0.05$) decrease in calretinin expression was observed in the $Tg^{+/-}$ (Fig. 9). The attenuation in calretinin$^+$ cells suggests

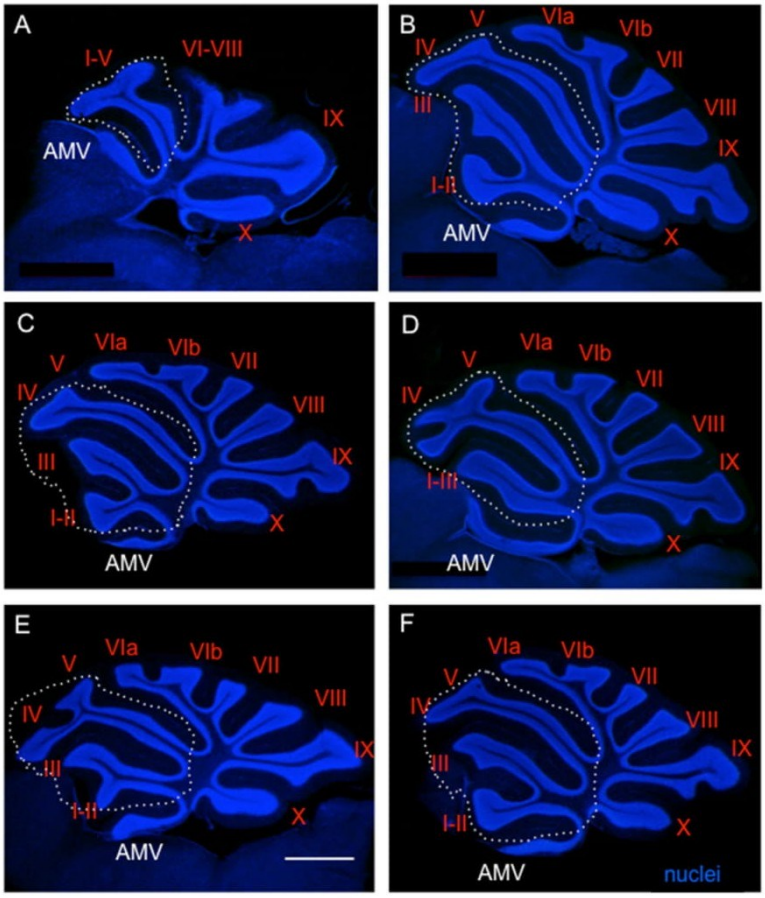

Fig. 6 Morphological changes in the adult transgenic cerebellum. Hoechst staining of the granule cell layer nuclei of the cerebellum shows a differential penetrance leading to variable foliation defects in $Tg^{+/-}$. Severe foliation defects (**a**) compared to less affected $Tg^{+/-}$ (**b**–**f**). The formation of the anterior lobe (lobules I–V) is altered in all $Tg^{+/-}$. The area of the anterior lobe is outlined by *white dashed line* and shows defects in all transgenic mice, including the AMV aberration. *AMV*, anterior medullary velum. *Scale bar* 1000 μm

changes in Ca^{2+} homeostasis in cerebellar neurons, which would be expected to affect vestibular information processing in the cerebellum, as UBCs are known to amplify the vestibular input. An alteration of sensory data processing in the cerebellum could affect the behavioral phenotype of $Tg^{+/-}$ mice.

Next, we analyzed molecular changes in the $Tg^{+/-}$ cerebellum. *Isl1* is expressed in the developing auditory and vestibular neurons [51] but is not expressed in the cerebellum. In order to investigate if the global overexpression of *Isl1* under *Pax2* regulatory sequences led to exogenous expression in the developing cerebellum, we performed immunohistochemistry on sagittal sections of the cerebellar vermis of transgenic mice and their *WT* littermates. *Pax2* identifies the entire population of GABAergic interneurons (basket, stellate, Golgi, and Lugaro cells) in the cerebellar cortex and in the deep cerebellar nuclei [23]. Accordingly, Isl1 protein was detected in the $Pax2^{+}$ cells of the internal granule layer of all lobules at P3 (detail of lobule IX in Fig. 10). This finding was also supported by the detection of *Isl1* mRNA in the $Tg^{+/-}$ cerebellum in 1-, 7-, and 11-month-old mice using RT-qPCR (Fig. 11a).

Gene Expression Profiling in the Cerebellum

In order to further analyze the molecular changes induced by the misexpression of *Isl1*, we analyzed the mRNA expression of selected genes in the cerebellum of 1-month-old mice. We selected a broad spectrum of genes, whose products play a role in the specification and maintenance of different types of neurons (*Atoh1*, *Neurod1*, *Pax6*, *Pax2*, *Shh*, *Ngn2*, *Math3*, *Lhx1*), Ca^{2+} homeostasis (*Cacng1*, calretinin, and parvalbumin), and in neurotransmitter signaling or are structural subunits of the glutamatergic (*Dlg4*, *Slc17a7*, *Grin1*) or GABAergic neurons (*Slc32a1*, *Gphn*). Additionally, we also analyzed the expression of *Isl1* mRNA in the cerebellum and its potential target molecule mRNAs (*Lhx3*, *Neurod4*, *Ngn2*, *Isl2*). Of all the analyzed genes, we detected significant changes in the expression of *Pax6*, *Cacng1*, *Neurod4*, calretinin, and *Dlg4* in the transgenic cerebellum

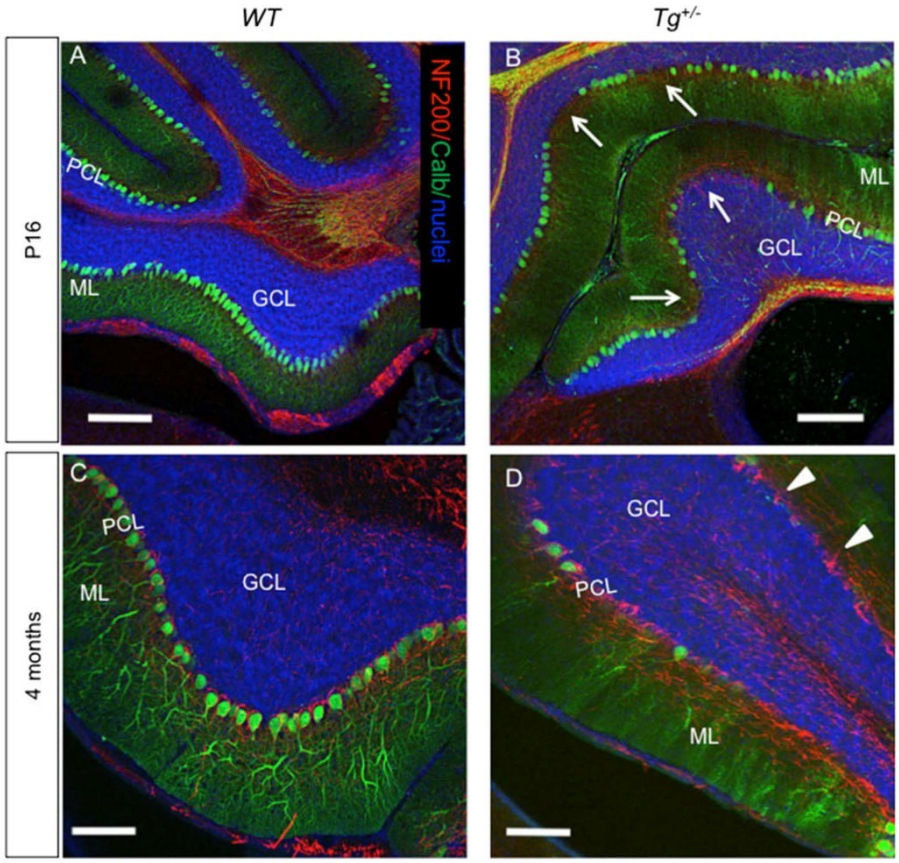

Fig. 7 Changes in Purkinje cells in the anterior lobe (detail of lobules I–II). **a**, **b** Purkinje cells (*PCs*) are oriented in a monolayer with dendrites projecting into the ML at P16, as visualized by calbindin staining (*green*; *nuclear staining*, *blue*). More calbindin-negative PCs are visible in the $Tg^{+/-}$ anterior lobe (**b**, *arrows*). The density of PC dendrites stained by calbindin is noticeably reduced in $Tg^{+/-}$ compared to *WT* (**a**) at P16. **c**, **d** A profound reduction of calbindin expression in PCs and PC dendrites in the ML progresses with increasing age in the $Tg^{+/-}$ anterior lobe (**d**), as visualized by lack of staining with anti-calbindin. Anti-NF200 staining (*red*) of basket interneuron fibers wrapped around Purkinje cell bodies (*arrowheads*) is still detected in 4-month-old $Tg^{+/-}$ mice. *ML*, molecular layer; *PCL*, PC layer; *GCL*, granule cell layer. *Scale bar* 200 μm (**a**–**b**), 100 μm (**c**, **d**)

compared to *WT* (Fig. 11b). Thus, the expression profile of transgenic cerebella was significantly altered compared to *WT*.

Discussion

To explore the gain-of-function role of *Isl1* in the developing cerebellar and vestibular system, we used an overexpression model of *Isl1* under the *Pax2* regulatory sequence. We present data showing that *Isl1* overexpression causes molecular and morphological changes in the cerebellum and vestibular system that may cause hyperactivity, including circling behavior of $Tg^{+/-}$ mice. The circling behavior of mutant mice has traditionally been related to vestibular defects (e.g., Bronx-Waltzer mouse [52]) but also to motor control defects in the forebrain, particularly to an imbalance of nigrostriatal function [10]. Below we will first provide the arguments for an ear phenotype being related to circling followed by the correlation of the posterior midbrain and cerebellum with hyperactivity and circling. We suggest that hyperactivity is most likely related to cerebellar malformation, including the progressive loss of calcium binding proteins but not including mild vestibular defects.

Behavioural Phenotype Associated with Isl1 Transgenic Expression

In tests evaluating behavioral phenotype, $Tg^{+/-}$ mice exhibit hyperactivity without balance deficits. In the air-righting test, the mutant mice were indistinguishable from control *WT* mice, suggesting that $Tg^{+/-}$ mice do not have a deficit in balance and coordination. Additionally, transgenic mice demonstrated enhanced performance on the accelerating rotarod task than the littermate controls. This was an unexpected finding; however, similar results were reported by other investigators when better performance in the rotarod task was associated with the hyperactivity. For example, heregulin mutants [53], $Pcmt1^{-/-}$ [54], or hA53T transgenic mice [55] demonstrate improved performance compared to control *WT* mice in this test. Interestingly, these mice have cerebellar abnormalities and hyperactivity in open-field tests. Hyperactivity without motor abnormalities and superior rotarod performance was also

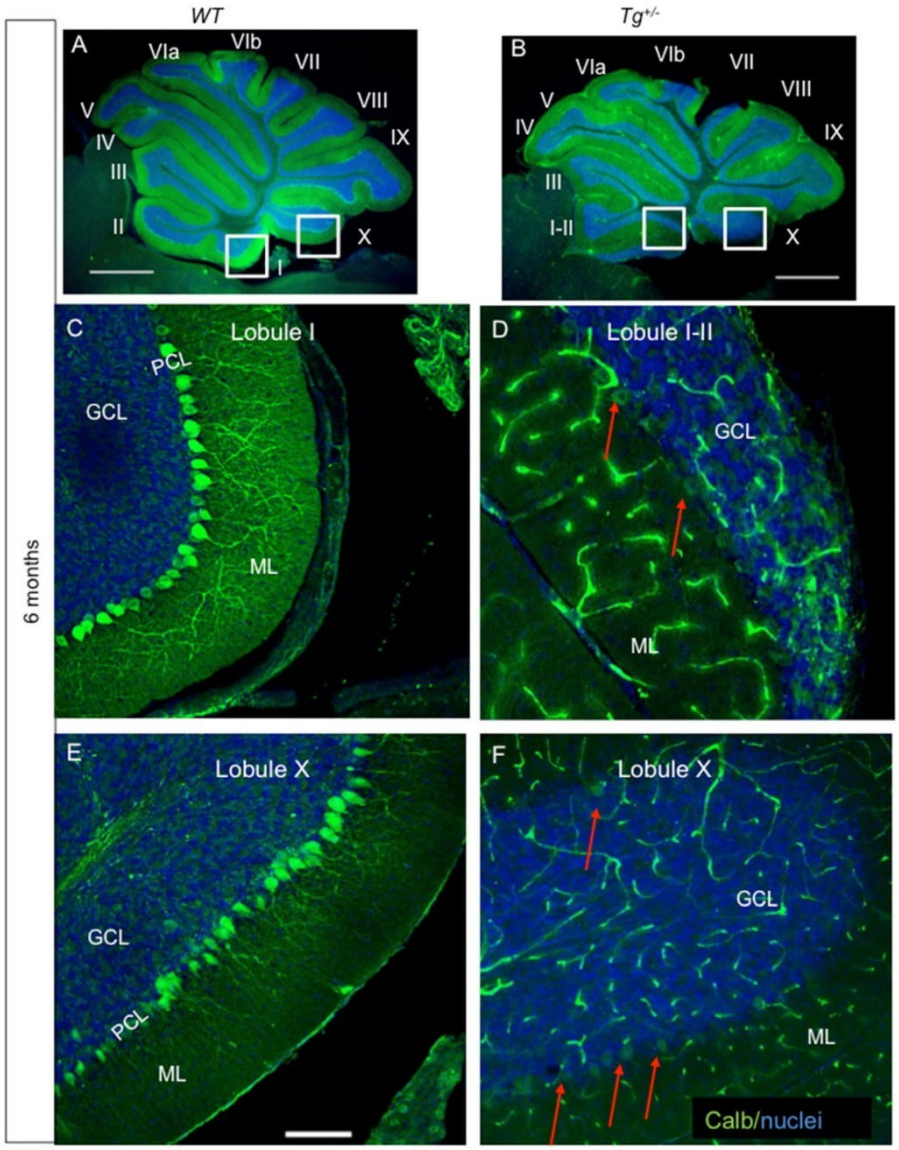

Fig. 8 Reduction of Purkinje cell (*PC*) immunogenicity and apparent loss of PC dendrites in the molecular layer of the adult transgenic cerebella. PCs form a monolayer with dense network of dendrites in the ML throughout all the lobules in control cerebellum (**a**). At 6 months, a profound loss of calbindin expression in PCs and PC dendrites in the ML progresses in all lobules of the $Tg^{+/-}$ cerebella (**b**) as visualized by lack of staining with anti-calbindin (*green*). A near complete loss of calbindin expression in PCs and PC dendrites (*arrows* in **d**, **f**) is detected in the $Tg^{+/-}$ cerebella compared to *WT*, in detail shown in the lobules I–II and X (**c**, **e**). *ML*, molecular layer; *PCL*, PC layer; *GCL*, granule cell layer. *Scale bar* 1000 μm (**a**, **b**); 250 μm (**c**–**f**)

observed in rats with cerebellar neuronal damage (microneuronal hypoplasia) induced by low-dose X-ray radiation [56]. Better rotarod performance is associated with hyperactivity rather than with improved motor functions. These studies, including our data, link cerebellar abnormalities with a hyperactive phenotype.

The Overexpression of Isl1 Affects the Differentiation of Vestibular End Organs

During early development, vestibular neurons delaminate from the ear and migrate to the vestibular ganglia before projecting back with their dendrites to form the vestibular ganglion located between the ear and brainstem [57]. Consistent with the expression of Isl1 and Pax2 in the sensory neurons of the ear [25, 51], we found a slight acceleration in early fiber development [29], but later innervation of the $Tg^{+/-}$ was comparable to *WT* littermates (Fig. 2). In newborn mice, utricle and canal cristae were all labeled at similar intensities. However, the saccule was labeled less (Fig. 2). The saccule is an otolith organ involved in vertical linear movement detection and the sensing of gravity. The saccule shares an embryological origin with the cochlea, arising from the pars inferior of the inner ear [58]. Interestingly, a parallel decline in cochlear and saccular function has been associated with aging in humans [59] and with the shared susceptibility of the saccule

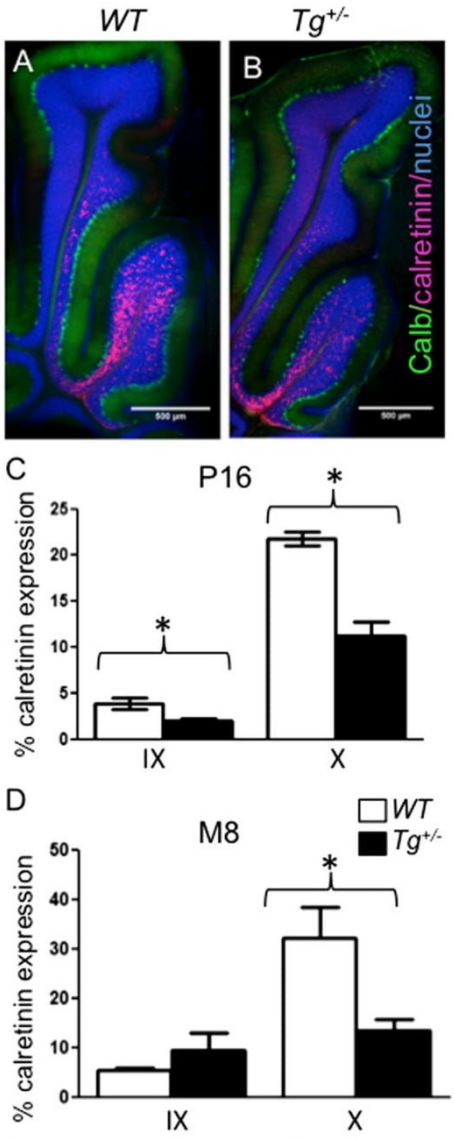

Fig. 9 Altered distribution of calretinin-labelled cells in lobules X and IX of the transgenic cerebellum. Calretinin$^+$ cells are primarily found in lobules X and half of IX as shown by calretinin staining (*red*) in both *WT* (**a**) and $Tg^{+/-}$ (**b**) cerebella. Double staining with anti-Calbindin (*Calb*, *green*) and anti-Calretinin (*red*) and visualization of nuclei with Hoechst staining of 100 μm sections of P16 cerebella. *Scale bar* 500 μm. Quantification of calretinin staining in lobules IX and X of the cerebellum at P16 (**c**) and 8-month-old (**d**) using ImageJ. The values represent an average percentage of calretinin$^+$ area/lobule area ± SEM ($n = 6$ $Tg^{+/-}$ and 6 *WT*/each age group), *t* test *, $P < 0.05$

and cochlea in pathological processes of Meniere's disease [60]. Coincidently, the $Tg^{+/-}$ mice show cochlear dysfunction as well as reduced size of the saccule that may be associated with the behavioral disorder similar to behavioral disorders observed in individuals with severe inner ear defects [10, 61]. Despite these measurable changes, it seem unlikely that changes in a sensory epithelium dedicated to the perception of vertical alterations in linear acceleration should be responsible for hyperactivity and unilateral rotations described here (Fig. 1). While we cannot rule this out, the data provided below on the cerebellum and midbrain of these transgenic mice correlates better with the behavioral phenotype.

Morphological and Molecular Changes in the Cerebellum and Midbrain

The cerebellum begins to form at embryonic day 9 (E9) in the mouse and continues through to postnatal development [62]. It is comprised of ten lobules, which are histologically uniform and divided into distinct layers. The analysis of cerebellar morphology of $Tg^{+/-}$ showed foliation defects in the anterior lobe, including a partial fusion of lobules I–III, altered layer formation of lobule I fused with the anterior medullary velum, and a defect in the formation of IV/V lobules. In addition, the inferior colliculus was reduced in $Tg^{+/-}$. A strikingly similar phenotype was reported in the engrailed1 (*En1*) conditional mutant with $En1^{flox}$ allele deleted with the null $En1^{Cre}$ knock-in allele [63]. En1 is necessary for the initial formation of the midbrain, and anterior hindbrain and *En1*-null mutants have a complete deletion of this region [64]. *En1* is required for the development of the anterior five cerebellar folia (I–V) and the inferior colliculus. Since *Pax2* and *En1* expression domains overlap and a molecular interaction is needed for the stable differentiation of the isthmus region [27], it is possible that the Isl1 protein of the *Pax2-Isl1* transgene product interacts with En1 signaling to produce a phenotype in the cerebellum and midbrain as in $En1^{flox/Cre}$ mutants. This suggestion is supported by similar losses of neurons in *Isl1* and *En1* mutants [15] and other data on Lim protein interactions with En1 proteins [65]. Since our data provide the first in vivo evidence for some direct or indirect interaction of Isl1 and En1 in the cerebellum and midbrain, we suggest that the Isl1 protein partially disables En1 signaling, thus resulting in a similar phenotype (compare Fig. 2 in [63] with our Fig. 4f). Unfortunately, no behavioral details were provided for the *En* mutants [63], and none of the other changes in protein expression we report here have been described in this mutant. Data from functional MRI studies in humans suggests that sensorimotor tasks are processed in lobules IV–V and VIII and that the activation of sensory motor regions is associated with the activation of anterior lobules (I–V) of the cerebellum [66] that also contains its own body representation in humans. We suggest that the cerebellar changes are related to the altered behavior, possibly in combination with the progressive decline of calcium-binding proteins discussed below.

The cerebellum contains five major types of neurons that use either glutamate (granule neurons, UBCs, deep nuclei neurons) or GABA as neurotransmitter (inhibitory

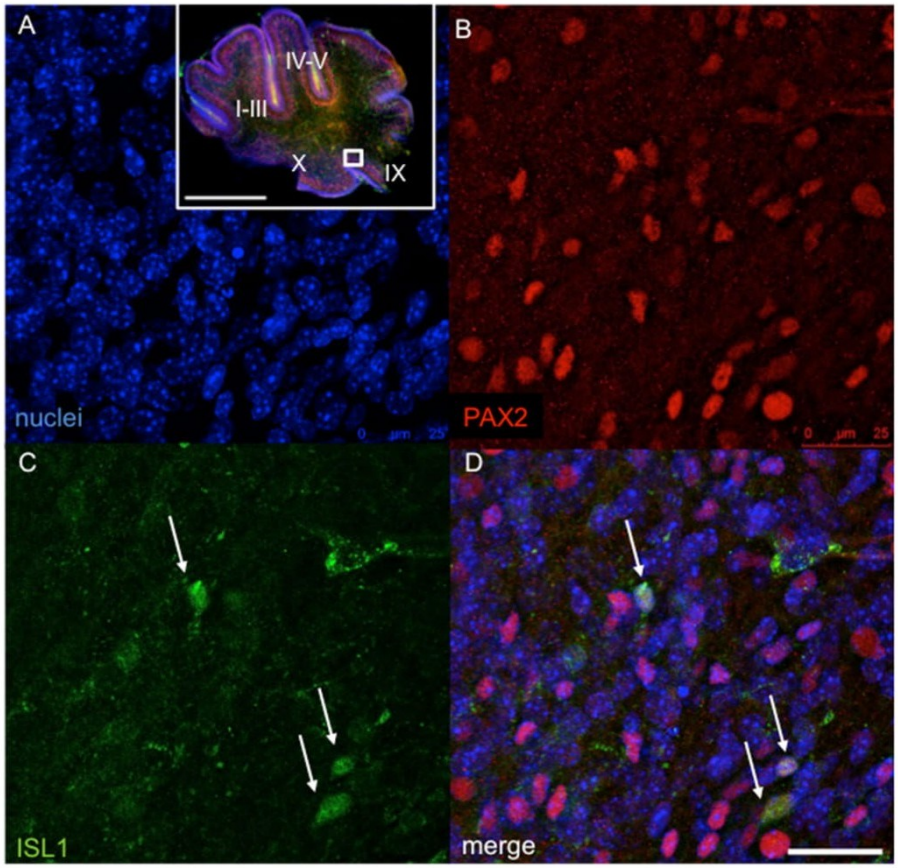

Fig. 10 The expression of Isl1 in the transgenic cerebellum at P3. Confocal microscopy of 100 μm sections shows the expression of Isl1 in the transgenic cerebellum (lobule IX) indicated by *white arrows*. Double staining with anti-Pax2 (**b**, *red*) and anti-Isl1 (**c**, *green*) and visualization of nucleus with Hoechst staining (**a**) and overlay of fluorescent channels (**d**). *Scale bar* 500 μm (whole cerebellum), 25 μm (detail **a**–**d**)

interneurons and Purkinje cells). GABAergic neurons originate in the ventricular zone in the roof for the fourth ventricle, and all three glutamatergic types come from the rhombic lip [67]. All three glutamatergic cerebellar neuron types derive from *Pax6*$^{+}$, *Atoh1*$^{+}$ progenitors [68]. Starting at E13.5, Pax2 is expressed in prospective GABA interneuron precursors in the cerebellar cortex that generate inhibitory interneurons in the cerebellar nuclei, Golgi and Lugaro cells in the granular layer, and basket and stellate cells in the molecular layer [28]. *Isl1* transgenic expression in Pax2^{+} cells might alter cell fate of Pax2^{+} GABAergic neuron population. The aberrations in the cell lineages are further supported by RT-qPCR results showing a significantly altered expression of *Pax6*, *Neurod4*, *Dlg4*, and *calretinin* mRNA in the cerebellum of 1-month-old *Tg*$^{+/-}$. All these genes are associated with glutamatergic neurons suggesting changes in the cell homeostasis of the cerebellum.

The dysfunction in GABA signaling in *Tg*$^{+/-}$ mice is demonstrated by our behavioral studies showing that a subconvulsive dose of picrotoxin normalizes the open-field hyperactive behavior of *Tg*$^{+/-}$ mice. Circling behavior and hyperactivity in mice are also a common presentation of the dysfunction of the striatum [69, 70]. The GABA-mediated striatonigral pathway has been indicated as a major output system from the striatum controlling circling activity [71]. Although our analysis of Isl1 expression in the striatum at E14.5 did not show any differences, we cannot exclude an attenuation in the input from the vestibular system that may cause a change in the striatum and/or striatonigral pathway of *Tg*$^{+/-}$ resulting in hyperactivity and circling.

Purkinje cells belong to GABAergic neuronal subtypes; however, their progenitors do not express *Pax2* [72]. Purkinje cells play a key role in connectivity forming a cortico-nucleo-olivary loop important for motor behavior [6]. Proper connectivity is critical for motor coordination, and the degeneration of the cerebellar circuits is associated with several neurological degenerative diseases. With increasing age, we detected reduced Purkinje cell calbindin expression in the transgenic cerebellum. This may indicate that Isl1 also affects the maintenance of Purkinje cells and their calcium homeostasis.

Another important calcium binding protein is calretinin, which is expressed in UBC, Lugaro-like, granular, Purkinje,

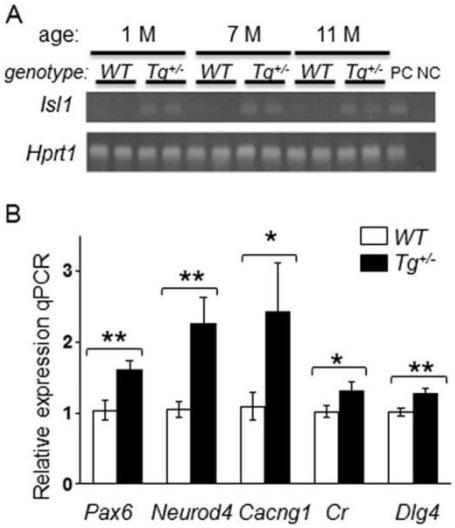

Fig. 11 RT-qPCR analysis of gene expression changes induced by the transgenic expression of *Isl1* in the cerebellum. **a** Representative 2 % agarose gel electrophoresis of RT-qPCR products shows the expression of *Isl1* in $Tg^{+/-}$ cerebella of 1-, 7-, and 11-month-old mice (two samples/genotype/age). *Hprt1* was used as the reference gene. Lane: *PC*, positive control (hindbrain); *NC*, negative control (H_2O). **b** The expression of genes was analyzed in *WT* and $Tg^{+/-}$ cerebella from 1-month-old mice; the relative expression levels were quantified using $-\Delta\Delta$Cq method. The data represent the expression of mRNA relative to the control cerebella, normalized by the reference gene *Hprt1*. $^*P < 0.05$; $^{**}P < 0.01$, *t* test. The values are means ± SEM (each experiment in duplicate; $N = 8$/group). *Dlg4*, discs large homolog 4; *Cacng1*, voltage-dependent calcium channel gamma subunit 1; *Cr*, calretinin

and astrocyte cells of the cerebellum [49]. We specifically analyzed calretinin expression in the vermis of lobule X and the ventral portion of lobule IX, where UBCs are particularly concentrated [50]. UBCs are a distinct type of glutamatergic interneurons in the cerebellar cortex and cochlear nucleus. It is thought that they serve as amplifiers of vestibular signals through a powerful feed-forward link due to the transfer of a signal from a single mossy fiber to a number of neighboring granule cells [3, 73]. A significant decrease in calretinin expression was observed in the lobule X and IX of $Tg^{+/-}$ compared to *WT* littermates at P16 and in adults (Fig. 9). This could be explained by UBC cell death, possibly as a result of altered innervation from the saccule [3]. Conversely, the reduction in the number of calretinin$^+$ cells may reflect the downregulation of calretinin expression as a response to a decrease in sensory input. The effect could also be a consequence of aberrations in the cell lineages of the Pax2$^+$ precursors. The impairment of Ca^{2+} homeostasis in Purkinje cells as well as the reduction of calretinin-mediated Ca^{2+} buffering would predict modifications in intracellular calcium concentration resulting in altered information processing and thus motor alterations such as hyperactivity.

Conclusion

Based on our behavioral study, the transgenic expression of Isl1 specifically affects GABA signaling. We found that Isl1 overexpression in the developing vestibular ear results in a smaller saccule with a significantly reduced number of hair cells and innervation. We observed both morphological and molecular changes in the cerebellum, especially at the vestibule-cerebellum and the anterior lobe, which may be associated with altered functions and abnormal behavior of the $Tg^{+/-}$ mice. Additionally, in the $Tg^{+/-}$ midbrain, the inferior colliculus was severely reduced. Taken together, the development of the cerebellum, midbrain, and the vestibular end organs is altered by the transgenic expression of Isl1. It is intriguing to consider whether an alternation of transcription regulation in the development of the vestibular system may contribute to psychiatric and motor disorders that show correlation with the shrinking of the anterior lobe of the cerebellum [74]. A most interesting correlation exists between our hyperactive mice and the age-related shrinking of the cerebellum [75] and altered GABA signaling [76, 77] in people with attention deficit hyperactivity disorder (ADHD). It remains to be seen if our Isl1 transgenic mice can serve as a model for ADHD. We are currently evaluating standard treatment of ADHD such as Ritalin for its effect on our transgenic mice [78].

Acknowledgments This work was supported by the Czech Science Foundation (Grant Agreement No. 13-07996S); by BIOCEV CZ.1.05/1.1.00/02.0109 from the ERDF; by "Biotechnological expert" CZ.1.07/2.3.00/30.0020 from the European Social Fund and the state budget of the Czech Republic; and by the Czech Ministry of Education, Youth and Sports (MEYS, Grant Agreement No. AVOZ50520701). We thank Dr. A. Kubik-Zahorodna of the Czech Centre for Phenogenomics (LM2011032 INFRAFRONTIER-CZ by the MEYS) for expert advice on the behavioral tests on the rotarod. We also thank Dr. D. Buckiova for an initial input and expertise involving experimental work on vestibular end organs.

Compliance with Ethical Standards

Conflict of Interest The authors declare that they have no competing interests.

References

1. Forbes PA, Siegmund GP, Schouten AC, Blouin J-S (2014) Task, muscle and frequency dependent vestibular control of posture. Front Integr Neurosci 8:94

2. Beisel KW, Wang-Lundberg Y, Maklad A, Fritzsch B (2005) Development and evolution of the vestibular sensory apparatus of the mammalian ear. J Vestib Res Equilib Orient 15(5-6):225–241
3. Maklad A, Fritzsch B (2003) Partial segregation of posterior crista and saccular fibers to the nodulus and uvula of the cerebellum in mice, and its development. Brain Res Dev Brain Res 140(2):223–236
4. Barmack NH, Yakhnitsa V (2008) Functions of interneurons in mouse cerebellum. J Neurosci 28(5):1140–1152
5. Bermingham NA, Hassan BA, Wang VY, Fernandez M, Banfi S, Bellen HJ, Fritzsch B, Zoghbi HY (2001) Proprioceptor pathway development is dependent on Math1. Neuron 30(2):411–422
6. Llinas R, Negrello MN (2015) Cerebellum. Scholarpedia 10(1): 4606
7. Straka H, Fritzsch B, Glover JC (2014) Connecting ears to eye muscles: evolution of a 'simple' reflex arc. Brain Behav Evol 83(2):162–175
8. Goodworth AD, Mellodge P, Peterka RJ (2014) Stance width changes how sensory feedback is used for multi-segmental balance control. J Neurophysiol. doi:10.1152/jn.00490.2013
9. Stiles L, Smith PF (2015) The vestibular-basal ganglia connection: balancing motor control. Brain Res 1597:180–188
10. Antoine MW, Hubner CA, Arezzo JC, Hebert JM (2013) A causative link between inner ear defects and long-term striatal dysfunction. Science 341(6150):1120–1123
11. Tsuchida T, Ensini M, Morton SB, Baldassare M, Edlund T, Jessell TM, Pfaff SL (1994) Topographic organization of embryonic motor neurons defined by expression of LIM homeobox genes. Cell 79(6): 957–970
12. Nichols DH, Pauley S, Jahan I, Beisel KW, Millen KJ, Fritzsch B (2008) Lmx1a is required for segregation of sensory epithelia and normal ear histogenesis and morphogenesis. Cell Tissue Res 334(3):339–358
13. Shirasaki R, Pfaff SL (2002) Transcriptional codes and the control of neuronal identity. Annu Rev Neurosci 25:251–281
14. Cai CL, Liang X, Shi Y, Chu PH, Pfaff SL, Chen J, Evans S (2003) Isl1 identifies a cardiac progenitor population that proliferates prior to differentiation and contributes a majority of cells to the heart. Dev Cell 5(6):877–889
15. Pfaff SL, Mendelsohn M, Stewart CL, Edlund T, Jessell TM (1996) Requirement for LIM homeobox gene Isl1 in motor neuron generation reveals a motor neuron-dependent step in interneuron differentiation. Cell 84(2):309–320
16. Liang X, Song MR, Xu Z, Lanuza GM, Liu Y, Zhuang T, Chen Y, Pfaff SL et al (2011) Isl1 is required for multiple aspects of motor neuron development. Mol Cell Neurosci 47(3):215–222
17. Lu KM, Evans SM, Hirano S, Liu FC (2014) Dual role for Islet-1 in promoting striatonigral and repressing striatopallidal genetic programs to specify striatonigral cell identity. Proc Natl Acad Sci U S A 111(1):E168–E177
18. Ehrman LA, Mu X, Waclaw RR, Yoshida Y, Vorhees CV, Klein WH, Campbell K (2013) The LIM homeobox gene Isl1 is required for the correct development of the striatonigral pathway in the mouse. Proc Natl Acad Sci U S A 110(42):E4026–E4035
19. Li H, Liu H, Sage C, Huang M, Chen ZY, Heller S (2004) Islet-1 expression in the developing chicken inner ear. J Comp Neurol 477(1):1–10
20. Huang M, Sage C, Li H, Xiang M, Heller S, Chen ZY (2008) Diverse expression patterns of LIM-homeodomain transcription factors (LIM-HDs) in mammalian inner ear development. Dev Dyn 237(11):3305–3312
21. Hans S, Liu D, Westerfield M (2004) Pax8 and Pax2a function synergistically in otic specification, downstream of the Foxi1 and Dlx3b transcription factors. Development 131(20):5091–5102
22. Pfeffer PL, Payer B, Reim G, di Magliano MP, Busslinger M (2002) The activation and maintenance of Pax2 expression at the midhindbrain boundary is controlled by separate enhancers. Development 129(2):307–318
23. Maricich SM, Herrup K (1999) Pax-2 expression defines a subset of GABAergic interneurons and their precursors in the developing murine cerebellum. J Neurobiol 41(2):281–294
24. Christophorou NA, Mende M, Lleras-Forero L, Grocott T, Streit A (2010) Pax2 coordinates epithelial morphogenesis and cell fate in the inner ear. Dev Biol 345(2):180–190
25. Bouchard M, de Caprona D, Busslinger M, Xu P, Fritzsch B (2010) Pax2 and Pax8 cooperate in mouse inner ear morphogenesis and innervation. BMC Dev Biol 10:89
26. Fritzsch B, Jahan I, Pan N, Elliott KL (2015) Evolving gene regulatory networks into cellular networks guiding adaptive behavior: an outline how single cells could have evolved into a centralized neurosensory system. Cell Tissue Res 359(1):295–313
27. Wang VY, Zoghbi HY (2001) Genetic regulation of cerebellar development. Nat Rev Neurosci 2(7):484–491
28. Zordan P, Croci L, Hawkes R, Consalez GG (2008) Comparative analysis of proneural gene expression in the embryonic cerebellum. Dev Dyn 237(6):1726–1735
29. Chumak T, Bohuslavova R, Macova I, Dodd N, Buckiova D, Fritzsch B, Syka J, Pavlinkova G (2015) Deterioration of the medial olivocochlear efferent system accelerates age-related hearing loss in Pax2-Isl1 transgenic mice. Mol Neurobiol
30. Simmons D, Duncan J, de Caprona DC, Fritzsch B (2011) Development of the inner ear efferent system. In: Ryugo DK, Fay RR, Popper AN (eds) Auditory and vestibular efferents. Springer, New York, pp 187–216
31. Duncan J, Kersigo J, Gray B, Fritzsch B: Combining lipophilic dye, in situ hybridization, immunohistochemistry, and histology. Journal of visualized experiments 2011(49).
32. Tonniges J, Hansen M, Duncan J, Bassett M, Fritzsch B, Gray B, Easwaran A, Nichols MG (2010) Photo- and bio-physical characterization of novel violet and near-infrared lipophilic fluorophores for neuronal tracing. J Microsc 239(2):117–134
33. Pfaffl MW (2001) A new mathematical model for relative quantification in real-time RT-PCR. Nucleic Acids Res 29(9):e45
34. Bohuslavova R, Kolar F, Kuthanova L, Neckar J, Tichopad A, Pavlinkova G (2010) Gene expression profiling of sex differences in HIF1-dependent adaptive cardiac responses to chronic hypoxia. J Appl Physiol 109(4):1195–1202
35. Khan Z, Carey J, Park HJ, Lehar M, Lasker D, Jinnah HA (2004) Abnormal motor behavior and vestibular dysfunction in the stargazer mouse mutant. Neuroscience 127(3):785–796
36. Brooks SP, Dunnett SB (2009) Tests to assess motor phenotype in mice: a user's guide. Nat Rev Neurosci 10(7):519–529
37. Carter RJ, Lione LA, Humby T, Mangiarini L, Mahal A, Bates GP, Dunnett SB, Morton AJ (1999) Characterization of progressive motor deficits in mice transgenic for the human Huntington's disease mutation. J Neurosci 19(8):3248–3257
38. Cristina C, Diaz-Torga G, Baldi A, Gongora A, Rubinstein M, Low MJ, Becu-Villalobos D (2005) Increased pituitary vascular endothelial growth factor-a in dopaminergic D2 receptor knockout female mice. Endocrinology 146(7):2952–2962
39. Autry AE, Adachi M, Nosyreva E, Na ES, Los MF, Cheng PF, Kavalali ET, Monteggia LM (2011) NMDA receptor blockade at rest triggers rapid behavioural antidepressant responses. Nature 475(7354):91–U109
40. Naydenov AV, Horne EA, Cheah CS, Swinney K, Hsu KL, Cao JK, Marrs WR, Blankman JL et al (2014) ABHD6 blockade exerts antiepileptic activity in PTZ-induced seizures and in spontaneous seizures in R6/2 mice. Neuron 83(2):361–371
41. Smith AM, Wellmann KA, Lundblad TM, Carter ML, Barron S, Dwoskin LP (2012) Lobeline attenuates neonatal ethanol-mediated changes in hyperactivity and dopamine transporter function in the prefrontal cortex in rats. Neuroscience 206:245–254

42. Maklad A, Kamel S, Wong E, Fritzsch B (2010) Development and organization of polarity-specific segregation of primary vestibular afferent fibers in mice. Cell Tissue Res 340(2):303–321
43. Leonard RB, Kevetter GA (2002) Molecular probes of the vestibular nerve. I. Peripheral termination patterns of calretinin, calbindin and peripherin containing fibers. Brain Res 928(1-2):8–17
44. Desai SS, Ali H, Lysakowski A (2005) Comparative morphology of rodent vestibular periphery. II. Cristae ampullares. J Neurophysiol 93(1):267–280
45. Desai SS, Zeh C, Lysakowski A (2005) Comparative morphology of rodent vestibular periphery. I. Saccular and utricular maculae. J Neurophysiol 93(1):251–266
46. Park JJ, Tang Y, Lopez I, Ishiyama A (2001) Age-related change in the number of neurons in the human vestibular ganglion. J Comp Neurol 431(4):437–443
47. Melcher JR, Kiang NY (1996) Generators of the brainstem auditory evoked potential in cat. III: identified cell populations. Hear Res 93(1-2):52–71
48. Resibois A, Rogers JH (1992) Calretinin in rat brain: an immunohistochemical study. Neuroscience 46(1):101–134
49. Lugli A, Forster Y, Haas P, Nocito A, Bucher C, Bissig H, Mirlacher M, Storz M et al (2003) Calretinin expression in human normal and neoplastic tissues: a tissue microarray analysis on 5233 tissue samples. Hum Pathol 34(10):994–1000
50. Nunzi MG, Birnstiel S, Bhattacharyya BJ, Slater NT, Mugnaini E (2001) Unipolar brush cells form a glutamatergic projection system within the mouse cerebellar cortex. J Comp Neurol 434(3):329–341
51. Radde-Gallwitz K, Pan L, Gan L, Lin X, Segil N, Chen P (2004) Expression of Islet1 marks the sensory and neuronal lineages in the mammalian inner ear. J Comp Neurol 477(4):412–421
52. Nakano Y, Jahan I, Bonde G, Sun X, Hildebrand MS, Engelhardt JF, Smith RJ, Cornell RA et al (2012) A mutation in the Srrm4 gene causes alternative splicing defects and deafness in the Bronx waltzer mouse. PLoS Genet 8(10):e1002966
53. Gerlai R, Pisacane P, Erickson S (2000) Heregulin, but not ErbB2 or ErbB3, heterozygous mutant mice exhibit hyperactivity in multiple behavioral tasks. Behav Brain Res 109(2):219–227
54. Vitali R, Clarke S (2004) Improved rotorod performance and hyperactivity in mice deficient in a protein repair methyltransferase. Behav Brain Res 153(1):129–141
55. Graham DR, Sidhu A (2010) Mice expressing the A53T mutant form of human alpha-synuclein exhibit hyperactivity and reduced anxiety-like behavior. J Neurosci Res 88(8):1777–1783
56. Altman J (1987) Morphological and behavioral markers of environmentally induced retardation of brain development: an animal model. Environ Health Perspect 74:153–168
57. Mao Y, Reiprich S, Wegner M, Fritzsch B (2014) Targeted deletion of Sox10 by Wnt1-cre defects neuronal migration and projection in the mouse inner ear. PLoS One 9(4):e94580
58. Fritzsch B, Pan N, Jahan I, Duncan JS, Kopecky BJ, Elliott KL, Kersigo J, Yang T (2013) Evolution and development of the tetrapod auditory system: an organ of Corti-centric perspective. Evol Devel 15(1):63–79
59. Zuniga MG, Dinkes RE, Davalos-Bichara M, Carey JP, Schubert MC, King WM, Walston J, Agrawal Y (2012) Association between hearing loss and saccular dysfunction in older individuals. Otol Neurotol 33(9):1586–1592
60. Morita N, Kariya S, Farajzadeh Deroee A, Cureoglu S, Nomiya S, Nomiya R, Harada T, Paparella MM (2009) Membranous labyrinth volumes in normal ears and Meniere disease: a three-dimensional reconstruction study. Laryngoscope 119(11):2216–2220
61. Cushing SL, Papsin BC, Rutka JA, James AL, Gordon KA (2008) Evidence of vestibular and balance dysfunction in children with profound sensorineural hearing loss using cochlear implants. Laryngoscope 118(10):1814–1823
62. Hatten ME, Heintz N (1995) Mechanisms of neural patterning and specification in the developing cerebellum. Annu Rev Neurosci 18: 385–408
63. Sgaier SK, Lao Z, Villanueva MP, Berenshteyn F, Stephen D, Turnbull RK, Joyner AL (2007) Genetic subdivision of the tectum and cerebellum into functionally related regions based on differential sensitivity to engrailed proteins. Development 134(12):2325–2335
64. Wurst W, Auerbach AB, Joyner AL (1994) Multiple developmental defects in Engrailed-1 mutant mice: an early mid-hindbrain deletion and patterning defects in forelimbs and sternum. Development 120(7):2065–2075
65. Timmer JR, Wang C, Niswander L (2002) BMP signaling patterns the dorsal and intermediate neural tube via regulation of homeobox and helix-loop-helix transcription factors. Development 129(10): 2459–2472
66. Stoodley CJ, Schmahmann JD (2009) Functional topography in the human cerebellum: a meta-analysis of neuroimaging studies. NeuroImage 44(2):489–501
67. Wang VY, Rose MF, Zoghbi HY (2005) Math1 expression redefines the rhombic lip derivatives and reveals novel lineages within the brainstem and cerebellum. Neuron 48(1):31–43
68. Fink AJ, Englund C, Daza RA, Pham D, Lau C, Nivison M, Kowalczyk T, Hevner RF (2006) Development of the deep cerebellar nuclei: transcription factors and cell migration from the rhombic lip. J Neurosci 26(11):3066–3076
69. Schwarting RK, Huston JP (1996) The unilateral 6-hydroxydopamine lesion model in behavioral brain research. Analysis of functional deficits, recovery and treatments. Prog Neurobiol 50(2-3):275–331
70. Schirmer M, Kaiser A, Lessenich A, Lindemann S, Fedrowitz M, Gernert M, Loscher W (2007) Auditory and vestibular defects and behavioral alterations after neonatal administration of streptomycin to Lewis rats: similarities and differences to the circling (ci2/ci2) Lewis rat mutant. Brain Res 1155:179–195
71. Smith AD, Llinás R, Kostyuk PG (1980) Commentaries in the neurosciences. Pergamon Press Ltd, Oxford
72. Mizuhara E, Minaki Y, Nakatani T, Kumai M, Inoue T, Muguruma K, Sasai Y, Ono Y (2010) Purkinje cells originate from cerebellar ventricular zone progenitors positive for Neph3 and E-cadherin. Dev Biol 338(2):202–214
73. Kalinichenko SG, Okhotin VE (2005) Unipolar brush cells—a new type of excitatory interneuron in the cerebellar cortex and cochlear nuclei of the brainstem. Neurosci Behav Physiol 35(1):21–36
74. Hulst T, van der Geest JN, Thürling M, Goericke S, Frens MA, Timmann D, Donchin O (2015) Ageing shows a pattern of cerebellar degeneration analogous, but not equal, to that in patients suffering from cerebellar degenerative disease. NeuroImage 116:196–206
75. Berquin P, Giedd J, Jacobsen L, Hamburger S, Krain A, Rapoport J, Castellanos F (1998) Cerebellum in attention-deficit hyperactivity disorder: a morphometric MRI study. Neurology 50(4):1087–1093
76. Courvoisie H, Hooper SR, Fine C, Kwock L, Castillo M (2004) Neurometabolic functioning and neuropsychological correlates in children with ADHD-H: preliminary findings. J Neuropsychiatry Clin Neurosci 16(1):63–69
77. Edden RA, Crocetti D, Zhu H, Gilbert DL, Mostofsky SH (2012) Reduced GABA concentration in attention-deficit/hyperactivity disorder. Arch Gen Psychiatry 69(7):750–753
78. Breggin P (2007) Talking back to Ritalin: what doctors aren't telling you about stimulants and ADHD. Da Capo Press, Boston

5.2 Nezbytná role SOX2 pro vývoj neuronů a senzorických buněk vnitřního ucha

Pro objasnění funkce transkripčního faktoru SOX2 během vývoje vnitřního ucha jsme použili systém Cre-loxP pro vytvoření podmíněné delece genu *Sox2* v ISL1 pozitivních buňkách. Konkrétně byly myši *Isl1-Cre* nesoucí gen pro Cre rekombinázu vložený do endogenního lokusu genu *Isl1* zkříženy s myším kmenem mající gen *Sox2* ohraničený *loxP* sekvencemi (*Sox2*$^{f/f}$) za účelem získání mutantních jedinců *Isl1-Cre*$^{+/-}$*; Sox2*$^{f/f}$ (*Sox2CKO*). Myši *Sox2*$^{+/f}$ nebo *Sox2*$^{f/f}$ byly použity jako kontroly. Imunohistologická barvení potvrdila shodující se expresi ISL1 a Isl1-Cre. Myší kmen *Isl1-Cre* byl vybrán z důvodu exprese Isl1-Cre v senzorických i neurálních prekurzorech od raného vývoje vnitřního ucha.

Heterozygotní jedinci se zachovalou jednou alelou *Sox2* (*Isl1-Cre; Sox2*$^{f/+}$) byli životaschopní a bez zjevného fenotypu, zatímco homozygoti s podmíněnou delecí obou alel umírali krátce po narození a měli menší abnormálně vyvinuté oči. Trojrozměrná rekonstrukce vnitřního ucha v E14,5 odhalila chybějící kristy i anteriorní a posteriorní kanál, menší utrikulus a sakulus a o 20 % zkrácenou kochleu u *Sox2CKO*. Excise *Sox2* v některých orgánech vnitřního ucha byla zpožděná, protože byl tento transkripční faktor detekován v E11,5 a E13,5 v utrikulu, sakulu a kochleární bázi, zatímco v kristách nebyla jeho exprese u mutanta nikdy potvrzena. Reziduální exprese SOX2 byla dostatečná k diferenciaci limitovaného počtu vláskových buněk, které byly detekovány v utrikulu, sakulu a bazální části sluchového ústrojí. Mutantní kochlea v oblasti báze obsahovala vláskové buňky, které se lišily svou velikostí, orientací a organizací stereocílií ve srovnání s vláskovými buňkami kontrol, zatímco vláskové buňky v utrikulu byly svojí morfologií srovnatelné mezi mutantem a kontrolou. V kochleární bázi byla detekována reziduální exprese *Atoh1* mRNA korespondující s expresí SOX2 a potvrzující jednoznačnou závislost *Atoh1* na SOX2. Souhrnně tyto výsledky ukazují na důležitost SOX2 pro přežití senzorických prekurzorů a diferenciaci vláskových buněk. Některé vláskové buňky Cortiho orgánu byly pozitivní na marker vláskových buněk (myosin VIIa) i marker nervových vláken (acetylovaný α-tubulin) naznačující možnou roli SOX2 při segregaci neuronálního a senzorického fenotypu. Po podmíněné deleci *Sox2* nebyl ve vnitřním uchu detekován *Fgf10*, jehož exprese je tak přímo nebo nepřímo ovlivňována SOX2.

V E10,5 neuroblasty u *Sox2CKO* delaminovaly podobně jako u kontrol a exprese transkripčních faktorů NEUROD1 a PAX2 byla srovnatelná mezi kontrolou a mutantem v E11,5. O několik dní později (E13,5) však došlo k úbytku vestibulárních vláken a v E14,5 -

E15,5 byla potvrzena masivní apoptóza neuronů vestibulárního ganglia. Neurony spirálního ganglia byly u mutanta detekovány pouze v bázi a v E15,5 taktéž podléhaly programované buněčné smrti. Nervová vlákna těchto neuronů vedla jednak k reziduálním vláskovým buňkám v kochleární bázi a jednak i do oblastí bez senzorického epitelu. Apikální neurony se u *Sox2CKO* vůbec nediferencovaly.

SCIENTIFIC REPORTS

OPEN

Received: 07 July 2016
Accepted: 07 November 2016
Published: 05 December 2016

Incomplete and delayed Sox2 deletion defines residual ear neurosensory development and maintenance

Martina Dvorakova[1,2,*], Israt Jahan[3,*], Iva Macova[1,2], Tetyana Chumak[4], Romana Bohuslavova[1], Josef Syka[4], Bernd Fritzsch[3,†] & Gabriela Pavlinkova[1,†]

The role of Sox2 in neurosensory development is not yet fully understood. Using mice with conditional *Islet1-cre* mediated deletion of *Sox2*, we explored the function of Sox2 in neurosensory development in a model with limited cell type diversification, the inner ear. In *Sox2* conditional mutants, neurons initially appear to form normally, whereas late- differentiating neurons of the cochlear apex never form. Variable numbers of hair cells differentiate in the utricle, saccule, and cochlear base but sensory epithelium formation is completely absent in the apex and all three cristae of the semicircular canal ampullae. Hair cells differentiate only in sensory epithelia known or proposed to have a lineage relationship of neurons and hair cells. All initially formed neurons lacking hair cell targets die by apoptosis days after they project toward non-existing epithelia. Therefore, late neuronal development depends directly on Sox2 for differentiation and on the survival of hair cells, possibly derived from common neurosensory precursors.

SRY-box (Sox) transcription factors are essential for embryonic and adult neuronal stem cell development[1]. Sox2 and other Sox genes dynamically specify the proliferating neuronal lineage, upregulate the differentiating transcription of basic helix-loop-helix (bHLH) factors and are ultimately downregulated by bHLH transcription factors to allow the differentiation of neurons and glia cells[2] in sequential transcriptional waves[3]. This process is conserved across neurosensory evolution[4] but is difficult to assess in the brain due to the complexity of a multitude of cell fate decisions. The developing inner ear has just two neurosensory cell types: hair cells (HCs) for mechanotransduction and sensory neurons to conduct information to the brain[5,6]. The ear provides a simpler model to study Sox2 involvement in specification, proliferation, and differentiation compared to the brain.

The mammalian inner ear has six sensory epithelia: Five vestibular (the maculae of utricle and saccule, and the cristae of the three semicircular canal ampullae) and the organ of Corti, the auditory sensory organ of the cochlea. Inner ear neuronal development primarily depends on *Neurogenin1* (*Neurog1*) and *Neurod1* for neuronal specification and differentiation. Sensory fate specification occurs after neurogenesis and requires the expression of *Atoh1*[7–9]. The expression of these bHLH transcription factors requires additional signaling molecules to regulate the transition from active proliferation to a progenitor cell state primed for commitment and differentiation. In particular, Sox2 may play an important role in this transition during inner ear development. The very early expression of Sox2 through the otic placode overlaps with the earliest forming neurons[7,10] and it is expressed in both neurogenic and sensory progenitors[11]. Sox2 may also be involved in non-sensory development[12]. Experimental data indicate that there are complex antagonistic and cooperative interactions between Sox2 and bHLH transcription factors during the development of the inner ear. Sox2 activates *Atoh1* and *Neurog1*, but also promotes negative regulators of *Atoh1* and *Neurog1* like *Neurod1*, thereby suppressing premature HC and neuronal differentiation in mice and chickens[13,14]. The results in chickens[15] suggest that Sox2 is part of a regulatory network responsible for the specification of neuronal *versus* prosensory cell fates in inner ear development.

[1]Institute of Biotechnology CAS, Prague, Czechia. [2]Faculty of Science, Charles University, Prague, Czechia. [3]Department of Biology, University of Iowa, Iowa City, IA, USA. [4]Institute of Experimental Medicine CAS, Prague, Czechia. *These authors contributed equally to this work. †These authors jointly supervised this work. Correspondence and requests for materials should be addressed to G.P. (email: gpavlinkova@ibt.cas.cz)

However, the role of Sox2 in the transcriptional network that controls neurosensory development in mice, beyond promoting it, remains unclear.

To analyze the molecular effects of *Sox2* deletion on the neurosensory development of the ear, we generated a new mouse model of *Sox2* conditional deletion, *Islet1-cre;Sox2$^{f/f}$* (*Isl1-cre;Sox2$^{f/f}$*). We chose *Isl1-cre* to achieve a partial overlap of *cre* and *Sox2* expression in the sensory epithelium and delaminating neurons in the inner ear[11,12,16,17]. The delayed elimination of Sox2 by Isl1-cre does not affect the earliest specification events in the developing ear, as these *Isl1-cre;Sox2$^{f/f}$* mutants show an initial formation of vestibular neurons and spiral ganglion (SG) neurons in the cochlear base. In contrast, SG neurons, which differentiate last, never form in the apex. Additionally, conditional mutant mice do not develop cristae of the semicircular canal ampullae and show correlated semicircular canal defects. In contrast, the utricle, saccule and base of the cochlea develop a variable number of HCs receiving an aberrant innervation from the few surviving neurons. All initially formed neurons lacking hair cell targets die by apoptosis days after they project toward non-existing epithelia. In summary, our data indicate that some HCs are refractory to the delayed loss of Sox2 and neuronal formation and viability depends on Sox2 both directly and indirectly.

Results

Sox2, _Isl1_ and _Isl1-cre_ are partially co-expressed in the otocyst. To analyze the molecular effects of *Sox2* deletion on the neurosensory development of the inner ear, we generated a new mouse model of *Sox2* conditional deletion using *Isl1-cre/+* with a direct *cre* knockin into the endogenous *Isl1* locus[18]. First, we characterized Isl1 and Isl1-cre protein early expression in the otocyst at E9.5 and found that their expression patterns overlap (Supplementary Fig. 1a). Isl1 and Isl1-cre were expressed in the delaminated vestibular neurons and also within the otic neurosensory epithelium at E9.5 (Supplementary Fig. 1a',a"). Similarly, the cells co-expressing Isl1 and Sox2 were detected in the otic epithelium as early as E9.5 (Supplementary Fig. 1a", arrows). However, Isl1 and Isl1-cre are not as widely expressed as Sox2 in the early sensory epithelium of the otic vesicle. Next, we analyzed the cre-mediated excision within the developing inner ear using a R26R-*lacZ* reporter line and *in situ* hybridization for *Isl1* mRNA. At E10.5, cre-mediated β-gal reporter expression showed cre recombination in the tissues corresponding to the expression of *Isl1* mRNA and protein (Supplementary Fig. 1b-c'). *Isl1* mRNA, cre, and protein are expressed in the progenitor cells of the sensory epithelium and in delaminating sensory neurons, consistent with previously reported data[16,17].

Conditional deletion of Sox2 causes inner ear dysmorphology. Heterozygous *Isl1-cre/+;Sox2$^{f/+}$* mice are viable and can be used as breeding stock. The morphology of the inner ear and hearing functions were comparable to wild type mice (Supplementary Fig. 2). The decreased gene dose of *Sox2* in heterozygous *Isl1-cre/+ ;Sox2$^{f/+}$* mice did not affect the normal development and maintenance of the sensory organs of the inner ear in any detectable way. In contrast, *Isl1-cre/+;Sox2$^{f/f}$* mutants (Sox2 CKO) died immediately after birth, although they did not exhibit any external morphological defects beyond a reduced and misshapen eye. These data demonstrate that *Isl1-cre* can be used for the recombination of *Sox2$^{f/f}$* in common precursors for sensory epithelia and sensory neurons and that homozygous mice develop a severe enough phenotype that they die at birth.

A computer assisted 3D-reconstruction revealed profound differences in the ear at E12.5 and E14.5 (Fig. 1a-b'). The *Sox2* CKO inner ears had no semicircular canal ampullae or cristae of the ampullae, and only rudiments of the posterior and anterior semicircular canals with the horizontal canal being the only canal ever forming. The formation of a horizontal canal is consistent with previous reports that this canal can form in the absence of a crista[19], whereas the formation of the vertical canals depends on Fgf10/BMP4 interactions expressed in the cristae of the anterior and posterior vertical canal ampullae[20]. The utricle and saccule were smaller, and the cochlear duct was 20% shorter compared to controls at E14.5. This phenotype was comparable to previous reports on the *Lcc* (light coat and circling; a mutant generated by a X-ray-irradiation-induced mutation with a severe inner ear malformation due to the absence of Sox2 in the developing inner ear)[21]. Scanning electron microscopy showed a profound reduction of sensory epithelia in Sox2 CKO. Only individual HCs or clusters of HCs formed in the basal half of the cochlea with undifferentiated epithelial cells between them (Fig. 1d), while the spiral sulcus and tectorial membrane formed normally. HCs in the Sox2 CKO cochlea differed in their size, orientation, and bundle organization (Fig. 1d'). There was no sign of HC differentiation in the entire apex, instead a flat epithelium was observed, as previously described for the *Lcc* mutant[21]. Differentiated HCs in the utricle in terms of cell size and stereocilia formation were comparable between Sox2 CKO and controls (Fig. 1e,f).

Incomplete and delayed Isl1-cre recombination of floxed _Sox2_ alters inner ear gene expression. We next investigated how rapidly Sox2 protein disappears after *Isl1-cre* expression. E10.5 ears already showed a reduced overlap of Isl1 and Sox2 immunostaining in the Sox2 CKO, indicating a loss of Sox2^{+} cells in the neurosensory epithelium (Supplementary Fig. 3a,b). Some detectable Sox2 protein may be found in the Sox2 CKO ear at E11.5 (Supplementary Fig. 3b'). At E13.5, Sox2 was expressed throughout the entire length of the control cochlea, whereas, in the Sox2 CKO cochlea, Sox2 was detected only in the base (Supplementary Fig. 3c,d). Therefore, we next investigated how rapidly *Sox2* mRNA disappears after Isl1-cre mediated recombination (Supplementary Fig. 3e–h). These data show a surprisingly uneven loss of *Sox2* expression in the Sox2 CKO: whereas no *Sox2* signal was detectable in all three cristae of the semicircular canal ampullae, the utricle showed a minor, and the saccule and cochlea a more obvious, reduction at E11.5 (Supplementary Fig. 3f,f'). At E13.5, there was no expression of *Sox2* mRNA in the cristae of the semicircular canal ampullae and the apex of the cochlea, limited expression in the base of the cochlea, and weak expression in the utricle and saccule (Supplementary Fig. 3h) compared to controls (Supplementary Fig. 3g). Notably, neither at E11.5 nor at E13.5 was there any expression of *Sox2* in all three cristae of the semicircular canal ampullae or apical half of the growing cochlear duct. These data suggest that Isl1-cre rapidly and effectively recombines floxed *Sox2* in certain areas of

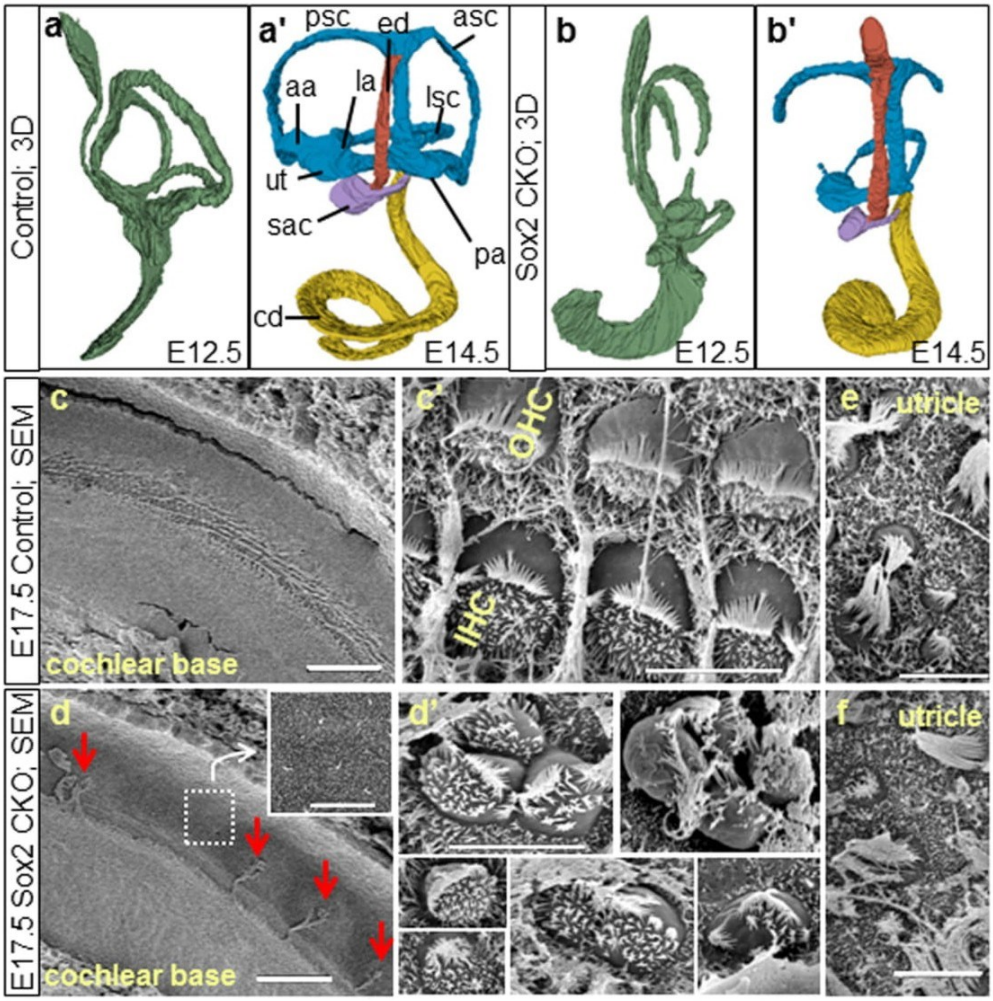

Figure 1. Altered morphology of the Sox2 CKO inner ear. (**a**-**b'**) 3D-reconstruction reveals severe changes in the developing inner ear at E12.5 and E14.5. (**b,b'**) No ampullae of semicircular canals and only rudiments of the posterior and anterior semicircular canals are present in Sox2 CKO. The utricle and saccule are smaller. (**a',b'**) The cochlear duct (cd) has decreased coiling and is shorter compared to controls. (**c**–**f**) Scanning electron microscopy shows a few individual cells and small clumps of cells with a hair cell-like phenotype in the base of the Sox2 CKO cochlea (arrows). (**d**) The rest of the organ of Corti is missing as shown by the overview of the whole cd width and by magnification of the sensory epithelium area. (**d'**) HCs vary in size, orientation and bundle organization. (**e**,**f**) The cellular phenotype of differentiated HCs in the Sox2 CKO utricle is comparable to controls. aa, anterior ampulla; asc, anterior semicircular canal; cd, cochlear duct; ed, endolymphatic duct; la, lateral ampulla; lsc, lateral semicircular canal; pa, posterior ampulla; psc, posterior semicircular canal; sac, saccule; ut, utricle; OHC, outer hair cells; IHC, inner hair cells. Scale bars: 50 μm (c,d), 5 μm (c',d',e,f).

Isl1 expression but not so in others. As Sox2 expression precedes Isl1-expression, this suggests delayed Isl1-cre recombination. Using Isl1-cre to delete *Atoh1*$^{f/f}$ (Atoh1 CKO), we showed that Isl1-cre has a uniform effect in all sensory epithelia of the inner ear with a complete loss of HCs (Supplementary Fig. 4). As opposed to Pax2-cre deletion of *Atoh1*[22], Isl1-cre deletion of *Atoh1* shows no residual Sox2 expression in sensory epithelia and concomitant innervation. Atoh1 CKO data combined with Pax2-cre *Atoh1* data suggest a simple delayed recombination of *Sox2* by Isl1-cre in the epithelium.

Since *Sox2* is completely lost in all three cristae of the semicircular canal ampullae (Supplementary Fig. 3f) and cristae formation critically depends on Fgf10 for normal development[23], we next tested the expression of *Fgf10* mRNA (Supplementary Fig. 3i,j). No canal crista labeling for *Fgf10* could be detected and late developmental stages showed limited *Fgf10* labeling in some saccular neurons of Sox2 CKO. These data imply an unexpected level of dependency of Fgf10 on Sox2. How direct or indirect this effect is, is yet to be determined.

Biphasic loss of neurons indicates direct and indirect effects of Sox2 CKO. The expression of Neurog1 and neuronal delamination is among the earliest specification events in the developing ear[7,24]. The initial

onset of Sox2 expression is nearly simultaneous with Neurog1 specifying neurogenic progenitors in the otic placode as early as E8.5[25]. One day later at E9.5, Isl1 is expressed in the delaminated vestibular neurons and in the neuroblast precursor cells within the otic epithelium[17]. Consistent with expression patterns, the early neurogenic specification events were unaffected by Isl1-cre mediated *Sox2* recombination, as demonstrated by a comparable formation of the delaminated vestibular neurons between Sox2 CKO and controls at E10.5 (Supplementary Fig. 3a,b). Furthermore, the expression of early neuronal differentiation marker, Neurod1, was comparable between controls and Sox2 CKO at E11.5, which is consistent with normal neuron differentiation (Supplementary Fig. 3k,l). Similarly, in the E11.5 inner ear, there was no obvious change in the expression of Pax2 (Supplementary Fig. 3m,n), one of the earliest genes expressed during inner ear development[26]. Neurofilament immunocytochemistry showed a limited growth of fibers toward the region of the anterior and horizontal semicircular canal crista in the Sox2 CKO inner ear, whereas growth toward the utricle, saccule, and posterior canal crista was similar between Sox2 CKO and controls (Fig. 2a,b). Later stages had fibers that did not innervate the 'crista organ region' but formed loops in the area where these organs should have been (Fig. 2a',b'), which is similar to previous records on Fgf10 mutants[23]. These fibers of cristae of the semicircular canal ampullae remained until E14.5 (Fig. 2a",b"), when they regressed and disappeared nearly completely by E18.5, leaving only a variable innervation to the utricle and saccule (Supplementary Fig. 6c–f). Our data suggest that many vestibular neurons form, develop, and project but are only later eliminated. Consistent with the progressive loss of vestibular fibers, we found increased Caspase 3 immunolabeling in the vestibular ganglion neurons in older stages (Fig. 2c-d'"), indicating rapid apoptosis of most vestibular neurons, likely due to the lack of neurotrophins[27] and/or HCs[22]. Quantification of Caspase 3 positive cells (E11.5–15.5) revealed a significant increase of Caspase 3 in the Sox2 CKO mutant (Supplementary Fig. 5). SG neurons form only near the base (Fig. 2b,b'", Supplementary Fig. 6b,b') but never in the apex of the mutant. Fewer basal SG neurons are present after E15.5, and by E18.5 only a few neurons are left projecting toward the base and occasionally sending fibers toward the apex (Supplementary Fig. 6e). Since only basal turn SG neurons ever form, we also found Caspase 3 immunocytochemical signals only in the base at E15.5 (Fig. 2d"), indicating a loss of initially formed SG neurons due to the absence of sensory epithelium.

Delayed deletion of *Sox2* allows limited HC differentiation in some epithelia. To define the extent of cellular changes in the inner ear of Sox2 CKO, the expression of specific markers for neuronal innervation (tubulin) and HCs (Myo7a) was analyzed. The Sox2 CKO sensory epithelium of the utricle, saccule, and cochlear base was smaller with a reduced domain of $Sox2^{+}$ at E14.5 (Fig. 3a–d, Supplementary Fig. 7). No Sox2 protein was ever detected in the apex despite transient labeling of the base (Fig. 3b, Supplementary Fig. 3d). In the cochlear base, the strong Sox2 expression domain was shifted toward the greater epithelial ridge (GER), whereas scattered cells with a very limited Sox2 expression were detected in the organ of Corti (Fig. 3b, dotted area). Consistent with the residual expression of Sox2 in the CKO utricle, saccule, and basal turn of the cochlea, we found Myo7a positive HCs only in these epithelia (Fig. 3e–l). We never found any Myo7a positive cells in the apex of the cochlea or cristae of the semicircular canal ampullae. This suggests that a limited amount of Sox2 expression for a yet to be determined time is needed to maintain and differentiate HC precursors into HCs. A complete deletion of Sox2 in the cristae of the semicircular canal ampullae and the apex leads to a complete loss of all HC differentiation. We next quantified the number of Myo7a positive cells and found that the utricle and saccule showed a profound variability (Fig. 3n, Supplementary Fig. 8, Table S1). Detailed quantification using Myo7a as a HC marker revealed a reduction of HCs even in the best cases and in most cases down to around 10% of the control littermates.

The remaining differentiated HCs dictate the residual pattern of innervation. The patterning of the inner ear, and in particular the innervation of the cochlea, requires a multitude of known and unknown molecules to guide the nerve fibers to the sensory epithelia and to sort the pattern of innervation to the distinct cell types within the sensory epithelia[6,28]. The absence of Sox2 seems to have no effect on the initial growth of fibers that is apparently primarily directed along Schwann cells[29]. Since only scattered HCs remain, an unusual pattern of innervation emerges in all sensory epithelia with fibers showing directional growth toward remaining HCs but also transient expansion into HC-free territories like the apex (Fig. 3m). In the basal turn of the organ of Corti, spiraling fibers may be found that are directed toward the apex (Fig. 3j,m, Supplementary Fig. 6) and not the base, as is typically the case for type II SGN fibers[6,30]. In general, the remaining HCs were the target of residual innervation, but fibers could overshoot and extend into HC-free territory, suggesting guiding issues possibly related to the Sox2 deletion in the neurons and/or supporting cells. A similar phenotype of fibers extending into HC-free territory was reported in mice with a loss of Schwann cells[29]. The variation in the number and distribution of the remaining HCs, combined with the transient viability of neurons outside HC areas, apparently determines the variation in the pattern of residual innervation.

Differentiated HCs in the Sox2 CKO inner ear have unusual features. Closer inspection of epithelia with a higher number of Myo7a positive cells revealed a variable degree of differentiation of HCs in terms of stereocilia development, cell size, distribution, and viability (Fig. 1, Fig. 4a-a",b). HCs differentiate as distinct types recognizable by their stereocilia with a complete absence of innervation[7,31]. Four distinct types of HCs are found in the mammalian inner ear with respect to stereocilia arrangement and stereocilia diameters (type I + II vestibular HCs, inner and outer HCs of the cochlea). In fact, inner and outer HCs are identified (as the name implies) based on their position relative to pillar cells. In the vestibular organs, type I and type II hair cells are known to be distinct based on the stereocilia bundle[32]. Furthermore, cochlea stereocilia bundles are very different from those of vestibular organs. While the molecular components determining the polarity within a given HC and across sensory epithelia are emerging[33,34], there is limited evidence on the molecular basis of vestibular versus cochlear HC bundle organization or the distinct differences in stereocilia diameters of inner and outer HCs[30]. Sox2 seems to play a minor role in this process, as many differentiating HCs in the Sox2 CKO have the

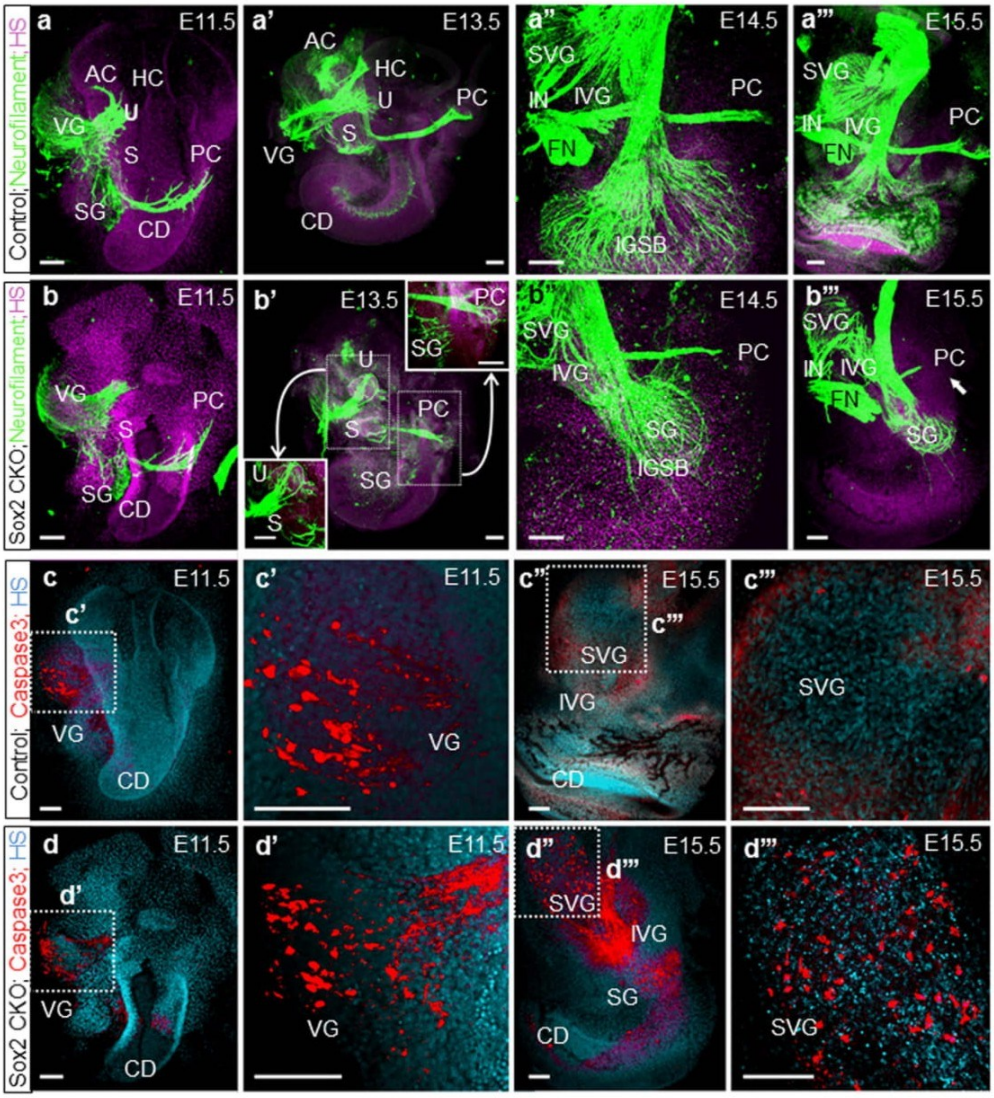

Figure 2. Isl1-cre mediated Sox2 loss disrupts neuron formation and results in massive neuronal degeneration by activation of Caspase3. (**a,b**) Immunofluorescence staining of neurofilament in the Sox2 CKO shows similar formation of vestibular neurons at E11.5 compared to controls. (**a',b'**) At E13.5, fibers are aberrantly projecting toward the utricle (or combined utricle and anterior and horizontal canal cristae) and posterior canal cristae of the Sox2 CKO. (**a",b",a"',b"'**) Fibers to the posterior canal crista start to retract in the absence of target HCs starting at E14.5 in the mutant. (**b"'**) Only a few radial fibers are formed near the base of the E15.5 Sox2 CKO cochlea. (**c, c',d,d'**) Immunofluorescence of activated Caspase3 reveals positive staining restricted mainly in the VG in the E11.5 Sox2 CKO comparable to the control littermates. (**c",c"',d",d"'**) However, Caspase3 mediated cell death is massively progressed to IVG, SVG, and SG at E15.5 compared to no caspase positive cells in the control littermates. Scale bars: 100 μm. AC, anterior canal crista; CD, cochlear duct; FN, facial nerve; HS, Hoechst nuclear stain; IGSB, intraganglionic spiral bundle; IVG, inferior vestibular ganglion; IN, intermediate nerve; HC, horizontal canal crista; PC, posterior canal crista; S, saccule; SG, spiral ganglion; SVG, superior vestibular ganglion; U, utricle; VG, vestibular ganglia.

sensory-epithelium-specific polarity and bundle organization. While stereocilia specific to all four types of HCs were found in the Sox2 CKO inner ear, some HCs showed a mixed diameter of stereocilia, indicating an incomplete segregation of the two vestibular and cochlear HC types after transient and limited expression of Sox2 (Fig. 4a-a",b). Whether this is a direct effect of Sox2 or is related to the previously described effect of the level of Atoh1 in cochlear HC differentiation[35] remains to be seen.

We also found many ectopic Myo7a positive HCs in GER, as well as in the area of Hensen/Claudius cells (lateral to the organ of Corti) in the Sox2 CKO cochlear base (Fig. 4c-d'). The combination of p75 and Myo7a immunolabeling shows an unusual configuration and distribution of p75 positive cells near the remaining Myo7a

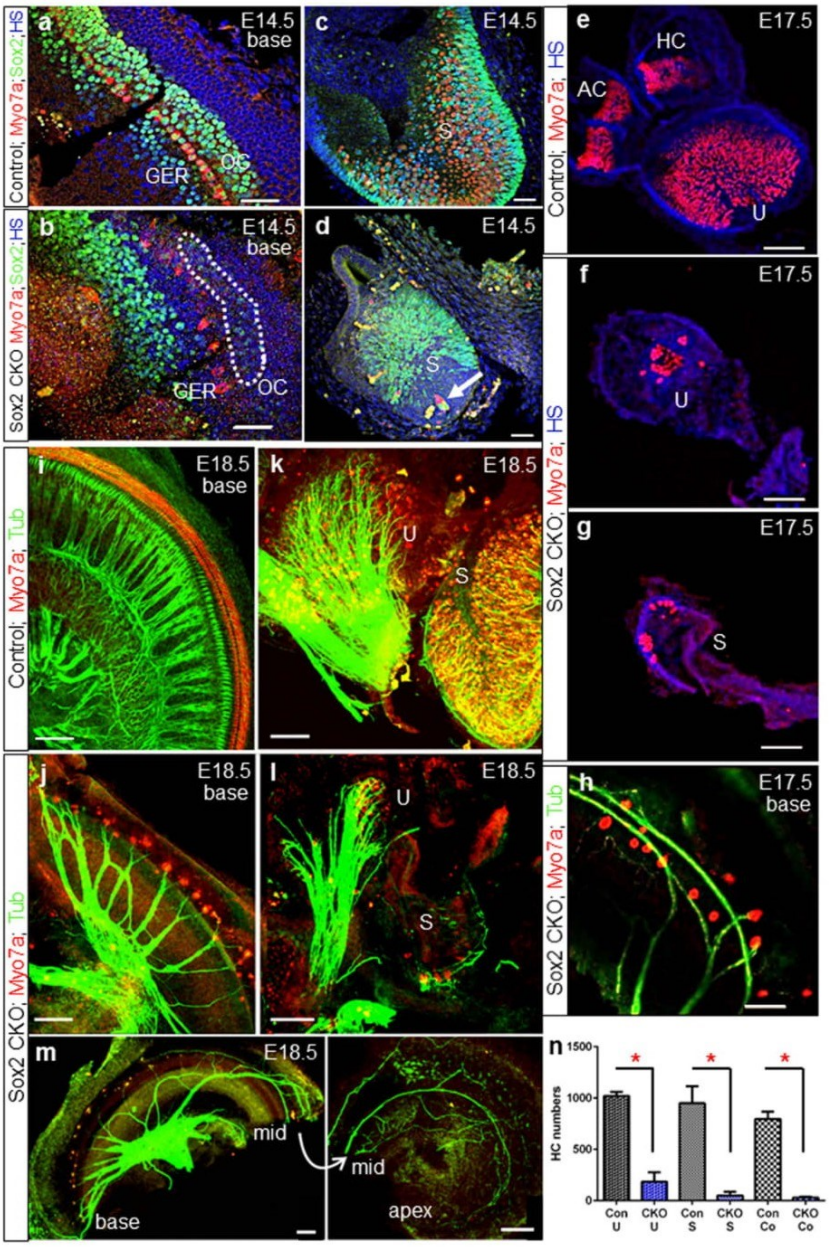

Figure 3. Delayed deletion of Sox2 results in the differentiation of some neurosensory cells in the basal cochlear turn and in the vestibular organs. (**a,b**) Sox2$^+$ cells in the Sox2 CKO cochlea are detected only in the base at the age of E14.5 and disappear later in development. (**b**) The strong Sox2 expression domain is shifted toward the GER. Similarly, Myo7a$^+$ cells do not differentiate in the proper area of OC. Some weak Sox2 expression remains in the OC area of Sox2 CKO (dotted area). (**c,d**) Variable numbers of HCs (Myo7a$^+$) and supporting cells (Sox2$^+$) develop in the Sox2 CKO vestibular system. (**d**) HCs in the saccule also develop in the area that lacks supporting cells (arrow). (**e–h**) Some poorly differentiated Myo7a$^+$ HCs are present in the utricle, saccule and basal turn of the cochlea of the Sox2 CKO at E17.5. (**i–m**) At E18.5, the innervation of mutant cochlea, saccule and utricle is severely reduced and shows an unusual pattern compared to controls. Fibers show mostly directional growth toward remaining HCs but also transient expansion into HC-free regions. (**n**) The quantification of Myo7a positive HCs after whole mount immunostaining shows a striking reduction of HCs in the Sox2 CKO inner ear compared to littermate controls for the utricle (U), saccule (S) and cochlea (Co). Myo7a$^+$ HCs were counted after whole mount immunostaining using LAS AF Lite draw counter to avoid counting error. The total number of HCs was determined in the entire utricle and saccule, and in the entire Sox2 CKO cochlea. The number of HCs in the control cochlea represents the total number of HCs in 1.5 mm of the base. The values represent means ± SD (N = 4–7 individuals/group). *P < 0.0001, *t*-test. Scale bars: 50 μm (a–h), 100 μm (i–m). AC, anterior crista; GER, greater epithelial ridge; HC, horizontal crista; OC, organ of Corti; S, saccule; U, utricle.

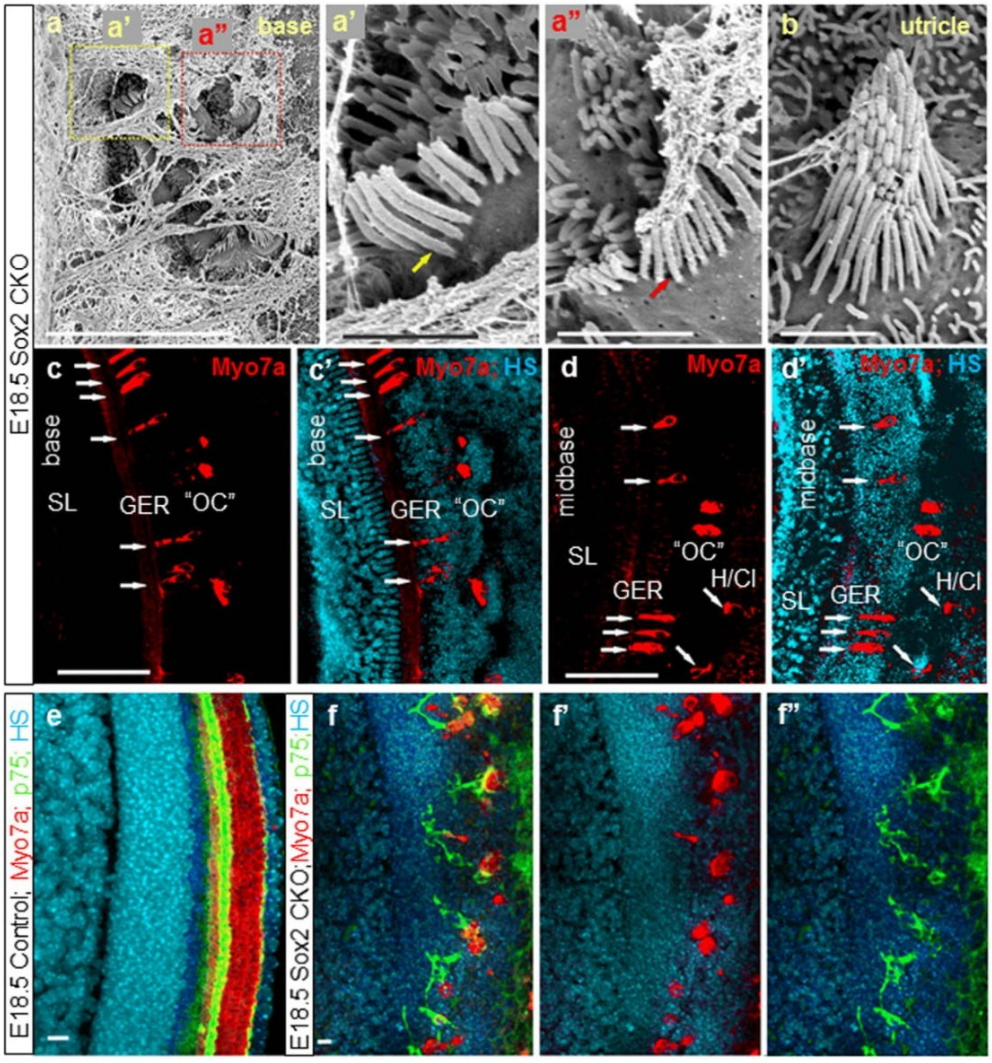

Figure 4. Aberrant HCs in ectopic topology and abnormal pillar cells are formed in the Sox2 CKO. Patches of HCs in the base of the E18.5 Sox2 CKO cochlea are covered by a tectorial membrane with HCs in the topology of inner HCs displaying both large diameter (**a,a'**) and small diameter (**a,a"**) stereocilia reminiscent of inner and outer HCs, respectively. (**b**) Vestibular HCs show normal organization of stereocilia but many display variability in stereocilia diameter in a single HC, normally associated with either type I or type II vestibular HCs. (**c-d'**) Scattered Myo7a positive HCs are detected in the area corresponding topologically to the organ of Corti (OC); however, forming atypical organ of Corti ("OC") in the mutant. Immunostaining of Myo7a reveals formation of HCs in the ectopic topologies, medial to OC, in the GER, as well as lateral to OC (in the area of Hensen/Claudius cells) (white arrows) in addition to the area of "OC" in the E18.5 Sox2 CKO. (**e-f"**) The combination of p75 and Myo7a immunolabeling shows an unusual configuration and distribution of p75 positive cells near the remaining Myo7a positive HCs in E18.5 Sox2 CKO compared to the single row of $p75^{+}$ inner pillar cells in control littermates (**e**). Scale bars: 10 μm (a,e-f"), 1 μm (a',a",b), 100 μm (c-d'). GER, greater epithelial ridge; H/Cl, Hensen/Claudius cells; OC, organ of Corti; "OC", atypical organ of Corti in the mutant; SL, spiral limbus.

positive HCs in E18.5 Sox2 CKO compared to the single row of $p75^{+}$ inner pillar cells in control littermates (Fig. 4e-f"). Nuclear staining revealed apoptosis in many HCs, suggesting that the variability in numbers is driven by two processes: the reduced formation of viable HCs and the loss of some unviable HCs. Longitudinal studies of Sox2 protein levels in viable and non-viable HCs are needed to clarify how early Sox2 protein levels define HC viability. Since both the level[34] and duration of Atoh1 expression[36] determine the normal differentiation of HCs, we investigated the expression of *Atoh1* using *in situ* hybridization[33]. Compared to the profound labeling of control littermates, we only found a limited, patchy expression of *Atoh1* in the basal turn of the cochlea (Fig. 5a-b"), corresponding to the expression of Sox2 in the base of the Sox2 CKO. These results confirm that *Atoh1* expression and the possible level of expression critically depend on Sox2. The dose effect of Sox2 in activating the

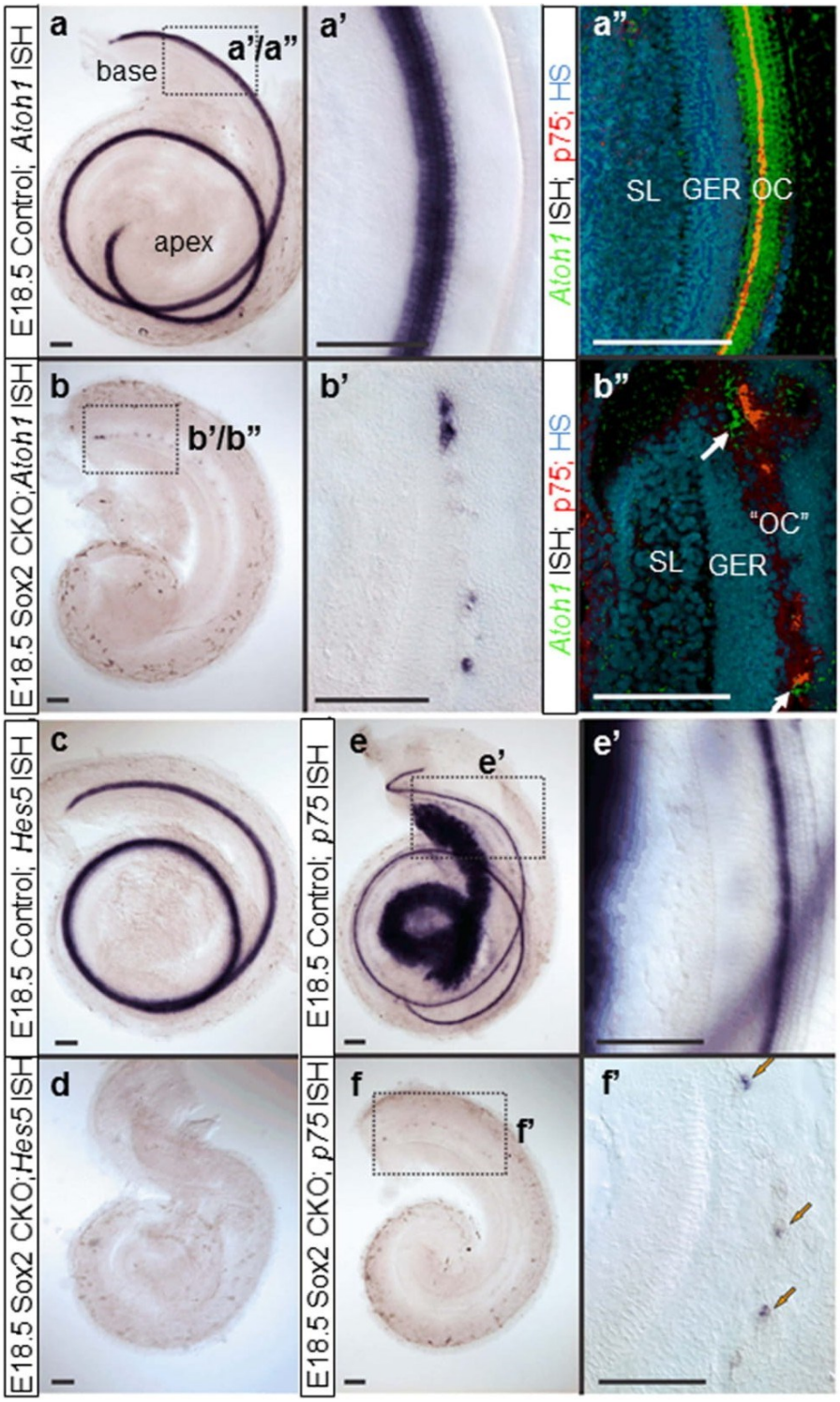

Figure 5. Loss of Sox2 affects downstream gene expression in the organ of Corti. (**a,a',b,b'**) *Atoh1* expression is dramatically reduced in Sox2 CKO mice at E18.5. (**a",b"**) *Atoh1* ISH signal converting into a fluorescent signal shows the relative topology to the inner pillar cell marker p75. Note that the scattered HCs are found medial and lateral to p75 positive cells (white arrows; b"). However, p75 expression (arrows) is discontinuous in the base (**b",f,f'**) and absent in the apex compared to prominent labeling in the inner pillar cells and the spiral ganglion neurons in control animals (**e,e'**). (**c**,**d**) Another supporting cell marker, *Hes5*, shows no expression at all in the Sox2 CKO mice at E18.5. Scale bars: 100 μm. GER, greater epithelial ridge; OC, organ of Corti; "OC", atypical organ of Corti in the mutant; SL, spiral limbus.

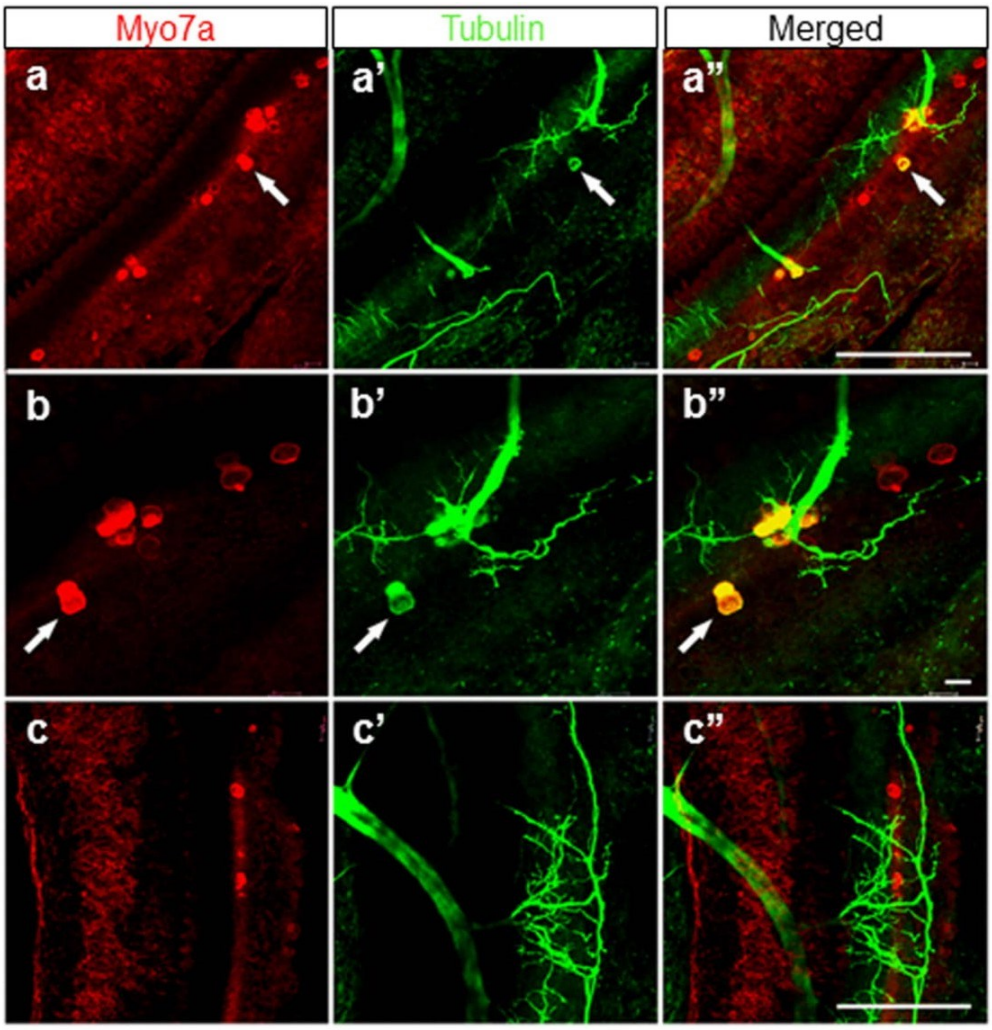

Figure 6. Some HCs are positive for both Myo7a and tubulin. These single or groups of Myo7a positive HCs of E18.5 Sox2 CKO mice show a patchy distribution (**a**,**b**,**c**) and an unusual pattern of innervation (**a'**,**b'**,**c'**). Note that most fibers are targeted toward Myo7a positive HCs, others are sometimes widely distributed in the topological equivalent of the organ of Corti. (**a"**,**b"**,**c"**) Some Myo7a positive cells are also positive for antibody directed against tubulin, normally a reliable neuronal marker in the ear. Scale bars: 100 μm, except b,b" that indicates 10 μm.

transcription of *Atoh1* has previously been shown in cochlear explant cultures[37]. Correspondingly, as shown by the HC marker (Myo7a), the HCs formed small clusters only in the basal turn of the cochlea (Fig. 3). The Sox2 CKO phenotype confirms that *Atoh1* expression and subsequent HC differentiation depends on Sox2, because *Atoh1* expression and differentiated HCs were detected only in the cochlear base of the Sox2 CKO, where Sox2 is initially expressed. However, the unusual cluster pattern and features of these differentiated HCs suggest that the induction of *Atoh1* expression and subsequent HC differentiation require a specific level and duration of Sox2 expression.

In the ear, HCs are normally negative for tubulin, which serves as a neuronal marker, even when neurons are experimentally converted to HCs[14]. In the Sox2 CKO, however, many remaining HCs showed positive staining for tubulin in addition to the HC marker, Myo7a (Fig. 6). Sox2 levels and timing of expression may therefore also play a role in the segregation of neuronal and HC phenotype that is incomplete for some HCs in our conditional mutant.

The molecular effects of Sox2 deletion on supporting cells. HCs and supporting cells are intertwined during development using the delta-notch signaling pathway[9] that critically depends on normal differentiation of HCs for proper signaling[36]. In contrast to the massive expression of the downstream factor *Hes5* of this signaling pathway in controls (Fig. 5c), we found virtually no expression in the Sox2 CKO mutant (Fig. 5d).

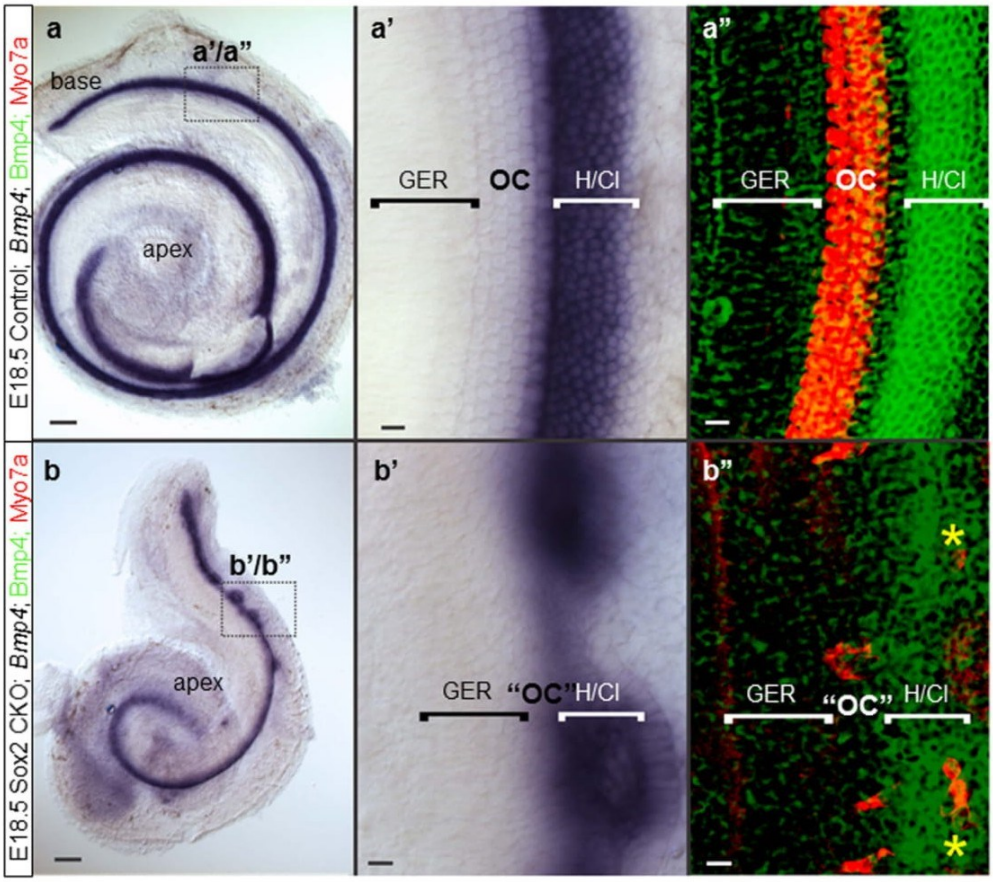

Figure 7. The cellular boundaries of the inner ear are changed in the Sox2 CKO. (**a,a',b,b'**) Loss of Sox2 results in aberration of *Bmp4* expression. Instead of being separated by the organ of Corti from the GER, *Bmp4* expression is adjacent to the GER. (**b, b',b"**) Only the base shows rings of lateral *Bmp4* expression and Myo7a positive HCs are both in the center of these rings as well as at the boundary between GER and *Bmp4* domain (b"; yellow asterisks). (**a'-a"**) In controls, the *Bmp4* expression in Hensen/Claudius cells is always lateral to the organ of Corti. Scale bars: 10 μm except 100 μm in a and b. GER, greater epithelial ridge; H/Cl; Hensen/Claudius cells; OC, organ of Corti; "OC", atypical organ of Corti in the mutant.

Given that neither Hes5 nor Sox2 can be used as general markers of supporting cells, we used only very early markers to further test the effect of the Sox2 CKO on the possible dependency of gene expression and differentiation of supporting cells. One of the earliest markers we found to be expressed in supporting cells is p75 in inner pillar cells[35]. p75 protein was found both lateral and medial to *Atoh1* positive cells (Fig. 5a",b"), suggesting that the remaining HCs are both inner and outer HCs. This is also consistent with HC bundle differentiation (Fig. 4a-a"). Of note, the remaining spiral ganglion neurons of the base showed no signal for *p75* expression compared to the strong *p75* expression in the spiral ganglion neurons of controls (Fig. 5e,e',f,f'). Closer examination of the morphology of the p75 positive presumptive pillar cells showed unusually shaped cells with no resemblance to inner pillar cells and variable topology to the remaining HCs (Fig. 4e-f").

Since most markers of the cells inside the organ of Corti were absent or highly unusual, we next investigated the expression pattern of markers outside the organ of Corti, *Fgf10* immediately medial in GER and *Bmp4* immediately lateral to the organ of Corti in Claudius cells. Previous work has shown that *Fgf10* expression in GER cells critically depends on unknown signals from the organ of Corti for its maintenance[22,38]. We found no *Fgf10* expression past E13.5 (Supplementary Fig. 3i,j). In contrast, *Bmp4* was unaffected by the loss of the organ of Corti and showed expression along the entire Sox2 CKO cochlear duct (Fig. 7), consistent with previous reports[22,38]. However, *Bmp4* expression was not lateral to the organ of Corti but rather adjacent to GER (Fig. 7a',b'), forming rings around sets of remaining, more lateral HCs (Fig. 7b", asterisks). Some additional HCs were found right at the boundary of GER and *Bmp4* domain, suggesting that these are residual inner HCs (Fig. 7b").

Combined, these data suggest that Sox2 is not only expressed in supporting cells[39], but may play a direct role in their differentiation. Conditional Sox2 deletion in supporting cells, sparing HCs, is needed to verify this suggestion.

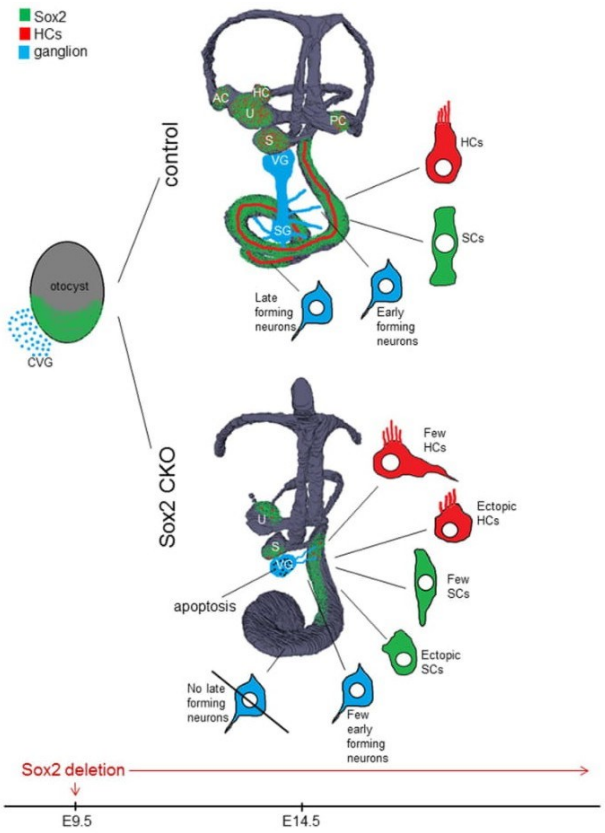

Figure 8. Summary of Sox2 CKO inner ear changes. *Sox2* deletion by Isl1-cre results in profound morphological changes at E14.5: all three cristae of the semicircular canal ampullae are missing, all remaining sensory organs are smaller and have a decreased size of the sensory area. Neuronal formation is eliminated in the apex of the cochlea, whereas vestibular and basal turn neurons gradually die due to limited support by the reduced sensory epithelia. Loss of innervation toward all epithelia except for the apex of the cochlea is secondary to the lack or reduced differentiation of HCs, which is either completely absent in the apex and semicircular canal cristae, or variably disabled in the base of the cochlea, utricle, and saccule. Many HCs have an unusual neurosensory phenotype. Similarly, supporting cells (SCs) have atypical features, altered expression of markers, and abnormal distribution, forming the aberrant organ of Corti. Many ectopic HCs and SCs are also found in the cochlear base. The spatial distribution of Sox2 expression is shown in green, blue color shows neurons, and red depicts HCs. AC, anterior crista; CVG, cochleovestibular ganglion; HC, horizontal crista; HCs, hair cells; PC, posterior crista; S, saccule; SCs, supporting cells; SG, spiral ganglion; U, utricle; VG, vestibular ganglion.

Discussion

Our conditional deletion of *Sox2* using Isl1-cre provides the first mouse model that tests *in vivo* the function of Sox2 in inner ear sensory neuron formation, inner ear sensory epithelia formation, and HC/supporting cell differentiation. Previous work has only provided indirect evidence for the role of Sox2, using a partially uncharacterized Sox2 model with limited or no expression of Sox2 in the ear[21,39] or induced delayed loss of Sox2 on HCs using inducible Sox2-creER mediated recombination[40] or worked in chickens[13,15]. Our data confirm and extend previous findings, but put them for the first time on a solid experimental basis consistent with the emerging concept of Sox-mediated neurosensory precursor development regulation[2,41,42]. The inner ear changes induced by the deletion of Sox2 in our Sox2 CKO mutant are summarized in Fig. 8.

Inner ear sensory neuron formation requires a series of transcription factors starting with the expression of the bHLH genes Neurog1[7,24], Neurod1[43] and followed by several other factors needed to fully differentiate the neurons, guide their migration away from the ear, and process growth to the ear[6,44]. Neurons delaminate from multiple sites in the sensory epithelia or areas adjacent to the sensory epithelia such as the region between the cochlear base and the saccule[10,45]. Additionally, neurons delaminate from the cochlea with a large number of neurons delaminating from the apex[46]. Spiral ganglion neurons exit the cell cycle in a base to apex progression[8]. In the Sox2 CKO, all early forming vestibular neurons seem to develop normally. However, the formation of late-forming spiral ganglion neurons of the cochlear apex is absent, indicating a dependency on the continuous expression of Sox2 for their formation. Given that apical spiral ganglion neurons are among the last neurons of the ear to exit the cell cycle[47], we suggest that neuronal precursor expansion and maintenance depends on Sox2.

Since Neurog1 expression, and thus neuronal precursor specification, precedes the onset of Isl1 expression[17,24] and Isl1-cre-mediated recombination by about 2 days (Supplementary Fig. 1), we presume that an earlier function of Sox2 protein is to stabilize early neuronal development by interacting with bHLH genes, as previously suggested[2,15]. A critical test of our hypothesis using an inducible *Sox2-creER* line was recently performed for the cochlea but the possible effects of a delayed loss of *Sox2* on ear neuronal development were not reported[40].

The embryonic viability of sensory neurons critically depends on two neurotrophins, Bdnf and Ntf3, released from the differentiating sensory epithelia[27,28]. In our Sox2 CKO, the targeted innervation of vestibular neurons to the area of the cristae of the semicircular canal ampullae was initially formed even in the complete absence of target HCs (Fig. 2a,b), suggesting pathfinding along the ear[48], possibly involving Schwann cells[29]. However, later in the development, the fibers retracted in the absence of sensory epithelia as in other mutants without cristae formation[23]. Thus, the absence of sensory epithelia results in the delayed loss of innervation. In contrast, the pattern of innervation within a sensory epithelium critically depends on the density and distribution of HCs as is very obvious in the unusual innervation pattern encountered in the base of the cochlea (Figs 2 and 3). Our data therefore suggest a biphasic loss of neurons in our Sox2 CKO: late-forming neurons never develop due to a loss of Sox2, which is required to initiate their differentiation, whereas early forming neurons die after differentiation proportionally to the reduced presence of HCs to support them. We also presume this to be true for the reported absence of neurons in *Lcc* mutants[25]. We predict that the recently reported delayed Sox2 deletion[40] should show a comparable pattern of neuronal loss in the cochlea.

Multiple lines of research have established that Sox transcription factors are needed to maintain pluripotency, but also to initiate differentiation through the upregulation of other transcription factors, in particular bHLH factors and other Sox factors[2,41], which subsequently form a negative feedback loop to suppress early Sox factors for normal differentiation[4,42]. Previous work has demonstrated a critical dependence of all HC development on Sox2[21] but some sensory epithelia in addition critically depend on Sox4/11[49]. Data in the ear show a loss of Sox2 in differentiated HCs due to Atoh1 repression[39] but also that Sox2 expression is needed for Atoh1 upregulation[40]. Our data support this, since *Atoh1* was expressed only in areas with residual Sox2 expression in the Sox2 CKO inner ear. However, for the first time, our data show that some yet to be defined level and time of Sox2 expression is needed for normal HC development. We showed that the level of *Atoh1* depends on the level of Sox2 expression. To define the spatiotemporal expression pattern of *Atoh1* and *Sox2* would require multicolor quantitative PCR to show the co-localization of *Atoh1* and *Sox2* mRNA in a given hair cell precursor over time. Our Sox2 CKO data demonstrate that different sensory epithelia vary remarkably in HC formation: some epithelia never form (cristae of the semicircular canal ampullae, apical turn of the organ of Corti), while others are variably reduced (utricle, saccule, basal turn of the organ of Corti). There are two other possibilities beyond a simple delay in *Sox2* recombination that could explain the differential loss of sensory epithelia: Isl1-cre could distinctly affect some but not other epithelia precursors, leading to their complete or partial loss. However, this possibility is effectively ruled out by our analysis of the inner ear of *Isl1-cre; Atoh1$^{f/f}$* mutants. Our data show a uniform effect of Isl1-cre in all sensory epithelia of *Isl1-cre; Atoh1$^{f/f}$* mutants with no differentiated HCs in the inner ear (Supplementary Fig. 4). Alternatively, since only epithelia known or suspected to have common neuronal/hair cell progenitors[7–9] retain HCs, it might be possible that only HCs derived from such common neurosensory progenitors form, whereas epithelia without such common precursors develop no HCs at all (cristae of the semicircular canal ampullae, apical turn of the organ of Corti). The expression of neuronal markers in some of these HCs (Fig. 6) supports this notion, but lineage tracing is needed to prove this suggestion.

Previous work has demonstrated that the level and duration of Atoh1 expression driven by multiple transcription factors[42] is crucial for HC differentiation and survival[33,34,36,38]. Using *in situ* hybridization, we found limited and transient expression of *Atoh1* mRNA, presumably leading to a differential loss of differentiating HCs, as previously reported[34,38]. We find profound variability of remaining HCs, which indicates that the compounding effect of Isl1-cre expression onset, effective recombination delay of *Sox2* and retention of Sox2 protein introduce HC specific irregularity into the differentiation process, compounded by alterations in Atoh1 expression.

Atoh1 is not only expressed in HCs but in the majority of neurons in the brain, among other cell types[35,50]. However, only in the ear, Atoh1 seems to control the formation of stereocilia and their organization in a dose dependent fashion[36]. Establishing the expression profile of transcription factors in the few HCs of the basal turn of our Sox2 CKO, which differentiate with some degree of normality, could provide candidate genes that can help to define the activation cascade needed to differentiate normal stereocilia needed for functional hair cells.

The organ of Corti has only two HC types but a rich variety of supporting cell types, each with unique properties and markers expressed in them[35], forming multiple feedback loops through the expression of diffusible factors, as well as the delta-notch lateral inhibition interactions[9] with HCs[36]. HC defects could thus result in supporting cell defects, as recently reported[36]. However, certain unusual features, such as the morphology of inner pillar cells (Fig. 4e-f") or the unusual distribution of *Bmp4* medial to remaining HCs (Fig. 7b"), suggest that Sox2 may have a more direct role to play in cell fate execution of supporting cells that needs to be explored using supporting cell specific deletion.

In summary, our data on this novel conditional mutation of the important developmental transcription factor Sox2 show a much deeper involvement of Sox2 in neurosensory development of the ear at various levels beyond HC differentiation[21,40]. First, our Sox2 CKO mutant with a delayed deletion of Sox2 indicates that neuronal development depends directly on Sox2, as the latest-forming spiral ganglion neurons never form. Second, our data confirm that the differentiation of HCs depends on Sox2. Furthermore, a variability in differentiation of HCs (cell number, size, stereocilia development, incomplete segregation neuronal and HC phenotype) suggests dependency on the level and duration of Sox2 expression. Third, Sox2 deletion affects the development of supporting cells, as shown by the altered expression of Hes5 and p75, and by the variable topology and unusual shape of p75 positive inner pillar cells. Fourth, the formation of boundaries between the organ of Corti and GER in the cochlea is affected by the loss of Sox2. Selective conditional deletion of Sox2 in neurons, HCs, or supporting cells using

differentially delayed cre expression is now needed to sort out the specific function of Sox2 in these cell types and to clarify questions raised by our novel mouse model.

Methods

Animals. This study was performed in agreement with the Guide for the Care and Use of Laboratory Animals (National Research Council. Washington, DC. The National Academies Press, 1996.). The experimental design was approved by the Animal Care and Use Committee of the Institute of Molecular Genetics, Czech Academy of Sciences. The experimental mice were housed in a controlled environment (12-h light-12-h dark cycles) with free access to food and water. All experiments were performed with the littermates cross-bred from two transgenic mouse lines: *Sox2*^{flox} (*Sox2*$^{tm1.1Lan}$/*J*) and *Isl1-cre* (*Isl1*$^{tm1(cre)Sev}$/*J*) from The Jackson Laboratory. Breeding pairs contain a mouse with two floxed *Sox2* alleles (*Sox2*$^{f/f}$) and a mouse with one floxed *Sox2* allele together with one *Isl1-cre* allele (*Isl1*$^{cre/+}$;*Sox2*$^{f/+}$). Experimental mutant mice (*Isl1-cre;Sox2*$^{f/f}$) survive until birth but they are not viable. The noon of the day the vaginal plug was found was designated as E0.5. Genotyping was performed by PCR on tail DNA. The annealing temperature was 55 °C for *cre* amplification and 64 °C for *Sox2* amplification. The primers and corresponding PCR products were as follows: cre forward (Fwd) (5′-GCC TGC ATT ACC GGT CGA TGC AAC GA-3′) and cre reverse (Rev) (5′-GTG GCA GAT GGC GCG GCA ACA CCA TT-3′) with 700 bp product; Sox2 Fwd (5′-TGG AAT CAG GCT GCC GAG AAT CC-3′), Sox2 Rev wild type (5′-TCG TTC TGG CAA CAA GTG CTA AAG C-3′) with 427 bp product or Sox2 Rev mutant (5′-CTG CCA TAG CCA CTC GAG AAG-3′) with 546 bp product. Additional crossing with transgenic lines the *Isl1-cre* (*Isl1*$^{tm1(cre)Sev}$/*J*) and floxed *Atoh1*[51] was used to generate conditional *Atoh1* knock-out mice (*Isl1-cre; Atoh1*$^{f/f}$; Atoh1 CKO). Genotyping primers for *Atoh1*^{flox} were Atoh1loxF (5′-CAG ATC CCA CAG AAG TGA CG-3′) and Atoh1loxR (5′-ACA CTG CTG GAC ACA CTT GG-3′).

Hearing function evaluation. To assess the auditory function of the experimental animals recording of auditory brainstem responses (ABR) and distortion product otoacoustic emissions (DPOAE) was performed. All tests were carried out on anaesthetized mice as previously described[52]. Briefly, hearing thresholds were determined at 2, 4, 8, 16, 32 and 40 kHz and DPOAEs were recorded at individual frequencies over the frequency range 4–38 kHz with a resolution of four points per octave. The average values per group were calculated and the results (mean ± SD) were plotted in audiograms (ABR thresholds) and DP-grams (DPOAEs).

Histology of the inner ear. Embryos were dissected in cold PBS and fixed in 4% paraformaldehyde.

3D reconstruction. Inner ears were dehydrated in ethanol series and stained with 0.5 μg/ml Rhodamine B isothiocyanate in 100% ethanol[53]. Samples were then cleared by MSBB solution and mounted onto a glass slide prior to imaging. Images were taken by Zeiss LSM 5 DUO or Leica SPE confocal microscopes and processed in ImageJ[54]. 3D structures of inner ears were reconstructed from confocal stacks in 3D Slicer by manually segmenting areas of interest.

Scanning electron microscopy. All of the excessing structures and membranes were removed from the sensory organs. Samples in porous specimen pots were extensively washed and dehydrated through an alcohol series followed by absolute acetone. Tissues were critical point dried in liquid CO_2 in a K 850 unit (Quorum Technologies Ltd, Ringmer, UK). The dried samples were mounted onto carbon conductive double sided adhesive discs and sputter-coated with 20 nm of gold in a Polaron Sputter-Coater (E5100) (Quorum Technologies Ltd, Ringmer, UK). The final samples were examined in a FEI Nova NanoSem 450 scanning electron microscope (FEI Czech Republic s.r.o.) at 5 kV using a secondary electron detector.

X-gal staining. The mouse line *Isl1-cre* was bred with R26R-*lacZ* (*Gt(ROSA)26Sor*^{tm1Sor}, Jackson Laboratory) and animals carrying both loci were subjected to X-gal staining. Fixed tissues were washed in detergent solution (0.1 M phosphate buffer (pH 7.3), 2 mM MgCl2, 0.01% sodium deoxycholate, 0.02% IGEPAL CA-630) and then incubated at 37 °C in X-gal staining solution (1 mg/ml X-gal, 5 mM potassium ferrocyanide, 5 mM potassium ferricyanide, 20 mM TrisCl (pH 7.3). Samples were washed in PBS with 25 mM EDTA and imaged by a Nikon SMZ dissection microscope.

Immunohistochemistry. For vibratome sections, samples were embedded in 4% agarose gel and sectioned at 80 μm on a Leica VT1000S vibratome. Vibratome sections, whole inner ears or whole embryos were defatted in 70% ethanol and then rehydrated and blocked with serum. Samples were then incubated with primary antibodies. The primary antibodies used were anti-Sox2 (1:500, #AB5603, Millipore or 1:250, #sc-17320, Santa Cruz Biotechnology), anti-Islet1/2 (1:200, #39.4D5, DSHB), anti-Islet1 (1:130, #39.3F7, DSHB) anti-Myo7a (1:500, #25-6790, Proteus Biosciences Inc), anti-acetylated Tubulin (1:400, #T6793, Sigma), anti-cre (1:500, #908001, BioLegend), anti-Cleaved Caspase 3 (1:100, #9661, Cell Signaling), anti-Neurofilament 200 (1:200, #N4142, Sigma-Aldrich) and anti-p75 (1:1000, #N3908, Sigma-Aldrich). Anti-Isl1/2 (#39.4D5) and anti-Isl1 (#39.3F7) antibodies developed by Jessell, T.M./Brenner-Morton, S. were obtained from the Developmental Studies Hybridoma Bank, created by the NICHD of the NIH and maintained at The University of Iowa, USA. Secondary antibodies used were Alexa Fluor 488 (#115-545-146, Jackson Immuno Research), Alexa Fluor 594 (#111-585-144, Jackson Immuno Research), DyLight 488 (#205-485-108, Jackson Immuno Research) and DyLight 594 (#205-515-108, Jackson Immuno Research). Samples were counterstained with Hoechst nuclear stain. Samples were mounted on slides in Polymount or Antifade medium and analyzed by Zeiss LSM 5 DUO, Zeiss LSM 880 or Leica SPE confocal microscopes. Images were processed in ImageJ. Individual cochleae were flat-mounted with the sensory epithelium facing up. The entire length of the cochlear duct from the hook region along the basilar

membrane was measured by ImageJ. Myo7a positive HCs were quantified after whole mount immunostaining using LAS AF Lite draw counter. The total number of HCs was determined in the entire utricle and saccule, and in the entire Sox2 CKO cochlea. The number of HCs in the control cochlea represents the total number of HCs in 1.5 mm of the base of the cochlea. Caspase3 positive cells were quantified in the vestibular ganglion at E11.5-E13.5 and in the superior vestibular ganglion at E14.5-E15.5 in both control and Sox2 CKO mice after the whole mount immunostaining with the anti-Caspase3 antibody. The statistical significant differences between control and Sox2 CKO mice were analyzed by Student's *t* test (significance assigned at the $P < 0.05$ level; GraphPad, 2005, USA).

In situ hybridization. *In situ* hybridization was performed using a RNA probe labeled with digoxigenin as previously described[14]. Plasmids containing cDNAs [gifts from H. Zoghbi (Atoh1), D. Wu (BMP4), A. Groves (Hes5), K Cheah (Sox2), D. Ornitz Fgf10)] were used to generate the RNA probe by *in vitro* transcription. After being anesthetized with 2,2,2 tribromoethanol (Avertin), mice were perfused in 4% paraformaldehyde (PFA) and fixed overnight in 4% PFA. The ears were dissected in 0.4% PFA and dehydrated and rehydrated in graded methanol series and then digested briefly with 20 μg/ml of Proteinase K (Ambion, Austin, TX, USA) for 15–20 minutes. The samples were then hybridized overnight at 60 °C to the riboprobe in hybridization solution. The samples were incubated overnight with an anti-digoxigenin antibody after washing off the unbound probe (Roche Diagnostics GmbH, Mannheim, Germany). After a series of washes, the samples were reacted with nitroblue phosphate/5-bromo, 4-chloro, 3-indolil phosphate (BM purple substrate, Roche Diagnostics, Germany) which is enzymatically converted to a purple colored product. The ears were mounted flat in glycerol and viewed in a Nikon Eclipse 800 microscope using differential interference contrast microscopy and images were captured with Metamorph software. The ears of the littermate of different genotype for the same gene expression were performed in the same reaction tubes to maintain the reaction accuracy.

Lipophilic Dye Tracing. We studied the pattern of innervation in whole or dissected ears using lipophilic dye tracing in aldehyde fixed tissue as previously described[55]. Briefly, we inserted filter strips loaded with differently colored lipophilic dyes into the cochlear/vestibular nuclei of the brainstem around rhombomere 5 to label afferents and into rhombomere 4 near the midline to label facial motoneurons/efferents to the ear[56]. After appropriate diffusion time of the lipophilic tracer, we prepared the ears as whole mounts removing the lateral wall of the otic capsule, mounted with glycerol on a glass slide using appropriate spacers to avoid distortion and imaged using a Leica SP5 confocal microscope. Image stacks were collected and single images or sets of the stacks were obtained to provide detailed information about the progressive development of the ear innervation and loss over time. Selected ears were further dissected to reveal the detailed innervation of flat mounted sensory epithelia. Images were compiled into plates to show the most pertinent details using Corel Draw. Only general image modifications such as contrast or brightness adjustments were used to enhance the visual appeal without affecting the scientific content. All material was after imaging used for either *in situ* hybridization or immunological studies as previously described[57].

References

1. Kondoh, H. & Lovell-Badge, R. *Sox2: Biology and Role in Development and Disease.* 3–15 (Elsevier, 2016).
2. Reiprich, S. & Wegner, M. From CNS stem cells to neurons and glia: Sox for everyone. *Cell Tissue Res* **359,** 111–124 (2015).
3. Telley, L. *et al.* Sequential transcriptional waves direct the differentiation of newborn neurons in the mouse neocortex. *Science* **351,** 1443–1446 (2016).
4. Fritzsch, B., Jahan, I., Pan, N. & Elliott, K. L. Evolving gene regulatory networks into cellular networks guiding adaptive behavior: an outline how single cells could have evolved into a centralized neurosensory system. *Cell Tissue Res* **359,** 295–313 (2015).
5. Fritzsch, B., Pan, N., Jahan, I. & Elliott, K. L. Inner ear development: building a spiral ganglion and an organ of Corti out of unspecified ectoderm. *Cell Tissue Res* **368,** 7–24 (2015).
6. Dabdoub, A., Fritzsch, B., Popper, A. N. & Fay, R. R. *The Primary Auditory Neurons of the Mammalian Cochlea*. Vol. 52 (Springer, 2016).
7. Ma, Q., Anderson, D. J. & Fritzsch, B. Neurogenin 1 null mutant ears develop fewer, morphologically normal hair cells in smaller sensory epithelia devoid of innervation. *J Assoc Res Otolaryngol* **1,** 129–143 (2000).
8. Matei, V. *et al.* Smaller inner ear sensory epithelia in Neurog 1 null mice are related to earlier hair cell cycle exit. *Developmental Dynamics* **234,** 633–650 (2005).
9. Raft, S. & Groves, A. K. Segregating neural and mechanosensory fates in the developing ear: patterning, signaling, and transcriptional control. *Cell Tissue Res*, **359,** 315–32 (2014).
10. Yang, T., Kersigo, J., Jahan, I., Pan, N. & Fritzsch, B. The molecular basis of making spiral ganglion neurons and connecting them to hair cells of the organ of Corti. *Hear Res* **278,** 21–33 (2011).
11. Mak, A. C., Szeto, I. Y., Fritzsch, B. & Cheah, K. S. Differential and overlapping expression pattern of SOX2 and SOX9 in inner ear development. *Gene Expr Patterns* **9,** 444–453 (2009).
12. Gu, R. *et al.* Lineage tracing of Sox2− expressing progenitor cells in the mouse inner ear reveals a broad contribution to non-sensory tissues and insights into the origin of the organ of Corti. *Developmental Biology* **414,** 72–84 (2016).
13. Neves, J., Uchikawa, M., Bigas, A. & Giraldez, F. The prosensory function of Sox2 in the chicken inner ear relies on the direct regulation of Atoh1. *PLoS one* **7,** e30871 (2012).
14. Jahan, I., Pan, N., Kersigo, J. & Fritzsch, B. Neurod1 suppresses hair cell differentiation in ear ganglia and regulates hair cell subtype development in the cochlea. *PloS one* **5,** e11661 (2010).
15. Evsen, L., Sugahara, S., Uchikawa, M., Kondoh, H. & Wu, D. K. Progression of neurogenesis in the inner ear requires inhibition of Sox2 transcription by Neurogenin1 and Neurod1. *J Neurosci* **33,** 3879–3890 (2013).
16. Huang, M. *et al.* Diverse expression patterns of LIM-homeodomain transcription factors (LIM-HDs) in mammalian inner ear development. *Developmental Dynamics* **237,** 3305–3312 (2008).
17. Radde-Gallwitz, K. *et al.* Expression of Islet1 marks the sensory and neuronal lineages in the mammalian inner ear. *J Comp Neurol* **477,** 412–421 (2004).
18. Yang, L. *et al.* Isl1Cre reveals a common Bmp pathway in heart and limb development. *Development* **133,** 1575–1585 (2006).
19. Pauley, S., Lai, E. & Fritzsch, B. Foxg1 is required for morphogenesis and histogenesis of the mammalian inner ear. *Developmental Dynamics* **235,** 2470–2482 (2006).
20. Chang, W., Brigande, J. V., Fekete, D. M. & Wu, D. K. The development of semicircular canals in the inner ear: role of FGFs in sensory cristae. *Development* **131,** 4201–4211 (2004).

21. Kiernan, A. E. *et al.* Sox2 is required for sensory organ development in the mammalian inner ear. *Nature* **434,** 1031–1035 (2005).
22. Pan, N. *et al.* Conditional deletion of Atoh1 using Pax2-Cre results in viable mice without differentiated cochlear hair cells that have lost most of the organ of Corti. *Hear Res* **275,** 66–80 (2011).
23. Pauley, S. *et al.* Expression and function of FGF10 in mammalian inner ear development. *Developmental dynamics* **227,** 203–215 (2003).
24. Ma, Q., Chen, Z., del Barco Barrantes, I., de la Pompa, J. L. & Anderson, D. J. neurogenin1 is essential for the determination of neuronal precursors for proximal cranial sensory ganglia. *Neuron* **20,** 469–482 (1998).
25. Puligilla, C., Dabdoub, A., Brenowitz, S. D. & Kelley, M. W. Sox2 induces neuronal formation in the developing mammalian cochlea. *J Neurosci* **30,** 714–722 (2010).
26. Bouchard, M., de Caprona, D., Busslinger, M., Xu, P. & Fritzsch, B. Pax2 and Pax8 cooperate in mouse inner ear morphogenesis and innervation. *BMC Dev Biol* **10,** 89 (2010).
27. Fritzsch, B., Kersigo, J., Yang, T., Jahan, I. & Pan, N. In *The Primary Auditory Neurons of the Mammalian Cochlea* 49–84 (Springer New York, 2016).
28. Rubel, E. W. & Fritzsch, B. Auditory system development: primary auditory neurons and their targets. *Annu Rev Neurosci* **25,** 51–101 (2002).
29. Mao, Y., Reiprich, S., Wegner, M. & Fritzsch, B. Targeted deletion of Sox10 by Wnt1-cre defects neuronal migration and projection in the mouse inner ear. *PloS one* **9,** e94580 (2014).
30. Fritzsch, B., Dillard, M., Lavado, A., Harvey, N. L. & Jahan, I. Canal cristae growth and fiber extension to the outer hair cells of the mouse ear require Prox1 activity. *PloS one* **5,** e9377 (2010).
31. Kersigo, J. & Fritzsch, B. Inner ear hair cells deteriorate in mice engineered to have no or diminished innervation. *Front Aging Neurosci* **7,** 33 (2015).
32. Fritzsch, B., Silos-Santiago, I., Bianchi, L. M. & Farinas, I. In *Seminars in cell & developmental biology*. Vol. 8, 277–284 (Elsevier, 1997).
33. Jahan, I., Pan, N., Kersigo, J. & Fritzsch, B. Beyond generalized hair cells: molecular cues for hair cell types. *Hear Res* **297,** 30–41 (2013).
34. Sheykholeslami, K. *et al.* A new mutation of the Atoh1 gene in mice with normal life span allows analysis of inner ear and cerebellar phenotype in aging. *PloS one* **8,** e79791 (2013).
35. Jahan, I., Pan, N., Elliott, K. L. & Fritzsch, B. The quest for restoring hearing: understanding ear development more completely. *Bioessays* **37,** 1016–1027 (2015).
36. Jahan, I., Pan, N., Kersigo, J. & Fritzsch, B. Neurog1 can partially substitute for Atoh1 function in hair cell differentiation and maintenance during organ of Corti development. *Development* **142,** 2810–2821 (2015).
37. Ahmed, M. *et al.* Eya1-six1 interaction is sufficient to induce hair cell fate in the cochlea by activating atoh1 expression in cooperation with sox2. *Dev Cell* **22,** 377–390 (2012).
38. Pan, N. *et al.* A novel Atoh1 "self-terminating" mouse model reveals the necessity of proper Atoh1 level and duration for hair cell differentiation and viability. *PloS one* **7,** e30358 (2012).
39. Dabdoub, A. *et al.* Sox2 signaling in prosensory domain specification and subsequent hair cell differentiation in the developing cochlea. *Proceedings of the National Academy of Sciences* **105,** 18396–18401 (2008).
40. Kempfle, J. S., Turban, J. L. & Edge, A. S. Sox2 in the differentiation of cochlear progenitor cells. *Sci Rep* **6,** 23293 (2016).
41. Reiprich, S. *et al.* In *GLIA*. Vol 57, Issue S13, S26–S171 (2009).
42. Cheah, K. S. E. & Xu, P.-X. In *Sox2* (ed Robin Lovell-Badge) 263–280 (Academic Press, 2016).
43. Kim, W.-Y. *et al.* NeuroD-null mice are deaf due to a severe loss of the inner ear sensory neurons during development. *Development* **128,** 417–426 (2001).
44. Goodrich, L. V. In *The Primary Auditory Neurons of the Mammalian Cochlea* 11–48 (Springer, 2016).
45. Fritzsch, B. *et al.* Development and evolution of inner ear sensory epithelia and their innervation. *Journal of neurobiology* **53,** 143–156 (2002).
46. Farinas, I. *et al.* Spatial shaping of cochlear innervation by temporally regulated neurotrophin expression. *J Neurosci* **21,** 6170–6180 (2001).
47. Ruben, R. J. Development of the inner ear of the mouse: a radioautographic study of terminal mitoses. *Acta oto-laryngologica* Suppl 220, 221 (1967).
48. Coate, T. M. & Kelley, M. W. In *Seminars in cell & developmental biology*. Vol. 24, 460–469 (Elsevier, 2013).
49. Gnedeva, K. & Hudspeth, A. SoxC transcription factors are essential for the development of the inner ear. *Proceedings of the National Academy of Sciences* **112,** 14066–14071 (2015).
50. Mulvaney, J. & Dabdoub, A. Atoh1, an essential transcription factor in neurogenesis and intestinal and inner ear development: function, regulation, and context dependency. *J Assoc Res Otolaryngol* **13,** 281–293 (2012).
51. Shroyer, N. F. *et al.* Intestine-specific ablation of mouse atonal homolog 1 (Math1) reveals a role in cellular homeostasis. *Gastroenterology* **132,** 2478–2488 (2007).
52. Chumak, T. *et al.* Deterioration of the Medial Olivocochlear Efferent System Accelerates Age-Related Hearing Loss in Pax2-Isl1 Transgenic Mice. *Mol Neurobiol* **53,** 2368–83 (2015).
53. Kopecky, B. J., Duncan, J. S., Elliott, K. L. & Fritzsch, B. Three-dimensional reconstructions from optical sections of thick mouse inner ears using confocal microscopy. *J Microsc* **248,** 292–298 (2012).
54. Preibisch, S., Saalfeld, S. & Tomancak, P. Globally optimal stitching of tiled 3D microscopic image acquisitions. *Bioinformatics* **25,** 1463–1465 (2009).
55. Fritzsch, B., Duncan, J. S., Kersigo, J., Gray, B. & Elliott, K. L. In *Auditory and Vestibular Research: Methods and Protocols.* (ed B. Sokolowski) 221–246 (Springer, 2016).
56. Simmons, D., Duncan, J., de Caprona, D. C. & Fritzsch, B. In *Auditory and vestibular efferents* 187–216 (Springer New York, 2011).
57. Duncan, J. S., Elliott, K. L., Kersigo, J., Gray, B. & Fritzsch, B. Combining Whole-Mount *In Situ* Hybridization with Neuronal Tracing and Immunohistochemistry. *In Situ Hybridization Methods* 339–352 (2015).

Acknowledgements

This work was supported by the Czech Science Foundation (Grant Agreement No. 13-07996S to GP); by BIOCEV CZ.1.05/1.1.00/02.0109 from the ERDF; by the Czech Ministry of Education, Youth and Sports (Grant Agreement No. AVOZ50520701); by the Charles University in Prague (GA UK No. 780216 to MD and No. 324615 to IM); and by the National Institute on Deafness and Other Communication Disorders (NIDCD) (R03 DC013655 to IJ) and Hearing Health Foundation (Emerging Research Grant to IJ). We thank the Office of the Vice President for Research (OVPR) and multiple colleagues for the donation of riboprobes and mice, University of Iowa College of Liberal Arts and Sciences (CLAS), the P30 core grant for support (DC 010362), A. Pavlinek and K Thompson for text editing, and O. Benada of the Electron Microscopy Group (Institute of Microbiology CAS) for assistance with SEM.

Author Contributions

All authors have read and approved the manuscript. The work presented here was done in collaboration among all authors. G.P. and B.F. conceived the study, designed experiments, and co-wrote the paper with the help of I.J. and M.D. M.D. and I.J. performed all experiments and analyze data with the exception of ABR and DPOEA analyses. T.C. performed ABR and DPOEA analyses. I.M. performed Atoh1 mutation analyses and data collection. J.S. co-defined the research theme and co-designed physiological experiments.

Additional Information

Supplementary information accompanies this paper at http://www.nature.com/srep

Competing financial interests: The authors declare no competing financial interests.

How to cite this article: Dvorakova, M. *et al.* Incomplete and delayed Sox2 deletion defines residual ear neurosensory development and maintenance. *Sci. Rep.* **6**, 38253; doi: 10.1038/srep38253 (2016).

Publisher's note: Springer Nature remains neutral with regard to jurisdictional claims in published maps and institutional affiliations.

5.3 Defekt primární tonotopické organizace a dysfunkce centrální sluchové dráhy v důsledku ztráty NEUROD1 ve vnitřním uchu

Systém Cre-loxP a myší kmen *Isl1-Cre* byl využit i při přípravě experimentálního modelu s podmíněnou delecí genu *Neurod1* (*Neurod1CKO*). Isl1-Cre je aktivní v neurosensorických prekurzorech během vývoje vnitřního ucha, ale není exprimována v centrálních částech sluchově rovnovážného systému včetně kochleárního jádra a *colliculus inferior*. Pomocí Isl1-Cre je tedy možné oddělit primární vliv delece *Neurod1* ve vnitřním uchu od sekundárních změn v centrálních částech sluchové dráhy. Toto nebylo možné u předchozích modelů s delecí genu *Neurod1*.

Náš unikátní myší model s homozygotní podmíněnou delecí *Neurod1* byl schopný přežít do dospělosti, což nám umožnilo provést i fyziologické měření sluchových a vestibulárních funkcí. Dospělí mutanti nevykazovali žádné motorické dysfunkce, které by naznačovaly významné změny ve vestibulárním systému. Imunohistologickými metodami bylo zjištěno, že kochlea je zkrácená o 40 % u *Neurod1CKO* oproti kochlee dospělých kontrolních jedinců. Toto zkrácení mělo pravděpodobně za následek dezorganizaci senzorického epitelu v apexu, kde docházelo ke zmnožení řad vláskových i podpůrných buněk a transdiferenciaci vnějších vláskových buněk na vnitřní vláskové buňky.

Podmíněná delece *Neurod1* nejvíce ovlivnila vývoj neuronů spirálního ganglia, jejichž počet byl snížen o 80 %. Rovněž počet aferentních zakončení na vnitřních vláskových buňkách, tzn. „ribbon“ synapsí, byl signifikantně redukován u *Neurod1CKO* v porovnání s kontrolními jedinci. Ačkoli počet neuronů spirálního ganglia u mutantů byl významně nižší, neuronová vlákna tvořila hustou síť inervující sensorické buňky v kochlee. Několik významných rozdílů v kochleární inervaci mezi kontrolami a *Neurod1CKO* však bylo identifikováno: u *Neurod1CKO* byla radiální vlákna delší a mezi jednotlivými svazky byly větší rozestupy; eferentní vlákna netvořila typický svazek označovaný jako „intraganglionic spiral bundle“; těla neuronů byla nepravidelně uspořádaná v různě velkých shlucích a v apexu neurony úplně chyběly. Snížený počet neuronů ve spirálním gangliu lze vysvětlit změnami v migraci neuroblastů a změnami v segregaci vestibulárního a spirálního ganglia. U *Neurod1CKO* se vytvořilo neoddělené „spiro-vestibulární“ ganglium v oblasti korespondující vestibulárnímu gangliu kontrol, které obsahovalo spirální i vestibulární neurony inervující jednak rovnovážné orgány a jednak senzorické buňky sluchového ústrojí. Navigace axonů neuronů byla poškozena

jak u neuronů ve „spiro-vestibulárním“ gangliu, tak u neuronů lokalizovaných ve spirálním gangliu. U mutantů byly detekovány axony neuronů spirálního ganglia vedoucí do orgánů vestibulárního systému a naopak neurony vestibulárního ganglia inervovaly vláskové buňky kochley. Tyto experimenty navíc poprvé ukázaly, že neurony spirálního ganglia u *Neurod1CKO* inervovaly více než jednu vnitřní vláskovou buňku.

Podobně dezorganizovaná byla i vlákna vedoucí z vnitřního ucha *Neurod1CKO* do centrální sluchové a vestibulární dráhy. Aferentní vlákna v kochleárním jádře byla nesegregovaná mezi dorsální a ventrální částí, přičemž DCN bylo téměř bez inervace. V kochleárním jádře mutanta byla také nalezena vlákna vedoucí z rovnovážných orgánů vnitřního ucha, která by měla správně vést do mozečku podobně jako u kontrol. Změny během vývoje vnitřního ucha při podmíněné deleci *Neurod1* měly sekundární efekt na vývoj kochleárního jádra, jehož objem byl u mutantů redukován o 40 % a morfologicky srovnatelné chundelaté buňky byly odlišně distribuované ve ventrální části, VCN. Pomocí imunohistologického barvení protoonkogenu c-Fos, který je aktivován již po patnácti minutách po akustickém stimulu, bylo možné analyzovat tonotopickou organizaci centrální sluchové dráhy. Po akustické stimulaci určitou frekvencí byl u kontrolních myší v kochleárním jádře detekován úzký izofrekvenční pás aktivovaných neuronů odpovídající tonotopickému uspořádání pro danou frekvenci. Naproti tomu u *Neurod1CKO* byly aktivované neurony rozsety po celém kochleárním jádře a jejich počet byl přibližně dvojnásobný v porovnání s kontrolami. Tyto výsledky ukazují poškozenou tonotopii v souvislosti s delecí *Neurod1*.

Další naše experimenty byly zaměřeny na charakterizaci neuronálních odpovědí při zpracování zvukového signálu v *colliculus inferior.* Mezi vyhodnocovanými parametry byly: (a) charakteristická frekvence, což je frekvence tónu, při níž je práh odpovědi nejnižší; (b) frekvenční prahová křivka, která ohraničuje excitační oblast neuronu; (c) funkce RIF („rate-intensity function”) měřící velikost odpovědi neuronu v závislosti na intenzitě zvuku; (d) spontánní aktivita neuronů a (e) frekvenční selektivita neuronu. Tyto analýzy ukázaly, že myši *Neurod1CKO* byly schopny rozlišit akustické signály v omezeném rozpětí 9 až 28 kHz v porovnání s kontrolami, u kterých byly naměřeny odpovědi v rozmezí od 2 do 80 kHz. Také byla u mutantů zhoršena selektivita frekvencí, kdy při izolovaném zvuku mělo excitační pole v *colliculus inferior* více amplitud místo jedné charakteristické odpovídající dané frekvenci. Inhibiční oblasti odpovědi neuronů u dvou-tónové stimulace byly redukovány do několika

malých ploch u *Neurod1CKO* místo typických dvou velkých postranních oblastí u kontrol. Další charakterizace neuronů v *colliculus inferior Neurod1CKO* odhalily zvýšenou spontánní aktivitu neuronů, jiné procentuální zastoupení druhů neuronů, menší úspěšnost a synchronizaci odpovědí na zvuk v podobě klikání. Změny funkčních vlastností neuronů v *colliculus inferior* se projevily i u behaviorálních reakcí mutantů *Neurod1CKO* na zvukové podněty. Behaviorální testy ukázaly, že myši *Neurod1CKO* měly snížené prahy reakcí na zvuk a některé jejich motorické dovednosti byly ovlivněné zvuky, což ukazuje na abnormální propojení sluchové a rovnovážné dráhy.

Neurod1 Is Essential for the Primary Tonotopic Organization and Related Auditory Information Processing in the Midbrain

Iva Macova,[1,4]* Kateryna Pysanenko,[2]* Tetyana Chumak,[2] Martina Dvorakova,[1,4] Romana Bohuslavova,[1] Josef Syka,[2] Bernd Fritzsch,[3] and Gabriela Pavlinkova[1]

[1]Institute of Biotechnology CAS, Vestec, Czechia 25250, [2]Institute of Experimental Medicine CAS, Prague, Czechia 14220, [3]Department of Biology, University of Iowa, Iowa City, Iowa 52242, and [4]Faculty of Science, Charles University, Prague, Czechia 12843

Hearing depends on extracting frequency, intensity, and temporal properties from sound to generate an auditory map for acoustical signal processing. How physiology intersects with molecular specification to fine tune the developing properties of the auditory system that enable these aspects remains unclear. We made a novel conditional deletion model that eliminates the transcription factor NEUROD1 exclusively in the ear. These mice (both sexes) develop a truncated frequency range with no neuroanatomically recognizable mapping of spiral ganglion neurons onto distinct locations in the cochlea nor a cochleotopic map presenting topographically discrete projections to the cochlear nuclei. The disorganized primary cochleotopic map alters tuning properties of the inferior colliculus units, which display abnormal frequency, intensity, and temporal sound coding. At the behavioral level, animals show alterations in the acoustic startle response, consistent with altered neuroanatomical and physiological properties. We demonstrate that absence of the primary afferent topology during embryonic development leads to dysfunctional tonotopy of the auditory system. Such effects have never been investigated in other sensory systems because of the lack of comparable single gene mutation models.

Key words: auditory pathway; cochlear nucleus; inferior colliculus; Neurod1 mutation; plasticity; sensory topographical map

Significance Statement

All sensory systems form a topographical map of neuronal projections from peripheral sensory organs to the brain. Neuronal projections in the auditory pathway are cochleotopically organized, providing a tonotopic map of sound frequencies. Primary sensory maps typically arise by molecular cues, requiring physiological refinements. Past work has demonstrated physiologic plasticity in many senses without ever molecularly undoing the specific mapping of an entire primary sensory projection. We genetically manipulated primary auditory neurons to generate a scrambled cochleotopic projection. Eliminating tonotopic representation to auditory nuclei demonstrates the inability of physiological processes to restore a tonotopic presentation of sound in the midbrain. Our data provide the first insights into the limits of physiology-mediated brainstem plasticity during the development of the auditory system.

Introduction

Sensory systems develop topographic maps of sensory inputs in nervous systems: the somatosensory system projects topographical maps of the skin to the brainstem, midbrain, and cortex (Penfield and Boldrey, 1937; Renier et al., 2017), the olfactory system projects odor properties to a given olfactory glomerulus (Mombaerts, 1999; Gogos et al., 2000), the retina develops a topographical map in the midbrain (Sperry, 1963; Goodhill, 2007; Huberman et al., 2008), and vestibular, lateral line, and electroreceptive organs project to specific nuclei of the hindbrain and midbrain to establish computational maps (Krahe and Maler, 2014; Chagnaud et al., 2017). In the auditory system, cochlear sensory hair cells are connected to the brain by spiral ganglion (SG) neurons that are organized within the cochlea in an orderly fashion according to frequency, so called tonotopic organization, with high frequencies at the base and low frequencies at the apex

Received Oct. 10, 2018; revised Nov. 17, 2018; accepted Dec. 5, 2018.

Author contributions: I.M. and K.P. wrote the first draft of the paper; J.S., B.F., and G.P. edited the paper; R.B., J.S., B.F., and G.P. designed research; I.M., K.P., T.C., M.D., R.B., and B.F. performed research; I.M., K.P., T.C., M.D., R.B., B.F., and G.P. analyzed data; B.F. and G.P. wrote the paper.

This work was supported by the Czech Science Foundation (17-04719S to G.P.), by BIOCEVCZ.1.05/1.1.00/02.0109 from the ERDF, by the Czech Academy of Sciences RVO: 86652036, by Charles University (GA UK 324615 to I.M. and GAUK 780216 to M.D.), and by the NIH (R01 AG060504 to B.F.). We thank Dr. K. Kandler for helpful comments on an earlier version of the paper, Dr. D. Šuta for help processing single-unit data, and A. Pavlinek for editing the paper.

The authors declare no competing financial interests.

*I.M. and K.P. contributed equally to this work.

Correspondence should be addressed to Gabriela Pavlinkova at Gabriela.Pavlinkova@ibt.cas.cz or Bernd Fritzsch at bernd-fritzsch@uiowa.edu.

https://doi.org/10.1523/JNEUROSCI.2557-18.2018

 0270-6474/19/390984-21$15.00/0

(Rubel and Fritzsch, 2002; Muniak et al., 2016). This tonotopic (or cochleotopic) organization is maintained throughout the auditory pathways (Kandler et al., 2009). The formation of a tonotopic map requires the precise projection of the SG neuron afferents of the cochlea onto the first auditory nuclei of the hindbrain, the cochlear nuclei (CN). In contrast to the better-characterized visual system or olfactory system, only some molecular mechanisms are known to lead to the cochleotopic mapping of spiral ganglion afferents onto the CN (Cramer and Gabriele, 2014; Goodrich, 2016; Yang et al., 2017) but it is unknown how much the initial cochleotopic map is physiologically refined (Marrs and Spirou, 2012). Developing second-order maps are highly plastic (Hubel et al., 1977; Renier et al., 2017) and convergence of multiple sensory organs can plastically reshape primary sensory maps as a compromise between activity and molecular cues (Constantine-Paton and Law, 1978; Elliott et al., 2015). Indeed, the auditory system is well known for having a high level of plastic changes throughout life (Syka, 2002; Eggermont, 2017) but how embryonic development affects and possibly limits these later plastic changes remains unclear because of the lack of models (Kral et al., 2016) beyond simply removing parts of the cochlea (Harrison, 2016).

In the formation of the primary tonotopic map, several factors apparently define the precision of some SG neuron projections (Cramer and Gabriele, 2014; Lu et al., 2014; Goodrich, 2016; Yang et al., 2017). The basic helix-loop-helix (bHLH) gene *Neurod1* (Liu et al., 2000) was shown to be essential for inner ear neuronal development as well as normal growth of the cochlea. Subsequent work on mutants null for *Neurod1* showed retention of some sensory neurons using specific neuronal tracing techniques (Kim et al., 2001). NEUROD1 cross-regulates other transcription factors in neurons and hair cells, leading to the transformation of some neurons to intraganglionic hair cells, and transformation of some outer hair cells to inner hair cells (Jahan et al., 2010b). In addition, deletion of *Neurod1* leads to gross projection mapping errors of the few remaining neurons (Jahan et al., 2010a) that go beyond those described in other primary sensory system (Huberman et al., 2008). In previously generated mutants, *Neurod1* deletion occurs both in the ear and the central auditory nuclei, which limits SG neuronal viability and hampers physiological assessment of the wiring defects (Gurung and Fritzsch, 2004; Fritzsch et al., 2006; Jahan et al., 2010a).

We therefore generated a novel mutant with a conditional deletion of *Neurod1* only in the ear to spare many SG neurons and to retain *Neurod1* expression in the auditory nuclei and auditory midbrain. We show here how a shortened and nearly overlapping cochleotopic projection from SG neurons to the CN is expanded across the entire inferior colliculus (IC), affecting the frequency, intensity, and temporal processing of the central auditory system of adult mice at the physiological and behavioral level. Unique to our study are the consequences of compressing the unsegregated and disorganized peripheral projection map of SG neurons onto the tonotopic organization of the central auditory pathways. This type of disorganization of a neural map of the sensory periphery is nearly impossible to achieve with other sensory systems that would require, for example, trigeminal neurons to the face to also innervate the foot or retina ganglion neurons to connect to both eyes and the brain.

Materials and Methods

Animals

All experiments using animals were performed according to protocols approved by the Animal Care and Use Ethics Committee of the Institute of Molecular Genetics, Czech Academy of Sciences. The experimental mice were housed in a controlled environment (12 h light/dark cycles) with *ad libitum* access to food and water. All experiments were performed with littermates (males and females) crossbred from two transgenic mouse lines: floxed *Neurod1* (*Neurod1*$^{loxP/loxP}$; Goebbels et al., 2005) and *Islet1*-cre (*Isl1*-cre; Isl1$^{tm1(cre)Sev/J}$) from The Jackson Laboratory. Breeding pairs contain a mouse with two floxed *Neurod1* alleles (*Neurod1*$^{loxP/loxP}$) and a mouse with one floxed *Neurod1* allele together with one *Isl1*-cre allele (*Isl1*$^{cre/+}$; *Neurod1*$^{loxP/+}$). Genotyping was performed by PCR on tail DNA. The specific primers used were the following: Isl1-cre F 5′-GCC TGC ATT ACC GGT CGA TGC AAC GA-3′ and Isl1-cre R 5′-GTG GCA GAT GGC GCG GCA ACA CCA TT-3′ with a 700 bp product; Neurod1 F 5′-ACC ATG CAC TCT GTA CGC ATT-3′ and Neurod1 R 5′-GAG AAC TGA GAC ACT CAT CTG-3′ with a 400 bp product for the WT allele or 600 bp for the floxed allele. Heterozygous mice *Isl1*$^{cre/+}$; *Neurod1*$^{loxP/+}$ (*HET*) were comparable to the control mice (*Isl1*$^{+/+}$; *Neurod1*$^{loxP/loxP}$ or *Isl1*$^{+/+}$;*Neurod1*$^{loxP/+}$) without any detectable morphological and functional differences. *Neurod1*cKO offspring were recovered at expected Mendelian ratios from E9.5 to P0 birth (123 litters collected and genotyped: 234 *Neurod1cKO*: 260 *HET*: 534 control offspring). The sex ratio of *Neurod1*cKO mice at weaning showed the same representation of males and females as the control mice.

Morphology of the cochlea, cochlear nuclei, and IC

X-gal staining. The mouse line *Isl1*-cre was bred with R26R-*lacZ* (*Gt(ROSA)26Sor*^{tm1Sor}; The Jackson Laboratory) and animals carrying both loci were subjected to X-gal staining (Dvorakova et al., 2016).

Lipophilic dye tracing. We studied the pattern of innervation in whole or dissected ears using lipophilic dye tracing in aldehyde fixed tissue as previously described (Fritzsch et al., 2016a). At least three mutants and similar numbers of control littermates of both sexes were shipped to the University of Iowa and used for different stage (E13.5, E14.5, E16.5, 6 at E18.5, P0, P3 and 6 at P7). We inserted filter strips loaded with different colored lipophilic dyes into the cochlear apex, base, vestibular end organs, cochlear/vestibular nuclei of the brainstem around rhombomere 5 to label afferents, and into rhombomere 4 near the midline to label facial motoneurons/efferents to the ear (Simmons et al., 2011). After allowing appropriate time for diffusion of the lipophilic tracer (between 48 and 120 h), we prepared the ears as whole mounts, mounted with glycerol on a glass slide, using appropriate spacers to avoid distortion, and imaged them using a Leica SP8 confocal microscope. Image stacks were collected and single images or sets of stacks were obtained to provide detailed information about the progressive development and loss of ear innervation over time. Selected ears were further dissected to reveal the detailed innervation of the flat mounted sensory epithelia. Images were compiled into plates to show the most pertinent details using Corel Draw. Only general image modifications, such as contrast or brightness adjustments, were used to enhance the visual appeal without affecting the scientific content.

Immunohistochemistry and morphological evaluations. For whole mounts, dissected tissues were fixed in 4% paraformaldehyde (PFA). For vibratome sections, 4% PFA-fixed samples were embedded in 4% agarose gel and sectioned at 80 μm on a Leica VT1000S vibratome. The primary antibodies used were rabbit anti-Myo7a (1:500; 25-6790, Proteus BioSciences), rabbit or mouse anti-NeuN (1:500, ab177487, Abcam; or 1:100, MAB377, Merck), mouse anti-acetylated α-tubulin (1:400; T6793, Sigma-Aldrich), mouse anti-tubulin β3 (Tuj1; 1:500; 801202, BioLegend), rabbit anti-neurofilament 200 (1:200; N4142, Sigma-Aldrich), rabbit anti-Prox1 (1:500; 925201, BioLegend), mouse anti-VGLUT1 (1:200; MAB5502, Merck), rabbit anti-parvalbumin (1:2000; ab11427, Abcam), rabbit anti-calretinin (1:100; sc-50453, Santa Cruz Biotechnology), goat anti-prestin (1:50; sc-22692, Santa Cruz Biotechnology), goat anti-Neurod1 (1:100; sc-1084, Santa Cruz Biotechnology),

mouse anti-Islet1 (1:50; Developmental Studies Hybridoma Bank 39.3F7 was deposited to the DSHB by T. M. Jessell/S. Brenner-Morton), and mouse anti-C-terminal binding protein 2 (CtBP2; 1:200; 612044, BD Biosciences). The secondary antibodies used were AlexaFluor 488 AffiniPure Goat Anti-Mouse IgG (1:500; 115-545-146, Jackson ImmunoResearch), AlexaFluor 594 AffiniPure Goat Anti-Rabbit (1:500; 111-585-144, Jackson ImmunoResearch), and DyLight488-conjugated AffiniPure Mouse Anti-Goat IgG (1:500; 205-485-108, Jackson ImmunoResearch). Nuclei were stained by Hoechst 33258 (1:2000; 861405, Sigma-Aldrich). Samples were mounted in Aqua-Poly/Mount (18606, Polysciences) or in prepared Antifade medium and images were taken on Zeiss LSM 5 DUO, Zeiss LSM 880, or Leica SPE confocal microscopes. ImageJ and ZEN software were used for image processing.

For neuron quantification, neurons were counted in all NeuN/Tuj1 stained vibratome sections containing a SG using the "Cell Counter" ImageJ plugin, as described previously (Bohuslavova et al., 2017). Briefly, the total number of neurons from all sections per individual cochlea was determined (n = 3/genotype/age). The mean number of neurons in control mice represented 100% of the SG neurons. To determine the length of the cochleae, individual adult cochleae were flat-mounted with the sensory epithelium facing up and the entire length of the cochlear duct from the hook region along the basilar membrane was measured using the "Measure line" ImageJ plugin (n = 3/genotype). The volume of the CN and IC was established by analyzing parallel serial equally spaced sections through the brain. Eighty micrometer coronal vibratome sections were prepared by sectioning five brains of control and five brains of mutant mice. The areas of the left and right CN and IC were determined in each section using ImageJ, and the volume of the organs was calculated. Volumes of paired organs were normalized to body weight. The quantification of neuron soma size was done using the lipophilic tracer dye labeled samples. The area of neuron somas (80 neurons/2 mutants) was determined in image stacks using ImageJ. Data are provided as mean ± SD.

c-Fos staining. Auditory stimulation was described previously (Karmakar et al., 2017). For each experiment, two 2-month-old mice (control and *Neurod1*cKO pair) were placed in a small wire cage under a speaker in a soundproof room. These animals were kept in silence for 1 h and then 15 kHz tone pips at 75 dB sound pressure level (SPL) followed for 90 min. Immediately after sound exposure, mice were transcardially perfused by 4% PFA and brains were dissected and fixed in 4% PFA for 1 h. Tissues were mounted into 4% agarose in PBS and 80 μm coronal sections were cut on a Leica VT1000S vibratome. Sections were blocked in 2.5% normal goat serum, 0.5% Tween and 0.1% Triton in PBS. To detect activated neurons in the CN, we used primary rabbit anti-c-Fos antibody (1:5000; PC38, Calbiochem) and secondary goat anti-rabbit antibody conjugated by AlexaFluor 594 (1:500; 111-585-144, Jackson ImmunoResearch). Stained sections were mounted in Antifade medium and pictures were taken on a Zeiss LSM 880. c-Fos$^+$ neurons in the CN were counted using Cell Counter (ImageJ) and statistics were made using GraphPad software (unpaired t test, n = 4/genotype).

Hearing function evaluation

Auditory brainstem response (ABR) and distortion product otoacoustic emission (DPOAE) tests were performed on mice as described previously (Chumak et al., 2016). Briefly, for ABR recording, responses to tone bursts (3 ms duration, 1 ms rise/fall times, frequencies of 2, 4, 8, 16, 32, and 40 kHz) and clicks of different intensity were recorded. The response threshold to each frequency was determined as the minimal tone intensity that still evoked a noticeable potential peak in the expected time window of the recorded signal. Click-evoked ABR responses were used to analyze the amplitude of single ABR waves and the latency of positive ABR peaks I to IV. For comparison of amplitude-intensity functions, the amplitude of a single ABR wave was calculated as the peak to peak interval and normalized in relation to the wave amplitude at 90 db SPL because of significant differences in ABR wave amplitude between the groups. For DPOAE tests, cubic (2 F1–F2) distortion product otoacoustic emissions over a F2 frequency range from 4 to 38 kHz were recorded (control, n = 12; *Neurod1*cKO, n = 8).

Table 1. Number of animals used

	No. of animals	
Experimental approach	*WT*	*Neurod1*cKO
Histology of the inner ear	39	38
Histology of the brain	20	17
Dye tracing	27	27
Physiology	30	25

Behavioral tests

In the behavioral tests, eight mice were used from both experimental groups (control and *Neurod1*cKO) at the age of 2–3 months. All behavioral tests were performed in a sound-attenuated chamber (Coulbourn Habitest, model E10–E21) located in a soundproof room. During the testing procedure, the mouse was confined to a small wire mesh cage on a motion-sensitive platform. The animal's reflex movements were detected and transduced by a piezoelectric accelerometer. The amplified voltage signal was acquired and processed using a TDT system III with Enhanced Real-Time Processor RP2.1 (Tucker Davis Technologies) and custom-made software programmed in MATLAB. The startle responses were evaluated in a 100 ms window beginning at the onset of the startle stimulus. The magnitude of the acoustic startle reflex was given by the maximal peak-to-peak amplitude of transient voltage occurring in the response window. Acoustic startle stimuli (tone pips or noise bursts) and prepulse stimuli were generated by the TDT system and presented via a loudspeaker (SEAS, 29AF/W) placed 12 cm above the platform inside the chamber. Stimulus presentation and data acquisition were controlled by a custom-made application in MATLAB. The acoustic startle reflex (ASR; a transient motor response to an intense, unexpected stimulus) was used as an indicator of the behavioral responsiveness to sound stimuli. The ASRs to 4, 8, 16, and 32 kHz tone pips and white noise (WN) bursts (50 ms duration, 3 ms rise/fall times, varying intensity levels) were recorded. Each test session contained the following: a baseline trial (−10 dB SPL stimulus intensity) and 13 startle stimuli of different intensities (50, 55, 60, 65, 70, 75, 80, 85, 90, 100, 110, 115, and 120 dB SPL). The intertrial interval varied from 15 to 50 s.

In the prepulse inhibition procedure, three different trial types were used: a baseline trial without any stimulus, an acoustic startle pulse alone (WN at 110 dB SPL, 50 ms, 3 ms rise/fall times), and a combination of the prepulse and startle pulse. The interstimulus interval between the prepulse and the startle stimulus was set to 50 ms; each of the trial types was presented three times. The intertrial interval was randomized and varied from 15 to 30 s. The efficacy of the prepulse inhibition (PPI) of the ASR was expressed as an ASR ratio in percentage: 100% corresponds to the amplitude of the ASR without a prepulse; smaller values of the ASR ratio indicate greater PPI. As a prepulse we used: either (1) WN bursts or tone pips (50 ms duration, 3 ms rise/fall time) at frequencies of 4, 8, and 16 kHz at increasing intensities; or (2) a gap in the background WN of low intensity (65 dB SPL). Both, when presented before the startle stimulus, are expected to decrease the amplitude of the startle response that followed.

Vestibular tests

To evaluate the motor coordination of the mice from both strains (control, n = 4; *Neurod1*cKO, n = 3), we used three stable rods of varying thickness and length (rod 1: 25 mm diameter, 50 cm distance from the open end to the end line; rod 2: 20 mm, 35 cm to the end line; and rod 3: 15 mm diameter, 35 cm to the end line). Two times were measured: orientation time, time taken to turn 180° from the starting position toward the shelf; and transit time, the time taken to travel to the end line (Deacon, 2013). For statistical purposes, we set the maximal test time at 300 s. If the mouse fell off a rod, the maximal score (300 s) was assigned for that particular rod. All tests were performed in an anechoic soundproof room and acoustic stimuli were delivered in free-field conditions via a two-driver loudspeaker system (Selenium 6W4P woofer and RAAL70–20 tweeter). Four types of trials were used: silence, the presence of a continuous broad band noise with intensity 80 dB SPL and presence of a 600 ms series of 100 μs clicks at an intensity of 70 dB SPL with

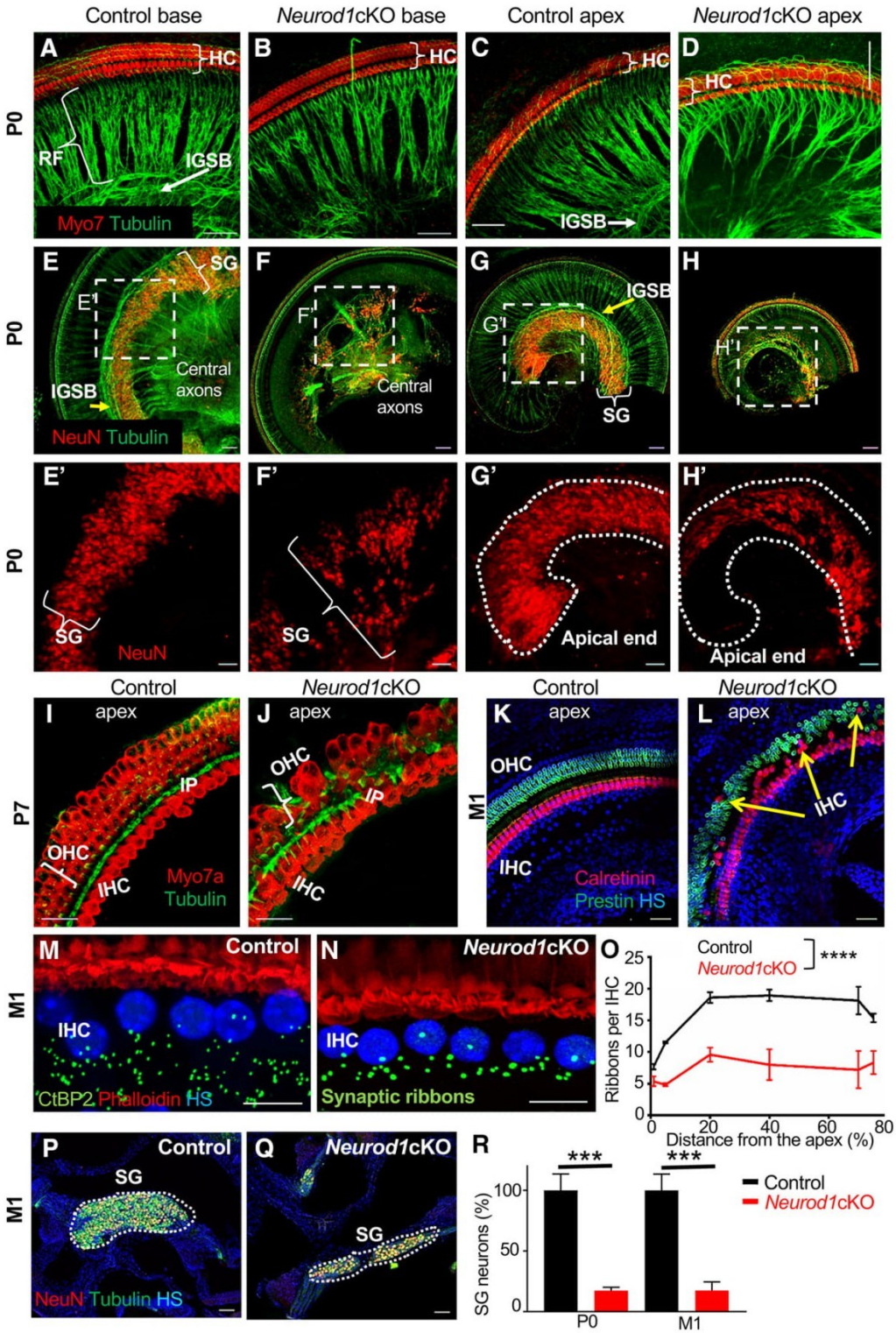

Figure 1. Morphology of the *Neurod1*cKO inner ear is altered. ***A–D***, Whole-mount immunostaining with anti-Myo7a [a marker of hair cells (HCs)] and anti-acetylated α-tubulin (nerve fibers) antibodies shows subtle changes in a number of radial fibers (RFs), lack of the intraganglionic spiral bundle (IGSB; arrow), noticeable disorganization of RFs, and overshooting fibers in the apex of *Neurod1*cKO cochlea (***C***, ***D***). Scale bar, 50 μm. ***E–H***, Whole-mount immunostaining of SG neurons (anti-NeuN, a neuronal soma marker) and innervation shows reduction and disorganization of SG neurons in mutants. Scale bar, 50 μm. ***E′–H′***, Higher-magnification images demonstrate a decreased number and altered distribution of SG neurons. Scale bar, 20 μm. ***I***, ***J***, Immunohistochemistry for Myo7a and for β tubulin (a marker of inner pillar supporting cells) shows the disorganization of OHCs (red) and inner pillar cells (IPs; green) in the apex in *Neurod1* cKO compared with the organ of Corti of control littermates at P7. Scale bar, 20 μm. HS, Hoechst nuclear staining. ***K***, ***L***, Immunohistochemistry for prestin (a marker for OHC) and calretinin (*Figure legend continues.*)

interstimulus intervals linearly decreasing and increasing from 25 to 6.6 ms and back to 25 ms.

Extracellular recording of the neuronal activity in the IC

For extracellular recording, *Neurod1*cKO ($n = 9$; 432 units from the IC) and control mice ($n = 10$; 480 units) were tested. The surgery and extracellular recording in the IC were performed in mice anesthetized with 35 mg/kg ketamine (Calypsol, 50 mg/ml) and 6 mg/kg xylazine (Xylapan, 20 mg/ml) in saline via intraperitoneal injection. Approximately every hour, additional subcutaneous injections of one-half of the original dose of the anesthetics were administered to keep a sufficient level of anesthesia. Basic reflexes (pedal reflex or eye blink reflex), respiratory rate, and heart rate, were monitored. For access to the IC, an incision was made through the skin of the skull and underlying muscles were retracted to expose the dorsal cranium. A holder was glued to the skull and small holes were drilled over both ICs. Neuronal activity (multiple units) in the IC was recorded using a 16-channel, single shank probe (NeuroNexus Technologies) with 50 μm between the electrode spots. The signal obtained from the electrode was amplified 10000 times, bandpass filtered over the range of 300 Hz to 10 kHz and processed by a TDT System III (Tucker Davis Technologies) using an RX5–2 Pentusa Base Station. The data were recorded and processed in BrainWare software (Jan Schnupp, Tucker Davis Technologies) for artifact rejection and separation of single units on the basis of spike-shape clustering and then analyzed with custom software based on MATLAB (MathWorks). The recorded data were processed and analyzed with custom software based on MATLAB. The stimulation signals were generated using a TDT System III with the RP 2.1 Enhanced Real-Time Processor. Acoustic stimuli were delivered in free-field conditions via a two-driver loudspeaker system (Selenium 6W4P woofer and RAAL70–20 tweeter) placed 70 cm in front of the animal's head.

Frequency-intensity mapping. To determine the neuronal receptive fields, pure tones (frequency 2–40 kHz with 1/8 octave step, 60 ms duration, 5 ms rise/fall times, various intensity with 5 dB step) were presented in a random order, each stimulus appearing three times. A discrete matrix corresponding to the response magnitude evoked by each of the frequency-intensity combinations was thereby obtained, smoothed using cubic spline interpolation and used for extraction of the basic parameters: the excitatory response threshold (the lowest stimulus intensity that excited the neuron, measured in dB SPL), the characteristic frequency (CF), the frequency with the minimal response threshold (measured in Hz), and the bandwidth of the excitatory area 10, 20, and 30 dB above the excitatory threshold, expressed by quality factor Q (Q = CF/bandwidth).

Two-tone stimulation. To detect inhibitory areas, a two-tone stimulation was used. Pure tone at the neuron's CF fixed 10 dB above the threshold at CF and pure tone pips of variable frequency and intensity, analogous to those used for the excitatory area mapping, were simultaneously presented. Similar to frequency-intensity mapping, a two-dimensional matrix was obtained, and the presence of the low- and high-frequency sideband inhibitory areas was evaluated.

Rate intensity function of the IC neurons. Neuronal responses to broadband noise (BBN) bursts of variable intensity (10 dB steps, 50 repetitions) were used to construct the rate intensity function (RIF). On each RIF, two points of interest were defined: R10, describing the starting point of the RIF's rise, and R90, describing the RIF's transition to the saturated region. A 100% scale was assigned to the neuron's total range of response amplitudes, with 0% corresponding to spontaneous activity and 100% corresponding to its maximum response magnitude. The two points of interest, R10 and R90, correspond to 10 and 90% of this scale, respectively. On each RIF, two points of interest were defined: R10, describing the starting point of the RIF's rise, and R90, describing the RIF's transition to the saturated region (Bures et al., 2010). The RIF was qualified as saturating if the response magnitude within the top 10 dB interval of the highest stimulus intensities was flat ($\pm$10%). The RIF was qualified as non-monotonic if the response magnitude at the highest stimulus intensity was smaller than the maximum response magnitude by >20%. The remaining RIFs were qualified as strictly monotonic. RIFs were further used for evaluating the following parameters: the percentage of saturating, non-monotonic, and strictly monotonic RIFs; the sound pressure level (S10) corresponding to point R10; the relative response at R10; the dynamic range (DR) of the RIF: DR = S90–S10); and the maximum response magnitude. Spontaneous activity of the IC neurons was determined at the 0 dB SPL BBN stimulation. A Fisher's exact test was used to examine the relationship between mutant and control neurons with a certain RIF.

Temporal properties of the IC neurons. Two types of stimuli were used: (1) a 600 ms series of 100 μs clicks at an intensity of 70 dB SPL for control and 80 dB SPL for *Neurod1*cKO mice with interstimulus intervals linearly decreasing and increasing from 25 to 6.6 ms and back to 25 ms, and (2) trains of five clicks at an intensity of 70 dB SPL for control and 80 dB SPL for *Neurod1*cKO mice with various interclick intervals (100, 50, 30, 20, 15, 10, and 5 ms). In the case of the long changing clicks stimulus, we calculated the percentage of the clicks in the train to which the neurons responded in the time window that started 5 ms after the click and lasted 5 ms. For trains of five clicks with different interspike intervals we computed the vector strength (VS) values along with the Rayleigh statistics that were computed for each spike pattern; only responses with Rayleigh statistics of least 5.991 were considered as significantly phase-locking (Zhou and Merzenich, 2008). The VS quantifies how well the individual spikes are synchronized (phase-locked) with a periodic signal.

Experimental design and statistical analysis

All comparisons were made between animals with the same genetic background, typically littermates. The number of mice used for different analyses was as follows:

The number of samples (n) for each comparison can be found in the individual method descriptions and are given in the corresponding figures. Note that for histology and dye tracing we used the left and right ears as independent samples, doubling the total given in Table 1. Phenotyping and data analysis were performed blind to the genotype of the mice. All values are presented either as the mean $\pm$ SD or SEM. For statistical analysis, GraphPad Prism software was used. To assess differences in the mean, two-sided Student's t tests, one-way or two-way ANOVA with Bonferroni's multiple-comparison test, multiple t test with Holm–Sidak comparison method, χ^2 test, and unpaired two-tailed t tests were used. Significance was determined as $^*p < 0.05$, $^{**}p < 0.01$, or $^{***}p < 0.001$. Complete results of the statistical analyses, including exact p values are included in the figure legends.

Results

Neurod1-deficient mice retain many SG neurons

Neurod1 was eliminated specifically in the inner ear by crossing *Neurod1*$^{loxP/loxP}$ mice (Goebbels et al., 2005) with *Islet1*^{cre} mice (Dvorakova et al., 2016; *Neurod1*cKO). *Neurod1*cKO mice are viable without any obvious abnormal motor activity behavior that would indicate major defects in the vestibular system. To evaluate the cochlear phenotype of *Neurod1*cKO mutants, we stained cochlear whole mounts with antibody to Myo7a, a hair cell marker. The organization of the organ of Corti of mutants was comparable to controls, with three rows of outer hair cells (OHCs) and one row of inner hair cells (IHCs; Fig. 1*A–D*). In contrast to previous work showing that all (Liu et al., 2000) or

←

(*Figure legend continued.*) (a marker for IHCs) shows trans-differentiated IHCs instead of OHCs (arrows) in the apex of the mutant cochlea at 1 month of age (M1). Scale bar, 20 μm. ***M***, ***N***, Confocal analysis of immunostaining for a synaptic ribbon protein (CtBP2) in the IHC area shows a reduction of ribbons in mutant adult mice compared with the controls. Phalloidin labels F-actin in stereocilia of hair cells. HS, Nuclear staining Hoechst. Scale bar, 10 μm. ***O***, Quantification of ribbon synapses per IHC area along the tonotopic axis. Data are expressed as the mean $\pm$ SEM; $n = 3$; two-way ANOVA. $^{****}p < 0.0001$. ***P***, ***Q***, Immunohistochemistry for NeuN in SG neurons at M1, the dotted line indicates the boundaries of SG in the vibratome sections of the cochlea. Scale bar, 50 μm. ***R***, Quantification of SG neurons in the control and *Neurod1*cKO cochlea at P0 and M1. Data are represented as the mean $\pm$ SEM; $n = 3$/genotype/age. Two-tailed unpaired t test. $^{***}p < 0.001$.

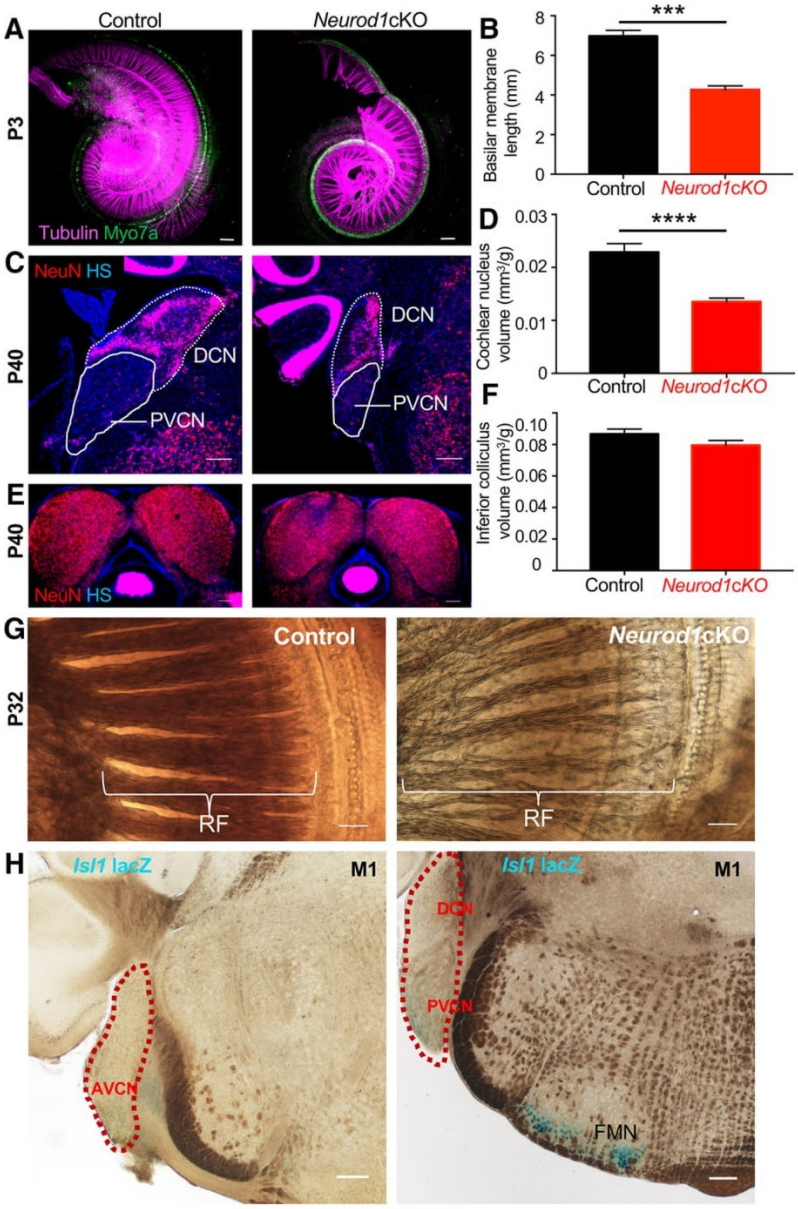

Figure 2. Deletion of *Neurod1* affects the size of the components of the auditory pathways. ***A***, ***B***, Representative image of a whole-mount of control and *Neurod1*cKO cochlea at P3. Hair cells labeled with anti-Myo7a (green) and neuronal fibers with anti-β-tubulin (magenta). Note a reduced density of radial fibers in *Neurod1*cKO cochlea. Scale bar, 100 μm. Quantification of cochlear length at 4 weeks of age ($n = 3$). ***C***, Sections of the CN immunostained with anti-NeuN (red) of adult control and *Neurod1*cKO, showing the DCN and PVCN. The line indicates the boundaries of the CN. HS, Nuclear staining Hoechst. Scale bar, 200 μm. ***D***, Quantification of the volume of the adult CN normalized to body weight ($n = 5$). ***E***, ***F***, Immunostaining of coronal brain sections for NeuN and quantification of the volume of the adult control and *Neurod1*cKO IC, normalized to body weight ($n = 5$). Scale bar, 200 μm. Data (***B***, ***D***, ***F***) are the mean $\pm$ SEM. Two-tailed unpaired *t* test. $^{***}p < 0.001$, $^{****}p < 0.0001$. ***G***, In the adult cochlea, decreased density and increased length of radial fibers (RFs) stained by OsO4 in *Neurod1*cKO are noticeable compared with the control. Scale bar, 100 μm. ***H***, Using a LacZ reporter (R26R mouse line), Isl1-cre-mediated β-galactosidase reporter expression shows no Cre recombination in the CN in the brain sections. The dotted line indicates the boundaries of the CN. Cre recombination is detected by the LacZ reporter in the facial motor nucleus (FMN). Scale bar, 200 μm.

nearly all SG neurons degenerate in different *Neurod1* mutants (Kim et al., 2001; Jahan et al., 2010a), we detected dense radial fibers and SG neurons in the cochlea of *Neurod1*cKO (Fig. 1*A–D*,*E–H*,*E′–H′*). However, there were noticeable abnormalities associated with aberrant innervation and migration of neurons in the cochlea, e.g., elongated and reduced radial fibers, increased spacing between radial fiber bundles, no intraganglionic spiral bundle formed by efferent axons, spread out and missing SG neurons, disorganized central axons, and complete absence of SG at the apical end. In the apex of *Neurod1*cKO, radial fiber bundles were noticeably disarranged with crossing fibers (Fig. 1*D*) and the epithelium was disorganized with missing OHCs, trans-differentiated OHCs into IHCs, and disarranged β-tubulin$^+$ supporting pillar cells (Fig. 1*I–L*). This sensory epithelium phenotype of trans-differentiation of some OHCs into IHCs was comparable to previous reports on different *Neurod1* deletion mutants (Liu et al., 2000; Kim et al., 2001; Jahan et al., 2010a). We also directly assessed the synapses between auditory nerve terminals and IHCs by immunostaining the cochlear sensory epithelium for CtBP2, a major component of presynaptic ribbons in the adult animals (Chumak et al., 2016). Ribbon counts showed an average reduction of 58% in *Neurod1*cKO compared with controls, indicating a reduction of IHC afferent ribbon synapses (Fig. 1*M–O*). The total number of SG neurons positioned inside the *Neurod1*cKO cochlea was reduced at P0 by 80% compared with control littermates but the number of surviving SG neurons was maintained during postnatal development up to adulthood (Fig. 1*P–R*).

*Neurod1*cKO mice have a shortened cochlea, smaller cochlear nuclei, normal size of the IC, and altered ABR

The dissected cochleae of control and *Neurod1*cKO mice were mounted, imaged in a confocal microscope and the length of the organ of Corti was measured (Fig. 2*A*) and found to be on average ~40% shorter in the adult mutant (Fig. 2*B*). Note that the density of radial fibers in *Neurod1*cKO is reduced compared with littermate control. Although their density was evidently lower than in controls, radial fibers were preserved in adult mutant cochlea (Fig. 2*G*). We next measured the volume of the CN at the entry of the auditory nerve in coronally sectioned adult brains. The volume of the CN was reduced by ~39% (Fig. 2*C*,*D*). Because *Islet1*^{cre} is not expressed in the CN (Fig. 2*H*), the size reduction is not likely because of *Neurod1* deletion in the CN (Fritzsch et al., 2006) but is exclusively a secondary effect of reduced afferent input consistent with the effects of neonatal cochlear ablation previously reported (Rubel and Fritzsch, 2002). In contrast to the CN, sections of the IC showed no significant reduction in the adult mutant mice, indi-

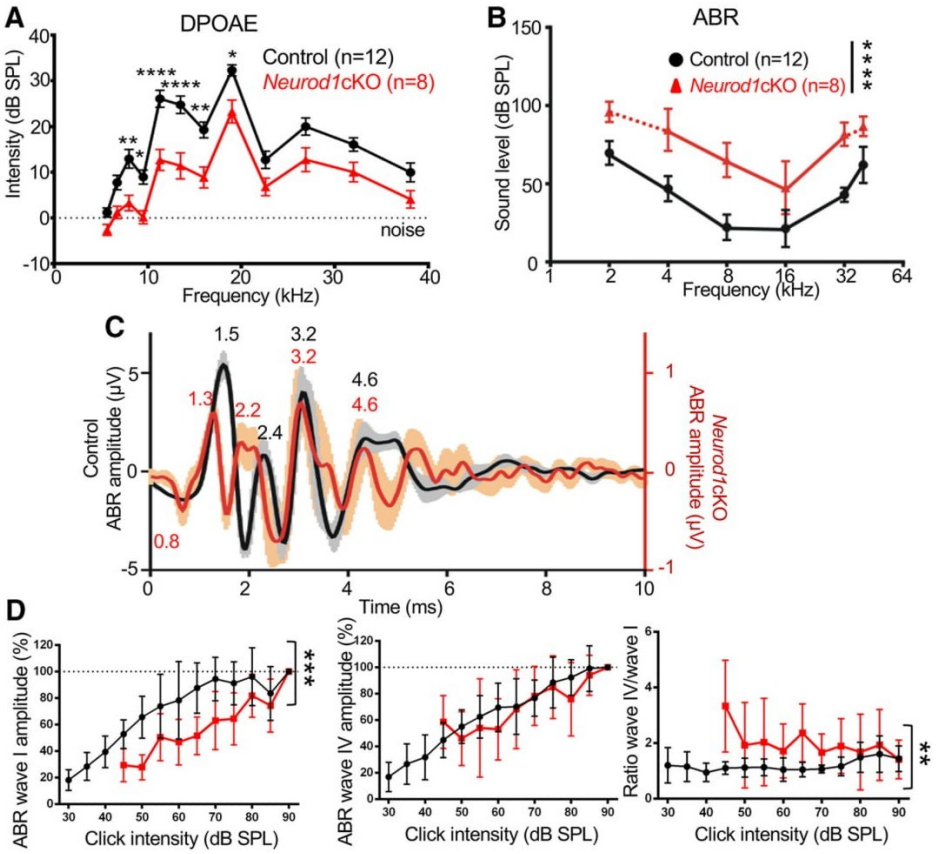

Figure 3. DPOAEs and ABRs are altered in *Neurod1*cKO. ***A***, OHC function assessed by DPOAE shows significantly reduced levels in the low-frequency range. Data are the mean ± SEM; n = 12/control, n = 8/*Neurod1*cKO; two-way ANOVA with Bonferroni *post hoc* test. *$p < 0.05$, **$p < 0.01$, ****$p < 0.0001$. ***B***, The average ABR thresholds of control (n = 12) and *Neurod1*cKO mice (n = 8). Five of the 8 *Neurod1*cKO animals did not have any response to the highest measured intensity at 2 or 40 kHz, indicated by the dotted line. Data are the mean ± SD; two-way ANOVA. ****$p < 0.0001$. ***C***, Averaged ABR response curves evoked by an 80 dB SPL click; control in black, *Neurod1*cKO in red. The solid line shows the average and the shading indicates ±SEM. The ABR wave amplitudes of the mutant were five times lower than the control. Averaged individual ABR wave latency values are shown by the corresponding peaks. ***D***, Averaged click-evoked ABR amplitude-intensity functions normalized to the wave amplitude at 90 dB SPL for ABR waves I and IV, and the ratio of ABR wave IV amplitude to wave I amplitude. Data are represented as the mean ± SD; two-way ANOVA. **$p < 0.01$, ***$p < 0.001$.

cating that the reduction of the CN does not result in a matching reduction of the IC (Fig. 2*E*,*F*).

We evaluated DPOAE, as an objective measure of the function of the cochlear OHCs and cochlear amplification, using frequency range from 4 to 38 kHz (Fig. 3*A*). Based on the base-apical gradient from high to low frequencies (Müller et al., 2005), we detected significant DPOAE changes in the frequency range between 4 and 18 kHz corresponding to the locations of the OHCs in the mid-apex and the apex of the cochlea. These data indicate that OHC dysfunction mostly correlates with the morphological disorganization of the epithelium detected in the apex (Fig. 1*I–L*). Hearing of mice was assessed with ABRs, which measure electrical activity associated with the propagation of acoustic information through auditory nerve fibers to higher auditory centers. The ABR thresholds of mutant mice were elevated compared with the thresholds of control animals throughout the entire measured frequency range, with a relatively even threshold shift in all frequencies averaging ~35 dB of SPL (Fig. 3*B*). Using click-evoked ABR, we evaluated waveform characteristics (Fig. 3*C*). ABR wave amplitudes were five times lower, but the absolute latency of peak I was shorter in *Neurod1*cKO mice. Wave I reflects the synchronous firing of the auditory nerve, whereas waves II–IV are attributed to the electrical activity of downstream circuits in the CN, superior olivary complex, and IC, respectively (Martin and Rickets, 1981). We expected that CN responses should be more affected compared with IC responses because of the overall size reductions. The shorter wave I latency in *Neurod1*cKO indicates altered properties of SG neurons in information processing. The relative interpeak latency between peaks I and II was retained within normal limits, whereas the interval between peaks II and III was prolonged, most likely because of the reduced size of the CN of *Neurod1*cKO. The timing and distribution of ABR III and IV peaks were comparable between control and mutant mice. After normalization and direct comparison of wave I with wave IV, we found that the 3:1 ratio of controls changed to a 1:1 ratio in the *Neurod1*cKO mice (Fig. 3*D*). Moreover, normalization showed that although attenuated, the overall intensity function of wave IV was near normal, whereas wave I was offset even more with higher intensities. These data indicate that morphological changes in the cochlea and CN translate to ABR differences.

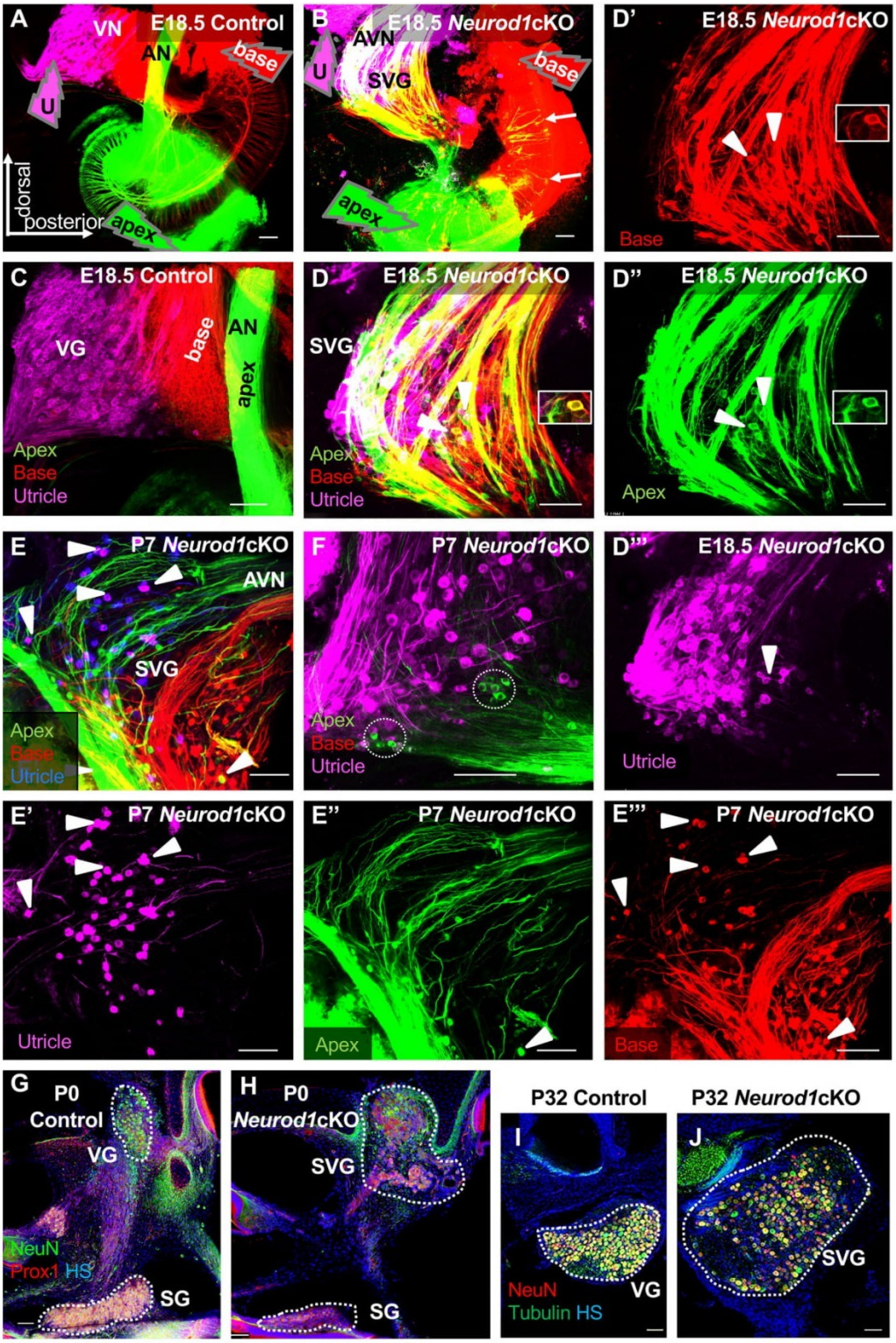

Figure 4. Translocated SG neurons form an aberrant, unsegregated spiro-vestibular ganglion in *Neurod1*cKO. ***A–F***, Representative images of triple-dye labeling from the anterior vestibular end organs [labeled as utricle (U); magenta], apex (green), and base (red) of the cochlea shows the distribution of vestibular and SG neurons in whole-mounted collapsed stacks (***A–D***) and optical confocal sections (***E***, ***F***). Dye injection sites are indicated by arrowheads and labeled correspondingly "apex", "base", "U" (***A***, ***B***). In the control (***A***, ***C***), neurons located in the vestibular ganglion (VG) of the control are only labeled by utricular dye applications (***A***, ***C***, magenta; basal turn, red; apex, green) injections label only fibers in the AN and utricular injection labels fibers of the vestibular nerve (VN). In *Neurod1*cKO (***B–F***), neurons labeled by dyes injected into the cochlear base and apex, and the utricle combine to form an aberrant enlarged ganglion, the SVG, (*Figure legend continues.*)

Spiral ganglion neurons form an aberrant "spiro-vestibular" ganglion

The application of different colored lipophilic dyes into the apex (green) and base of the cochlea (red), and anterior vestibular end organs (utricle, anterior and horizontal canal cristae; magenta) showed an aberrant distribution of spiral and vestibular ganglion neurons into a "spiro-vestibular" ganglion (SVG) complex in *Neurod1*cKO (Fig. 4*B*,*D*) in contrast to the vestibular ganglion of control mice with neurons exclusively labeled by anterior vestibular dye applications (Fig. 4*A*,*C*). Additionally, apex-dye application labeled fibers were detected in the base of the *Neurod1*cKO cochlea (Fig. 4*B*, arrows). In controls, the segregated central axons of neurons labeled by dyes injected into the base and apex in the auditory nerve (AN) were separated from the vestibular nerve (labeled by the dye injection into vestibular end organs; Fig. 4*A*,*C*). In contrast, the segregation of central axons was lost as basal and apical afferents completely overlapped with vestibular axons in the auditory-vestibular nerve (AVN) in *Neurod1*cKO (Fig. 4*B*, in detail *D*,*E*). Note that double-labeled neurons (from base/apex or base/utricular injections) were detected only in the *Neurod1*cKO at E18.5 and P7 (Fig. 4*D–D‴*,*E–E‴*, arrowheads), indicating multiple branches of some single SG neurons and abnormal innervation within the cochlea and between the cochlea and vestibular organs. Soma size of SVG neurons labeled from dye injections into the apex of the cochlea (green) was noticeable smaller in mutants (Fig. 4*F*; area: 253 ± 80 μm^2) compared with adjacent vestibular neurons labeled from anterior vestibular organ applications (magenta; area: 364 ± 74 μm^2; $n = 80$ neurons/2 mutants, t test, $p < 0.001$). We verified the tracing data using PROX1 immunocytochemistry that labels only SG neurons in wild-type (Fritzsch et al., 2010). In *Neurod1*cKO, PROX1$^+$ translocated SG neurons were detected in the area of the vestibular ganglion, thus forming a mammalian SVG (Fig. 4*H*) instead of the normally distinct SG in Rosenthal's canal and a vestibular ganglion between the ear and the brain of controls (Fig. 4*G*). The adult SVG of *Neurod1*cKO mice was enlarged and deformed compared with control animals (Fig. 4*I*,*J*). Our data confirm previous suggestions of such unusual migration of some SG neurons to colocalize with vestibular neurons in $Pax2^{cre}Neurod1^{loxP/loxP}$ (Jahan et al., 2010b) or $Wnt1^{cre}Sox10^{loxP/loxP}$ mice (Mao et al., 2014). We showed not only translocated SG neurons and the formation of the aberrant SVG but also single ganglion neurons having multiple branches within the cochlea (double-labeled by base/apex injections) and between the cochlea and vestibular end organs (double-labeled by cochlear/vestibular injections) in *Neurod1*cKO.

Spiral ganglion neurons are miswired in the cochlea of *Neurod1*cKO

Having recognized the major effects of *Neurod1* deletion on the cochlea and auditory nucleus size, overall physiology, and abnormal arrangement of SG neurons together with vestibular ganglion neurons in the SVG complex (Fig. 4), we next wanted to establish the details of the SG connection between the organ of Corti and vestibular organs as well as connection between the cochlea and the CN. We first investigated whether SG neuron projections are restricted to the CN by backfilling afferents in the ear through dye tracing injections into the CN (red) and cerebellum (green). These dye-tracing data showed that afferents in the cochlea of controls were strictly labeled through dye injected into the CN (Fig. 5A, red). In contrast, some SG neurons in the developing cochlea of *Neurod1*cKO mutants projected to the cerebellum, because their afferents were colabeled through dye injected into the cerebellum (Fig. 5*B*, overlapping yellow fibers in the *Neurod1*cKO cochlea). Note that the location of the vestibular ganglion (green dye tracing injection into the cerebellum) was anterior to the auditory nerve in controls (Fig. 5*A*) but posterior to the aberrant SVG ganglion in *Neurod1*cKO (Fig. 5*B*) consistent with the reorganization of anterior posterior fibers and cell distributions in the SVG (Fig. 4*B*,*D*). We next wanted to establish whether the branches of cochlear projecting neurons also reach vestibular organs in the ear by injecting dye into the cochlea, posterior canal crista and utricle ($n = 9$ at E14.5, E16.5, E18.5). Applying dye to the posterior vertical canal crista consistently labeled fibers in the cochlea in a pattern reminiscent of backfilling from the cerebellum in *Neurod1*cKO (Fig. 5*C*,*D*). Neurons labeled with posterior canal injections had multiple branches toward the developing organ of Corti (Fig. 5*D′*, in detail *D″*) that overlapped with fibers to the base and to the posterior canal crista after dye was applied to the apex (Fig. 5 *D′*, inset, green), indicating the presence of neurons projecting to both the cochlea and the posterior canal crista. No such labeled intertwined innervation was found in the control cochlea at E14.5 nor were fibers labeled from the cerebellum (Fig. 5*A*). Later at E16.5, posterior vertical canal injections labeled at most a few efferent collaterals in control animals (Fig. 5*E*), similar to previous descriptions of branching of the efferent axons in the ear (Simmons et al., 2011; Sienknecht et al., 2014). In contrast, posterior vertical canal injection labeled SG fibers in the base, middle, and apex of the shortened cochlea of *Neurod1*cKO (Fig. 5*F*,*F′*). Not only translocated SG neurons but also vestibular ganglion neurons in the SVG innervated the cochlear hair cells, as indicated by an unusual innervation pattern near inner hair cells in *Neurod1*cKO (Fig. 5*F′*, arrow). These fiber terminations are comparable to rerouted vestibular fibers in neurotrophin mutants (Tessarollo et al., 2004; Fig. 5*F′*, inset), implying that some neurons reach both the organ of Corti as well as vestibular organs.

We next investigated in more detail the branching of SG neurons within the cochlea and between the cochlea and vestibular organs. In controls, dye injections into the cochlear apex (green) and base (red) resulted in a spatially restricted labeling of SG neurons and fibers in the cochlea according to the injection site without any labeling detected from injections to anterior vestibular organs (Fig. 6*A*). In addition to the projection of afferents from the ear to the brain, the ear is also innervated by efferents

←

(*Figure legend continued.*) as shown in whole mounts (***B***, ***D***) or optical sections (***E***, ***F***). In mutants, there is a tendency of fibers labeled from the apex (green) to be more anterior in the combined SVG and the combined AVN (***B***), whereas apical fibers run in the most posterior part of the AN in control animals (***A***, ***C***). Overlapping fibers (yellow) labeled by the basal and apical dye applications are present in the mutant cochlear base (***B***, arrows). Note that double-labeled SVG neurons can be seen after basal and apical injections (***D***, ***E***, yellow cells). The double-labeled cells after basal and anterior vestibular end organ injections can best be visualized when the dye is false colored in blue (***E***, double-labeled cells in magenta). ***D′–D‴***, ***E′–E‴***, Images of individual colors of the separate channels shown as a merged image in ***D*** and ***E*** (arrowheads indicate double-labeled cells from merged images). ***F***, A merged image shows only apical turn dye labeled SG neurons (green, dotted circles) near magenta labeled vestibular neurons in the SVG. Note that green cells are substantially smaller compared with the VG neurons labeled from anterior vestibular end organ dye application. Scale bars, 100 μm; dorsal is up and posterior is to the right in all dye-tracing images. ***G***, ***H***, Representative vibratome sections show translocated spiral ganglion PROX1$^+$ neurons in the SVG as detected by immunohistochemistry for PROX1 (a marker for SG neurons) and NeuN (a marker for differentiated neurons) in *Neurod1*cKO at P0. Scale bar, 100 μm. HS, Nuclear staining Hoechst. ***I***, ***J***, Immunohistochemistry for NeuN and β-tubulin in the adult control VG and *Neurod1*cKO SVG. Scale bar, 50 μm. Dotted lines indicate the boundaries of the SG, VG, and SVG.

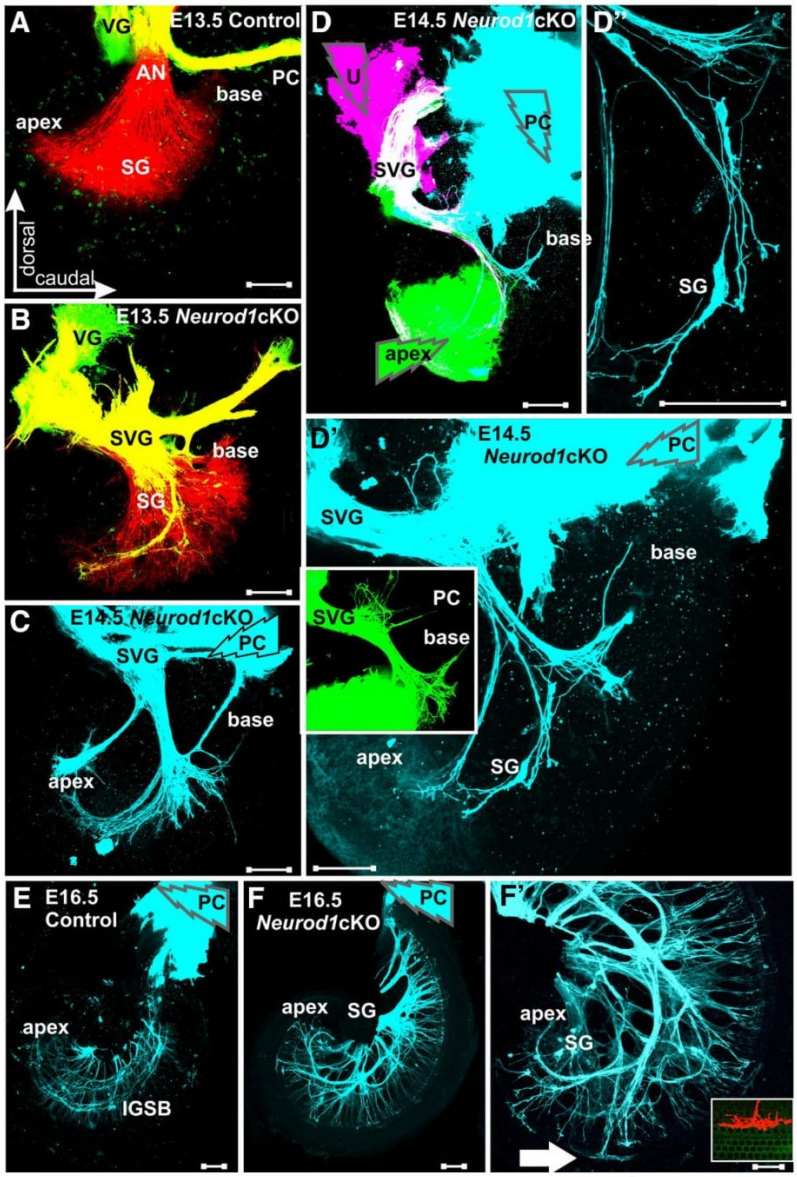

Figure 5. Loss of *Neurod1* causes projection defects of SG neurons. ***A***, ***B***, Only afferents to the cochlea are labeled by the lipophilic dye injected into the CN (red) but not by dye injected into the cerebellum (green) in the control at E13.5. In *Neurod1*cKO littermates, some SG neurons and fibers are labeled from cerebellar injections (***B***, yellow, representing green overlapping with red). Note that afferents in the cochlea are distributed irregularly in mutants compared with controls (***A***, ***B***, red). ***C–F′***, The cyan arrowheads show the approximate application site of the dye [posterior canal crista (PC)] that results in labeling of multiple cells and branches projecting to the developing organ of Corti in *Neurod1*cKO. Injection of three different colored dyes [utricle, magenta; PC, cyan; apex, green] into the E14.5 *Neurod1*cKO ear shows overlap of spiral and vestibular ganglion neurons in the spiro-vestibular ganglion and magenta fibers to the cochlea (***C***, ***D***, ***D′***). Higher-magnification of fibers in the cochlea labeled from PC injections shows multiple neuronal branches toward the developing organ of Corti hair cells (***D″***). The dye injected into the apex of *Neurod1*cKO (***D′***, inset, green) labels fibers reaching the base as well as fibers to the posterior canal crista in a pattern reminiscent of fibers labeled from PC injections. These neurons have branched axons that reach not only the brain but also the PC nerve. ***E***, ***F***, ***F′***, After PC dye application at E16.5, only a few efferent collaterals are labeled in controls that contribute to the intraganglionic spiral bundle (IGSB). In *Neurod1*cKO at E16.5, PC dye application labels SG neurons near the apex that terminate in an unusual pattern along IHC (***F′***, arrow). This pattern is comparable to the reported pattern of vestibular fibers in a replacement model of neurotrophins (***F′***, inset; data from Tessarollo et al., 2004), indicating that some SG neurons project like vestibular neurons in the brain, reach vestibular end organs (such as the canal crista) and terminate at the organ of Corti in a pattern comparable to rerouted vestibular neurons. Scale bars, 100 μm. PC, Posterior crista; U, utricle; VG, vestibular ganglion.

that are rerouted facial branchial motor neurons that end on hair cells instead of muscle fibers (Simmons et al., 2011; Fritzsch and Elliott, 2017). Typically, dye applications into the cochlea label efferent branches as the dye diffuse close to the radial fibers into the organ of Corti and efferent fibers can be distinguished by a recognizable intraganglionic spiral bundle, formed exclusively by efferents. Accordingly, in our controls, most efferent fibers were strictly either labeled by the dye applications to the apex or base in controls (Fig. 6*A′*, red or green). Note that fibers formed evenly spaced radial bundles. Overlapping (yellow) fibers represented efferents forming the intraganglionic spiral bundle and branching to reach multiple points along the cochlea in controls (Fig. 6*A′*). In contrast similar dye applications (into the base, apex, and anterior vestibular organs) labeled neurons and branches throughout the inner ear in *Neurod1*cKO, showing mingled bundles of fibers from the apex and base (Fig. 6*B*). Tracing data revealed at least three different groups of "SG neurons" within the cochlea: those restricted to base or apex, those overlapping between base and apex and those that have in addition branches to vestibular organs (Fig. 6*B–B‴*). A few SG neurons labeled from vestibular injections revealed multiple branches to reach different parts of the cochlea (Fig. 6*B′*). Thus, our tracing experiments show that both the branching properties and migration properties of inner ear sensory neurons are affected by the deletion of *Neurod1*, generating neurons that are colocalized with vestibular neurons (Fig. 4) and reach multiple parts of the organ of Corti as well as different vestibular organs (Figs. 5, 6).

To fully evaluate efferent innervation in the cochlea, we applied lipophilic dyes into the olivocochlear bundle (green) to label efferents and into the CN (red) to label SG neurons and afferent radial fibers reaching the organ of Corti. In control animals, efferents formed the intraganglionic spiral bundle along SG neurons and together with afferents formed evenly spaced radial bundles (Fig. 7*A*, in detail *A′*). In contrast, *Neurod1*cKO efferents reached outer hair cells like in control littermates but did not form the intraganglionic spiral bundle (Fig. 7*B*,*B′*). Accordingly, the function of outer hair cells of control and *Neurod1*cKO was comparable to the exception of the mid-apex, as shown by DPOAE tests (Fig. 3*A*). These data support the notion that much of the intracochlear trajectory of

efferents depends on the distribution of SG neurons but efferents can reach hair cells no matter the deviation from their normal trajectory.

Neurod1 deletion results in a loss of the tonotopic organization of the CN

Next, we evaluated the auditory nerve fiber projections to the brainstem cochlear nucleus complex, composed of the anterior ventral CN (AVCN), posterior ventral CN (PVCN), and dorsal CN (DCN; Muniak et al., 2013, 2016). In control animals, application of different colored lipophilic dyes into the apex (green) and base of the cochlea (red), and vestibular end organs (magenta) showed the segregation of central axons of SG neurons from the base and apex in the auditory nerve and that these discrete, non-overlapping bundles were separated from the vestibular nerve (Fig. 8*A*,*E*). In contrast, the segregation of central axons of SG neurons was lost as basal and apical afferents completely overlapped in the AVN (Fig. 8*B*, F). Dye applications in the control cochlea showed the tonotopic organization of the CN subdivisions, with low-frequency-encoding fibers from the apex terminating dorsally and high-frequency-encoding fibers from the base terminating ventrally in both the VCN and DCN (Fig. 8*A*,*E*). In the CN of *Neurod1*cKO, fibers labeled with lipophilic dye tracing from the entire cochlea were restricted to the VCN with just a few fibers occasionally expanding to the DCN (Fig. 8*B*,*F*–*F*″). Very large dye injections covering the basal half and apical half resulted in segregated projections with almost no space between apical and basal afferents in control animals (Fig. 8*G*). In contrast, comparable injections in *Neurod1*cKO mutants showed the entering fibers overlapped in the AVN and were mostly restricted to the VCN with just a few fibers occasionally expanding to the DCN (Fig. 8*H*,*I*). In essence, the DCN remained virtually non-innervated by cochlear afferents and the dorsal part of both AVCN and PVCN likewise received only sporadic and variable individual fibers, indicating a relocation of high-frequency-encoding basal turn fibers. In controls, cochlear afferents formed parallel fibers, the isofrequency bands (Fig. 8*C*,*G*, inset), whereas *Neurod1*cKO afferents neither expanded across the entire CN nor showed a parallel fiber organization (Fig. 8*D*,*H*,*I*). As expected from overlapping peripheral connections of neurons in the SVG (Fig. 4) as well as neurons in cochlea reaching vestibular organs (Figs. 5, 6), we also found fibers in the CN of *Neurod1*cKO labeled by the application of lipophilic dye into vestibular end organs (Fig. 8*F*″). Thus, *Neurod1*cKO mutants have both the peripheral and central connections of spiral and vestibular neurons incompletely segregated and miswired with overlapping central axons of SG neurons in the auditory-vestibular nerve and limited projections of widely ramifying fibers to the ventral part of CN that showed variable and inconsistent segregation (Fig. 8*J*, summary).

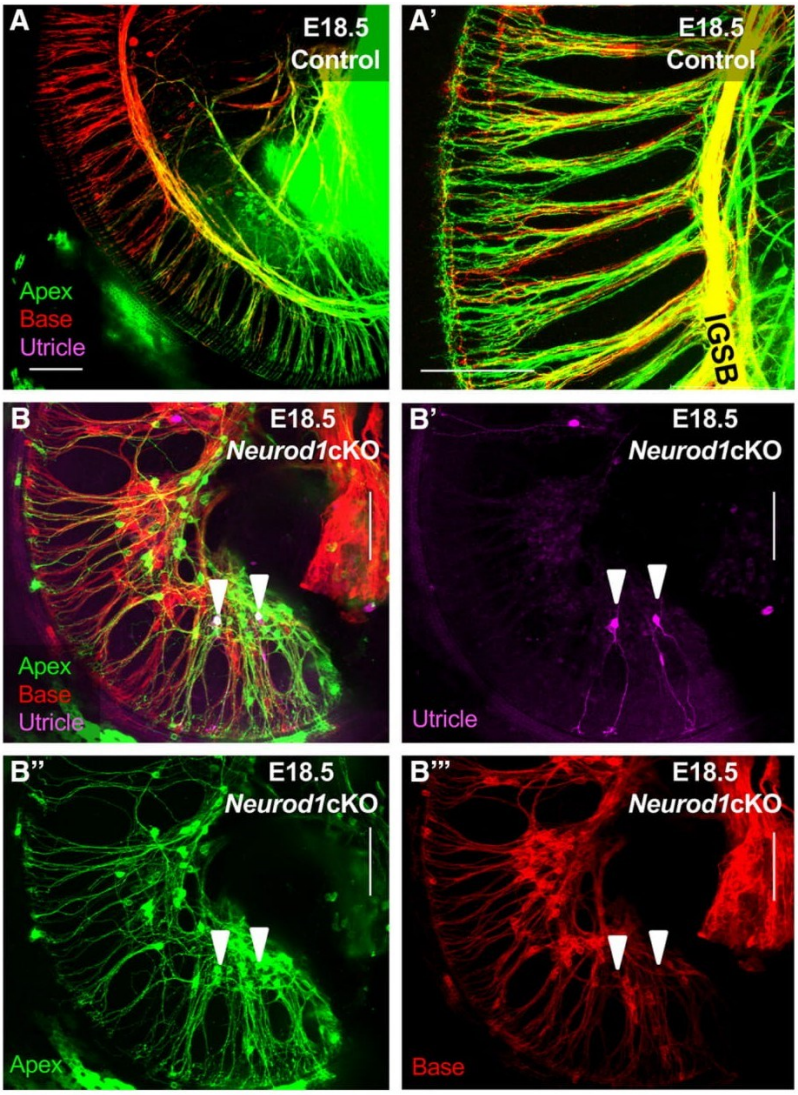

Figure 6. Distribution and multiple branches of SG neurons reveal disorganization in the *Neurod1*cKO cochlea. ***A***, ***B***, The application of different colored dyes into the apex (green), base (red), and utricle (magenta) shows a spatially restricted labeling of SG neurons and fibers based on the injection site in controls (***A***), whereas both fibers and neurons are labeled throughout the *Neurod1*cKO cochlea by the utricle, base and apex injections (***B***). ***A′***, In controls, overlapping (yellow) efferent fibers superimpose in the intraganglionic bundles (IGSB). Some efferent fibers are labeled either by the dye application to the apex or base in controls (red or green) and together with afferents form evenly spaced radial bundles. ***B′*–*B‴***, images of individual colors of the separate channels shown as a merged image in ***B***. Note that SG neurons near the apex are double labeled with magenta (utricle) and green (apex) as indicated by arrowheads, and show in addition two or more local branches to different parts of the cochlea (***B′***). Scale bars, 100 μm.

Since the size of the CN depends on the full complement of afferents and the survival of CN neurons depends on innervation (Rubel and Fritzsch, 2002; Syka, 2002), we next investigated the survival of one class of neurons that receive input from auditory nerve fibers through the large end bulbs of Held, the bushy cells in the AVCN (Muniak et al., 2016). Although the size of the AVCN in *Neurod1*cKO was reduced, SG afferents of *Neurod1*cKO and

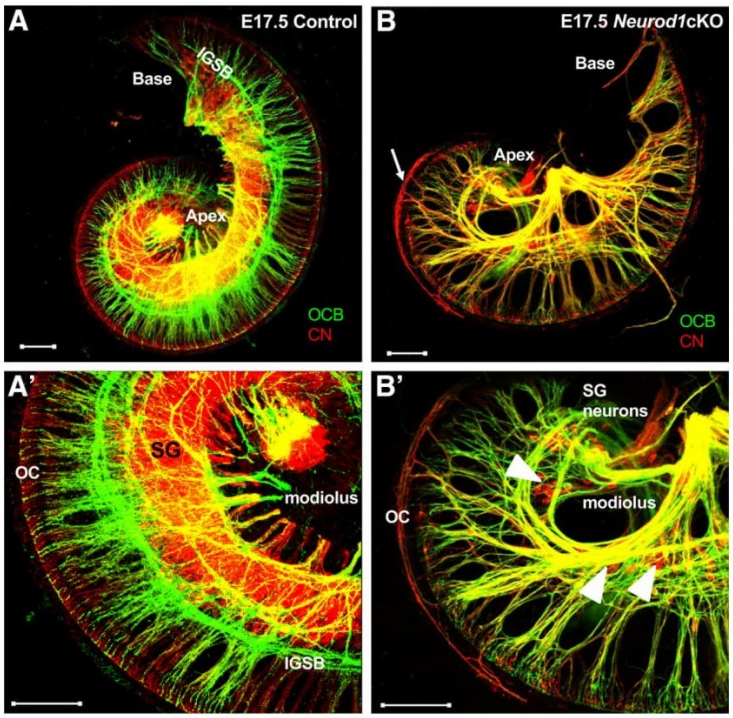

Figure 7. Disorganized inner ear efferents reach the organ of Corti in the *Neurod1*cKO cochlea. ***A***, ***A′***, In control animals, the injections of lipophilic dye into the olivocochlear bundle (OCB; green) labels inner ear efferent fibers forming the intraganglionic bundle (IGSB) and dye application into the CN (red) labels SG neurons and afferent radial fibers reaching the organ of Corti (OC). ***B***, ***B′***, In *Neurod1*cKO, the same dye applications label the scattered SG neurons (red dye-labeled; arrowheads) in the cochlea and show strong efferent innervation that lacks an IGSB formation. Note also the profound innervation of the OHC region of the OC only in the apex of the *Neurod1*cKO mutant (***B***, arrow). Scale bars, 100 μm.

control formed morphologically comparable clusters of boutons that wrap the somas of their targets with the end bulbs of Held, as shown by excitatory VGLUT1 synaptic marker labeling (Fig. 9*A–B′*). However, innervation patterns of afferents outside the overlapping area in AVCN of *Neurod1*cKO (Fig. 8*D*,*H*,*I*) suggest an unusual distribution that does not conform to the regular pattern of stratified afferent projections in controls (the isofrequency bands in Fig. 8*C*,*G*, inset), which represent the tonotopic input of the organ of Corti onto the CN (Muniak et al., 2013, 2016).

c-Fos shows a distorted frequency map representation in the CN

We next wanted to investigate whether SG afferents formed functional synapses onto AVCN bushy cells and how distinct frequencies are mapped throughout the system in terms of the activation of the immediate early response of c-Fos, a technique shown to allow such mapping (Tomková et al., 2015; Karmakar et al., 2017). We subjected freely moving adult mice (2 months old) to pure tone auditory stimulation with 15 kHz pips at 75 dB for 90 min in a sound-proof chamber. We used a 15 kHz tone that drives cochlear activation near the middle in controls and likely also in *Neurod1*cKO mutants, assuming the apex and base shorten equally. Consistent with previous reports (Karmakar et al., 2017), in control mice, we found a narrow band of c-Fos $^{+}$ cells near the center of the AVCN, corresponding with the known isofrequency representation (Fig. 9*C*). In contrast, in *Neurod1*cKO, 15 kHz-stimulation activated AVCN neurons but the c-Fos activation area was spread all over the AVCN and the number of activated neurons was doubled (*Neurod1*cKO 20.7 $\pm$ 2.5; control 9.8 $\pm$ 1.4, $p = 0.0099$; Fig. 9*D*). These data indicate that the pure tone stimulation of 15 kHz activated AVCN neurons but the tonotopic precision of SG axon targeting was degraded with a spread of activation to many surrounding frequencies.

Frequency tuning, intensity, and temporal coding properties of IC units are distorted in *Neurod1*cKO

With this background on neuroanatomical, quantitative and frequency related c-Fos activity changes in mind, we next investigated the tuning properties of IC neurons at various frequencies as well as other parameters of their function i.e., two-tone suppression, intensity, and temporal resolution as the IC is the first level of auditory space map projection and shows some amelioration of primary afferent dysfunction (Buran et al., 2010; Pelgrim et al., 2018).

The study of the tuning characteristics of IC neurons revealed striking differences in the shape of the excitatory receptive fields between the *Neurod1*cKO and control mice. Instead of simple narrow V-shape receptive fields (a mono-peak response) seen in the controls, we recorded mostly wide receptive fields with two or more peaks in clusters of IC neurons of *Neurod1*cKO mice (Fig. 10*A*), suggesting multiple inputs from the lower levels of the auditory system. Two-tone stimulation, used to detect inhibitory areas surrounding the excitatory tuning curves, showed the presence of low- and high-frequency sideband inhibitory areas in controls, and small and disorganized inhibitory areas in *Neurod1*cKO (Fig. 10*B*). Because we mostly recorded the multiple-unit activity of neuronal clusters in the IC, we wanted to establish whether the multipeaked broad tuning curves in mutants are formed by the integration of responses of several neurons with different best frequencies or whether they reflect a miswiring of auditory fibers occurring below the IC. We found that the multipeaked broad tuning curves in the responses of neuronal clusters were also observed in the tuning curves of isolated single units recorded at the same electrode (Fig. 10*C–H*).

The investigation of responsiveness of IC units of the mutant mice to different sound frequencies revealed a frequency range with a limited presence of CFs from 9 up to 28 kHz (Fig. 11*A*). These features are consistent with the observed shortening of the cochlea, and the reduced amplitude of the ABR. In addition, the excitatory thresholds of IC units were higher in mutants than in control animals in all measured frequencies (Fig. 11*A*). One commonly used metric of auditory tuning is the "quality factor", or Q, defined as the CF divided by the bandwidth, typically measured 10 dB above the minimum threshold. Comparing the data of control and mutant mice, the tuning curves recorded at individual electrodes in the IC of mutant mice had a significantly lower quality factor Q_{10}, indicating that their frequency selectivity was worse (Fig. 11*B*).

To assess the responsiveness of neurons to sound intensity, we recorded the responses of IC multiunits to WN bursts of variable

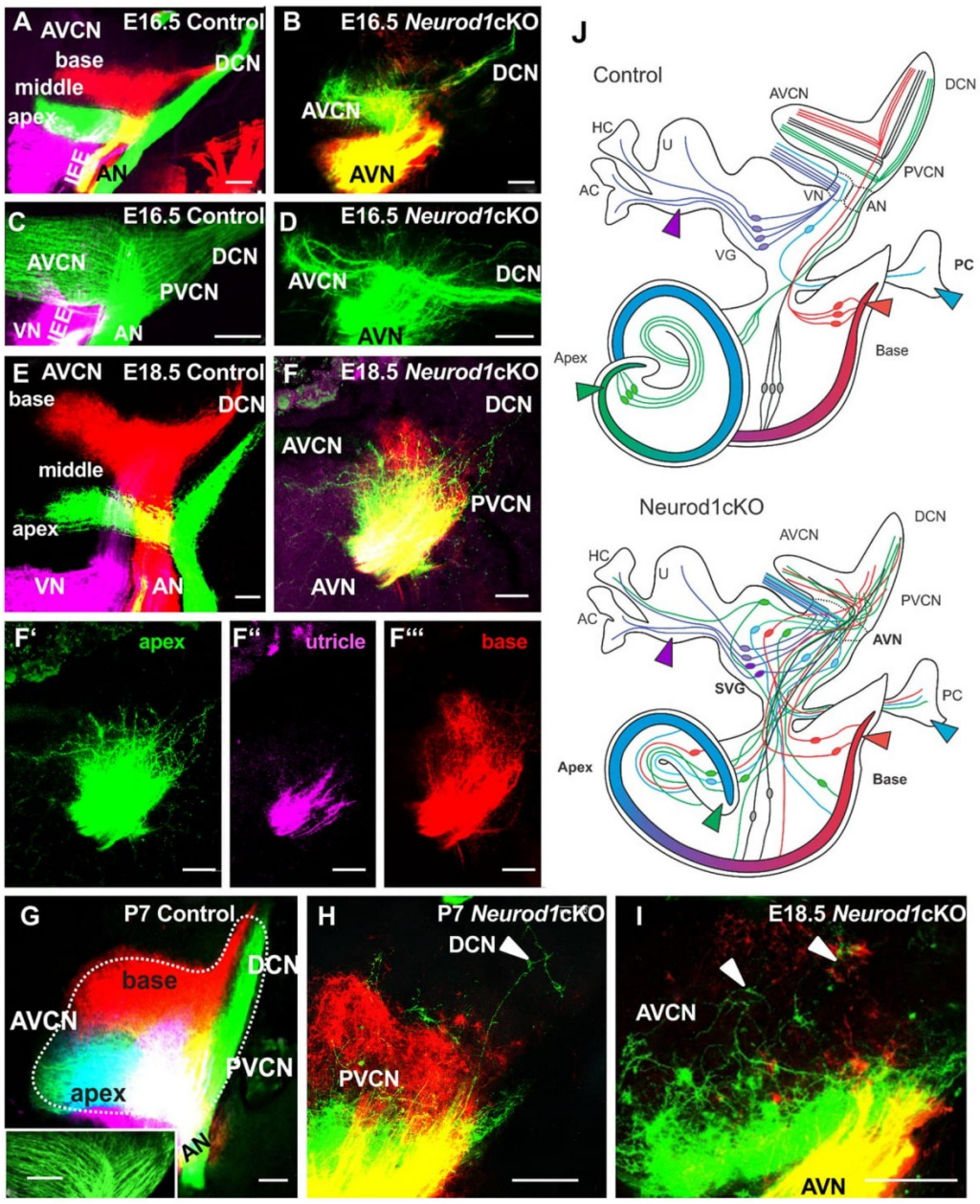

Figure 8. *Neurod1*cKO SG neurons project unsegregated widely ramifying central axons to the CN. ***A***, ***C***, ***E***, Injections of different colored dyes (magenta, vestibular organs; red, base; green, apex) label distinct bundles of neuronal fibers (AN) projecting to the CN and vestibular nuclei in controls. The tonotopic organization of the CN subdivisions in controls is shown in the AVCN and the DCN with low-frequency fibers labeled from the apex and high-frequency from the base and no labeling between (the middle cochlea; ***A***, ***E***, ***G***). The only mixed bundle (yellow) are inner ear efferents (IEEs; ***A***). In *Neurod1*cKO, neuronal fibers completely overlap forming a mixed-labeled AVN (yellow) and are restricted to the ventral part of the CN with just a few fibers occasionally expanding to the DCN (***B***, ***D***, ***F***). The overlapping fibers in the AVCN indicate a loss of the tonotopic organization of the central projections (***B***, yellow fibers). ***C***, ***D***, Higher-magnification shows central afferents as parallel fibers (isofrequency bands) in control AVCN and DCN, whereas central projections of afferents in mutants branch in a restricted and erratic pattern in the CN (green dye injection into the apex). ***E***, ***F***, The tonotopic organization of the CN subdivisions with low-frequency-encoding fibers from the apex (green) terminating ventrally and high-frequency-encoding fibers from the base (red) terminating dorsally in the control AVCN and DCN. In contrast, disorganized fibers labeled by dye injected in the apex of *Neurod1*cKO project into the ventral part of the AVCN, whereas virtually only sporadic fibers labeled by basal dye injection reach only PVCN subdivisions. ***F′***–***F‴***, Single color images show the incomplete cochlear projection segregation as well as some "vestibular" fibers projecting to the CN of *Neurod1*cKO (***F″***) that never happens in control animals (***A***, ***C***, ***E***). ***G***, Very large lipophilic dye injections result in barely segregated projection with almost no space between apical and basal afferents in controls. Inset, Cochlear afferents organized as parallel fibers in isofrequency bands. ***H***, ***I***, Comparable large dye injections label sporadic and divergent fibers mostly in the ventral part of the CN of *Neurod1*cKO at P7 and E18.5. Note that single afferents project widely ramifying across the CN complex (***H***, ***I***, arrowheads). Scale bars, 100 μm. ***J***, Schematics of changes in *Neurod1*cKO: (1) SG neurons are miswired and misplaced into an aberrant SVG, (2) overlapped central auditory and vestibular afferents form the AVN, and 3) the CN has reduced projections without tonotopic organization both in terms of branch distribution within the cochlea and to the CN. The triangles indicate the application sites of the dyes in the base, apex, utricle (U), and posterior canal crista (PC). AC, Anterior crista; HC, horizontal crista; VG, vestibular ganglion; VN, vestibular nerve.

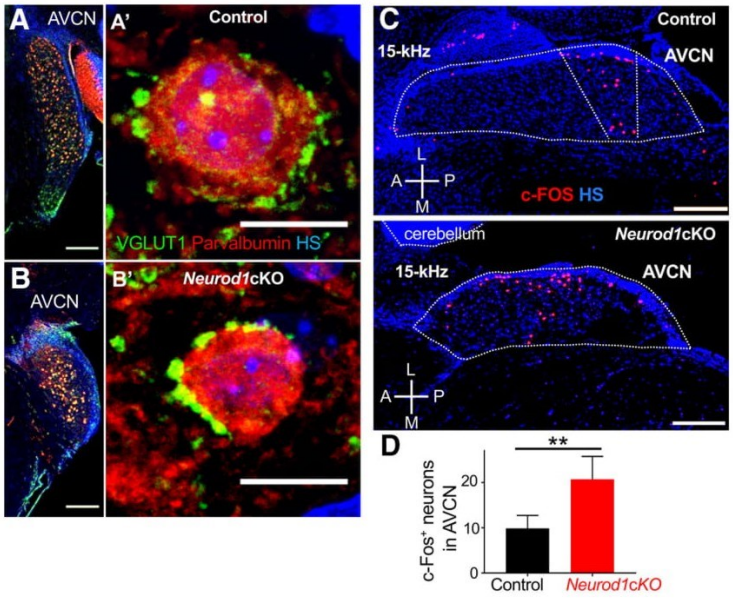

Figure 9. The formation of isofrequency bands in the anteroventral CN of *Neurod1*cKO is altered. ***A***, ***A′***, ***B***, ***B′***, Auditory nerve synaptic terminals of control and mutant mice are comparable, as anti-VGLUT1 labels the endbulb of Held synapses and anti-parvalbumin labels the bushy cell soma in the AVCN of the adult control and *Neurod1*cKO. ***C***, Activated neurons are labeled by anti-c-Fos antibody in response to 15 kHz pure tone stimulation in the AVCN of 2 months old controls and *Neurod1*cKO. Dotted line indicates boundaries of the AVCN. A, Anterior; L, lateral; M, medial; P, posterior. ***D***, The total number of c-Fos $^{+}$ neurons determined in the sections of the AVCN of control ($n = 4$) and *Neurod1*cKO mice ($n = 4$). Two sections were evaluated per each individual mouse. Values are mean ± SEM. $^{**}p = 0.0099$, *t* test. Scale bars: 200 μm; ***A′***, ***B′***, 10 μm. HS, Nuclear staining Hoechst.

intensity and used them to construct RIFs. The percentage of multiunits with non-monotonic responses (i.e., encoding the increasing intensity initially by increasing spike rate, and then decreasing spike rate as sound intensity is further increased) was doubled in the IC of *Neurod1*cKO (35%) compared with controls (16%; $p < 0.0001$; *Neurod1*cKO $n = 9$; 432 IC recording sites and control $n = 10$; 480 IC recording sites; Fig. 11*C*). Saturated rate intensity functions were present only in 7% of the measured IC multiunits in *Neurod1*cKO compared with 37% in the controls ($p < 0.0001$), whereas monotonic rate-intensity functions represented 55% of the recorded neuronal clusters in *Neurod1*cKO compared with 47% in the controls ($p = 0.0007$). As a result, the IC multiunits in *Neurod1*cKO had a narrower dynamic range (23.38 ± 0.31 dB vs control 24.23 ± 0.29 dB, $p < 0.05$) as well as significantly lower maximum response magnitudes (*Neurod1*cKO 16.96 ± 0.44 spikes/s; control 25.26 ± 0.51 spikes/s, $p < 0.0001$; Fig. 11*D*). Additionally, it was necessary to use significantly higher WN intensity in *Neurod1*cKO to reach the R10, representing 10% of the RIF response magnitude (53.8 ± 0.5 dB SPL; control 34.3 ± 0.4 dB SPL, $p < 0.0001$; Fig. 11*D*), as a consequence of a higher excitatory threshold. However, at this low suprathreshold noise level, *Neurod1*cKO IC units showed facilitated evoked activity (0.15 ± 0.0029 vs control 0.12 ± 0.00091, $p < 0.0001$). We also observed significantly higher spontaneous activity in the *Neurod1*cKO IC units than in controls (*Neurod1*cKO 6.21 ± 0.34 spikes/s; control 1.5 ± 0.11 spikes/s, $p < 0.0001$; Fig. 11*D*).

We performed acoustical stimulation of the IC units with two types of click trains, a long one with changing frequency of clicks in the train and a train of five clicks with different interclick intervals from 100 up to 5 ms. In *Neurod1*cKO, this revealed a significantly lower efficiency in recognizing individual clicks in the complex train (*Neurod1*cKO 23.96 ± 1.07%; control 49.86 ± 1.47%, $p < 0.0001$; Fig. 11*E*); and a lower degree of response synchronization with clicks in the train for the whole range of interclick intervals, suggesting a reduction in the precise response timing in the *Neurod1*cKO (Fig. 11*F*).

Auditory behavior of *Neurod1*cKO is altered

Previous work has demonstrated that even minor frequency presentation mistakes in the CN can lead to system effects, revealed by altered auditory behavior (Karmakar et al., 2017; Cruces-Solís et al., 2018). The thresholds and growth of the ASR were measured for tonal and WN startle stimuli in a continuous-noise and in a noiseless background. In mutants, ASR thresholds were significantly reduced for startle tone stimuli of 8 kHz (*Neurod1*cKO 72.14 ± 2.67 dB SPL; control 81.43 ± 3.78 dB SPL, $p < 0.001$; $n = 8$/group) and 16 kHz (*Neurod1*cKO 66.43 ± 6.27 dB SPL; control 83.57 ± 3.78 dB SPL, $p < 0.0001$), suggesting that instead of perceiving a pure tone, mutants perceive noise-like stimuli. This is further supported by the fact that the startle thresholds of mutants in response to pure tone stimulation were similar to those for WN (Fig. 12*A*). The differences in thresholds in response to WN between control and mutant mice were not significant. Consistent with the lower dynamic range, lower maximum response and higher percentage of non-monotonic responses of IC multiunits (Fig. 11*C*,*D*), we found that *Neurod1*cKO mice had a reduced amplitude of the startle response at higher intensities of noise startle stimuli (Fig. 12*B*). However, the 16 kHz stimulation resulted in significantly larger amplitudes of the response at low and middle intensities in mutants (Fig. 12*C*). To further assess complex auditory discrimination behavior in *Neurod1*cKO mutants, we subjected control and mutant adult mice to a PPI paradigm, which is an operational measure of sensory-motor gating. We used either WN or pure tone pips at increasing intensities as a non-startling acoustic stimulus (prepulse) that preceded the startle stimulus in a quiet background. PPI with WN as the prepulse resulted in mutants with a larger inhibition of the startle response than in controls (Fig. 12*D*). PPI growth functions demonstrated that the prepulse WN bursts can significantly modulate the startle response at sound pressures as low as 10 dB SPL in mutant mice, indicating heightened sensitivity of the central auditory system. Similarly, subsequent comparisons revealed that the PPI of *Neurod1*cKO for 16 kHz prepulses (a preserved audible frequency in the mutant IC) was enhanced starting at 40 dB SPL compared with control mice (Fig. 12*E*). Additionally, mutant mice showed higher sensitivity to increasing intensities of the continuous background WN than controls (Fig. 12*F*). Thus, *Neurod1*cKO displayed hyperacusis-like behavioral ASR and PPI responses parallel to animal models with noise-induced cochlear neuropathy, which is also associated with increased behavioral salience of still-audible sounds (Hickox and Liberman, 2014).

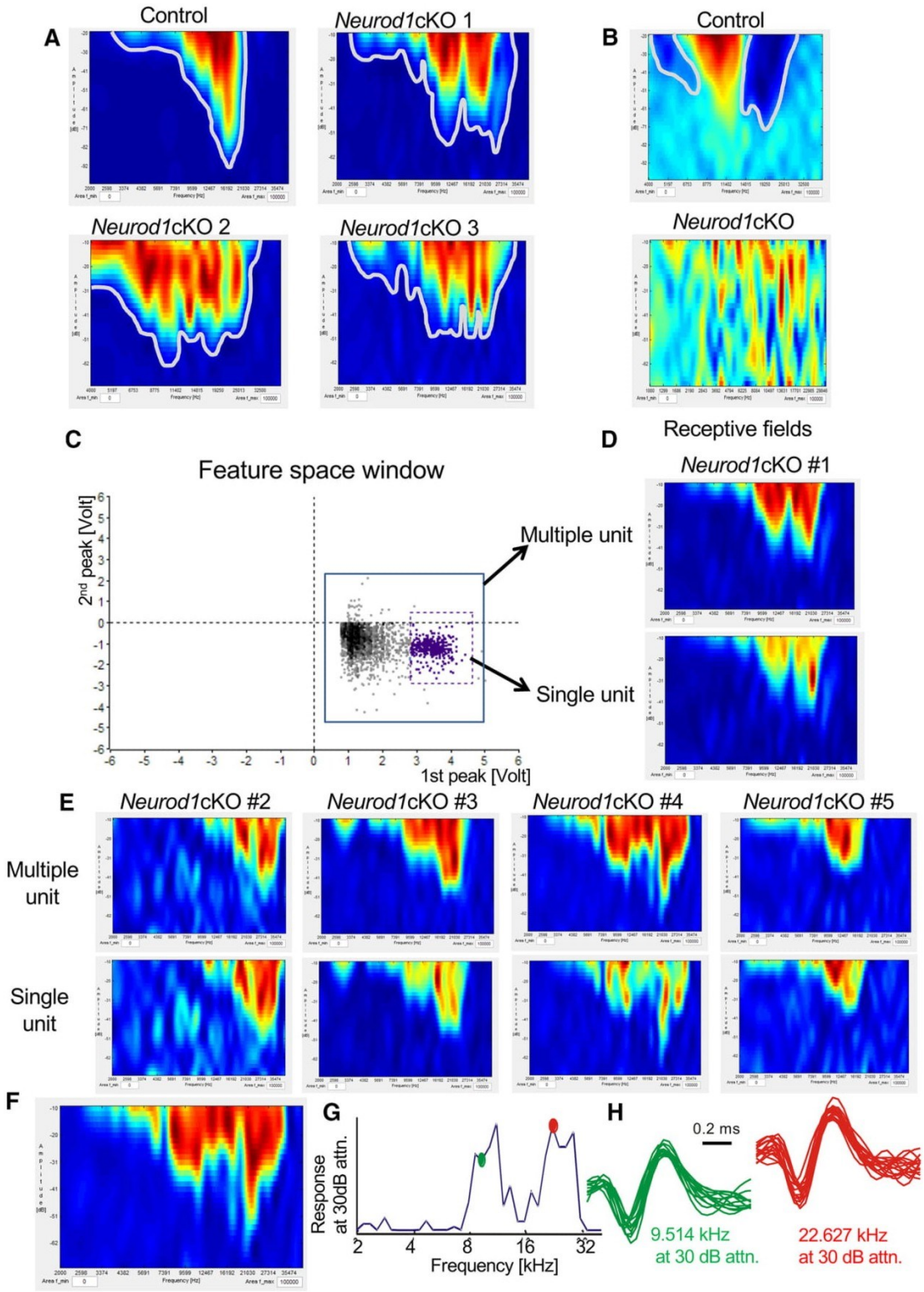

Figure 10. Deletion of *Neurod1* affects the IC tuning curves of multiple and isolated single units. ***A***, Representative examples of tuning curves recorded in the IC in control and *Neurod1*cKO mice. ***B***, Response map to two-tone stimulation (fixed tone of 13 kHz), shows low- and high-frequency sideband inhibitory areas in control (the areas are outlined by white lines) and small and disorganized inhibitory areas in *Neurod1*cKO mice. ***C***, Feature space window (in which each action potential is represented by a single point) with a delineated cluster of action potentials (purple dashed box) belonging to isolated single units recorded at the electrode channel. Action potentials corresponding to multiple unit activity are within the larger box (*Figure legend continues.*)

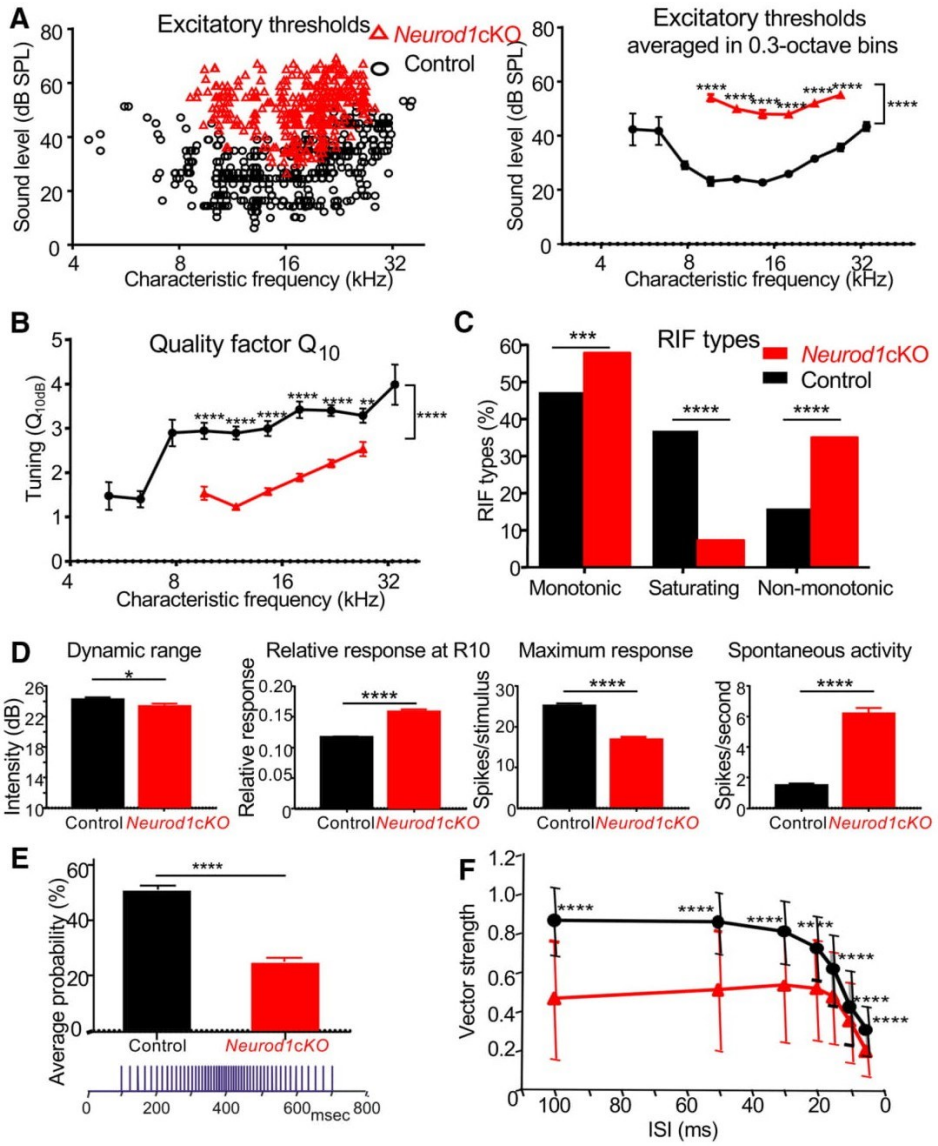

Figure 11. Characteristics of IC neurons are affected by acoustic information processing in the periphery. ***A***, The dependence of IC excitatory thresholds on the CF of neuronal clusters (multiunits) in control and *Neurod1*cKO mice. Excitatory thresholds are shown as individual units and as averages in 0.3 octave bins. Data are mean ± SEM. Two-way ANOVA with Bonferroni *post hoc* test. $^{****}p < 0.0001$. ***B***, Sharpness of the neuronal tuning expressed by quality factor Q_{10} (the ratio between the CF and bandwidth at 10 dB above the minimum threshold) averaged in 0.3 octave bins. Data are represented as the mean ± SEM; two-way ANOVA with Bonferroni *post hoc* test. $^{****}p < 0.0001$, $^{**}p < 0.01$. ***C***, Percentages of strictly monotonic, saturating and non-monotonic RIFs. Fisher's exact test. $^{***}p < 0.001$, $^{****}p < 0.0001$. ***D***, Comparison of the RIF parameters in control and *Neurod1*cKO mice: dynamic range, relative response at the RIFs point R10 (10% of the RIF response magnitude), maximum response magnitude and spontaneous activity. Data are the mean ± SD; unpaired *t* test. $^{*}p < 0.05$, $^{****}p < 0.0001$. For all extracellular recordings *Neurod1*cKO ($n = 9$; 432 units from the IC) and control mice ($n = 10$; 480 units) were used. ***E***, The average probability of a response to individual clicks in the series of clicks. Inset, Diagram of the clicks train, where the rate continuously speeds up and then slows down again (mean ± SEM; $n = 10$/control, $n = 9$/*Neurod1*cKO; $^{****}p < 0.0001$, unpaired *t* test). ***F***, Degree of synchronization for different interstimulus intervals (ISIs) expressed using the vector strength computed for responses to click trains with different interclick intervals (mean ± SD; $n = 10$/control, $n = 9$/*Neurod1*cKO; $^{****}p <$ 0.0001, two-way ANOVA with Bonferroni *post hoc* test).

←

(*Figure legend continued.*) (indicated by solid blue line). ***D***, ***E***, Examples of the tuning curves representing multiple unit activity and the activity of a single isolated unit from five different recordings in *Neurod1*cKO mice. ***F***, Tuning curve of a multiple unit in *Neurod1*cKO mice; for the same recording, frequency profile of the same response to tonal stimulation at different frequencies with bimodal frequency tuning (at 30 dB sound attenuation) is calculated from single-unit activity (***G***). ***H***, Action potential curves, recorded at two different points marked with the corresponding color in the frequency profile at (***E***), demonstrating very similar spike shapes and therefore classified as generated by the same neuron (single unit).

Neurod1 deletion results in aberrant vestibular function

Finally, we investigated the possibility of interference of vestibular function of *Neurod1*cKO with auditory stimuli. This would be expected given the distribution of SG neurons in the aberrant SVG, shared central projections after labeling vestibular and cochlear afferents, and labeled neurons in the SG by dye injected into vestibular organs (Figs. 4, 6, 8). Thus, these results demonstrate interconnections of afferents between cochlear and vestib-

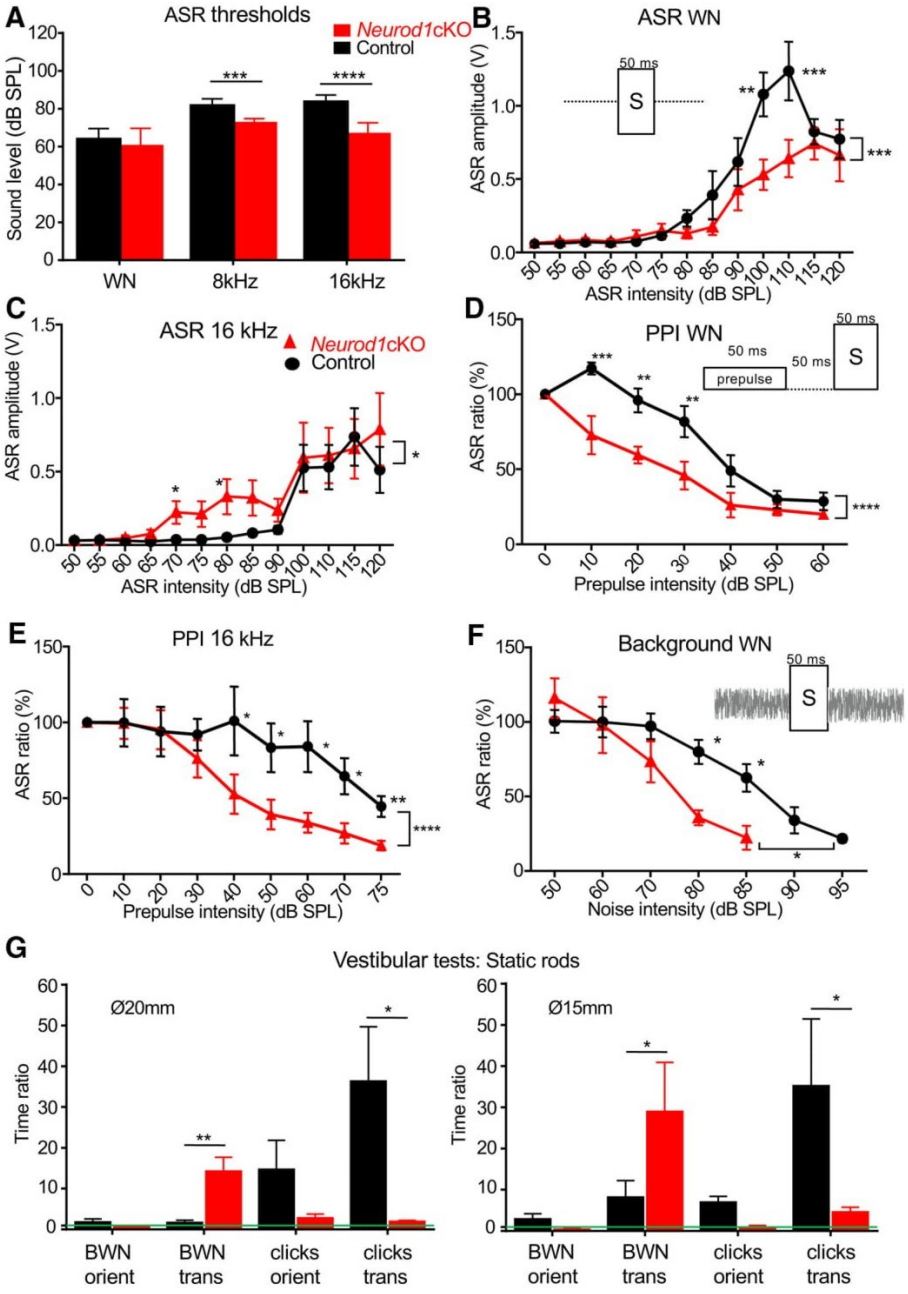

Figure 12. ASR and PPI responses are altered in *Neurod1*cKO. ***A***, Thresholds of ASRs for WN, and tone pips at 8 and 16 kHz in control and *Neurod1*cKO mice. Data are the mean ± SEM, $n = 8$/group. Statistical significance determined by the Holm–Sidak method, *t* test. $^{*}p < 0.05$, $^{**}p < 0.01$, $^{***}p < 0.001$. Amplitude-intensity ASR functions for WN (***B***), and for tone pips of 16 kHz (***C***) in control and *Neurod1*cKO mice. Data are the mean ± SEM, $n = 8$/group. ***D***, Efficacy of the WN and (***E***) 16 kHz tone prepulse intensity on the relative ASR amplitude; 100% corresponds to the ASR amplitude without a prepulse (uninhibited ASR). Data are the mean ± SEM, $n = 8$/group. ***F***, Impact of a continuous background WN with increasing intensity on the relative ASR amplitude; 100% corresponds to the amplitude of uninhibited ASR (response in silence). Data are the mean ± SEM, $n = 8$/group. Two-way ANOVA with Bonferroni *post hoc* tests for ***B–F***. $^{*}p < 0.05$, $^{**}p < 0.01$, $^{***}p < 0.001$, $^{****}p < 0.0001$. ***G***, Ratio of the orientation (orient) and transition (trans) time in the presence of background WN (BWN) or series of clicks to the time in silence on rods of 20 or 15 mm diameters. The green line depicts the point when the ratio is 1 (no change in measured times with/without sound). Data are the mean ± SEM (control, $n = 4$; *Neurod1*cKO, $n = 3$). Statistical significance determined using two-way ANOVA with Sidak's multiple-comparison test. $^{*}p < 0.05$, $^{**}p < 0.01$.

ular sensory epithelia previously only shown in certain neurotrophin mutants (Tessarollo et al., 2004) and *Foxg1* mutant mice (Pauley et al., 2006). We tested whether the motor coordination of *Neurod1*cKO can be affected by acoustic stimulation. We conducted two different experiments, one with continuous WN at an 80 dB SPL intensity, and another with a 600 ms series of clicks with a changing frequency of spike occurrence at an intensity of 70 dB SPL. We measured turning time (time taken to perform an 180° turn from the starting position) and transition time on static rods of two different diameters. WN had a negative

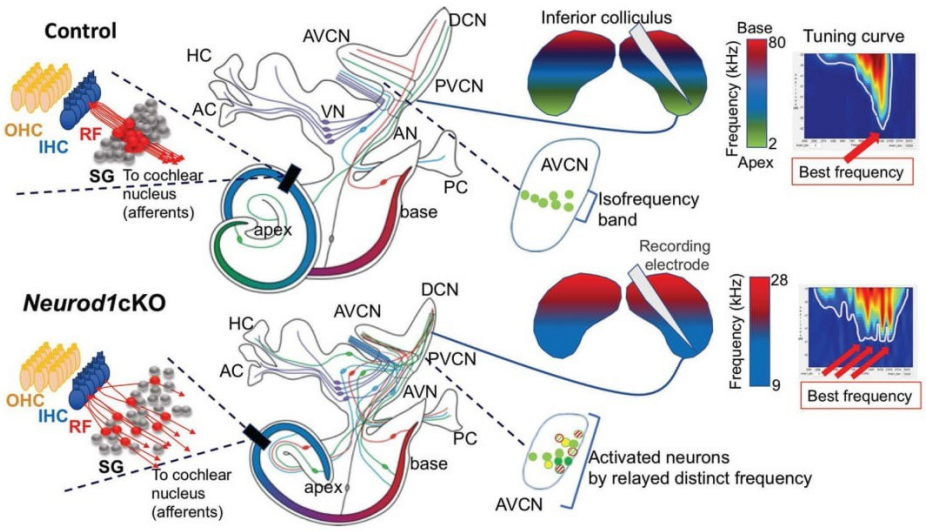

Figure 13. Model of tonotopic phenotype in *Neurod1*cKO. In control mice, spiral ganglion afferent neurons (SGN) are radially connected with a single ending to IHCs (10–20 neurons/1 IHC). IHCs at different parts of the cochlea are stimulated by different frequencies, forming a tonotopic map with high frequencies at the base and low frequencies at the apex. The auditory system is tonotopically organized at all levels including the auditory nerve. The CN is the first target of the auditory nerve. SGN axons project centrally into the AVCN, relaying distinct frequencies within their corresponding isofrequency band. The IC is a major center for the integration of auditory sensory information from ascending pathways, including the pathway from the CN. The tuning curve of each IC unit represents a combination of the frequency and amplitude that evokes a response. At one frequency, the best frequency, sensitivity is highest. In *Neurod1*cKO mutants, the SG is disorganized, with aberrant innervation and a reduced number of neurons, many of which are displaced in the spiro-vestibular ganglion. There is little cochleotopic organization of afferents to the organ of Corti, within the auditory nerve and in the CN. SG afferents relaying specific frequencies target more AVCN cells outside the isofrequency band. Characteristics of IC neurons are altered with an enlarged frequency range and higher excitatory thresholds. The tuning characteristics of IC neurons are broad with multiple peaks of "best frequency". AC, Anterior crista; AN, auditory nerve; HC, horizontal crista; PC, posterior crista; RF, radial fibers; VG, vestibular ganglion; VN, vestibular nerve.

effect on the transition time of *Neurod1*cKO mice on both rods (Fig. 12*G*). However, the train of clicks with changing frequency of occurrence had a lower impact on the mutant mice than on the controls. These results demonstrate that *Neurod1* deletion affected the processing of vestibular information during sound exposure. Although we cannot exclude the possibility that the altered motor behavior of *Neurod1*cKO mutants was the result of their increased sound sensitivity to WN exposure, our data indicate that the vestibular and auditory systems may be functionally interconnected. The possibility of an interconnection is supported by the observed shared central projections and distribution of SG neurons in the vestibular ganglion and their projection to both the cochlea and vestibular organs.

Discussion

The formation of a neural map of the sensory periphery is an essential feature of all sensory systems. Understanding the mechanisms of formation, plasticity, and wiring of the sensory maps in both neonatal and adult states is a major endeavor in neuroscience. Sensory maps of the retina, somatosensory space, and cochlea show plastic reorganization of central map properties as a result of loss or modifications of specific features, for example filling in lost fingers or expanding size of somatosensory maps according to their use (Buonomano and Merzenich, 1998; Zhou and Merzenich, 2008), filling in lost areas of the retina (Baker et al., 2005; Keck et al., 2008), and even providing some hearing after destruction of SG neurons (Chambers et al., 2016; Wang, 2016). In contrast to all these data on ontogenetic and adult map effects, for the first time we succeeded to eliminate auditory primary map formation during development altogether. We genetically engineered a new mouse model lacking cochleotopic projections to the CN and tonotopic segregation in the ear. Using this new model, we have explored the ability of second-order neurons projecting from the CN to the IC to self-organize a secondary frequency map in the absence of a refined cochleotopic map. To the best of our knowledge, this is the first time that a single gene mutation results in physiologically uncorrectable primary map mistakes of both the peripheral and central innervation.

We show that genetically induced abnormal inner ear development results in a shorter cochlea, miswired and displaced SG neurons, and reduced spatially unsegregated central axons of SG neurons. The SG-to-CN afferent projections are represented by widely ramifying fibers that mostly reach the ventral part of the CN (Fig. 8). The tonotopic order of SG projections to all three CN subdivisions and their precise parallel fiber organization into isofrequency bands are largely absent in *Neurod1*cKO. The processing of the limited frequency range of the periphery and CN is expanded across the entire IC (Fig. 13, schematic). These alterations of cochlear mapping onto the CN and CN onto the IC result in altered tuning characteristics of IC neurons in *Neurod1*cKO mutants, including an enlarged frequency range, higher excitatory thresholds, and worsened tuning capabilities. In association with the broad and multipeaked tuning curves of IC units, lower thresholds of startle responses to pure tones in mutants were measured, suggesting that mutants apparently perceive noise-like stimuli rather than pure tones. Modifications in intensity coding in the IC of *Neurod1*cKO mutants indicate a central reorganization of the tuning properties of the auditory system with changes in the balance of inhibition and excitation as a response to the peripheral auditory deficiency. Furthermore, increased spontaneous activity of IC units in *Neurod1*cKO suggests hypersensitivity to sound in the central auditory pathways. Thus, our data provide evidence that a disorganized primary tonotopic auditory map leads to higher-order tono-

topic information processing problems in the IC that are not self-correcting as seems to be the case for simple intensity distortions (Pelgrim et al., 2018).

Central reorganization of the auditory system has been previously demonstrated in studies using noise exposure or other cochlear damage protocols (Kandler et al., 2009; Harrison, 2016). However, unique to our study are the consequences of simultaneously disorganizing and compressing the primary sensory projection map onto the precise tonotopic organization of the central auditory pathways. Our data are in line with recent evidence from the CN and primary sound localization circuits that precise tonotopy depends on refinement at the subcellular and circuit level (summarized by Kandler et al., 2009; Clause et al., 2014). The smaller size of the CN and reduced cochlear nuclear circuits have been reported in genetically produced mutations, blocking synaptic transmission from hair cells and/or activation of SG neurons, and in cochlear ablation studies (Rubel and Fritzsch, 2002; Seal et al., 2008; Tritsch and Bergles, 2010; Tritsch et al., 2010); however, although reduced, the cochlear nuclear circuits that are established in these animals maintain their normal topographic organization patterns (Cao et al., 2008; Wright et al., 2014). This indicates that the reduction in the size of the CN of our *Neurod1*cKO mutant might only have a minimal contribution to the observed differences in the topographic disorganization of the CN and the responses of IC neurons, including wide and multipeaked tuning curves. Minor distortions of neuroanatomical mapping to the CN have been reported before, such as distortions in the patterning of the SG axons (Yang et al., 2017), and distortions of cochleotopic projections in *Npr2* mutants (Lu et al., 2014). Analysis of *Hoxa2* mutants imply that even relatively minor alterations in isofrequency mapping have behavioral consequences (Karmakar et al., 2017). Compared with these minor changes of topological projections, our profoundly disorganized and truncated cochleotopic mapping implies that NEUROD1 may specify some navigational cues in SG neurons that read diffusible gradients mediated by specific Wnt signals in the dorsal hindbrain (Yang et al., 2017), substrate cues (Gu et al., 2003; Lu et al., 2014), and physiological activity (Kandler et al., 2009; Marrs and Spirou, 2012; Elliott et al., 2015) to establish the cochleotopic map onto the CN. NEUROD1 variably regulates, directly or indirectly, ~3000 genes, including nearly all frizzled class receptor (*Fzd*) genes (Pataskar et al., 2016) relevant for Wnt signaling (Dijksterhuis et al., 2014). Without NEUROD1, spiral ganglia afferent fibers will experience expression changes in many genes possibly involved in neurite guidance. For example, alterations in local Fzd receptors could provide further mechanistic insights into the distorted mapping of *Neurod1*cKO SG neurons. In addition, bHLH proteins interact with Gata zinc-finger proteins (Rawnsley et al., 2013). There is an interesting resemblance of phenotypes between a delayed *Gata3* conditional KO (Duncan and Fritzsch, 2013) and our *Neurod1*cKO mutant. Both mutants have decreased number and misplaced SG neurons, and display incorrect patterning within the CN. However, the blurring of the boundaries between spiral and vestibular ganglion neurons with SVG formation and multiple branches within the inner ear represents a unique feature of our *Neurod1*cKO mutant. Although some afferents can still reach the CN, their inability to navigate properly results in reduced and disorganized coverage of the CN in the *Neurod1*cKO mutant. In particular, the well known regulation of neurotrophin receptors *Ntrk2* (TrkB) and *Ntrk3* (TrkC) by NEUROD1 (Kim et al., 2001) may regulate the branching of afferents previously described using neurotrophin and neurotrophin receptor deletions (Fariñas et al., 2001; Fritzsch et al., 2016b), and misexpression (Tessarollo et al., 2004; Yang et al., 2011). *Neurod1* mutation might also affect the central projections, as previously described in *Neurotrophin3* mutants, which use BDNF/Ntrk2 signaling to expand into the CN after a partial loss of basal turn SG neurons (Fritzsch et al., 1997). The expanded branching of afferents along the cochlea in our mutant, with basal turn SG neurons projecting to the apex (and vice versa; Fig. 6), generates broad mapping of large areas of the cochlea to only parts of the ventral CN (Fig. 13, summary) instead of a point to point connection as in control animals (Muniak et al., 2016).

The connectional reasons for the occurrence of the unusual multipeak broad tuning curves in the IC of our *Neurod1*cKO mutants are yet to be specified. Nevertheless, our data show that the peripheral deficit in sound encoding cannot be compensated up to the level of the IC. The tuning curves of single units in the IC of control mice have a characteristic V-shape with one peak and thus one best frequency. In the *Neurod1*cKO, there are either two-peak or multipeak tuning curves, suggesting multiple frequency inputs. Where this integration of inputs occurs must be shown in further experiments. Clearly, at the level of the cochlea, neurons of the SG are connected to more than one IHC as revealed by our dye tracing data, which show that single SG neurons reach multiple areas of the organ of Corti, for example a given neuron can reach both the base and apex (Fig. 6). This would explain the multipeaked tuning curves in the IC. However, we also cannot exclude more SG neurons with different frequency tuning being connected to several CN neurons as afferents are not segregated into isofrequency bands in the CN (Fig. 8).

In conclusion, our data demonstrate that the physiological tonotopic properties of the *Neurod1*cKO auditory system are changed at all levels investigated. It remains unclear how exactly the frequency presentation distortion of the cochlea onto the cochlear nuclei relates to these property changes and other well known plastic changes in the cortical auditory system (Harrison, 2016). Our behavioral data show that the startle response is affected and that the cross-innervation of vestibular end-organs affects complex vestibular functions after sound disturbance. Future work is needed to establish how tonotopic distortions affect space map formation (Syka, 2002; Eggermont, 2017) and cortical information processing (Kral et al., 2016) that could benefit cochlear implant treatment (Harrison, 2016). Using ouabain in our mouse model should allow to demonstrate that the reported recovery after afferent ablation (Chambers et al., 2016) relies on a developmental stabilization of tonotopic map features which we have disrupted here.

References

Baker CI, Peli E, Knouf N, Kanwisher NG (2005) Reorganization of visual processing in macular degeneration. J Neurosci 25:614–618. CrossRef Medline

Bohuslavova R, Dodd N, Macova I, Chumak T, Horak M, Syka J, Fritzsch B, Pavlinkova G (2017) Pax2-Islet1 transgenic mice are hyperactive and have altered cerebellar foliation. Mol Neurobiol 54:1352–1368. CrossRef Medline

Buonomano DV, Merzenich MM (1998) Cortical plasticity: from synapses to maps. Annu Rev Neurosci 21:149–186. CrossRef Medline

Buran BN, Strenzke N, Neef A, Gundelfinger ED, Moser T, Liberman MC (2010) Onset coding is degraded in auditory nerve fibers from mutant mice lacking synaptic ribbons. J Neurosci 30:7587–7597. CrossRef Medline

Bures Z, Grécová J, Popelár J, Syka J (2010) Noise exposure during early development impairs the processing of sound intensity in adult rats. Eur J Neurosci 32:155–164. CrossRef Medline

Cao XJ, McGinley MJ, Oertel D (2008) Connections and synaptic function in the posteroventral cochlear nucleus of deaf jerker mice. J Comp Neurol 510:297–308. CrossRef Medline

Chagnaud BP, Engelmann J, Fritzsch B, Glover JC, Straka H (2017) Sensing external and self-motion with hair cells, a comparison of the lateral line and vestibular systems from a developmental and evolutionary perspective. Brain Behav Evol 90:98–116. CrossRef Medline

Chambers AR, Resnik J, Yuan Y, Whitton JP, Edge AS, Liberman MC, Polley DB (2016) Central gain restores auditory processing following near-complete cochlear denervation. Neuron 89:867–879. CrossRef Medline

Chumak T, Bohuslavova R, Macova I, Dodd N, Buckiova D, Fritzsch B, Syka J, Pavlinkova G (2016) Deterioration of the medial olivocochlear efferent system accelerates age-related hearing loss in Pax2-Isl1 transgenic mice. Mol Neurobiol 53:2368–2383. CrossRef Medline

Clause A, Kim G, Sonntag M, Weisz CJ, Vetter DE, Rűbsamen R, Kandler K (2014) The precise temporal pattern of prehearing spontaneous activity is necessary for tonotopic map refinement. Neuron 82:822–835. CrossRef Medline

Constantine-Paton M, Law MI (1978) Eye-specific termination bands in tecta of three-eyed frogs. Science 202:639–641. CrossRef Medline

Cramer KS, Gabriele ML (2014) Axon guidance in the auditory system: multiple functions of Eph receptors. Neuroscience 277:152–162. CrossRef Medline

Cruces-Solís H, Jing Z, Babaev O, Rubin J, Gür B, Krueger-Burg D, Strenzke N, de Hoz L (2018) Auditory midbrain coding of statistical learning that results from discontinuous sensory stimulation. PLoS Biol 16:e2005114. CrossRef Medline

Deacon R (2013) Measuring motor coordination in mice. J Vis Exp 75: e2609. CrossRef Medline

Dijksterhuis JP, Petersen J, Schulte G (2014) WNT/Frizzled signalling: receptor–ligand selectivity with focus on FZD-G protein signalling and its physiological relevance: IUPHAR review 3. Br J Pharmacol 171:1195–1209. CrossRef Medline

Duncan JS, Fritzsch B (2013) Continued expression of GATA3 is necessary for cochlear neurosensory development. PLoS One 8:e62046. CrossRef Medline

Dvorakova M, Jahan I, Macova I, Chumak T, Bohuslavova R, Syka J, Fritzsch B, Pavlinkova G (2016) Incomplete and delayed Sox2 deletion defines residual ear neurosensory development and maintenance. Sci Rep 6:38253. CrossRef Medline

Eggermont JJ (2017) Acquired hearing loss and brain plasticity. Hear Res 343:176–190. CrossRef Medline

Elliott KL, Houston DW, Fritzsch B (2015) Sensory afferent segregation in three-eared frogs resemble the dominance columns observed in three-eyed frogs. Sci Rep 5:8338. CrossRef Medline

Fariñas I, Jones KR, Tessarollo L, Vigers AJ, Huang E, Kirstein M, de Caprona DC, Coppola V, Backus C, Reichardt LF, Fritzsch B (2001) Spatial shaping of cochlear innervation by temporally regulated neurotrophin expression. J Neurosci 21:6170–6180. CrossRef Medline

Fritzsch B, Elliott KL (2017) Evolution and development of the inner ear efferent system: transforming a motor neuron population to connect to the most unusual motor protein via ancient nicotinic receptors. Front Cell Neurosci 11:114. CrossRef Medline

Fritzsch B, Fariñas I, Reichardt LF (1997) Lack of neurotrophin 3 causes losses of both classes of spiral ganglion neurons in the cochlea in a region-specific fashion. J Neurosci 17:6213–6225. CrossRef Medline

Fritzsch B, Pauley S, Feng F, Matei V, Nichols DH (2006) The molecular and developmental basis of the evolution of the vertebrate auditory system. Int J Comp Psychol 19:1–25.

Fritzsch B, Dillard M, Lavado A, Harvey NL, Jahan I (2010) Canal cristae growth and fiber extension to the outer hair cells of the mouse ear require Prox1 activity. PloS One 5:e9377. CrossRef Medline

Fritzsch B, Duncan JS, Kersigo J, Gray B, Elliott KL (2016a) Neuroanatomical tracing techniques in the ear: history, state of the art, and future developments. In: Auditory and vestibular research: methods and protocols (Sokolowski B, ed), pp. 243–262. New York: Springer.

Fritzsch B, Kersigo J, Yang T, Jahan I, Pan N (2016b) Neurotrophic factor function during ear development: expression changes define critical phases for neuronal viability. In: The primary auditory neurons of the mammalian cochlea, pp. 49–84. New York: Springer.

Goebbels S, Bode U, Pieper A, Funfschilling U, Schwab MH, Nave KA (2005) Cre/loxP-mediated inactivation of the bHLH transcription factor gene NeuroD/BETA2. Genesis 42:247–252. CrossRef Medline

Gogos JA, Osborne J, Nemes A, Mendelsohn M, Axel R (2000) Genetic ablation and restoration of the olfactory topographic map. Cell 103:609–620. CrossRef Medline

Goodhill GJ (2007) Contributions of theoretical modeling to the understanding of neural map development. Neuron 56:301–311. CrossRef Medline

Goodrich LV (2016) Early development of the spiral ganglion. In: The primary auditory neurons of the mammalian cochlea, pp. 11–48. New York: Springer.

Gu C, Rodriguez ER, Reimert DV, Shu T, Fritzsch B, Richards LJ, Kolodkin AL, Ginty DD (2003) Neuropilin-1 conveys semaphorin and VEGF signaling during neural and cardiovascular development. Dev Cell 5:45–57. CrossRef Medline

Gurung B, Fritzsch B (2004) Time course of embryonic midbrain and thalamic auditory connection development in mice as revealed by carbocyanine dye tracing. J Comp Neurol 479:309–327. CrossRef Medline

Harrison RV (2016) Biologic development of the auditory system from periphery to cortex. In: Comprehensive handbook of pediatric audiology, p. 23. San Diego: Plural.

Hickox AE, Liberman MC (2014) Is noise-induced cochlear neuropathy key to the generation of hyperacusis or tinnitus? J Neurophysiol 111:552–564. CrossRef Medline

Hubel DH, Wiesel TN, LeVay S (1977) Plasticity of ocular dominance columns in monkey striate cortex. Philos Trans R Soc Lond B Biol Sci 278: 377–409. CrossRef Medline

Huberman AD, Feller MB, Chapman B (2008) Mechanisms underlying development of visual maps and receptive fields. Annu Rev Neurosci 31: 479–509. CrossRef Medline

Jahan I, Kersigo J, Pan N, Fritzsch B (2010a) Neurod1 regulates survival and formation of connections in mouse ear and brain. Cell Tissue Res 341:95–110. CrossRef Medline

Jahan I, Pan N, Kersigo J, Fritzsch B (2010b) Neurod1 suppresses hair cell differentiation in ear ganglia and regulates hair cell subtype development in the cochlea. PLoS One 5:e11661. CrossRef Medline

Kandler K, Clause A, Noh J (2009) Tonotopic reorganization of developing auditory brainstem circuits. Nat Neurosci 12:711–717. CrossRef Medline

Karmakar K, Narita Y, Fadok J, Ducret S, Loche A, Kitazawa T, Genoud C, Di Meglio T, Thierry R, Bacelo J, Lüthi A, Rijli FM (2017) Hox2 genes are required for tonotopic map precision and sound discrimination in the mouse auditory brainstem. Cell Rep 18:185–197. CrossRef Medline

Keck T, Mrsic-Flogel TD, Vaz Afonso M, Eysel UT, Bonhoeffer T, Hübener M (2008) Massive restructuring of neuronal circuits during functional reorganization of adult visual cortex. Nat Neurosci 11:1162–1167. CrossRef Medline

Kim WY, Fritzsch B, Serls A, Bakel LA, Huang EJ, Reichardt LF, Barth DS, Lee JE (2001) NeuroD-null mice are deaf due to a severe loss of the inner ear sensory neurons during development. Development 128:417–426. Medline

Krahe R, Maler L (2014) Neural maps in the electrosensory system of weakly electric fish. Curr Opin Neurobiol 24:13–21. CrossRef Medline

Kral A, Kronenberger WG, Pisoni DB, O'Donoghue GM (2016) Neurocognitive factors in sensory restoration of early deafness: a connectome model. Lancet Neurol 15:610–621. CrossRef Medline

Liu M, Pereira FA, Price SD, Chu MJ, Shope C, Himes D, Eatock RA, Brownell WE, Lysakowski A, Tsai MJ (2000) Essential role of BETA2/NeuroD1 in development of the vestibular and auditory systems. Genes Dev 14:2839–2854. CrossRef Medline

Lu CC, Cao XJ, Wright S, Ma L, Oertel D, Goodrich LV (2014) Mutation of Npr2 leads to blurred tonotopic organization of central auditory circuits in mice. PLoS Genetics 10:e1004823. CrossRef Medline

Mao Y, Reiprich S, Wegner M, Fritzsch B (2014) Targeted deletion of Sox10 by Wnt1-cre defects neuronal migration and projection in the mouse inner ear. PloS One 9:e94580. CrossRef Medline

Marrs GS, Spirou GA (2012) Embryonic assembly of auditory circuits: spiral ganglion and brainstem. J Physiol 590:2391–2408. CrossRef Medline

Martin MR, Rickets C (1981) Histogenesis of the cochlear nucleus of the mouse. J Comp Neurol 197:169–184. CrossRef Medline

Mombaerts P (1999) Molecular biology of odorant receptors in vertebrates. Annu Rev Neurosci 22:487–509. CrossRef Medline

Müller M, von Hünerbein K, Hoidis S, Smolders JW (2005) A physiological place–frequency map of the cochlea in the CBA/J mouse. Hear Res 202: 63–73. CrossRef Medline

Muniak MA, Rivas A, Montey KL, May BJ, Francis HW, Ryugo DK (2013)

3D model of frequency representation in the cochlear nucleus of the CBA/J mouse. J Comp Neurol 521:1510–1532. CrossRef Medline

Muniak MA, Connelly CJ, Suthakar K, Milinkeviciute G, Ayeni FE, Ryugo DK (2016) Central projections of spiral ganglion neurons. In: The primary auditory neurons of the mammalian cochlea, pp. 157–190. New York: Springer.

Pataskar A, Jung J, Smialowski P, Noack F, Calegari F, Straub T, Tiwari VK (2016) NeuroD1 reprograms chromatin and transcription factor landscapes to induce the neuronal program. EMBO J 35:24–45. CrossRef Medline

Pauley S, Lai E, Fritzsch B (2006) Foxg1 is required for morphogenesis and histogenesis of the mammalian inner ear. Dev Dyn 235:2470–2482. CrossRef Medline

Pelgrim M, Yamanbaeva G, Reisinger E, Strenzke N (2018) Sound encoding in the inferior colliculus of otoferlin Ile515Thr mutant mice. Laryngorhinootologie 97:S230–S231. CrossRef

Penfield W, Boldrey E (1937) Somatic motor and sensory representation in the cerebral cortex of man as studied by electrical stimulation. Brain 60:389–443. CrossRef

Rawnsley DR, Xiao J, Lee JS, Liu X, Mericko-Ishizuka P, Kumar V, He J, Basu A, Lu M, Lynn FC, Pack M, Gasa R, Kahn ML (2013) The transcription factor atonal homolog 8 regulates Gata4 and Friend of Gata-2 during vertebrate development. J Biol Chem 288:24429–24440. CrossRef Medline

Renier N, Dominici C, Erzurumlu RS, Kratochwil CF, Rijli FM, Gaspar P, Chédotal A (2017) A mutant with bilateral whisker to barrel inputs unveils somatosensory mapping rules in the cerebral cortex. eLife 6:e23494. CrossRef Medline

Rubel EW, Fritzsch B (2002) Auditory system development: primary auditory neurons and their targets. Annu Rev Neurosci 25:51–101. CrossRef Medline

Seal RP, Akil O, Yi E, Weber CM, Grant L, Yoo J, Clause A, Kandler K, Noebels JL, Glowatzki E, Lustig LR, Edwards RH (2008) Sensorineural deafness and seizures in mice lacking vesicular glutamate transporter 3. Neuron 57:263–275. CrossRef Medline

Sienknecht UJ, Köppl C, Fritzsch B (2014) Evolution and development of hair cell polarity and efferent function in the inner ear. Brain Behav Evol 83:150–161. CrossRef Medline

Simmons D, Duncan J, de Caprona DC, Fritzsch B (2011) Development of the inner ear efferent system. In: Auditory and vestibular efferents, pp. 187–216. New York: Springer.

Sperry RW (1963) Chemoaffinity in the orderly growth of nerve fiber patterns and connections. Proc Natl Acad Sci U S A 50:703–710. CrossRef Medline

Syka J (2002) Plastic changes in the central auditory system after hearing loss, restoration of function, and during learning. Physiol Rev 82:601–636. CrossRef Medline

Tessarollo L, Coppola V, Fritzsch B (2004) NT-3 replacement with brain-derived neurotrophic factor redirects vestibular nerve fibers to the cochlea. J Neurosci 24:2575–2584. CrossRef Medline

Tomková M, Tomek J, Novák O, Zelenka O, Syka J, Brom C (2015) Formation and disruption of tonotopy in a large-scale model of the auditory cortex. J Comput Neurosci 39:131–153. CrossRef Medline

Tritsch NX, Bergles DE (2010) Developmental regulation of spontaneous activity in the mammalian cochlea. J Neurosci 30:1539–1550. CrossRef Medline

Tritsch NX, Rodríguez-Contreras A, Crins TT, Wang HC, Borst JG, Bergles DE (2010) Calcium action potentials in hair cells pattern auditory neuron activity before hearing onset. Nat Neurosci 13:1050–1052. CrossRef Medline

Wang X (2016) The yin and yang of auditory nerve damage. Neuron 89:680–682. CrossRef Medline

Wright S, Hwang Y, Oertel D (2014) Synaptic transmission between end bulbs of held and bushy cells in the cochlear nucleus of mice with a mutation in otoferlin. J Neurophysiol 112:3173–3188. CrossRef Medline

Yang T, Kersigo J, Jahan I, Pan N, Fritzsch B (2011) The molecular basis of making spiral ganglion neurons and connecting them to hair cells of the organ of corti. Hear Res 278:21–33. CrossRef Medline

Yang T, Kersigo J, Wu S, Fritzsch B, Bassuk AG (2017) Prickle1 regulates neurite outgrowth of apical spiral ganglion neurons but not hair cell polarity in the murine cochlea. PloS One 12:e0183773. CrossRef Medline

Zhou X, Merzenich MM (2008) Enduring effects of early structured noise exposure on temporal modulation in the primary auditory cortex. Proc Natl Acad Sci U S A 105:4423–4428. CrossRef Medline

6 Diskuze

Tato práce analyzuje role transkripčních faktorů ISL1, SOX2 a NEUROD1 ve vývoji vnitřního ucha pomocí tří různých myších modelů – [Tg(*Pax2-Isl1*)], *Sox2CKO* a *Neurod1CKO*. Pro zkoumání funkcí transkripčních faktorů SOX2 a NEUROD1 ve vývoji vnitřního ucha jsme pro jejich tkáňově specifickou deleci použili *Isl1-Cre*. Isl1-Cre zprostředkovala účinnou rekombinaci v progenitorech senzorického epitelu i v delaminujících senzorických neuronech vnitřního ucha, ale zároveň nebyla exprimována v částech centrální sluchové dráhy včetně kochleárního jádra a *colliculus inferior*. Pomocí imunohistologického barvení bylo potvrzeno, že se exprese Cre rekombinázy shoduje s expresí ISL1. Tento výsledek potvrzuje předchozí publikované poznatky (Radde-Gallwitz, Pan *et al.* 2004, Huang, Sage *et al.* 2008).

6.1 Transgenní exprese ISL1 narušila funkci vnějších vláskových buněk Cortiho orgánu.

Pro studium funkce ISL1 ve sluchově rovnovážném ústrojí byl vytvořen nový myší model [Tg(*Pax2-Isl1*)] s transgenní expresí ISL1 řízenou regulační sekvencí pro gen *Pax2*. Tato regulační sekvence byla vybrána z důvodu velmi rané aktivity ve vnitřním uchu. Exprese PAX2 je u myšího embrya detekována již ve věku E8 ve ventrální části otocysty a později v diferencujících se vláskových buňkách všech senzorických orgánů vnitřního ucha (Lawoko-Kerali, Rivolta *et al.* 2002). Spolu s PAX8 je PAX2 nezbytný pro morfologii vnitřního ucha a specifikaci neurosenzorických buněk (Burton, Cole *et al.* 2004, Bouchard, de Caprona *et al.* 2010). Embryonální ektopická exprese ISL1 u [Tg(*Pax2-Isl1*)] ve vnitřním uchu měla za následek zvětšené kochleovestibulární ganglium v E10,5 a růst delších více větvených nervových vláken v E12,5. Tato urychlená diferenciace aferentních nervových vláken v periferní i centrální části sluchově rovnovážné soustavy nekorespondovala se žádnými změnami aferentní inervace u dospělých jedinců [Tg(*Pax2-Isl1*)]. Transgenní exprese ISL1 překvapivě negativně ovlivnila otoakustické emise (DPOAE) u stárnoucích mutantů. DPOAE byly u myší [Tg(*Pax2-Isl1*)] signifikantně snížené v celém rozsahu měřených frekvencí již u nejmladší skupiny (1-5 měsíců) a u starších jedinců (6-9 a 10-15 měsíců) emise nebyly vůbec detekovány. Se změnami otoakustických emisí také korelovaly prahy sluchových kmenových potenciálů (ABR), které se zvyšovaly u nejmladších jedinců [Tg(*Pax2-Isl1*)] nejprve pouze v oblasti vysokých frekvencí odpovídající bázi kochley a se zvyšujícím se věkem byly prahy zvýšené po celé délce kochley. Snížení otoakustických emisí často poukazuje na ztrátu vnějších

vláskových buněk nebo jejich nefunkčnost (Wu, Gao *et al.* 2004). Jednou z možných příčin ztráty funkce vnějších vláskových buněk je ztráta exprese proteinu prestinu, který je exprimovaný v laterální stěně maturovaných vnějších vláskových buněk a je zodpovědný za jejich smršťování a natahování při akustické stimulaci (Belyantseva, Adler *et al.* 2000, Liberman, Gao *et al.* 2002). Imunohistochemické barvení a analýzy kvantitativní PCR ukázaly, že u mutantů [Tg(*Pax2-Isl1*)] v porovnání s kontrolami nedocházelo ani k významné ztrátě vláskových buněk ani ke změnám exprese prestinu. Dalším možným důvodem zhoršené funkce vnějších vlaskových buněk mohou být změny v inervaci. Vnější vláskové buňky jsou inervovány aferentními spirálními neurony II. typu, které podle nejnovějších výsledků hrají roli v protekci senzorických buněk před nadměrným hlukem (Liu, Glowatzki *et al.* 2015). Synapse mezi vnějšími vláskovými buňkami a neurony II. typu jsou zpětně kontrolovány eferentními vlákny z mediální olivy superior v mozkovém kmeni (Fuchs a Lauer 2018). Mezi hlavní funkce eferentní inervace vnějších vláskových buněk patří přesná lokalizace zvuku (Andeol, Guillaume *et al.* 2011, Irving, Moore *et al.* 2011), ochrana při akustickém traumatu (Lauer a May 2011) a během stárnutí (Liberman, Liberman *et al.* 2014). Naše analýzy ukázaly, že počet eferentních zakončení na vnějších vláskových buňkách u [Tg(*Pax2-Isl1*)] byl významně snížen již ve dvou měsících. Toto snížení zřejmě souvisí s ektopickou expresí ISL1 v neuronech mozkového kmene mutantů vedoucí k narušení jejich funkce, zatímco u kontrol v mediální olivě superior není ISL1 exprimován.

Naše výsledky ukazují negativní efekt transgenní exprese ISL1 v porovnání s publikovanými výsledky popisující naopak prospěšný vliv navýšené exprese ISL1 z hlediska sluchových funkcí. Huang *et al.* (Huang, Kantardzhieva *et al.* 2013) použil pro navýšení exprese ISL1 regulační sekvenci genu *Pou4f3* (dříve označovaný jako *Brn3c*), která je aktivní v maturovaných vláskových buňkách od E14 a jejíž exprese přetrvává v senzorických buňkách i v dospělosti (Xiang, Gan *et al.* 1997). U těchto mutantů nadprodukce ISL1 prodloužila přežívání vláskových buněk a neuronů spirálního ganglia po akustickém traumatu (Huang, Kantardzhieva *et al.* 2013), zatímco u našeho mutanta [Tg(*Pax2-Isl1*)] transgenní exprese ISL1 byla spojena se zhoršením sluchových funkcí a rychlejší degenerací spirálního ganglia během stárnutí. Tyto rozdílné výsledky jsou dány použitím odlišných regulačních sekvencí pro transgenní expresi ISL1. U našeho modelu byla použita regulační sekvence *Pax2*, která v maturovaných vláskových buňkách není aktivní, ale je naopak aktivní v raných stádiích vývoje vnitřního ucha (Lawoko-

Kerali, Rivolta *et al.* 2002). Navíc regulační sekvence *Pax2* je aktivní v eferentních neuronech mozkového kmene a jak bylo ukázáno u našeho mutanta [Tg(*Pax2-Isl1*)], ektopická exprese ISL1 v těchto neuronech vedla k předčasné degeneraci eferentního systému vnitřního ucha. Na těchto modelech s transgenní expresí ISL1 je zřejmé, že vliv transkripčních faktorů na vývoj a funkci sluchového systému je závislý na jejich časové a prostorové expresi, která pak odlišně ovlivňuje jejich konečný účinek.

6.2 Transgenní exprese ISL1 ovlivnila vývoj a funkci centrální části vestibulárního systému.

Transgenní myši [Tg(*Pax2-Isl1*)] vykazovaly změny chování a to zejména hyperaktivitu a pohyb v kruhu, které jsou tradičně spojovány s defekty vestibulárního systému. Z tohoto důvodu kromě sluchového systému byl u našeho mutanta analyzován také vestibulární systém. Jediný defekt vestibulárního periferního aparátu nalezený u myší [Tg(*Pax2-Isl1*)] byl menší sakulus s menším počtem vláskových buněk. Tato změna koreluje s expresí *Pax2* ve vyvíjející se ventrální části otocysty (Torres, Gomez-Pardo *et al.* 1996), ze které vzniká kochlea a právě sakulus. Ektopicky exprimovaný ISL1 tedy může ovlivňovat expresi genů pro transkripční faktory důležité pro vývoj ventrální části otického váčku např. *Otx2* („Homeobox protein OTX2“) či *Gbx2* („Homeobox protein GBX-2“), u nichž bylo pomocí myších modelů nesoucí deleci některého z těchto genů ukázána jejich role na vývoji sakulu (Morsli, Tuorto *et al.* 1999, Lin, Cantos *et al.* 2005). Tato minimální morfologická změna v orgánech rovnovážného systému však nemůže být příčinou zjevného vestibulárního fenotypu u mutanta [Tg(*Pax2-Isl1*)], a proto byly další analýzy zaměřeny na centrální část vestibulární dráhy. Významné morfologické rozdíly ve vestibulární dráze byly detekovány hlavně v mozečku u [Tg(*Pax2-Isl1*)], kde docházelo ke špatnému rýhování laloků. Nejčastěji byly postiženy anteriorní laloky, kdy laloky I-III splývaly v jediný lalok. Obdobný defekt byl také zaznamenán u myší s podmíněnou delecí genu pro „Homeobox protein engrailed-1“ (*En1*), který taktéž hraje významnou roli během vývoje anteriorních laloků mozečku (Sgaier, Lao *et al.* 2007). EN1 je exprimován od raného věku E8,5 v dorsální části středního mozku, ze kterého vzniká *colliculus inferior* a anteriorní části mozečku podobně jako PAX2 (Joyner 1996). Transkripční faktor ISL1 není běžně v mozečku exprimován a můžeme tedy předpokládat, že jeho ektopická exprese u transgenních myší pravděpodobně způsobila přímou nebo nepřímou inhibici EN1 a tím také

stejný abnormální fenotyp mozečku. Dalším vývojovým defektem u myší [Tg(*Pax2-Isl1*)] byl výrazně menší *colliculus inferior* ve srovnání s kontrolami, což bylo opět popsáno u modelu s podmíněnou delecí *En1* (Sgaier, Lao *et al.* 2007).

Kromě morfologických změn v mozečku a *colliculus inferior* byly také zaznamenány odchylky na molekulární úrovni. PAX2 je v mozečku aktivní již od E13 avšak pouze v neuronech, v gliových buňkách nebyl detekován. Konkrétně transkripční faktor PAX2 specifikuje všechny druhy GABAergních inhibičních interneuronů v mozečku (hvězdicové, košíčkové a Golgiho buňky)(Maricich a Herrup 1999). Naopak glutamátové excitační neurony granulární vrstvy se vyznačují expresí proteinu DLG4 (označováný také jako PSD95) a transkripčního faktoru PAX6 (Fukaya, Ueda *et al.* 1999, Yeung, Ha *et al.* 2016). Hladina mRNA genů *Pax6* a *Dlg4* byla navýšena v mozečku [Tg(*Pax2-Isl1*)], což ukazuje na možnou roli ISL1 během specifikace neuronů. Dále byla u mutantů potvrzená zvýšená exprese genu pro transkripční faktor *Neurod4*, který je aktivován právě ISL1 (Dykes, Tempest *et al.* 2011). Kromě transkripčních faktorů byla také ovlivněna hladina mRNA některých genů pro proteiny vápníkové homeostáze – *Calb2* a *Cacng1*. *Calb2* je gen pro protein kalretinin a je exprimován v granulárních buňkách mozečku (Bastianelli 2003), zatímco *Cacng1* je exprimován zejména v kosterním svalstvu, ale jeho exprese byla potvrzena i v mozečku (Burgess, Gefrides *et al.* 2001). Výsledky kvantitativní PCR naznačují, že ektopická exprese ISL1 v mozečku zapříčinila změněný expresní profil neuronů, přičemž došlo k navýšení exprese genů typických pro granulární buňky (*Pax6*, *Dlg4* a *Calb2*), ke změně exprese transkripčních faktorů, jejichž exprese je přímo regulována ISL1 (*Neurod4*) a ke změně exprese genů důležitých pro vápníkovou homeostázi (*Cacng1* a *Calb2*).

V dalších analýzách byly nalezeny změny v GABA signalizaci. Po aplikaci pikrotoxinu, inhibitoru neurotransmiteru GABA (Gahwiler 1975), bylo hyperaktivní chování mutanta [Tg(*Pax2-Isl1*)] normalizováno. Správná signalizace je rozhodující pro koordinaci pohybu a degenerace mozkových obvodů je spojena s několika neurologickými degenerativními chorobami. Například myší a potkaní modely s poruchou pozornosti („Attention Deficit Hyperactivity Disorder“; ADHD) vykazují srovnatelné výsledky na rotarodu jako kontroly (Qian, Lei *et al.* 2010, Majdak, Ossyra *et al.* 2016) podobně jako v případě našeho hyperaktivního mutanta [Tg(*Pax2-Isl1*)]. Stejný fenotyp chování mají myši nesoucí mutaci A53R v *Snca* genu (gen pro protein α synuklein), které trpí Parkinsonovou nemocí (Graham a

Sidhu 2010, Paumier, Sukoff Rizzo *et al.* 2013). Naše výsledky ukazují, že změny v transkripční regulaci ve vývoji vestibulárního systému mohou přispět k psychiatrickým a motorickým poruchám, které také korelují se zmenšujícím se anteriorním lalokem mozečku související s věkem (Hulst, van der Geest *et al.* 2015) a změnou GABA signalizace, která byla zaznamenána u lidí s ADHD (Courvoisie, Hooper *et al.* 2004, Edden, Crocetti *et al.* 2012).

6.3 Opožděná a variabilní delece *Sox2* vede k abnormálnímu morfologickému vývoji vnitřního ucha s reziduálními neurosenzorickými buňkami.

Pro studium funkce transkripčního faktoru SOX2 byl vytvořen nový myší model s podmíněnou delecí *Sox2* (*Sox2CKO*) pomocí systému Cre-loxP křížením myších kmenů *Isl1-Cre* a *Sox2*$^{f/f}$. SOX2 je považován za jeden z nejranějších markerů otické plakody, jelikož jeho exprese je detekována ve většině prekurzorů vnitřního ucha již ve věku E8,5 (Wood a Episkopou 1999). ISL1 je také exprimován v otocystě, avšak ve stejném věku byl detekován pouze v několika buňkách (Radde-Gallwitz, Pan *et al.* 2004). Předpokládali jsme, že excise *Sox2* u myšího modelu *Sox2CKO* bude zpožděná i také proto, že delece pomocí Cre rekombinázy může být opožděná (Nagy 2000). Reziduální exprese SOX2 byla u mutanta detekována v sakulu, utrikulu a bazální části kochley, zatímco u kontroly byl SOX2 exprimován ve všech orgánech vnitřního ucha. Tento výsledek ukazuje na opožděnou deleci genu *Sox2* v experimentálním modelu *Sox2CKO*.

Podobně jako u myší s náhodnou inzercí plasmidu do genu *Sox2* nebo s mutací tohoto genu vzniklou rentgenovým zářením (Kiernan, Pelling *et al.* 2005) byly u *Sox2CKO* detekovány rozsáhlé morfologické malformace vnitřního ucha – chybějící polokruhovité kanály, menší vestibulární makuly a kratší kochlea potvrzující důležitost SOX2 během morfogeneze vnitřního ucha (Steevens, Glatzer *et al.* 2019). Dalším důležitým faktorem pro vývoj sluchově rovnovážného ústrojí je FGF10, po jehož deleci se nevytvářejí vestibulární kanály (Pauley, Wright *et al.* 2003). Po podmíněné deleci *Sox2* nebyl u mutanta pomocí *in situ* hybridizace detekován *Fgf10*, což ukazuje na přímou nebo nepřímou závislost exprese *Fgf10* na SOX2.

Naše výsledky potvrzují, že transkripční faktor SOX2 je nezbytný pro specifikaci a diferenciaci vláskových i podpůrných buněk (Dabdoub, Puligilla *et al.* 2008). Ve vnitřním uchu *Sox2CKO* byl detekován zbytkový senzorický epitel pouze v místech s pozůstatky exprese SOX2 (utrikulus, sakulus a kochleární báze). Ve stejných oblastech byla detekována exprese

transkripčního faktoru ATOH1, který je nezbytný pro diferenciaci vláskových buněk (Bermingham, Hassan *et al.* 1999). Naše výsledky jsou v souladu s předešlými publikacemi ukazující závislost *Atoh1* na SOX2 (Ahmed, Wong *et al.* 2012, Kempfle, Turban *et al.* 2016).

Některé senzorické orgány *Sox2CKO* neobsahovaly žádné sensorické buňky (kristy polokruhovitých kanálů a apex kochley), zatímco v některých orgánech vnitřního ucha byly zbytkové vláskové buňky detekovány (utrikulus, sakulus a kochleární báze). Jedno z možných vysvětlení by byla rozdílná účinnost Cre rekombinázy. Tato možnost byla vyloučena pomocí křížení myší *Isl1-Cre* a *Atoh1*$^{f/f}$, u nichž nebyly nalezeny vláskové buňky v žádném orgánu vnitřního ucha a rekombinace tak byla úplná jak v celé délce kochley, tak i ve všech vestibulárních orgánech. Dalším důvodem rozdílného výskytu senzorických buněk v orgánech vnitřního ucha by mohla být časově posunutá delece *Sox2* ve vnitřním uchu *Sox2CKO*. Nicméně exprese *Atoh1*, prvního diferenciačního markeru vláskových buněk, který je řízen transkripčním faktorem SOX2, začíná přibližně v E12,5 ve všech vestibulárních orgánech a až o den později je detekován v kochleární bázi (Pan, Jahan *et al.* 2012). Z tohoto důvodu by měly být reziduální vláskové buňky nalezeny ve všech vestibulárních orgánech, avšak v kristách *Sox2CKO* nebyly žádné vláskové buňky detekovány. Vysvětlením by mohl být odlišný původ vláskových buněk, které se vyvíjí ze senzorických a neurosenzorických prekurzorů (Fritzsch, Beisel *et al.* 2006). Vláskové buňky makul (utrikulus a sakulus) a kochleární báze jsou kromě senzorického i neurosenzorického původu, zatímco epitelové buňky krist a apexu vznikají výhradně jen ze senzorických prekurzorů (Matei, Pauley *et al.* 2005, Koundakjian, Appler *et al.* 2007, Raft, Koundakjian *et al.* 2007).

Změny v důsledku podmíněné delece *Sox2* nebyly zaznamenány pouze ve vývoji vláskových a podpůrných buněk, ale také ve spirálním a vestibulárním gangliu. Ve věku E18,5 bylo ve vnitřním uchu mutantů *Sox2CKO* detekováno pouze několik nervových vláken inervujících vestibulární orgány a bazální část kochley v porovnání s hustou inervací všech orgánů vnitřního ucha su kontrol. Kochleární apex byl zcela bez inervace u *Sox2CKO*. Neurony apexu se diferencují a ukončují buněčný cyklus nejpozději ze všech neuronů vnitřního ucha (Ruben 1967), což naznačuje, že v případě delece *Sox2* dochází ke specifikaci pouze raných nervových buněk, zatímco později diferencované neurony se ve vnitřním uchu nevyvíjejí. Ačkoli z počátku vývoje (E11,5) byla inervace srovnatelná mezi *Sox2CKO* a kontrolou, v následujících dnech docházelo k rozsáhlé apoptóze v oblasti vyvíjejícího se sluchově rovnovážného ganglia a poté

ke ztrátě nervových vláken. K apoptóze docházelo v období vývoje, kdy nervová vlákna začínají být závislá na neurotrofinech BDNF a NTF-3 produkovaných senzorickým epitelem (Fritzsch, Silos-Santiago *et al.* 1997, Farinas, Jones *et al.* 2001, Ramekers, Versnel *et al.* 2012). Naše výsledky poprvé ukazují, že ztráta inervace raně se vyvíjejících neuronů v důsledku delece *Sox2* je tedy pravděpodobně druhotným důsledkem ztráty vláskových a podpůrných buněk.

6.4 NEUROD1 je nezbytný pro tonotopické uspořádání sluchové dráhy.

Transgenní myši *Isl1-Cre* byly využity i pro získání dalšího nového myšího modelu s podmíněnou delecí genu *Neurod1* (*Neurod1CKO*). Kochlea dospělých myší *Neurod1CKO* je o 40 % kratší v porovnání s kontrolami. Toto zkrácení bylo popsáno i u myší s úplnou delecí genů *Neurog1* (Ma, Anderson *et al.* 2000) či *Neurod1* (Kim, Fritzsch *et al.* 2001) a podmíněnou delecí *Neurod1* řízenou Pax2-Cre (Jahan, Pan *et al.* 2010). Nejkratší kochlea byla detekována u experimentálního modelu nesoucí totální deleci *Neurog1*, u něhož kochlea dosahuje pouze 51% kochleární délky kontrol. Toto výraznější zkrácení může být zapříčiněno ranější expresí NEUROG1 oproti NEUROD1 a také tím, že NEUROG1 reguluje expresi *Neurod1* (Fritzsch, Eberl *et al.* 2010). Délka kochley u myší s podmíněnou delecí *Neurod1* řízenou Isl1-Cre a Pax2-Cre je srovnatelná. Se zkrácením kochley také souvisí dezorganizace buněk Cortiho orgánu, která byla detekována u všech výše zmíněných mutantů i u našich jedinců *Neurod1CKO*. Avšak jedinou oblastí se zmnoženými řadami senzorických buněk a chybně orientovanými vláskovými buňkami je vždy apex, takže dezorganizace epitelu je pravděpodobně druhotným výsledkem zkrácení kochley. Tuto hypotézu potvrzují Ma *et al.*, (Ma, Anderson *et al.* 2000), kteří u mutanta nezaznamenali zvýšený celkový počet vláskových buněk v celé délce Cortiho orgánu.

Nejvýraznější defekty vnitřního ucha u *Neurod1CKO* byly detekovány ve spirálním gangliu a inervaci. Předchozí publikace se vždy zaměřily pouze na nervová vlákna, kterých je u myší s mutací v genu *Neurod1* výrazně méně (Kim, Fritzsch *et al.* 2001, Jahan, Kersigo *et al.* 2010). My jsme také zaznamenali úbytek vláken, ale vůbec poprvé jsme kvantifikovali počet neuronů spirálního ganglia, jenž u *Neurod1CKO* dosahoval pouze 20 % z celkového počtu neuronů spirálního ganglia kontrolních myší. Došlo také ke snížení počtu nervových zakončení na vnitřních vláskových buňkách, tzv. „ribbon“ synapsí. Avšak tyto synapse jsou u mutanta redukovány pouze z 50 %, při čemž by však jeden neuron spirálního ganglia měl inervovat vždy pouze jednu vnitřní vláskovou buňku. Tento rozdíl mezi snížením počtu sluchových neuronů a

„ribbon“ synapsí lze vysvětlit dvěma mechanismy – vláskové buňky jsou inervovány i jinými neurony než sluchovými nebo spirální neurony inervují více sensorických buněk. Tyto hypotézy byly ověřeny metodou trasování neuronů lipofilickou próbou. Tyto analýzy ukázaly, že u mutanta jeden spirální neuron inervuje více než jednu vnitřní vláskovou buňku a že inervace jednotlivých orgánů vnitřního ucha u *Neurod1CKO* není oddělená. Neurony vestibulárního ganglia inervují jak rovnovážné orgány, tak i sluchové vláskové buňky, a neurony spirálního ganglia mají synapse jak v kochlee, tak ve vestibulárním ústrojí. Metodou trasování neuronů i histologickými metodami bylo dále u mutanta detekováno zvětšené vestibulární ganglium obsahující vestibulární i spirální neurony, které jsme nazvali „spiro-vestibulární“ ganglium. Všechny tyto defekty inervace vnitřního ucha mohou být zapříčiněny chybnou migrací neuroblastů a neuronů během vývoje, při nichž hraje NEUROD1 důležitou roli (Kim 2013). Obdobné abnormality (zvětšené nesegregované ganglium, menší hustota vláken) byly také detekovány u myší s podmíněnou delecí genu pro transkripční faktor SOX10 exprimovaný zejména v gliových buňkách vnitřního ucha (Mao, Reiprich *et al.* 2014). Na základě našich výsledků spolu se závěry zmíněných publikací lze usuzovat, že pro správnou migraci neuroblastů je tedy důležitá souhra neurálních i gliových transkripčních faktorů.

Změny ve vnitřním uchu po podmíněné deleci *Neurod1* se promítly i do centrálních částí sluchové dráhy. Ačkoli je NEUROD1 exprimován v kochleárním jádru, působením Isl1-Cre docházelo k jeho deleci pouze ve vnitřním uchu a my tak poprvé mohli sledovat změny v mozku způsobené abnormalitami na periferii sluchové dráhy. Menší počet neuronů spirálního ganglia a méně hustá inervace ovlivnila vývoj kochleárního jádra, jehož objem byl u mutanta v dospělosti cca o 39 % menší a obsahoval celkově méně chundelatých buněk. Zmenšené kochleární jádro bylo v minulosti detekováno po chirurgickém odstranění kochley u mladých hlodavců (Tierney, Russell *et al.* 1997). Dalším důsledkem rané ztráty Cortiho orgánu u myší je apoptóza neuronů spirálního ganglia a následně nervových buněk kochleárního jádra (Tong, Strong *et al.* 2015). K těmto negativním změnám v kochleárním jádru dochází vlivem ztráty aferetních vláken z vnitřního ucha, ke které však musí dojít během embryonálního nebo raného postnatálního vývoje. Ztráta inervace vnitřního ucha v dospělosti nemá na velikost kochleárního jádra vliv. Doposud nebyly publikovány výsledky ukazující, že vlivem ztráty spirálního ganglia dochází k porušení tonotopie kochleárního jádra (Wright, Hwang *et al.* 2014). Naše experimenty tak poprvé ukázaly, že ztráta tonotopického uspořádání v kochlee u *Neurod1CKO*, kdy bazální

neurony spirálního ganglia inervují kochleární bázi i apex a naopak apikální neurony mají nervová zakončení na vláskových buňkách po celé délce kochley, vedla ke změně tonotopie v centrálních částech sluchové dráhy v kochleárním jádře a *colliculus inferior*. Detekcí aktivovaných neuronů v kochleárním jádře pomocí protilátky proti c-Fos bylo ukázáno, že zatímco u kontrol bylo aktivováno pouze několik neuronů v úzkém izofrekvenčním pásu dané frekvence, u mutanta *Neurod1CKO* se aktivovalo dvakrát více neuronů v celém kochleárním jádře. Podobná ztráta tonotopie v kochleárním jádře byla zaznamenána u mutanta s delecí genů pro transkripční faktory *Hox2* („Homeobox proteins Hox2“) v důsledku zmnožení synapsí u neuronů kochleárního jádra při zachování normálního přenosu akustického signálu ve vnitřním uchu (Karmakar, Narita *et al.* 2017).

Naše funkční analýzy poprvé ukázaly, že změny frekvenčního rozsahu a přenosu akustického signálu z vnitřního ucha a kochleárního jádra vedou k funkční reorganizaci neuronů v *colliculus inferior* u *Neurod1CKO.* Následkem ztráty tonotopie a jednoneuronového spojení dochází ke změnám vlastností neuronů v *colliculus inferior*. Mění se např. prahy odpovědí, spontánní aktivita neuronů, frekvenční selektivita neuronů a velikost excitačních prahů. Poprvé jsme ukázali důsledky dezorganizované periferní projekční mapy neuronů spirálního ganglia na tonotopickou organizaci centrální sluchové dráhy. Změny frekvence, intenzity a zpracování akustické informace ovlivnily nejen fyziologické vlastnosti neuronů centrální sluchové dráhy, ale i zpracování zvukové informace na behaviorální úrovni. Reakce mutantů *Neurod1CKO* na zvukové podněty byly testovány měřením reflexní úlekové reakce na intenzivní akustický podnět a nadprahová citlivost sluchového systému byla testována pomocí prepulzní inhibice úlekové reakce. Změny v chování mutantů *Neurod1CKO* odráží změny nervových okruhů centrálních sluchových struktur včetně *colliculus inferior* a sluchové kůry. Plasticita a reorganizace neuronů se uplatňuje zejména během vývoje tonotopie v celé sluchové dráze (Kandler, Clause *et al.* 2009). Poprvé jsme ukázali, že mutace jednoho genu způsobuje fyziologicky neopravitelné chyby v nervových spojení jak na periferii, tak i v centrální části sluchové dráhy, které ukazují omezenou plasticitu mozku reagovat na výrazné změny tonotopie během embryonálního vývoje.

7 Závěr

Tato práce byla zaměřena na studium rolí vybraných transkripčních faktorů (ISL1, SOX2 a NEUROD1) během proliferace, specifikace a diferenciace neurosenzorických buněk vnitřního ucha. Pro studium funkcí těchto proteinů byly použity tři myší modely - [Tg(*Pax2-Isl1*)], *Sox2CKO* a *Neurod1CKO*.

Získané výsledky poprvé ukázaly, že presbyakuze (stařecká nedoslýchavost) by mohla být způsobena vedle ztráty vláskových buněk a neuronů spirálního ganglia i degenerací eferentních vláken vedoucích z mediální olivy superior mozkového kmene do vnitřního ucha. Ektopická exprese ISL1 řízená regulační sekvencí *Pax2*, která je aktivní i v mozkovém kmeni, vedla k 36% snížení objemu zakončení eferentních vláken na vláskových buňkách, což mělo za následek snížení funkčnosti těchto senzorických buněk a také zhoršení sluchových funkcí. Tyto výsledky jsou v souladu s předchozími výzkumy ukazujícími pozitivní vliv eferentních zakončení na životaschopnost vláskových buněk.

Negativní změny v důsledku ektopické exprese ISL1 byly zaznamenány i v dráze rovnovážné. U transgenního modelu [Tg(*Pax2-Isl1*)] byl detekován menší sakulus s menším počtem vláskových buněk, avšak mnohem větší abnormality byly odhaleny v mozečku a středním mozku na úrovni morfologické i molekulární. Mozeček a *colliculus inferior* byly u mutanta celkově významně menší ve srovnání s kontrolami a struktura mozečku byla navíc u [Tg(*Pax2-Isl1*)] abnormální. Dále byla ektopickou nadprodukcí ISL1 ovlivněna GABA signalizace, což se projevovalo hyperaktivitou. Myší model [Tg(*Pax2-Isl1*)] by proto mohl být využíván při studiu ADHD.

Experimenty na novém myším modelu se zpožděnou delecí genu *Sox2* odhalily dosud neznámou funkci transkripčního faktoru SOX2 během vývoje vnitřního ucha. Poprvé byla ukázána přímá závislost diferenciace neuronů vnitřního ucha na expresi SOX2, jelikož byly detekovány raně se vyvíjecí vestibulární neurony, zatímco později se utvářející apikální spirální ganglium zcela chybělo. Dále bylo potvrzeno, že diferenciace buněk senzorického epitelu je závislá na přesné hladině exprese SOX2. Nedostatečná hladina tohoto transkripčního faktoru vede k morfologickým abnormalitám vláskových i podpůrných buněk.

Podmíněná delece genu *Neurod1* vedla k abnormálnímu vývoji na všech úrovních sluchové dráhy. Hlavní příčinou těchto změn byla defektní proliferace a migrace neuroblastů spirálního ganglia, ve kterých NEUROD1 hraje zásadní roli. Nedostatek tohoto transkripční faktoru

zapříčinil výraznou redukci neuronů spirálního ganglia s nedokonalou tonotopií, dezorganizovanou aferentní a eferentní kochleární inervaci a zvětšené atypické spiro-vestibulární ganglium. Toto poškození inervace vnitřního ucha se následně projevilo zhoršenými funkcemi komponetů centrální sluchové dráhy - kochleárního jádra a *colliculus inferior,* ukazující omezené spektrum vnímaných frekvencí, poškozenou tonotopii, zhoršenou selektivitu frekvencí a abnormální zpracování zvukové informace na behaviorální úrovni.

Závěrem lze říci, že transkripční faktory ISL1, SOX2 a NEUROD1 jsou nezbytné pro správný vývoj buněk vnitřního ucha a že při změně v jejich expresi dochází k vážným abnormalitám vedoucích k poškození sluchu a rovnováhy.

8 Seznam literatury

Ahmed M., Wong E. Y., Sun J., Xu J., Wang F., Xu P. X. (2012). "Eya1-Six1 interaction is sufficient to induce hair cell fate in the cochlea by activating Atoh1 expression in cooperation with Sox2." Dev Cell **22**(2): 377-390.

Aitkin L. M., Dickhaus H., Schult W., Zimmermann M. (1978). "External nucleus of inferior colliculus: auditory and spinal somatosensory afferents and their interactions." J Neurophysiol **41**(4): 837-847.

Alvarez Y., Alonso M. T., Vendrell V., Zelarayan L. C., Chamero P., Theil T., Bosl M. R., Kato S., Maconochie M., Riethmacher D., Schimmang T. (2003). "Requirements for FGF3 and FGF10 during inner ear formation." Development **130**(25): 6329-6338.

Andeol G., Guillaume A., Micheyl C., Savel S., Pellieux L., Moulin A. (2011). "Auditory efferents facilitate sound localization in noise in humans." J Neurosci **31**(18): 6759-6763.

Ango F., Dos Reis R. (2019). "Sensing how to balance." Elife **8**.

Appler J. M., Lu C. C., Druckenbrod N. R., Yu W. M., Koundakjian E. J., Goodrich L. V. (2013). "Gata3 is a critical regulator of cochlear wiring." J Neurosci **33**(8): 3679-3691.

Balmer T. S., Trussell L. O. (2019). "Selective targeting of unipolar brush cell subtypes by cerebellar mossy fibers." Elife **8**.

Basch M. L., Brown R. M., 2nd, Jen H. I., Groves A. K. (2016). "Where hearing starts: the development of the mammalian cochlea." J Anat **228**(2): 233-254.

Bastianelli E. (2003). "Distribution of calcium-binding proteins in the cerebellum." Cerebellum **2**(4): 242-262.

Belyantseva I. A., Adler H. J., Curi R., Frolenkov G. I., Kachar B. (2000). "Expression and localization of prestin and the sugar transporter GLUT-5 during development of electromotility in cochlear outer hair cells." J Neurosci **20**(24): RC116.

Ben-Arie N., Bellen H. J., Armstrong D. L., McCall A. E., Gordadze P. R., Guo Q., Matzuk M. M., Zoghbi H. Y. (1997). "Math1 is essential for genesis of cerebellar granule neurons." Nature **390**(6656): 169-172.

Bermingham N. A., Hassan B. A., Price S. D., Vollrath M. A., Ben-Arie N., Eatock R. A., Bellen H. J., Lysakowski A., Zoghbi H. Y. (1999). "Math1: an essential gene for the generation of inner ear hair cells." Science **284**(5421): 1837-1841.

Blauwkamp M. N., Beyer L. A., Kabara L., Takemura K., Buck T., King W. M., Dolan D. F., Barald K. F., Raphael Y., Koenig R. J. (2007). "The role of bone morphogenetic protein 4 in inner ear development and function." Hear Res **225**(1-2): 71-79.

Bouchard M., de Caprona D., Busslinger M., Xu P., Fritzsch B. (2010). "Pax2 and Pax8 cooperate in mouse inner ear morphogenesis and innervation." BMC Dev Biol **10**: 89.

Burgess D. L., Gefrides L. A., Foreman P. J., Noebels J. L. (2001). "A cluster of three novel Ca2+ channel gamma subunit genes on chromosome 19q13.4: evolution and expression profile of the gamma subunit gene family." Genomics **71**(3): 339-350.

Burton Q., Cole L. K., Mulheisen M., Chang W., Wu D. K. (2004). "The role of Pax2 in mouse inner ear development." Dev Biol **272**(1): 161-175.

Cai C. L., Liang X., Shi Y., Chu P. H., Pfaff S. L., Chen J., Evans S. (2003). "Isl1 identifies a cardiac progenitor population that proliferates prior to differentiation and contributes a majority of cells to the heart." Dev Cell **5**(6): 877-889.

Cai T., Jen H. I., Kang H., Klisch T. J., Zoghbi H. Y., Groves A. K. (2015). "Characterization of the transcriptome of nascent hair cells and identification of direct targets of the Atoh1 transcription factor." J Neurosci **35**(14): 5870-5883.

Cai T., Seymour M. L., Zhang H., Pereira F. A., Groves A. K. (2013). "Conditional deletion of Atoh1 reveals distinct critical periods for survival and function of hair cells in the organ of Corti." J Neurosci **33**(24): 10110-10122.

Cai X., Kardon A. P., Snyder L. M., Kuzirian M. S., Minestro S., de Souza L., Rubio M. E., Maricich S. M., Ross S. E. (2016). "Bhlhb5::flpo allele uncovers a requirement for Bhlhb5 for the development of the dorsal cochlear nucleus." Dev Biol **414**(2): 149-160.

Champney T. H. (2015). Essential Clinical Neuroanatomy, Wiley-Blackwell**:** 320.

Chang W., Lin Z., Kulessa H., Hebert J., Hogan B. L., Wu D. K. (2008). "Bmp4 is essential for the formation of the vestibular apparatus that detects angular head movements." PLoS Genet **4**(4): e1000050.

Chellappa R., Li S., Pauley S., Jahan I., Jin K., Xiang M. (2008). "Barhl1 regulatory sequences required for cell-specific gene expression and autoregulation in the inner ear and central nervous system." Mol Cell Biol **28**(6): 1905-1914.

Chen P., Johnson J. E., Zoghbi H. Y., Segil N. (2002). "The role of Math1 in inner ear development: Uncoupling the establishment of the sensory primordium from hair cell fate determination." Development **129**(10): 2495-2505.

Chen P., Segil N. (1999). "p27(Kip1) links cell proliferation to morphogenesis in the developing organ of Corti." Development **126**(8): 1581-1590.

Chittka L., Brockmann A. (2005). "Perception space--the final frontier." PLoS Biol **3**(4): e137.

Cho J. H., Tsai M. J. (2004). "The role of BETA2/NeuroD1 in the development of the nervous system." Mol Neurobiol **30**(1): 35-47.

Chonko K. T., Jahan I., Stone J., Wright M. C., Fujiyama T., Hoshino M., Fritzsch B., Maricich S. M. (2013). "Atoh1 directs hair cell differentiation and survival in the late embryonic mouse inner ear." Dev Biol **381**(2): 401-410.

Čihák R. (2016). "Anatomie 3." Grada Publishing, a.s., Praha, Česká republika: 605-623.

Courvoisie H., Hooper S. R., Fine C., Kwock L., Castillo M. (2004). "Neurometabolic functioning and neuropsychological correlates in children with ADHD-H: preliminary findings." J Neuropsychiatry Clin Neurosci **16**(1): 63-69.

D'Mello A. M., Stoodley C. J. (2015). "Cerebro-cerebellar circuits in autism spectrum disorder." Front Neurosci **9**: 408.

Dabdoub A., Puligilla C., Jones J. M., Fritzsch B., Cheah K. S., Pevny L. H., Kelley M. W. (2008). "Sox2 signaling in prosensory domain specification and subsequent hair cell differentiation in the developing cochlea." Proc Natl Acad Sci U S A **105**(47): 18396-18401.

DeBry R. W., Seldin M. F. (1996). "Human/mouse homology relationships." Genomics **33**(3): 337-351.

Delacroix L., Malgrange B. (2015). "Cochlear afferent innervation development." Hear Res **330**(Pt B): 157-169.

Deng M., Yang H., Xie X., Liang G., Gan L. (2014). "Comparative expression analysis of POU4F1, POU4F2 and ISL1 in developing mouse cochleovestibular ganglion neurons." Gene Expr Patterns **15**(1): 31-37.

Driver E. C., Sillers L., Coate T. M., Rose M. F., Kelley M. W. (2013). "The Atoh1-lineage gives rise to hair cells and supporting cells within the mammalian cochlea." Dev Biol **376**(1): 86-98.

Duncan J. S., Fritzsch B. (2013). "Continued expression of GATA3 is necessary for cochlear neurosensory development." PLoS One **8**(4): e62046.

Dvorakova M., Macova I., Bohuslavova R., Anderova M., Fritzsch B., Pavlinkova G. (2019). "Early ear neuronal development, but not olfactory or lens development, can proceed without SOX2." Dev Biol.

Dykes I. M., Tempest L., Lee S. I., Turner E. E. (2011). "Brn3a and Islet1 act epistatically to regulate the gene expression program of sensory differentiation." J Neurosci **31**(27): 9789-9799.

Edden R. A., Crocetti D., Zhu H., Gilbert D. L., Mostofsky S. H. (2012). "Reduced GABA concentration in attention-deficit/hyperactivity disorder." Arch Gen Psychiatry **69**(7): 750-753.

Farinas I., Jones K. R., Tessarollo L., Vigers A. J., Huang E., Kirstein M., de Caprona D. C., Coppola V., Backus C., Reichardt L. F., Fritzsch B. (2001). "Spatial shaping of cochlear innervation by temporally regulated neurotrophin expression." J Neurosci **21**(16): 6170-6180.

Faye-Lund H., Osen K. K. (1985). "Anatomy of the inferior colliculus in rat." Anat Embryol (Berl) **171**(1): 1-20.

Fettiplace R. (2017). "Hair Cell Transduction, Tuning, and Synaptic Transmission in the Mammalian Cochlea." Compr Physiol **7**(4): 1197-1227.

Forge A., Wright T. (2002). "The molecular architecture of the inner ear." Br Med Bull **63**: 5-24.

Freyer L., Aggarwal V., Morrow B. E. (2011). "Dual embryonic origin of the mammalian otic vesicle forming the inner ear." Development **138**(24): 5403-5414.

Fritzsch B., Beisel K. W., Hansen L. A. (2006). "The molecular basis of neurosensory cell formation in ear development: a blueprint for hair cell and sensory neuron regeneration?" Bioessays **28**(12): 1181-1193.

Fritzsch B., Eberl D. F., Beisel K. W. (2010). "The role of bHLH genes in ear development and evolution: revisiting a 10-year-old hypothesis." Cell Mol Life Sci **67**(18): 3089-3099.

Fritzsch B., Matei V. A., Nichols D. H., Bermingham N., Jones K., Beisel K. W., Wang V. Y. (2005). "Atoh1 null mice show directed afferent fiber growth to undifferentiated ear sensory epithelia followed by incomplete fiber retention." Dev Dyn **233**(2): 570-583.

Fritzsch B., Silos-Santiago I., Bianchi L. M., Farinas I. (1997). "The role of neurotrophic factors in regulating the development of inner ear innervation." Trends Neurosci **20**(4): 159-164.

Fuchs P. A., Glowatzki E. (2015). "Synaptic studies inform the functional diversity of cochlear afferents." Hear Res **330**(Pt A): 18-25.

Fuchs P. A., Lauer A. M. (2018). "Efferent Inhibition of the Cochlea." Cold Spring Harb Perspect Med.

Fukaya M., Ueda H., Yamauchi K., Inoue Y., Watanabe M. (1999). "Distinct spatiotemporal expression of mRNAs for the PSD-95/SAP90 protein family in the mouse brain." Neurosci Res **33**(2): 111-118.

Gahwiler B. H. (1975). "The effects of GABA, Picrotoxin and bicuculline on the spontaneous bioelectric activity of cultured cerebellar Purkinje cells." Brain Res **99**(1): 85-95.

Galvez H., Tena J. J., Giraldez F., Abello G. (2017). "The Repression of Atoh1 by Neurogenin1 during Inner Ear Development." Front Mol Neurosci **10**: 321.

Graham D. R., Sidhu A. (2010). "Mice expressing the A53T mutant form of human alpha-synuclein exhibit hyperactivity and reduced anxiety-like behavior." J Neurosci Res **88**(8): 1777-1783.

Hawkins J. E. (2017). Human ear. Encyclopaedia Britannica. Chicago, USA, Encyclopaedia Britannica, inc. **2017**.

Henry K. R., Wallick M., Davis M. (1972). "Inferior collicular lesions: effects on audiogenic seizure and Preyer reflex." Physiol Behav **9**(5): 885-887.

Hobert O., Westphal H. (2000). "Functions of LIM-homeobox genes." Trends Genet **16**(2): 75-83.

Huang M., Kantardzhieva A., Scheffer D., Liberman M. C., Chen Z. Y. (2013). "Hair cell overexpression of Islet1 reduces age-related and noise-induced hearing loss." J Neurosci **33**(38): 15086-15094.

Huang M., Sage C., Li H., Xiang M., Heller S., Chen Z. Y. (2008). "Diverse expression patterns of LIM-homeodomain transcription factors (LIM-HDs) in mammalian inner ear development." Dev Dyn **237**(11): 3305-3312.

Huang W. H., Tupal S., Huang T. W., Ward C. S., Neul J. L., Klisch T. J., Gray P. A., Zoghbi H. Y. (2012). "Atoh1 governs the migration of postmitotic neurons that shape respiratory effectiveness at birth and chemoresponsiveness in adulthood." Neuron **75**(5): 799-809.

Hulst T., van der Geest J. N., Thurling M., Goericke S., Frens M. A., Timmann D., Donchin O. (2015). "Ageing shows a pattern of cerebellar degeneration analogous, but not equal, to that in patients suffering from cerebellar degenerative disease." Neuroimage **116**: 196-206.

Hume C. R., Bratt D. L., Oesterle E. C. (2007). "Expression of LHX3 and SOX2 during mouse inner ear development." Gene Expr Patterns **7**(7): 798-807.

Hwang C. H., Simeone A., Lai E., Wu D. K. (2009). "Foxg1 is required for proper separation and formation of sensory cristae during inner ear development." Dev Dyn **238**(11): 2725-2734.

Irving S., Moore D. R., Liberman M. C., Sumner C. J. (2011). "Olivocochlear efferent control in sound localization and experience-dependent learning." J Neurosci **31**(7): 2493-2501.

Ito M. (2006). "Cerebellar circuitry as a neuronal machine." Prog Neurobiol **78**(3-5): 272-303.

Ivanova A., Yuasa S. (1998). "Neuronal migration and differentiation in the development of the mouse dorsal cochlear nucleus." Dev Neurosci **20**(6): 495-511.

Izumikawa M., Minoda R., Kawamoto K., Abrashkin K. A., Swiderski D. L., Dolan D. F., Brough D. E., Raphael Y. (2005). "Auditory hair cell replacement and hearing improvement by Atoh1 gene therapy in deaf mammals." Nat Med **11**(3): 271-276.

Jahan I., Kersigo J., Pan N., Fritzsch B. (2010). "Neurod1 regulates survival and formation of connections in mouse ear and brain." Cell Tissue Res **341**(1): 95-110.

Jahan I., Pan N., Kersigo J., Fritzsch B. (2010). "Neurod1 suppresses hair cell differentiation in ear ganglia and regulates hair cell subtype development in the cochlea." PLoS One **5**(7): e11661.

Jahan I., Pan N., Kersigo J., Fritzsch B. (2015). "Neurog1 can partially substitute for Atoh1 function in hair cell differentiation and maintenance during organ of Corti development." Development **142**(16): 2810-2821.

Javitt D. C., Sweet R. A. (2015). "Auditory dysfunction in schizophrenia: integrating clinical and basic features." Nat Rev Neurosci **16**(9): 535-550.

Joyner A. L. (1996). "Engrailed, Wnt and Pax genes regulate midbrain hindbrain development." Trends in Genetics **12**(1): 15-20.

Kandler K., Clause A., Noh J. (2009). "Tonotopic reorganization of developing auditory brainstem circuits." Nat Neurosci **12**(6): 711-717.

Karmakar K., Narita Y., Fadok J., Ducret S., Loche A., Kitazawa T., Genoud C., Di Meglio T., Thierry R., Bacelo J., Luthi A., Rijli F. M. (2017). "Hox2 Genes Are Required for Tonotopic Map Precision and Sound Discrimination in the Mouse Auditory Brainstem." Cell Rep **18**(1): 185-197.

Kawamoto K., Ishimoto S., Minoda R., Brough D. E., Raphael Y. (2003). "Math1 gene transfer generates new cochlear hair cells in mature guinea pigs in vivo." J Neurosci **23**(11): 4395-4400.

Kelley M. W. (2006). "Regulation of cell fate in the sensory epithelia of the inner ear." Nat Rev Neurosci **7**(11): 837-849.

Kempfle J. S., Turban J. L., Edge A. S. (2016). "Sox2 in the differentiation of cochlear progenitor cells." Sci Rep **6**: 23293.

Khan S., Chang R. (2013). "Anatomy of the vestibular system: a review." NeuroRehabilitation **32**(3): 437-443.

Kiernan A. E., Cordes R., Kopan R., Gossler A., Gridley T. (2005). "The Notch ligands DLL1 and JAG2 act synergistically to regulate hair cell development in the mammalian inner ear." Development **132**(19): 4353-4362.

Kiernan A. E., Pelling A. L., Leung K. K., Tang A. S., Bell D. M., Tease C., Lovell-Badge R., Steel K. P., Cheah K. S. (2005). "Sox2 is required for sensory organ development in the mammalian inner ear." Nature **434**(7036): 1031-1035.

Kiernan A. E., Xu J., Gridley T. (2006). "The Notch ligand JAG1 is required for sensory progenitor development in the mammalian inner ear." PLoS Genet **2**(1): e4.

Kim W. Y. (2013). "NeuroD regulates neuronal migration." Mol Cells **35**(5): 444-449.

Kim W. Y., Fritzsch B., Serls A., Bakel L. A., Huang E. J., Reichardt L. F., Barth D. S., Lee J. E. (2001). "NeuroD-null mice are deaf due to a severe loss of the inner ear sensory neurons during development." Development **128**(3): 417-426.

Koundakjian E. J., Appler J. L., Goodrich L. V. (2007). "Auditory neurons make stereotyped wiring decisions before maturation of their targets." J Neurosci **27**(51): 14078-14088.

Králíček P. (2004). "Úvod do speciální neurofyziologie." Nakladatelství Karolinum, Praha, Česká republika: 67-86; 145-154.

Lahav A., Skoe E. (2014). "An acoustic gap between the NICU and womb: a potential risk for compromised neuroplasticity of the auditory system in preterm infants." Front Neurosci **8**: 381.

Lanford P. J., Lan Y., Jiang R., Lindsell C., Weinmaster G., Gridley T., Kelley M. W. (1999). "Notch signalling pathway mediates hair cell development in mammalian cochlea." Nat Genet **21**(3): 289-292.

Lauer A. M., May B. J. (2011). "The medial olivocochlear system attenuates the developmental impact of early noise exposure." J Assoc Res Otolaryngol **12**(3): 329-343.

Lawoko-Kerali G., Rivolta M. N., Holley M. (2002). "Expression of the transcription factors GATA3 and Pax2 during development of the mammalian inner ear." J Comp Neurol **442**(4): 378-391.

Lawoko-Kerali G., Rivolta M. N., Lawlor P., Cacciabue-Rivolta D. I., Langton-Hewer C., van Doorninck J. H., Holley M. C. (2004). "GATA3 and NeuroD distinguish auditory and vestibular neurons during development of the mammalian inner ear." Mech Dev **121**(3): 287-299.

Li S., Price S. M., Cahill H., Ryugo D. K., Shen M. M., Xiang M. (2002). "Hearing loss caused by progressive degeneration of cochlear hair cells in mice deficient for the Barhl1 homeobox gene." Development **129**(14): 3523-3532.

Liberman M. C., Gao J., He D. Z., Wu X., Jia S., Zuo J. (2002). "Prestin is required for electromotility of the outer hair cell and for the cochlear amplifier." Nature **419**(6904): 300-304.

Liberman M. C., Liberman L. D., Maison S. F. (2014). "Efferent feedback slows cochlear aging." J Neurosci **34**(13): 4599-4607.

Lim D. J. (1986). "Functional structure of the organ of Corti: a review." Hear Res **22**: 117-146.

Lin Z., Cantos R., Patente M., Wu D. K. (2005). "Gbx2 is required for the morphogenesis of the mouse inner ear: a downstream candidate of hindbrain signaling." Development **132**(10): 2309-2318.

Liu C., Glowatzki E., Fuchs P. A. (2015). "Unmyelinated type II afferent neurons report cochlear damage." Proc Natl Acad Sci U S A **112**(47): 14723-14727.

Liu K., Lin B., Zhao M., Yang X., Chen M., Gao A., Liu F., Que J., Lan X. (2013). "The multiple roles for Sox2 in stem cell maintenance and tumorigenesis." Cell Signal **25**(5): 1264-1271.

Liu M., Pereira F. A., Price S. D., Chu M. J., Shope C., Himes D., Eatock R. A., Brownell W. E., Lysakowski A., Tsai M. J. (2000). "Essential role of BETA2/NeuroD1 in development of the vestibular and auditory systems." Genes Dev **14**(22): 2839-2854.

Liu S., Wang Y., Lu Y., Li W., Liu W., Ma J., Sun F., Li M., Chen Z. Y., Su K. (2018). "The Key Transcription Factor Expression in the Developing Vestibular and Auditory Sensory Organs: A Comprehensive Comparison of Spatial and Temporal Patterns." Neural Plast **2018**: 7513258.

Liu W., Li G., Chien J. S., Raft S., Zhang H., Chiang C., Frenz D. A. (2002). "Sonic hedgehog regulates otic capsule chondrogenesis and inner ear development in the mouse embryo." Dev Biol **248**(2): 240-250.

Luo X. J., Deng M., Xie X., Huang L., Wang H., Jiang L., Liang G., Hu F., Tieu R., Chen R., Gan L. (2013). "GATA3 controls the specification of prosensory domain and neuronal survival in the mouse cochlea." Hum Mol Genet **22**(18): 3609-3623.

Ma Q., Anderson D. J., Fritzsch B. (2000). "Neurogenin 1 null mutant ears develop fewer, morphologically normal hair cells in smaller sensory epithelia devoid of innervation." J Assoc Res Otolaryngol **1**(2): 129-143.

Magarinos M., Contreras J., Aburto M. R., Varela-Nieto I. (2012). "Early development of the vertebrate inner ear." Anat Rec (Hoboken) **295**(11): 1775-1790.

Majdak P., Ossyra J. R., Ossyra J. M., Cobert A. J., Hofmann G. C., Tse S., Panozzo B., Grogan E. L., Sorokina A., Rhodes J. S. (2016). "A new mouse model of ADHD for medication development." Sci Rep **6**: 39472.

Mao M., Montgomery J. M., Kubke M. F., Thorne P. R. (2015). "The Structural Development of the Mouse Dorsal Cochlear Nucleus." J Assoc Res Otolaryngol **16**(4): 473-486.

Mao Y., Reiprich S., Wegner M., Fritzsch B. (2014). "Targeted deletion of Sox10 by Wnt1-cre defects neuronal migration and projection in the mouse inner ear." PLoS One **9**(4): e94580.

Maricich S. M., Herrup K. (1999). "Pax-2 expression defines a subset of GABAergic interneurons and their precursors in the developing murine cerebellum." J Neurobiol **41**(2): 281-294.

Masuda M., Pak K., Chavez E., Ryan A. F. (2012). "TFE2 and GATA3 enhance induction of POU4F3 and myosin VIIa positive cells in nonsensory cochlear epithelium by ATOH1." Dev Biol **372**(1): 68-80.

Matei V., Pauley S., Kaing S., Rowitch D., Beisel K. W., Morris K., Feng F., Jones K., Lee J., Fritzsch B. (2005). "Smaller inner ear sensory epithelia in Neurog 1 null mice are related to earlier hair cell cycle exit." Dev Dyn **234**(3): 633-650.

Merlo G. R., Paleari L., Mantero S., Zerega B., Adamska M., Rinkwitz S., Bober E., Levi G. (2002). "The Dlx5 homeobox gene is essential for vestibular morphogenesis in the mouse embryo through a BMP4-mediated pathway." Dev Biol **248**(1): 157-169.

Mikaelian D., Ruben R. J. (1965). "Development of Hearing in the Normal Cba-J Mouse: Correlation of Physiological Observations with Behavioral Responses and with Cochlear Anatomy." Acta Oto-Laryngologica **59**(2-6): 451-461.

Miyata T., Maeda T., Lee J. E. (1999). "NeuroD is required for differentiation of the granule cells in the cerebellum and hippocampus." Genes Dev **13**(13): 1647-1652.

Morsli H., Choo D., Ryan A., Johnson R., Wu D. K. (1998). "Development of the mouse inner ear and origin of its sensory organs." J Neurosci **18**(9): 3327-3335.

Morsli H., Tuorto F., Choo D., Postiglione M. P., Simeone A., Wu D. K. (1999). "Otx1 and Otx2 activities are required for the normal development of the mouse inner ear." Development **126**(11): 2335-2343.

Mulvaney J., Dabdoub A. (2012). "Atoh1, an essential transcription factor in neurogenesis and intestinal and inner ear development: function, regulation, and context dependency." J Assoc Res Otolaryngol **13**(3): 281-293.

Muniak M. A., Rivas A., Montey K. L., May B. J., Francis H. W., Ryugo D. K. (2013). "3D model of frequency representation in the cochlear nucleus of the CBA/J mouse." J Comp Neurol **521**(7): 1510-1532.

Nagy A. (2000). "Cre recombinase: the universal reagent for genome tailoring." Genesis **26**(2): 99-109.

Naya F. J., Huang H. P., Qiu Y., Mutoh H., DeMayo F. J., Leiter A. B., Tsai M. J. (1997). "Diabetes, defective pancreatic morphogenesis, and abnormal enteroendocrine differentiation in BETA2/neuroD-deficient mice." Genes Dev **11**(18): 2323-2334.

Nishimura K., Noda T., Dabdoub A. (2017). "Dynamic Expression of Sox2, Gata3, and Prox1 during Primary Auditory Neuron Development in the Mammalian Cochlea." PLoS One **12**(1): e0170568.

Nordang L., Cestreicher E., Arnold W., Anniko M. (2000). "Glutamate is the afferent neurotransmitter in the human cochlea." Acta Otolaryngol **120**(3): 359-362.

Nouvian R., Beutner D., Parsons T. D., Moser T. (2006). "Structure and function of the hair cell ribbon synapse." J Membr Biol **209**(2-3): 153-165.

Ohyama T., Groves A. K. (2004). "Generation of Pax2-Cre mice by modification of a Pax2 bacterial artificial chromosome." Genesis **38**(4): 195-199.

Pan N., Jahan I., Kersigo J., Duncan J. S., Kopecky B., Fritzsch B. (2012). "A novel Atoh1 "self-terminating" mouse model reveals the necessity of proper Atoh1 level and duration for hair cell differentiation and viability." PLoS One **7**(1): e30358.

Pan N., Jahan I., Kersigo J., Kopecky B., Santi P., Johnson S., Schmitz H., Fritzsch B. (2011). "Conditional deletion of Atoh1 using Pax2-Cre results in viable mice without differentiated cochlear hair cells that have lost most of the organ of Corti." Hear Res **275**(1-2): 66-80.

Pan N., Jahan I., Lee J. E., Fritzsch B. (2009). "Defects in the cerebella of conditional Neurod1 null mice correlate with effective Tg(Atoh1-cre) recombination and granule cell requirements for Neurod1 for differentiation." Cell Tissue Res **337**(3): 407-428.

Pauley S., Lai E., Fritzsch B. (2006). "Foxg1 is required for morphogenesis and histogenesis of the mammalian inner ear." Dev Dyn **235**(9): 2470-2482.

Pauley S., Wright T. J., Pirvola U., Ornitz D., Beisel K., Fritzsch B. (2003). "Expression and function of FGF10 in mammalian inner ear development." Dev Dyn **227**(2): 203-215.

Paumier K. L., Sukoff Rizzo S. J., Berger Z., Chen Y., Gonzales C., Kaftan E., Li L., Lotarski S., Monaghan M., Shen W., Stolyar P., Vasilyev D., Zaleska M., W D. H., Dunlop J. (2013). "Behavioral characterization of A53T mice reveals early and late stage deficits related to Parkinson's disease." PLoS One **8**(8): e70274.

Puligilla C., Dabdoub A., Brenowitz S. D., Kelley M. W. (2010). "Sox2 induces neuronal formation in the developing mammalian cochlea." J Neurosci **30**(2): 714-722.

Puligilla C., Kelley M. W. (2017). "Dual role for Sox2 in specification of sensory competence and regulation of Atoh1 function." Dev Neurobiol **77**(1): 3-13.

Purves D., Augustine G. J., Fitzpatrick D. (2001). Hair Cells and the Mechanoelectrical Transduction of Sound Waves. Neuroscience. Sunderland, USA, Sinauer Associates.

Qian Y., Lei G., Castellanos F. X., Forssberg H., Heijtz R. D. (2010). "Deficits in fine motor skills in a genetic animal model of ADHD." Behav Brain Funct **6**: 51.

Rabbitt R. D., Brownell W. E. (2011). "Efferent modulation of hair cell function." Curr Opin Otolaryngol Head Neck Surg **19**(5): 376-381.

Radde-Gallwitz K., Pan L., Gan L., Lin X., Segil N., Chen P. (2004). "Expression of Islet1 marks the sensory and neuronal lineages in the mammalian inner ear." J Comp Neurol **477**(4): 412-421.

Raft S., Koundakjian E. J., Quinones H., Jayasena C. S., Goodrich L. V., Johnson J. E., Segil N., Groves A. K. (2007). "Cross-regulation of Ngn1 and Math1 coordinates the production of neurons and sensory hair cells during inner ear development." Development **134**(24): 4405-4415.

Raft S., Nowotschin S., Liao J., Morrow B. E. (2004). "Suppression of neural fate and control of inner ear morphogenesis by Tbx1." Development **131**(8): 1801-1812.

Ramekers D., Versnel H., Grolman W., Klis S. F. (2012). "Neurotrophins and their role in the cochlea." Hear Res **288**(1-2): 19-33.

Ress D., Chandrasekaran B. (2013). "Tonotopic organization in the depth of human inferior colliculus." Front Hum Neurosci **7**: 586.

Riccomagno M. M., Takada S., Epstein D. J. (2005). "Wnt-dependent regulation of inner ear morphogenesis is balanced by the opposing and supporting roles of Shh." Genes Dev **19**(13): 1612-1623.

Riley H. A. (1930). "The Lobules of the Mammalian Cerebellum and Cerebellar Nomenclature." Archives of Neurology & Psychiatry **24**(2): 227-256.

Robles L., Ruggero M. A. (2001). "Mechanics of the mammalian cochlea." Physiol Rev **81**(3): 1305-1352.

Rose M. F., Ren J., Ahmad K. A., Chao H. T., Klisch T. J., Flora A., Greer J. J., Zoghbi H. Y. (2009). "Math1 is essential for the development of hindbrain neurons critical for perinatal breathing." Neuron **64**(3): 341-354.

Ruben R. J. (1967). "Development of the inner ear of the mouse: a radioautographic study of terminal mitoses." Acta Otolaryngol: Suppl 220:221-244.

Sandell L. L., Butler Tjaden N. E., Barlow A. J., Trainor P. A. (2014). "Cochleovestibular nerve development is integrated with migratory neural crest cells." Dev Biol **385**(2): 200-210.

Sento S., Ryugo D. K. (1989). "Endbulbs of held and spherical bushy cells in cats: morphological correlates with physiological properties." J Comp Neurol **280**(4): 553-562.

Seo S., Lim J. W., Yellajoshyula D., Chang L. W., Kroll K. L. (2007). "Neurogenin and NeuroD direct transcriptional targets and their regulatory enhancers." EMBO J **26**(24): 5093-5108.

Sgaier S. K., Lao Z., Villanueva M. P., Berenshteyn F., Stephen D., Turnbull R. K., Joyner A. L. (2007). "Genetic subdivision of the tectum and cerebellum into functionally related regions based on differential sensitivity to engrailed proteins." Development **134**(12): 2325-2335.

Shepard A. R., Scheffel J. L., Yu W. M. (2018). "Relationships between neuronal birthdates and tonotopic positions in the mouse cochlear nucleus." J Comp Neurol.

Sheykholeslami K., Thimmappa V., Nava C., Bai X., Yu H., Zheng T., Zhang Z., Li S. L., Liu S., Zheng Q. Y. (2013). "A new mutation of the Atoh1 gene in mice with normal life span allows analysis of inner ear and cerebellar phenotype in aging." PLoS One **8**(11): e79791.

Shore S. E., Zhou J. (2006). "Somatosensory influence on the cochlear nucleus and beyond." Hear Res **216-217**: 90-99.

Shou J., Zheng J. L., Gao W. Q. (2003). "Robust generation of new hair cells in the mature mammalian inner ear by adenoviral expression of Hath1." Mol Cell Neurosci **23**(2): 169-179.

Shrestha B. R., Chia C., Wu L., Kujawa S. G., Liberman M. C., Goodrich L. V. (2018). "Sensory Neuron Diversity in the Inner Ear Is Shaped by Activity." Cell **174**(5): 1229-1246.e1217.

Steevens A. R., Glatzer J. C., Kellogg C. C., Low W. C., Santi P. A., Kiernan A. E. (2019). "SOX2 is required for inner ear growth and cochlear nonsensory formation before sensory development." Development **146**(13).

Steevens A. R., Sookiasian D. L., Glatzer J. C., Kiernan A. E. (2017). "SOX2 is required for inner ear neurogenesis." Sci Rep **7**(1): 4086.

Stiebler I., Ehret G. (1985). "Inferior colliculus of the house mouse. I. A quantitative study of tonotopic organization, frequency representation, and tone-threshold distribution." J Comp Neurol **238**(1): 65-76.

Stojanova Z. P., Kwan T., Segil N. (2015). "Epigenetic regulation of Atoh1 guides hair cell development in the mammalian cochlea." Development **142**(20): 3529-3536.

Sun S., Babola T., Pregernig G., So K. S., Nguyen M., Su S. M., Palermo A. T., Bergles D. E., Burns J. C., Müller U. (2018). "Hair Cell Mechanotransduction Regulates Spontaneous Activity and Spiral Ganglion Subtype Specification in the Auditory System." Cell **174**(5): 1247-1263.e1215.

Tascioglu A. B. (2005). "Brief review of vestibular system anatomy and its higher order projections." Neuroanatomy **4**: 24-27.

Teudt I. U., Richter C. P. (2014). "Basilar membrane and tectorial membrane stiffness in the CBA/CaJ mouse." J Assoc Res Otolaryngol **15**(5): 675-694.

Tierney T. S., Russell F. A., Moore D. R. (1997). "Susceptibility of developing cochlear nucleus neurons to deafferentation-induced death abruptly ends just before the onset of hearing." J Comp Neurol **378**(2): 295-306.

Tong L., Strong M. K., Kaur T., Juiz J. M., Oesterle E. C., Hume C., Warchol M. E., Palmiter R. D., Rubel E. W. (2015). "Selective deletion of cochlear hair cells causes rapid age-dependent changes in spiral ganglion and cochlear nucleus neurons." J Neurosci **35**(20): 7878-7891.

Torres M., Giraldez F. (1998). "The development of the vertebrate inner ear." Mech Dev **71**(1-2): 5-21.

Torres M., Gomez-Pardo E., Gruss P. (1996). "Pax2 contributes to inner ear patterning and optic nerve trajectory." Development **122**(11): 3381-3391.

UniProt C. (2019). "UniProt: a worldwide hub of protein knowledge." Nucleic Acids Res **47**(D1): D506-D515.

Van Keymeulen A., Mascre G., Youseff K. K., Harel I., Michaux C., De Geest N., Szpalski C., Achouri Y., Bloch W., Hassan B. A., Blanpain C. (2009). "Epidermal progenitors give rise to Merkel cells during embryonic development and adult homeostasis." J Cell Biol **187**(1): 91-100.

Wan G., Corfas G., Stone J. S. (2013). "Inner ear supporting cells: rethinking the silent majority." Semin Cell Dev Biol **24**(5): 448-459.

Wang V. Y., Rose M. F., Zoghbi H. Y. (2005). "Math1 expression redefines the rhombic lip derivatives and reveals novel lineages within the brainstem and cerebellum." Neuron **48**(1): 31-43.

Waqas M., Sun S., Xuan C., Fang Q., Zhang X., Islam I. U., Qi J., Zhang S., Gao X., Tang M., Shi H., Li H., Chai R. (2017). "Bone morphogenetic protein 4 promotes the survival and preserves the structure of flow-sorted Bhlhb5+ cochlear spiral ganglion neurons in vitro." Sci Rep **7**(1): 3506.

Webster D. B., Trune D. R. (1982). "Cochlear nuclear complex of mice." Am J Anat **163**(2): 103-130.

Winer J. A., Larue D. T., Diehl J. J., Hefti B. J. (1998). "Auditory cortical projections to the cat inferior colliculus." J Comp Neurol **400**(2): 147-174.

Wood H. B., Episkopou V. (1999). "Comparative expression of the mouse Sox1, Sox2 and Sox3 genes from pre-gastrulation to early somite stages." Mech Dev **86**(1-2): 197-201.

Woods C., Montcouquiol M., Kelley M. W. (2004). "Math1 regulates development of the sensory epithelium in the mammalian cochlea." Nat Neurosci **7**(12): 1310-1318.

Wright S., Hwang Y., Oertel D. (2014). "Synaptic transmission between end bulbs of Held and bushy cells in the cochlear nucleus of mice with a mutation in Otoferlin." J Neurophysiol **112**(12): 3173-3188.

Wu X., Gao J., Guo Y., Zuo J. (2004). "Hearing threshold elevation precedes hair-cell loss in prestin knockout mice." Brain Res Mol Brain Res **126**(1): 30-37.

Xiang M., Gan L., Li D., Chen Z. Y., Zhou L., O'Malley B. W., Jr., Klein W., Nathans J. (1997). "Essential role of POU-domain factor Brn-3c in auditory and vestibular hair cell development." Proc Natl Acad Sci U S A **94**(17): 9445-9450.

Xu J., Ueno H., Xu C. Y., Chen B., Weissman I. L., Xu P. X. (2017). "Identification of mouse cochlear progenitors that develop hair and supporting cells in the organ of Corti." Nat Commun **8**: 15046.

Yamashita T., Zheng F., Finkelstein D., Kellard Z., Carter R., Rosencrance C. D., Sugino K., Easton J., Gawad C., Zuo J. (2018). "High-resolution transcriptional dissection of in vivo Atoh1-mediated hair cell conversion in mature cochleae identifies Isl1 as a co-reprogramming factor." PLoS Genet **14**(7): e1007552.

Yang H., Xie X., Deng M., Chen X., Gan L. (2010). "Generation and characterization of Atoh1-Cre knock-in mouse line." Genesis **48**(6): 407-413.

Yang J., Cong N., Han Z., Huang Y., Chi F. (2013). "Ectopic hair cell-like cell induction by Math1 mainly involves direct transdifferentiation in neonatal mammalian cochlea." Neurosci Lett **549**: 7-11.

Yang Q., Bermingham N. A., Finegold M. J., Zoghbi H. Y. (2001). "Requirement of Math1 for secretory cell lineage commitment in the mouse intestine." Science **294**(5549): 2155-2158.

Yeung J., Ha T. J., Swanson D. J., Goldowitz D. (2016). "A Novel and Multivalent Role of Pax6 in Cerebellar Development." J Neurosci **36**(35): 9057-9069.

Yoon H., Lee D. J., Kim M. H., Bok J. (2011). "Identification of genes concordantly expressed with Atoh1 during inner ear development." Anat Cell Biol **44**(1): 69-78.

Zheng J., Shen W., He D. Z., Long K. B., Madison L. D., Dallos P. (2000). "Prestin is the motor protein of cochlear outer hair cells." Nature **405**(6783): 149-155.

Zheng J. L., Gao W. Q. (2000). "Overexpression of Math1 induces robust production of extra hair cells in postnatal rat inner ears." Nat Neurosci **3**(6): 580-586.

Zhuang S., Zhang Q., Zhuang T., Evans S. M., Liang X., Sun Y. (2013). "Expression of Isl1 during mouse development." Gene Expr Patterns **13**(8): 407-412.